Ife Journal of Technology

Vol 20, No 1, 2011

Editorial Board

General Information

The Ife Journal of technology is an international journal published by the Faculty of Technology, Obafemi Awolowo University, Ile-Ife, Nigeria.

The journal accepts original manuscripts from anywhere in the world in all engineering and related disciplines as listed below:

i. Agricultural Engineering
ii. Chemical Engineering
iii. Civil Engineering
iv. Computer Science and Technology
v. Electronic and Electrical Engineering
vi. Food Science and Technology
vii. Materials Science and Engineering
viii. Mechanical Engineering
ix. Technology Planning, Development and Management
x. Other engineering and related topics

The journal provides a vehicle for the fast and wide dissemination of results and findings of well-conducted researches in engineering and related fields mainly as research papers (theoretical and experimental), research notes and review articles. The journal also publishes book reviews, news and announcements.

Frequency of Publication
The journal is published twice a year in May and November

Annual Subscription (including postage)

Within Nigeria:	Outside Nigeria
Individuals: N1200.00	Individuals: $50
Institutions: N2500.00	Institutions: $100

Advertisement Rates
Full page (inside): N10,000
Half page (Inside): N5000
Additional for color: N5,000

Correspondence
All correspondence should be addressed to:

The Editor,
Ife Journal of Technology,
Dean's Office
Faculty of Technology,
Obafemi Awolowo University,
Ile-Ife, Nigeria

Visit our website at http://www.ijtonline.org

IFE JOURNAL OF TECHNOLOGY

Vol. 20, No. 1, 2011

Published by Faculty of Technology, Obafemi Awolowo University,
Ile-Ife, Nigeria

ISSN: 1115-9782

Full Paper

MICROSTRUCTURAL RESPONSE OF POWDER METALLURGY (PM) RR1000 SUPERALLOY TO INERTIA FRICTION WELDING

K.M. Oluwasegun
Department of Materials Science and Engineering, Obafemi Awolowo University, Ile-Ife, Osun State 220005 Nigeria.

M.O. Adeoye
Department of Materials Science and Engineering, Obafemi Awolowo University, Ile-Ife, Osun State 220005 Nigeria
madeoye@oauife.edu.ng

O.E. Olorunniwo,
Department of Materials Science and Engineering, Obafemi Awolowo University, Ile-Ife, Osun State 220005 Nigeria.

P.O. Atanda
Department of Materials Science and Engineering, Obafemi Awolowo University, Ile-Ife, Osun State 220005 Nigeria.

ABSTRACT

The microstructural response of powder metallurgy RR1000 superalloy to inertia friction welding was investigated. It was observed that the rapid heating during inertial friction welding resulted in a significant grain-boundary liquation of solid-state γ' precipitates, low temperature melting depressant intermetallic compound, and secondary solidification MC carbides constituents, which were all present in the preweld heat-treated alloy. Liquation of these particles enhanced grain boundary microfissuring in the thermomechanical affected zone (TMAZ) of the weldment. However, contrary to the generally observed increase in HAZ cracking in superalloys with an increase in Ti and Al concentration, due to increase in the hardness of the alloy and rapid re-precipitation of γ' strengthening particles during cooling from welding temperature, a significantly reduced cracking was observed in inertia friction welded PM RR1000 compared to the conventional gas tungsten arc welded cast IN738. This was despite the hardness being higher in the former than in the latter. This may be related to the solid state welding phenomena proffered by inertia friction welding which precludes the formation of liquid melt during welding.

Keywords: *Hardness; Intermetallic compounds; Superalloy; Grain boundary wetting*

1. INTRODUCTION

RR1000 is an emerging precipitation-strengthened nickel based superalloy produced via powder metallurgy. This alloy possesses a very good hot-corrosion resistance, long-term stability, and high-temperature strength, primarily due to the precipitation hardening by γ' precipitates, an ordered intermetallic $Ni_3(Al,Ti)$ phase dispersed in the austenitic γ' matrix, and has been employed for use in aero-engines and large stationary power generation gas turbine discs. Powder metallurgy processing of the alloy results in a further improvement in its high-temperature properties and hot corrosion resistance and also permits the use of higher service temperatures, which is very important for enhancing the thermal efficiency of turbines (Silva and Brito, 2006). The hot-section components of the turbines generally experience very severe thermal and mechanical stresses for extended periods during service, which can cause cracking or material loss. For cost effectiveness, it is often advantageous to repair the damaged components rather than replace them, and inertia friction welding has been found as a better joining technique than the conventional welding method during repair to increase the component life. However, precipitation-strengthened nickel-base alloys that contain a high concentration of Al/Ti (›3 at%) exhibit only a limited weldability due to their high susceptibility to heat-affected zone (HAZ) cracking during welding and during the subsequent postweld heat treatment (PWHT) (Owezarski et al, 1966; Prager and Sines, 1970; Jahnke, 1982; Thamburaj et al, 1983; Ojo et al, 2004; Sidhu et al, 2005).

Cracking during welding of nickel base superalloy has been attributed mostly to shrinkage stresses caused by rapid re-precipitation of γ' particles during weld cooling and the propensity of the alloys to liquation cracking due to constitutional liquation of various phases present in the preweld microstructure of the base alloy (Owezarski et al, 1966) . Strain-age or PWHT cracking in all the precipitation-hardened superalloys, has also been reported to generally initiate in the HAZ that liquated during the welding process (Lim et al, 2002; Sidhu et al, 2005). The synergetic effect of thermally induced welding strain and very low ductility in the alloy due to localized melting of particle at grain boundaries results in HAZ liquation cracking. HAZ or thermomechanical affected zone (TMAZ) liquation is known to occur either by non-equilibrium interface melting below the solidus an alloy or by equilibrium supersolidus melting. Subsolidus HAZ liquation which commonly occurs by constitutional liquation of second phase particles is generally considered more detrimental to crack resistance in that it extends the effective melting range of an alloy and also influences the nature of supersolidus melting by pre-establishing non-equilibrium film at a lower temperature which changes the reaction kinetics during subsequent heating (Owezarski et al, 1966). This process, proposed by Pepe and Savage (Pepe and Savage, 1967) and observed by different investigators in various alloy system (Romig et al, 1988; Radhakrishnan and Thompson, 1991; Reiso et al, 1993), occurs by a eutectic-type reaction between a second phase particle and the matrix producing a non-equilibrium solute rich film at the particle/matrix interface. Thus the thermal history is particularly important if weld microstructures are to be optimized for subsequent joint performace. The present study is aimed at microstructural response of the newly developed PM RR1000 superalloy to inertia friction welding.

2. EXPERIMENTAL PROCEDURE

The base alloy in this work was a new generation PM nickel base superalloy RR1000, developed and provided by Rolls Royce Plc. The as received base alloy had been standard solution heat treated at 1120°C for 4 h and fully aged at 760°C for 8 h with subsequent air cooling after the PM process with the following composition (wt %) 15Cr, 16.5Co, 5Mo, 3Al, 3.9Ti, 2Ta, 0.2Hf, 0.02B, 0.05Zr, 0.02C and nickel balance. The as received inertial friction welded (IFW) samples were of dimensions 20 mm × 12 mm × 10 mm. The themomechanical affected zone microstructures of this alloy were simulated by a Gleeble thermomechanical simulation system by using cylindrical specimens of 8 mm diameter and 7.96 mm length which were heated to 1150, 1175, 1200 and 1225°C at a rate of 20°C/s and held for 1 s at all temperatures followed by water quenching, while another similar sample was air cooled. The specimen temperature was monitored with a chromel-alumel thermocouple spot welded to the specimens at the midsection of the gauge length. The specimens were water quenched from their high temperatures in order to preserve, as much as possible, the microstructural changes that occurred at the simulation temperatures. The as received inertial friction welded samples were sectioned transversely across the weldment while the Gleeble simulated samples were sectioned at the locations of the spot welded thermocouple. The sectioned samples were polished using standard metallographic techniques and were subsequently electrolytically etched in 10% orthophosphoric acid solution at 3.5 V for 3 s. TEM foils were prepared by twin jet electropolishing in a solution containing 35 cc $HClO_4$ in 500 cc methanol and 65 cc n-butanol at 20 V and a temperature ≤ -40°C. Vickers hardness test was carried out by employing a Mitutoyo vicker harness tester with a load of 1000 g. The microstructural studies of the specimens were carried out by the use of optical microscope, field emission gun XL30 scanning electron microscope and Philips CM20 transmission electron microscope, both electron microscopes equipped with energy dispersive X-ray (EDX) spectrometer.

3. RESULTS AND DISCUSSION

3.1. Microstructure of preweld material

The microstructure of the as-received preweld (solution treated) RR1000 superalloy is shown in Fig. 1. It consisted of extensive precipitation, ~48 vol %, of trimodal ordered intermetallic phase within the grain and at the grain boundary regions. It is seen that they have a spherical morphology. They consisted of a fairly regular distribution of primary γ', 0.8–2 μm in size, fine (~0.1 μm) spheroidal secondary γ', and very fine tertiary γ' (5-30 nm) (Fig. 1(a) and (b)). Figure 1(c) shows a thin film TEM bright field image of the spheroidal secondary γ' particles. Superlattice reflections in the SADP, shown confirmed them to be ordered intermetallic γ' phase with the usual orientation relationship of $\{100\}_{\gamma'}$ //$\{100\}_{\gamma}$ and $\langle 100\rangle_{\gamma'}$//$\langle 100\rangle_{\gamma}$ with the fcc-γ matrix. These secondary γ' particles have formed during cooling from the solution treatment temperature. Metal carbides (MC) rich in Ti were also observed in the alloy (Fig. 1(a) and 2(d)).

3.2. Microstructures of the actual and simulated TMAZ

The microstructure of the actual weldment and simulated TMAZ showed similar morphology of microcracks displaying a relatively irregular and jagged path typical of liquation cracks, with cracking occurring pre-dominantly in the TMAZ slightly away from the bond line (Fig. 2). Detailed examination of cracked regions at higher magnification by SEM revealed the existence of re-solidification constituents with eutectic morphology that is characteristic of γ-γ' eutectic which formed at the later stage of solidification in this alloy (Fig. 2(f)). The re-solidification constituents that formed mostly on one side of the cracks confirm the formation of liquid film on the grain boundaries in TMAZ by liquation mechanism. Microfissuring occurred by decohesion across the solid–liquid interfaces under the action of tensile welding stresses generated during cooling.

Moreover, many of the liquated grain boundaries were observed to exhibit liquid-film migration features (Fig. 2(d)), signifying the formation of grain-boundary liquid during the weld thermal cycle. The liquid was observed to be present in the form of thick, continuous layers, particularly along the grain-boundary regions in the immediate vicinity of the fusion zone. It has been reported that grain-boundary liquation, observed in welds of many fully austenitic iron and nickel-based alloys aggravate the intergranular microfissuring in these materials, which has generally been attributed to the inability of the intergranular liquid to accommodate thermal and mechanical stresses and mechanical constraint during weld cooling (Radhakrishnan and Thompson, 1991; Nakkalil et al, 1992; Ojo et al, 2004).

3.3. Constitutional liquation of γ' precipitates and its attendant effect on grain boundary microfissuring

Constitutional liquation of γ' precipitates, which are the principal precipitation-strengthening particles in RR1000 superalloy, was observed to be a significant phenomenon that occurred in the TMAZ of the present welds. The extent of γ' liquation in the welded samples was observed to increase with an increase in the peak temperatures experienced in the TMAZ as illustrated by the simulation results (Fig. 3(a) and (b)).This was also true for the actual welded sample with proximity to the fusion line (Fig. 4). The requirement for the occurrence of constitutional liquation of an intermetallic compound A_xB_y in an alloy is the existence of A_xB_y particles at temperatures equal to or above their eutectic temperature on heating (Ojo et al, 2004). Consequently, the susceptibility of an A_xB_y type second phase to constitutional liquation in the weld TMAZ must primarily be related to its solid state dissolution behavior, as complete dissolution prior to reaching the eutectic temperature will preclude the occurrence of liquation. It has been reported that the terminal eutectic temperature in a nickel base superalloy (Inconel 718) above which constitutional liquation of A_2B-type Laves phase and NbC particles were observed was found to correspond to the terminal reaction peak temperature during thermal analysis (Radhakrishnan and Thompson, 1991). Dissolution behavior of γ' precipitates was expected to deviate from equilibrium due to rapid thermal cycling

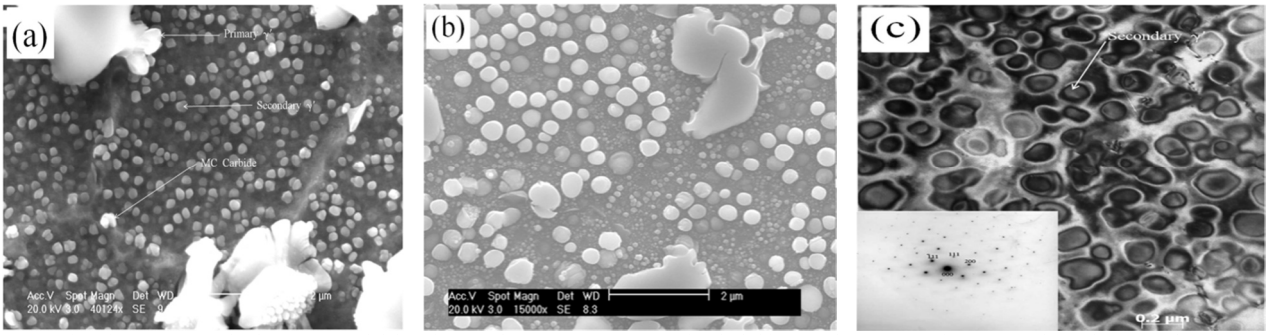

Fig. 1. (a) and (b) Micrographs showing trimodal distribution of γ' precipitate. (c) TEM bright field image showing secondary γ' particles with (inset) selected area diffraction pattern (SADP) from $[0\bar{1}1]$ *zone axis*

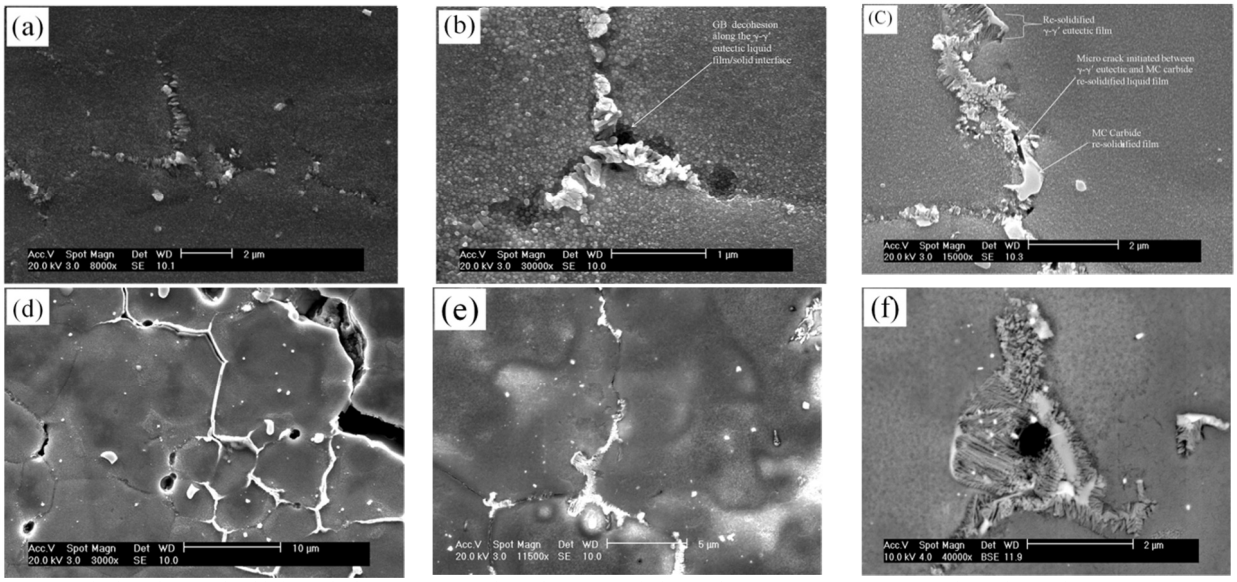

Fig. 2. SEM micrograph of (a) the actual welded sample showing microcracks at the TMAZ, (b) the simulation at 1175°C + water quench, (c) the simulation at 1200°C + water quench, (d and e) simulated TMAZ showing continuous layer of constitutional liquated particles. (f) Backscatter electron mode of SEM showing typical morphology of γ-γ' eutectic product and crack formed by decohesion of solid-liquid interface.

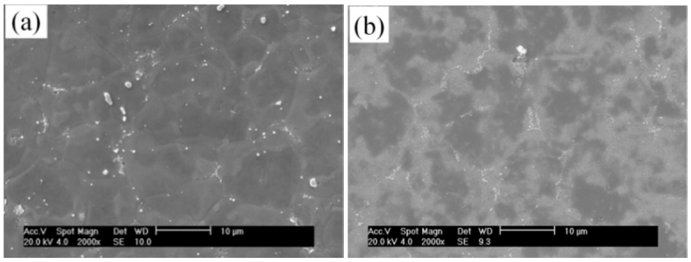

Fig. 3. SEM micrographs showing the extent of liquation at different peak simulation temperature (a) 1175°C and (b) 1200°C.

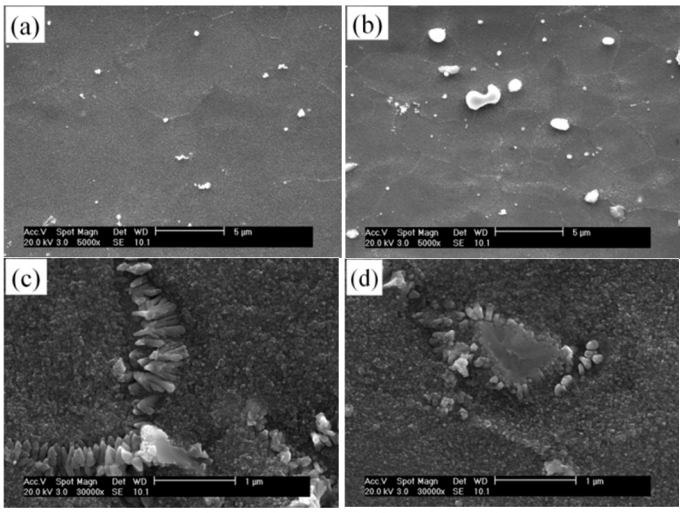

Fig.4. SEM micrographs showing the extent of γ' liquation as a function of distance from bond line (a) and (d) at 2 μm from bond line and (b) and (c) 4 μm from bond line.

involved during welding. Particle dissolution model under rapid heating condition by an analytical technique as well as through the additivity and isokinetic approach has been made (Bjorneklett et al, 1998). The results of the two methods, which were found to be in good agreement with numerical dissolution model and experimental results, show that the degree of particle dissolution depends on interplay between the heating rate and the initial particle size. The solid state dissolution of the γ' phase in Astroloy superalloy at equilibrium and under rapid heating was studied by Soucail and Bienvenu (Soucail and Bienvenu, 1996) in a separate work. Their results, which were in agreement with those of Bjorneklett et al. (1998) showed that there was a significant deviation from equilibrium under rapid heating condition, in that the temperature of complete solid state dissolution increased with increasing heating rate and this deviation was dependent on the initial particle size. This increase in complete dissolution temperature was found to be more pronounced with increase in particle size. An increase of about 120°C in complete dissolution temperature was reported for γ' precipitates with initial size of 0.8 μm under a heating rate of 8°C/s. In inertia friction welding process, like the one used in the present work, typical heating rate normally exceeds 150°C/s and as such, variations in γ' dissolution behaviour of γ' particles could be expected to depend on the particle's location and size, with the possibility of some coarse particles remaining undissolved above 1600°C (solvus temperature of primary γ') resulting in their constitutional liquation. Evidence of γ/γ' interface liquation was observed not only along the grain boundaries but more importantly within the grains of the TMAZ (Fig. 5). This figure is presented to prevent argument that liquation of intergranular γ' particles could not be used to confirm the occurrence of constitutional liquation of the precipitate, knowing that other liquation mechanisms may also be operative at grain boundaries, such as constitutional liquation of MC type carbides and possibly liquation due to segregation of low melting point depressing elements like titanium. Consequently intragranular particles shown in Fig. 5 is located up to 10 μm away from HAZ grain boundaries and distinctly separated from other liquating phases.

Susceptibility to cracking depends on penetration and wetting of grain boundary liquid film thickness and its stability to temperatures at which sufficient thermal and mechanical stresses are generated on cooling. This is very crucial because mere occurrence of liquation may not be sufficient to produce a crack susceptible microstructure. Grain boundary wetting is enhanced if the solid–liquid interfacial energy is small compared to the grain boundary energy. Considering that the metastable liquid produced by constitutional liquation always reacts with the solid through solute back diffusion, the non-equilibrium solid–liquid interface energy is very low (Askay et al, 1974), and as such extensive grain boundary penetration and wetting by film produced by constitutional liquation of γ' particles is expected. This was observed in all the samples with significant penetration and spreading of the film along the grain boundary (Figs. 2(c) to (f)), even to the lower temperature subsolidus region of the TMAZ.

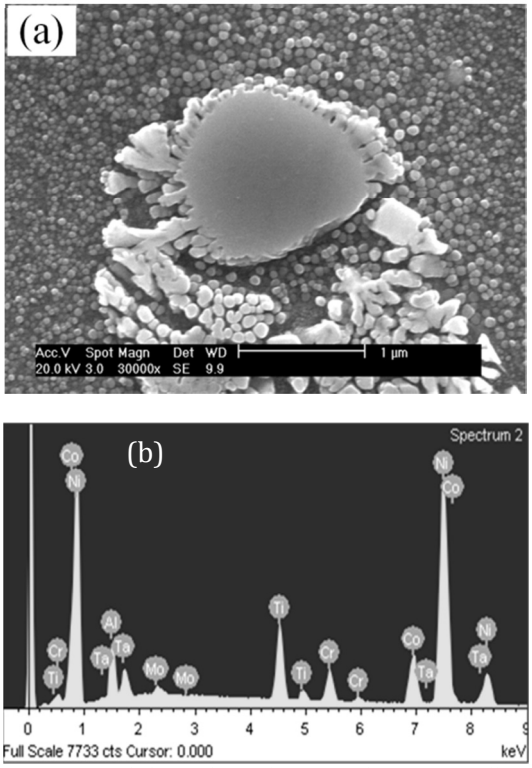

Fig. 5. (a) SEM micrograph showing liquated transgranular primary γ'. (b) EDX of liquated intragranular primary γ'.

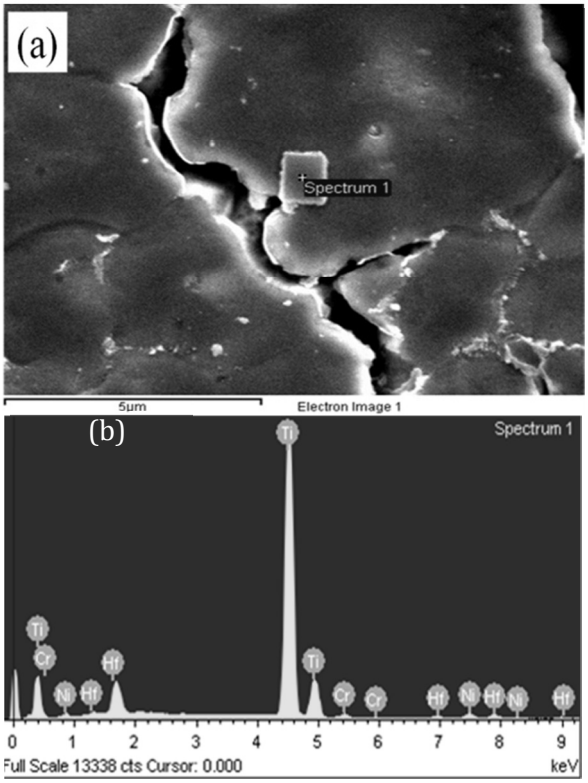

Fig.6. (a) SEM micrograph showing grain boundary Ni-Ti intermetallic particle. (b) EDX of the Ti rich precipitate.

3.4. The Role of MC and Ti-rich particles in the TMAZ microfissuring

The role of carbides in superalloys is complex and dynamic. Opinions seem to vary as to whether carbides are to be tolerated or are essential in the superalloy grain boundaries. However most investigators today feel carbides do exert a significant and beneficial effect on rupture strength at high temperature. However, our focus should not be drifted from the fact that carbide morphology can influence ductility and chemical stability of the matrix through removal of reacting elements. The solvus temperatures of MC carbides have been reported to be within the range of 1180-1190°C (Koul and Wallace,1982). The high heating rate of the weld region or of the simulated samples increases the solvus temperature of this particle as discussed in γ' liquation. The existence of these particles up to the temperature at which they can form an eutectic like reaction, MC + γ with the matrix γ resulted in constitutional liquation of Ti-rich MC to form liquid film spreading along the grain boundary (Fig. 2(d)).

The dissolution of the secondary γ' and liquation of both primary γ' and Ti- rich MC carbide in the TMAZ resulted in the microsegregation of Ti to the grain boundary due to the positive segregation behaviour proffers by its partition coefficient of 0.6 ($k < 1$) (Table 1). The enrichment of the grain boundary with Ti leads to the formation of Ni-Ti (Table 2) melting point depressant intermetallic particle. Ti has been discovered as one of the melting point depressant in Ni superalloy (Ernst et al, 1989). Thus, the presence of these Ti-rich particles at the grain boundary will enhance the stability of the liquid film resulting from the constitution liquation of γ' and MC carbide and consequently their penetration and wetting of the grain boundary which resulted in the revealed grain boundary microcracking (Fig. 6). The discussion above shows that grain boundary microfissuring cannot be considered in isolation due to constitutional liquation of γ' precipitates alone.

3.5. Microhardness and volume fraction studies

Figures 7a-c show the response of the alloy's hardness and primary γ' volume fraction to cooling from the weld simulated temperatures. It is generally believed that as cooling rate increases, there is a corresponding increase in hardness (Wusatowska-Sarnek et al, 2003). A high cooling rate results in a large degree of undercooling and increased supersaturation. This in return suppresses early precipitation during cooling and generates a large amount of nucleation sites and small size γ' (tertiary) with a small interparticle distance after cooling (Groh, 1996). Although it has been already stated in the present report that water quenching was chosen in order to preserve, as much as possible, the microstructural changes that occurred at the simulation temperatures. The observed variations in the hardness profile (Fig. 8) may be due to the temperature gradient from the weld line through the TMAZ. This temperature gradient during cooling may result in different re-precipitation responses of γ' precipitates in this region. The peak in hardness observed at 0.3 mm from weld line was due to the rapid nucleation and precipitation of tertiary γ' (Fig. 9a).

Table 1 Element partition coefficients in nickel based superalloy.

Element	Experimental k (Zhou et al, 1992)
Al	1.2
Co	1.1
Cr	1.05
Ni	1.05
Zr	0.06
Nb	0.4
Ti	0.6
Ta	0.7
Mo	0.85
W	1.4
Element	**Theoretical k (Taha and Kurz, 1981)**
B	0.0082
S	0.01
C	0.3

Table 2. Composition of the Ni-Ti intermetallic compound.

Element	Weight %	Atomic %
Ti	84.72	92.08
Cr	1.65	1.66
Ni	3.85	3.41
Hf	9.78	2.85

Constitutional liquation of primary γ' precipitates could also have been responsible for the trough in the hardness profile between 0.3 mm and 1 mm (Fig. 9c) in addition to the depletion of secondary γ' as reported by Preuss et al (2002) and also confirmed in the present work. The precipitation of the secondary γ' particles during cooling could be responsible for the next phase of increase in hardness from 1mm to approximately 2 mm from the bond line (Figs. 9 d-g). Further slow cooling from this region could result to the coarsening of secondary γ' until the distribution gives similar response to that of the base alloy (Fig. 9h). Figures 7a-b illustrate that the samples cooled from a simulation temperature of 1200°C give a similar response to the as-received IFW sample. This corroborates the report by Wang et al (2005) on the energy input based finite element process modeling of inertia welding (Fig. 10).

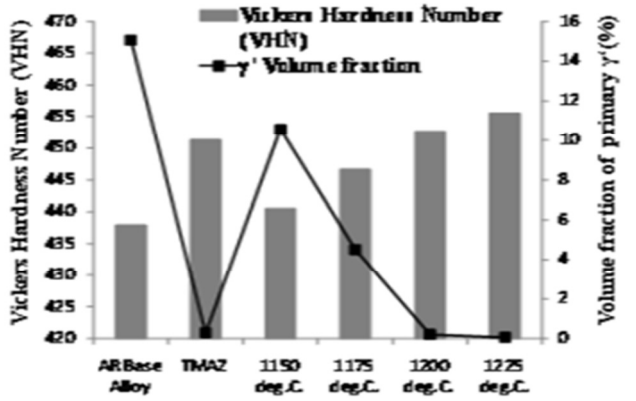

(a)

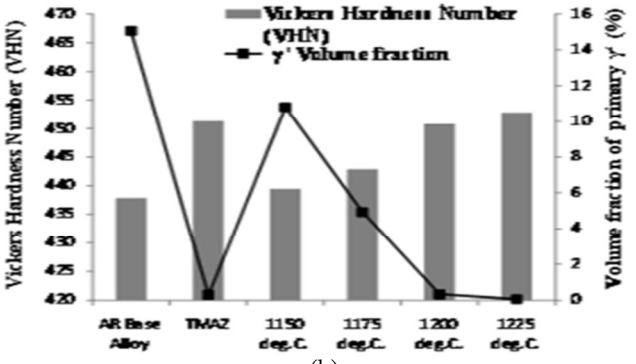

(b)

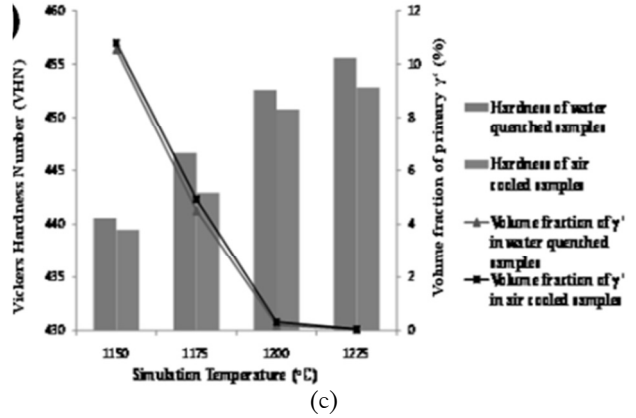

(c)

Fig.7. (a) Comparison of the hardness and primary γ' volume fraction of the base material and TMAZ with (a) water quenched samples(b) air cooled samples (c)The response of hardness and GB γ' particles to cooling rates from peak temperature in the simulated TMAZ.

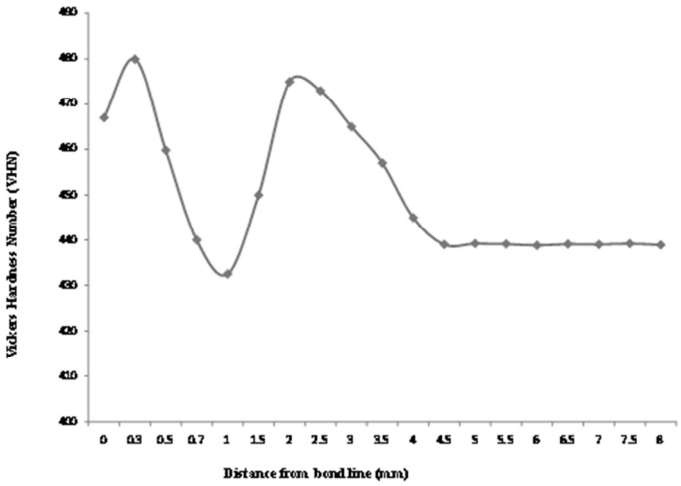

Fig.8. Response of the as received IFW RR1000 alloy's hardness to distance from the bond line

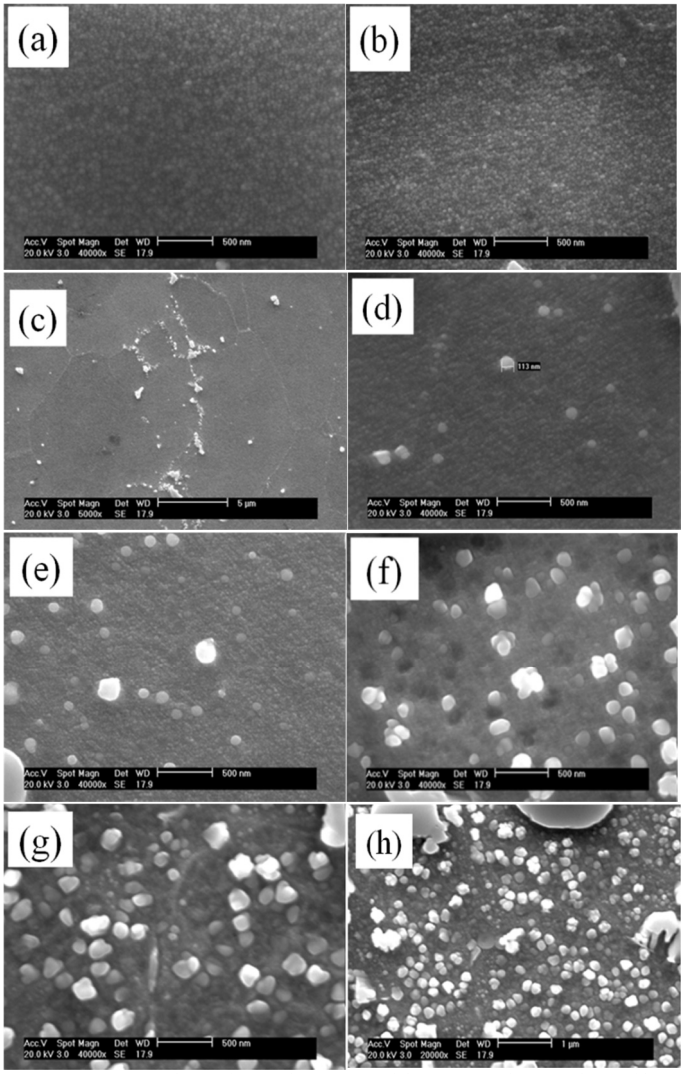

Fig. 9: SEM images of secondary and tertiary γ' of the IFW sample (a) at the bond line (b) 0.3 mm (c) 0.5 mm (d)1 mm (e) 1.5 mm (f) 1.7 mm (g) 2 mm and (h) 4 mm from the bond line.

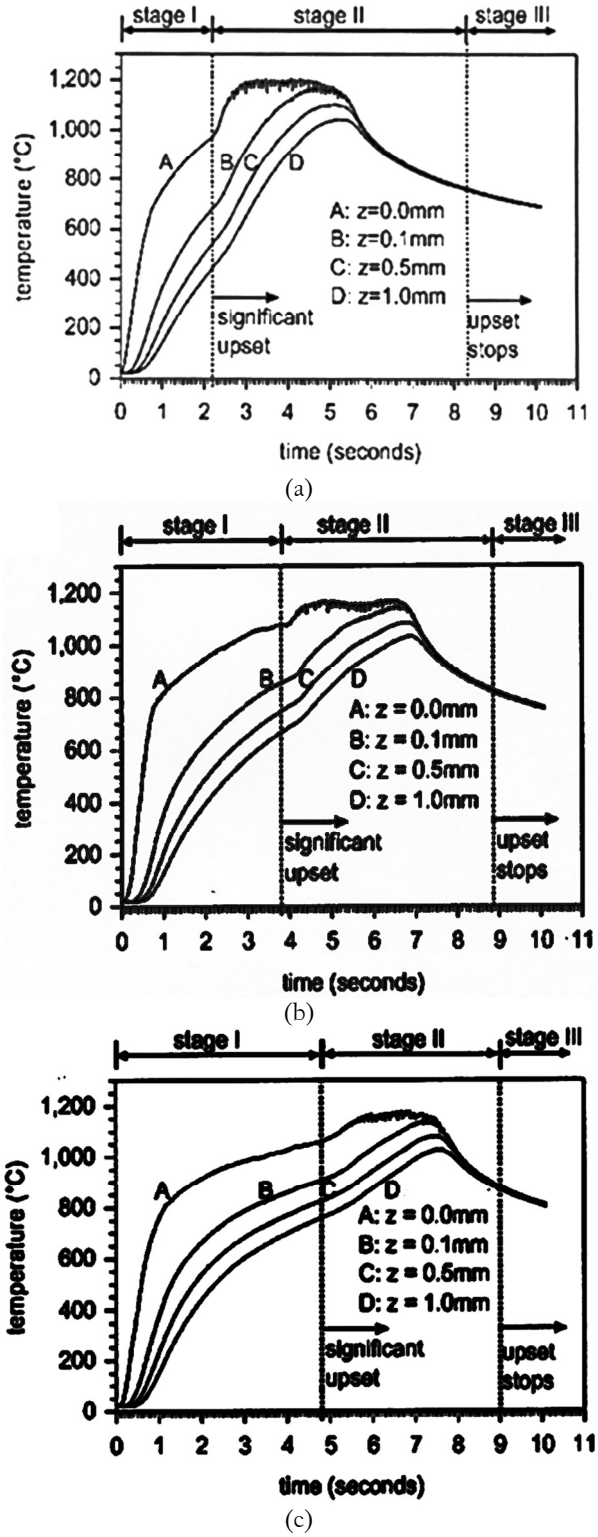

Fig. 10. The simulated thermal history of (a) low inertia, high initial rpm (b) medium inertia, medium initial rpm (c) high inertia, low initial rpm from the weld line. (Wang et al, 2005)

4. Conclusions

1. Re-solidified constituents were observed along cracked grain boundaries in the TMAZ of inertia friction welded RR1000 alloy and it is concluded that one of the factors responsible for TMAZ cracking in this alloy was grain boundary liquation.
2. Constitutional liquation of both intragranular and intergranular γ' precipitates was found to be contributing significantly to the TMAZ liquation.
3. Constitutional liquation of Ti-rich MC carbide precipitates was also found to contribute to the TMAZ liquation
4. Liquid films from liquated particles were observed to exhibit extensive penetration and wetting of grain boundaries even to the lower temperature subsolidus region of the TMAZ.
5. The results of the present study confirmed previous reports which indicated that rapid re-precipitation of γ' precipitates during solidification from weld temperature could contribute to TMAZ.
6. It is suggested that higher concentration of γ' forming elements in nickel base superalloys could promote constitutional liquation tendency of γ' particles by reducing the minimum required heating rate for particles of a given size to liquate, and by reducing the maximum γ' particle size that can withstand a particular heating rate without liquating.

Acknowledgements

The authors would like to appreciate Rolls Royce Plc for providing specimens and technical information.

References

Aksay, I.A.; Hoge, C.E. and Pask, J.A. 'Wetting under chemical-equilibrium and nonequilibrium conditions', J Phys Chem. 78:1178-1183, 1974.

Bjorneklett,; B.I.; Grong, O., Myhr, O.R. and Kluken, O.A. 'Additivity and isokinetic behaviour in relation to particle dissolution', Acta Mater. 46:6257, 1998.

Ernst, S.C.; Baeslack, W.A., Lippold J.C. 'Weldability of high-strength low-expansion Superalloys' Weld J. 68: 145, 1989.

Groh, J.R., 'Effect of cooling rate from solution heat treatment on waspaloy microstructure and properties', Superalloys', 621-626, 1996.

Jahnke, B. 'High-temperature electron beam welding of the nickel- base superalloy IN-738LC', Weld. J. 61: 343s–347s, 1982.

Koul, A.K.; and Wallace W. 'Note on the microstructural dependence of creep strength in inconel 700', Metallurgical and Materials Transactions A. 3A: 673- 675, 1982.

Lim, L.C.; Yi, J.Z., Liu, N. and Ma, Q. 'Mechanism of post-weld heat treatment cracking in Rene 80 nickel based superalloy', Mater. Sci. Technol. 18 (4): 407- 412, 2002.

Nakkalil, R.; Richards, N.L. and Chaturvedi, M.C. 'Influence of solidification mode on heat affected zone microfissuring in a nickel-iron base superalloy', Scripta Metall. Mater. 26: 1599–1603, 1992.

Ojo, O.A.; Richards, N.L. and Chaturvedi, M.C. 'Liquation of various phases in HAZ during welding of cast Inconel* 738LC', Mater. Sci. Technol. 20:1027–1034, 2004.

Ojo, O.A.; Richards, N.L. and Chaturvedi, M. C. 'Contribution of constitutional liquation of gamma prime precipitate to weld HAZ cracking of cast Inconel 738 superalloy', Scripta Mater. 50: 641, 2004.

Owczarski, W.A.; Duvall, D.S. and Sullivan, C.P. 'Model for heat-affected zone cracking in nickel-base superalloys', Weld. J. 45: 145s–155s, 1966.

Pepe, J.J.; and Savage, W.F. 'Effects of constitutional liquation in 18-Ni maraging steel weldments', Weld J. 46: 411s–422s, 1967.

Prager, M.; and Sines, G. 'Welding of precipitation-hardening nickel-base alloys', Weld. Res. Counc. Bull. No. 150:24–32, 1970.

Preuss, M.; Pang, J.W.L., Withers, P.J. and Baxter, G.J. 'Inertia welding nickel-based superalloy: Part I. Residual stress characterization', Metallurgical and Materials Transactions A: Physical Metallurgy and Materials Science, 33(10): 3215-3225, 2002.

Radhakrishnan, B. and Thompson, R.G. 'Phase diagram approach to study liquation cracking in alloy 718', Metall Trans;22A:887-902, 1991.

Radhakrishnan, B. and Thompson, R.G. 'The effect of weld heat-affected zone (HAZ) liquation kinetics on the hot cracking susceptibility of alloy-718', Metall. Trans. A, 24A:1409–15, 1993.

Reiso, O.; Ryum, N. and Strid, J. 'Melting of secondary-phase particles in Al-Mg-Si alloys', Metall Trans; 24A:2629-2641, 1993.

Romig, A.D. Jr.; Lippold, J.C. and Cieslak, M.J. 'Analytical electron microscope investigation of the phase transformations in a simulated heat-affected zone in alloy 800', Metall Trans;19A:35, 1988.

Sidhu, R.K.; Richards, N.L. and Chaturvedi, M.C. 'Effect of aluminium concentration in
filler alloys on HAZ cracking in TIG welded cast lnconel 738LC superalloy', Mater. Sci. Technol. 21 (10): 1119–31, 2005.

Sidhu, R.K.; Richards, N.L. and Chaturvedi, M.C. 'Post-weld heat treatment cracking inautogenous GTA welded cast Inconel 738LC superalloy', Mater. Sci. Technol. 23 (2): 203–13, 2007.

Silva, J.M. and A. Sousa E Brito. 'Microstructural evaluation of a new generation PM nickel base superalloy', Proceedings of the10th Portuguese Conference on Fracture, pp.1-6, 2006.

Soucail, M. and Bienvenu, Y. 'Dissolution of the γ′ phase in a nickel base superalloy at equilibrium and under rapid heating', Mater Sci Eng A. 220: 215, 1996.

Taha, M.; and Kurz, W. 'About microsegregation of nickel base superalloys'. Z. Metallkd. 72: 546-549, 1981.

Thamburaj, R.; Wallace, W. and Goldak, J.A. 'Post-weld heat-treatment cracking in Superalloys', Int. Met. Rev., 28 (1):1–22, 1983.

Wang L.; Preuss, M., Withers, P.J. Baxter, G. and Wilson, P. 'Energy-input-based finite-element process modelling of inertia welding', Metallurgical and Materials Transactions B: Process Metallurgy and Materials Processing Science, 36(4): 513-523, 2005.

Wusatowska-Sarnek, A.M.; Blackburn, M.J. and Aindow, M. 'Gamma Precipitation kinetics in P/M IN100 Thermec'2003, Pts 1-5,. 426-4: 767-772, 2003.

Zhou, J.; Wang, H. P., Doherty, R. and Perry, E. M. 'Solidification behavior and microstructure formation in a cast nickel based superalloy-experiment and modelling', in Proceedings of Superalloys Conference edited by S. D.Antolovich, R. W. Stusrud, R. A. Mackay, D. L. Anton, T. Khan, R. D. Kissinger and D. L. Klarstrom (The Minerals, Metals & Materials Society, 1992) p.165, 1992.

Full Paper

MODELLING HYDRAULIC BACKWASH IN ULTRAFILTRATION PROCESS: A STATISTICAL APPROACH

M.O. Daramola
Biochemical Engineering Laboratory,
Department of Chemical Engineering,
Obafemi Awolowo University, Ile Ife, Osun State, Nigeria
kennydara@yahoo.com

E.F. Aransiola
Biochemical Engineering Laboratory,
Department of Chemical Engineering,
Obafemi Awolowo University, Ile Ife, Osun State, Nigeria

E. Betiku
Biochemical Engineering Laboratory,
Department of Chemical Engineering,
Obafemi Awolowo University, Ile Ife, Osun State, Nigeria

A. G. Adeogun
National Center for Hydropower Research and Development
University of Ilorin, Ilorin, Nigeria.

ABSTRACT

Modelling of hydraulic backwash (*HB*) during ultrafiltration process is presented in this paper with the aim to studying the influence of operating parameters on *HB* using statistical approach under pilot scale conditions. The *HB* model describes change in transmembrane pressure (ΔTMP) as a function of backwash frequency, backwash flux and backwash time. The development and validation of the model was based on the experimental data from a series of experiments designed using full 2^3 factorial design method and implemented in SMART XIGA pilot plant with an 8-inch polyether sulfone (PES) membrane module. The results showed that *HB* is largely influenced by backwash time and backwash frequency but with insignificant influence from the backwash flux. However for further implementation in practice, due to changes in the feed water quality, a regular update of the models is necessary and can be easily obtained using the methodology presented in this paper.

Keywords: *ultrafiltration, backwash, filtration, modelling, response surface methodology*

1. INTRODUCTION

Over 70% of our Earth's surface is covered by water. Although water is seemingly abundant, the real issue is the amount of fresh water available. About 97.5% of all water on Earth is salt water, leaving only 2.5% as fresh water. Nearly 70% of that fresh water is frozen in the icecaps of Antarctica and Greenland; most of the remainder is present as soil moisture, or lies in deep underground aquifers as groundwater not accessible to human use. However, less than 1% of the world's fresh water (~0.007% of all water on earth) is accessible for direct human uses. This is the water found in lakes, rivers, reservoirs and those underground sources that are shallow enough to be tapped at an affordable cost. Only this amount is regularly renewed by rain and snowfall, and is therefore available on a sustainable basis (Wikipedia, 2009). To make the fresh water available for human usage, it has to be treated to a specific acceptable level at which no harm is done to human life. One of the cost effective processes of doing this is ultrafiltration (UF).

In the last decade, ultrafiltration applied to drinking water production has demonstrated its reliability and its cost effectiveness (Moll *et al*., 2007). However, membrane fouling and scaling, major problems in UF affect the performance of the process and eventually damage the membranes. In clarification and filtration operations, deposits from fouling create an additional resistance to mass transfer (Serra *et al*., 1998). Fouling decrease would increase permeate flux and so proportionally reduce plant size and /or operating costs. In UF, fouling decrease depends on the method of removal such as backwashing, backflushing etc. Also, accurate backwash modelling and optimization could be helpful to achieving greater backwash effectiveness and thus reducing fouling. In UF, backwashing can either be hydraulic backwashing (*HB*) or chemically enhanced backwashing (*CEB*) (Cheryan, 1998).

During *HB*, permeate flows back through the membrane, lifts off the cake and flushes it out of the module in dead-end mode. Each operating cycle is thus made up of a filtration phase followed by a backwash phase that allows the membrane to recover its initial properties. However, the efficiency of *HB* depends on the backwash flux, backwash frequency and the backwash time (Cheryan, 1998). The ideal situation regarding hydraulic backwash flux and frequency is to use a high backwash flux as frequently as possible. However, such practice results in a low net flux, as permeate is consumed in backwashing. Hence, the need to optimise the *HB*. However, optimizing this process depends on availability of accurate models that will adequately explain the interactions among the influencing factors. Consequently, the objective of this paper is to provide a methodology to find appropriate backwash models using the so-called Response Surface Methodology (*RSM*) (Box and Hunter, 1965) for further insight and optimization of the process because the effectiveness of cleaning procedures (e.g. *HB*) plays an important role in the performance of membranes (Heijman *et al*., 2007).

Response surface methodology (*RSM*) was initiated with the work of Box and Hunter (Box and Hunter, 1961a,b). This method employs statistically designed experiments to obtain appropriate data that can be analyzed statistically to produce concrete and valid conclusions. The essence of this is to obtain descriptions of the responses to the factors considered. These experiments usually developed for modelling phenomena lead to most favourable responses. Specifically, response surface design is classified as a simultaneous method being used in the stage of optimization (Kuehl, 2000; Lazic, 2004). Its application allows selecting the optimum combination of levels to obtain the best response for specific conditions (Montgomery, 1991). Based on the responses and the considered independent variables, polynomial models are developed.

The developed polynomial models are used as practical approach to the real response function (Anunziata and Cussa, 2008).

2 EXPERIMENTAL

2.1. Materials and methods

A two-level full 2^3 factorial design was used. The experiments were performed using *SMART-XIGA* pilot plant containing a 8-inch polyether sulfone (*PES*) capillary hollow fibre UF membrane module (Area 0.0754 m^2 ; number of fibre 120; effective length 25 cm) and operated dead-end mode to clean a sample of wastewater containing some impurities such as microorganisms, volatile organic compounds (VOC) etc. The fouled membrane was cleaned during *HB* by using some of the permeated. Nine experimental runs were performed and the change in transmembrane pressure, *TMP* (ΔTMP) in bar was estimated from Eq. (1). The experimental range and coded factors used in the experimentation are presented in Table 1. Fig. 1 shows the clean membrane and the experimental set-up. Schematic of a cube representing 2^3 factorial design implemented in this study is depicted in fig. 2.

$$\Delta TMP = TMP_f - TMP_o \quad (1)$$

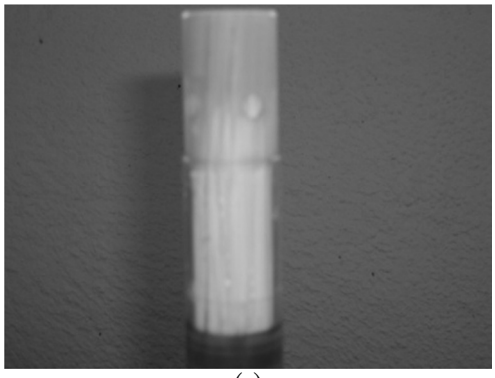

(a)

(b)

Fig. 1. (a) Clean capillary UF membrane module and (b) Experimental set-up

Table 1: Experimental range and coded levels of the three independent variables for HB

Variables	actual	coded	actual	coded	actual	coded
Backwash frequency	2	-1	3	0	4	+1
Backwash time(min)	0.5	-1	1	0	1.5	+1
Backwash flux ($l\,m^{-2}\,h^{-1}$)	150	-1	200	0	250	+1

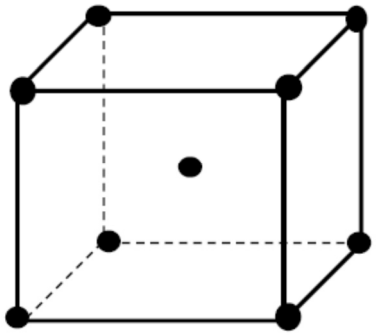

Fig. 2. Schematic of the cubic representation of the 2^3 factorial design (The black dot at the edges of the cube represents each experimental run with a nominal point at the centre).

2.2. Model formulation, development and validation

The model formulation was based on the second order regression polynomial with interactions included. The proposed mathematical relationship is given in Eq. (2).

$$\Delta TMP = \Delta TMP_O + \alpha_1 t_b + \alpha_2 B_f + \alpha_3 J_b + \alpha_4 t_b^{\,2} + \alpha_5 B_f^{\,2} + \alpha_6 J_b^{\,2} + \alpha_7 t_b J_b + \alpha_8 t_b B_f + \alpha_9 J_b B_f \quad (2)$$

where TMP_f is the final transmembrane pressure at the end of filtration, i.e. at T_f = 20 min., and TMP_o the transmembrane pressure of the membrane at the commencement of the filtration. J_b, t_b, and B_f, are backwash flux, backwash time and Backwash frequency, respectively. α_1, ... α_9 denote the regression coefficients related to linear, quadratic and interaction terms, ΔTMP is the predicted response.

Five models were considered based on the combination of B_f, t_b and J_b as shown in Table 2. Least square (LS) estimation method was used to estimate the regression coefficients. Selection of the most suitable regression model was based on the mean square error (MSE) and mean residuals. However, MSE was considered to be more significant in the selection. The model with the lowest MSE was considered as the most suitable candidate. Based on MSE, models 3 & 4 could be considered to be suitable but model 4 has lower mean residuals compared to model 3. Hence, model 4 was considered as the most suitable regression model.

Table 2: Different combinations of B_f, t_b, J_b in relation to ΔTMP

Model	ΔTMP_o	t_b	B_f	J_b	$t_b^{\,2}$	$B_f^{\,2}$	$J_b^{\,2}$	$B_f t_b$	$J_b t_b$	$J_b B_f$	Mean residuals	MSE
1	+	+	+	+	-	-	-	-	-	-	-6.11E-17	4.34E-05
2	+	+	+	+	+	+	+	-	-	-	0.7432	0.08
3	+	+	+	+	+	-	-	+	+	-	4.12E-15	2.48E-05
4	+	+	+	+	-	+	-	+	-	+	2.32E-15	2.48E-05
5	+	+	+	+	-	-	+	-	+	+	1.55E-15	4.34E-05

+ Combined; - Not combined

For model validation, a cross-validation method was used. In cross-validation method, a testing set of data which is a complimentary subset of the data used for model development is normally used.

3. RESULTS AND DISCUSSION

Eq. (3) is the resulted model (a reduced form of Eq. (2)) with standard deviations of the estimated coefficients. Fig. 3 gives the response surface and the contour plots based on Eq. (3). Table 3 depicts the results of cross-validation of the models.

$$\Delta TMP = -0.020 - 0.512 t_b + 0.074 B_f - 0.015 {B_f}^2 - 0.104 B_f t_b \quad (3)$$

$$(\pm 0.032)\ (\pm 0.472)\ (\pm 0.023)\ \ (\pm 0.004)\ \ (\pm 0.149)$$

Table 3 shows that the predicted ΔTMP_p agrees with the estimated ΔTMP from the experimental data to some extent with a mean square error (*MSE*) of 0.18 and thus confirming the validity of the model. Hence, there is a clear indication that the model is valid in the region of the nominal working points employed in this study.

Table 3: Results of model validation for HB using the 2^3 factorial design

No. of Expt.	J_b ($l\,m^{-2}\,h^{-1}$)	t_b (min)	B_f	ΔTMP (bar)	ΔTMP_p (bar)
1	0	0	0	0.036	0.054
2	+1	+1	+1	0.022	0.014
3	+1	+1	-1	0.044	0.051
4	+1	-1	+1	0.050	0.030
5	-1	+1	+1	0.013	0.014
6	-1	+1	-1	0.015	0.051
7	-1	-1	+1	0.032	0.030
8	+1	-1	-1	0.074	0.063
9	-1	-1	-1	0.080	0.063

** see Table 1 for coded levels. Filtration flux was 100 $l\,m^{-2}\,h^{-1}$ for all the experiments*

Depending on the process conditions, an individual experimental run can take several hours to more than one day. Hence, effective experimental designs must be chosen and thus, usually small data sets are obtained. In our application on the influencing factors related to *HB*, nine experimental runs (Table 3) have been performed, while the number of regression coefficients was five (Eq. 3). Consequently, the error characteristics, and especially the auto-correlation of the residuals, were difficult to evaluate and thus the standard deviations presented in (Eq. 3) are only rough indications. As an alternative to the stochastic approach, and most appropriate to small data sets, in the past, a so-called set-membership or bounded-error approach has been proposed.

In this approach, it is assumed that the measurement error is bounded, so that effectively at each sample instant, only intervals are considered instead of single points. For a full treatment of this approach, Walter (2002), Norton (2002), and Keesman (2002) should be consulted. In particular, for the linear estimation case exact solutions can be found. These exact solutions can be tightly bound by boxes, which can be found by solving a couple of linear programming (LP) problems. Assuming an error bound on ΔTMP of 0.005; the following bounded (interval) estimates of the coefficients in (Eq. 3) were found and presented in the second row of Table 4.

If the error bound chosen is too small, no feasible solution will be found. Hence, there exists a minimum error bound for which the interval estimates reduce to a single point. This point estimate is called the min-max estimate. For our application, the min-max estimate of the coefficients is presented in the third column of Table 4. Note that these min-max estimates are not too far from the least-squares estimates. The essence of this bounded-error approach is that now reliable uncertainty regions around the estimates are found.

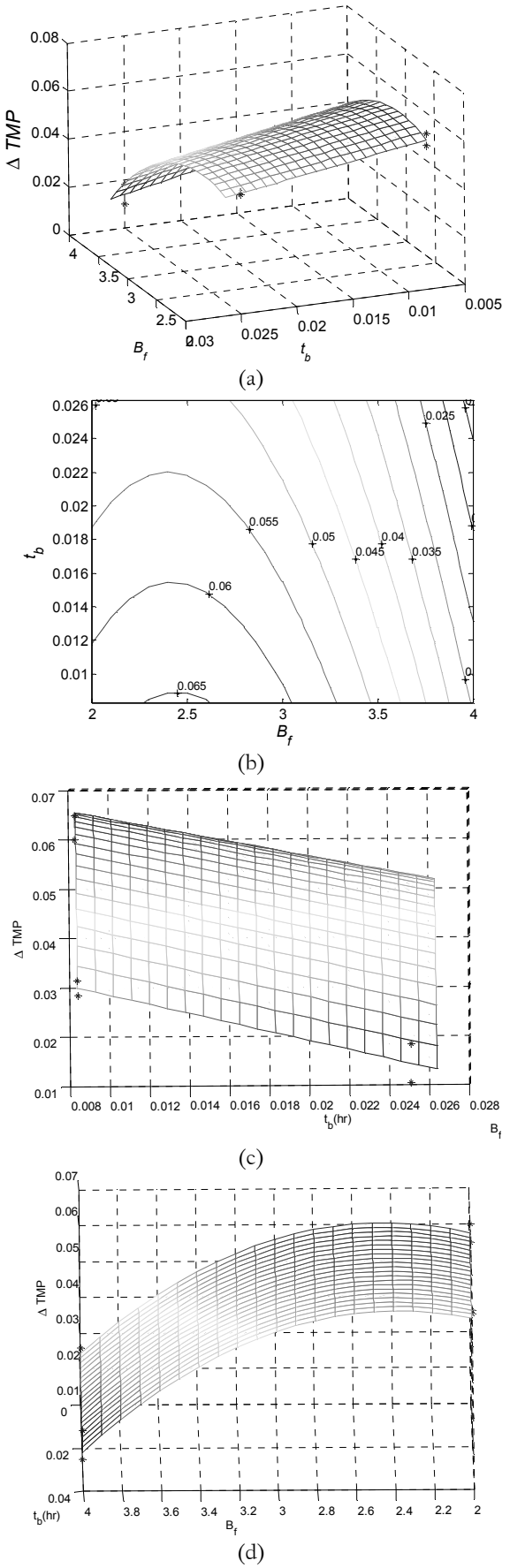

Fig. 3. Response surfaces and contour plots (plus data points) for HB (a) response surface showing relationship between ΔTMP and t_b and B_f (b) the contour plot relating ΔTMP to t_b and B_f (c) response surface showing the relationship between ΔTMP and t_b (d) the contour plot relating ΔTMP to t_b.

Table 4: Bounded-error estimation results for HB

ΔTMP_0	α_1	α_2	α_3	α_4
[-0.081 0.042]	[-1.62 0.60]	[0.028 0.119]	[-0.023 -0.007]	[-0.45 0.24]
-0.022	-0.518	0.076	-0.015	-0.114

From the contour plot of Fig. 3, it can be seen that the model predicts a small decrease of ΔTMP when B_f is smaller than 2.5. This is a rather unlikely phenomenon. If there is sufficient evidence that the maximum should be at B_f = 2, then this information can be easily incorporated into the empirical modelling approach. Setting $\left.\frac{\partial \Delta TMP}{\partial B_f}\right|_{B_f=2} = 0$, where the derivative can be easily found from (Eq. 3), leads to the following constraint between α_2 and α_3: $\alpha_2 + 2\alpha_3 B_f = 0$, so that $\alpha_2 = -4\alpha_3$. Hence, after substitution of this relationship, the model structure of (Eq. 3) becomes

$$\Delta TMP = \Delta TMP_0 + \alpha_1 t_b + \alpha_3 (-4B_f + B_f^2) + \alpha_4 t_b B_f \quad (4)$$

in which the coefficients have to be re-estimated.

Fig. 3 shows that as the t_b increases, the ΔTMP linearly decreases. It can be explained that the longer the time for backwashing, the lower the change in the TMP. This shows a good removal of the fouled layer. Meanwhile, it is expected that for $t_b \to 0$, ΔTMP will become very high (i.e. indicating no removal of foulant), indicating a hyperbolic relationship. Note, however, that the experimental data (Table 3) only support a linear relationship. Therefore, most likely the relationship between ΔTMP and t_b is inverse proportionality. However, this can only be verified through additional experimental runs to get more data points beyond the region considered in this study.

Also, Fig. 3 shows that as the backwash frequency B_f increases from 2 to 4, ΔTMP decreases quadratically with increasing B_f. It can be explained that at low frequencies, there is more formation of cake layer than can be removed with backwash. But as the frequency increases, the cake layer is washed off the membrane. This restores the original property of the membrane. Therefore, the model shows that the higher the frequency of hydraulic backwash, the lower the ΔTMP (i.e. the higher the degree of recovery of the initial membrane flux).

4. CONCLUSIONS

In this study, a model for hydraulic backwash has been developed and cross-validated using an empirical modelling approach, in particular the *RSM*. The modelling was based on experimental data from the *SMART-XIGA (Norit)* pilot plant, using 2^3 factorial designs to limit the number of experimental runs, with the aim of studying the full behaviour and possibilities for optimization of a UF plant. Cross-validation led to the conclusion that the model is reliable under the given experimental conditions. The model showed that *HB* is largely influenced by backwash time and backwash frequency with backwash flux having no effect. However, for further implementation in practice, due to changes in the feed water quality, a regular update of the models is necessary and can be obtained using the methodology presented in this paper.

ACKNOWLEDGEMENT

The authors hereby acknowledge Norit Membrane in The Netherlands for providing the membrane and the pilot plant used in this study and Systems and Control Group of Wageningen University and Research Centre, The Netherlands for providing the enabling environment for the experimentation.

REFERENCES

Anunziata, O.A. and Cussa, J. "Applying response surface design to the optimization of methane activation with ethane over Zn-H-ZSM-5-11 zeolite". *Chemical Engineering Journal* 138: 510 – 516, 2008.

Box, G.E.P. and Hunter, J.S. "The 2k-p fractional factorial designs, Part I". *Technometrics* 3: 311 – 351, 1961a.

Box, G.E.P. and Hunter, J.S. "The 2k-p fractional factorial designs, Part II". *Technometrics* 3: 449 – 458, 1961b.

Box, G.E.P. and Hunter, J.S. "The experimental study of physical mechanisms". *Technometrics*, 7: 23 - 42, 1965.

Cheryan, M. "Ultrafiltration and Microfiltration Handbook". Technomic Publishing Company, Lancaster, Pennsylvania, 1998.

Heijman, S.G.J., Vantieghem, M., Raktoe, S., Verberk, J.C. and van Dijk, J. *Journal of Membrane Science*, 287:119-125, 2007.

Keesman, K.J. "Nonlinear-Model Case in Bound-based Identification, in Control Systems, Robotics and Automation". In: Unbehauen H. (Ed), Encyclopaedia of Life Support Systems (EOLSS), Developed under the auspices of the UNESCO, Eolss Publishers, Oxford, UK (http://www.eolss.net), 2002.

Kuehl, R.O. "Design of experiments: Statistical Principles of Research Design and Analysis". 2nd ed., Duxbury Press, 2000.

Lazic, Z.R. "Design of experiments in Chemical Engineering". Wiley – VCH, Weinhein, 2004.

Moll, R., Veyret, D., Moulin, P. and Charbit, F. "Dean vortices applied to membrane Part I. Experimental approach". *Journal of Membrane Science*, 288: 307-320, 2007.

Montgomery, D.C. "Design and analysis of experiments". John Wiley and Sons, Inc., 1991.

Norton, J.P. "Linear-Model Case in Bound-based Identification, in Control Systems, Robotics and Automation". In: Unbehauen H. (Ed), Encyclopaedia of Life Support Systems (EOLSS), Developed under the auspices of the UNESCO, Eolss Publishers, Oxford, UK (http://www.eolss.net), 2002.

Serra, C., Clifton, M.J., Moulin, P., Rouch, J. and Aptel, P. "Dead-end ultrafiltration in hollow fibre modules: module design and process simulation". *Journal of Membrane Science*, 145:159 – 172, 1998.

Walter, E. "Bound-based Identification, in Control Systems, Robotics and Automation". In: Unbehauen H. (Ed), Encyclopaedia of Life Support Systems (EOLSS), Developed under the auspices of the UNESCO, Eolss Publishers, Oxford, UK (http://www.eolss.net), 2002.

Wikipedia, http://en.wikipedia.org. (Accessed Oct. 14, 2009).

Full Paper

INFLUENCE OF pH AND METAL CONCENTRATION ON Cu ADSORPTION BY TWO SOILS OF CONTRASTING FEATURE

J.A. Osunbitan
Department of Agricultural Engineering
Obafemi Awolowo University,
Ile – Ife, Nigeria.
josunbit@oauife.edu.ng

K.O. Adekalu
Department of Agricultural Engineering
Obafemi Awolowo University,
Ile – Ife, Nigeria.

P.O. Aina
Department of Soil Science
Obafemi Awolowo University,
Ile – Ife, Nigeria.

ABSTRACT

The influence of soil pH and soil copper concentration on the adsorption of the metals by the soil particles was studied in batch conditions. The metal was introduced into the soil through the application of copper based fungicide. Copper adsorption was studied by means of adsorption isotherms using Cu concentrations range of 3.25 g/*l* to 4.5 g/*l* and solution pH of 3, 4, 5 and 6. Results indicated that the four solution pH were significantly ($P < 0.05$) different in their effects on the adsorption of the metal to the two soils. The two soils are also significantly different in their adsorption capacity. The adsorbed copper increased with increase in solution pH and copper concentration with the maximum adsorption occurring at pH of 6 and copper concentration of 4.00 g/*l*. However, concentrations 4.25 g/*l* and 4.50 g/*l* were not significantly different in their effects on the amount of copper adsorbed by the two soils. The amount of copper adsorbed per unit mass of the soil on the average increased from 15.25mg/g at pH 3 to 26.13 mg/g at pH 6 while it increased on the average from 19.20 mg/g at copper concentration of 3.25 g/l to 21.30 mg/g at copper concentration of 4.50g/l. Regression analysis revealed a strong correlation between adsorbed copper and solution pH within individual copper concentrations. From the isotherm analysis, sorption of copper to the two soil types considered was best described by Langmuir equation.

Keywords: *Kocide 101, Adsorption isotherm, equilibrium concentration, solution pH*

1. INTRODUCTION

Land application of fertilizers and pesticides in agriculture has contributed to a continuous accumulation of heavy metals in soils (Adriano, 1986; Sarkar, 2002; Krumholz *et al*., 2003). The behaviour of metals in soil is governed largely by sorption and desorption reactions with different soil constituents (Singh *et al*., 2001). The adsorption of chemicals to sediments and soils is an important process that affects a chemical's distribution in the environment. If a chemical is adsorbed to soil particles, it will remain on the soil surface and will not reach ground water. If a chemical is not adsorbed, it will leach through the soil profile and may reach ground waters and the surface waters thereby contaminating them. Availability of trace elements to plants is affected by a variety of factors including soil solution pH, soil texture, and soil moisture, temperature, oxide content, carbonate content, organic matter content, and clay mineralogy (Goldberg *et al*., 2005).

The total soluble copper in acid soils is found as organic matter complexes (Sposito, 1989; Baker, 1993). Thus the copper availability for plants depends on its characteristics of adsorption (Raghupathi and Vasuki, 1993). Copper is a very common substance that occurs naturally in the environment and spreads through the environment through natural phenomena. Copper can be released into the environment by both natural sources and human activities. Examples of natural sources are wind-blown dust, decaying vegetation, forest fires and sea spray. A few examples of human activities that contribute to copper release into the environment include mining, metal production, wood production, application of copper fungicides and phosphate fertilizer production. Because copper is released both naturally and through human activity, it is spread widely in the environment. Most copper compounds will settle and be bound to either water sediment or soil particles. Soluble copper compounds which form the largest threat to human health usually occur in the environment after release through application in agriculture.

Copper enters agricultural ecosystems through applications of copper – containing fungicides, stable manures, and liquid or solid wastes from copper related mining and manufacturing. When copper is released into soil, it can become strongly attached to the organic material and other components (e.g., clay, sand, etc.) in the top layers of soil and may not move very far when it is released. When copper and copper compounds are released into water, the copper that dissolves can be carried in surface waters either in the form of copper compounds or as free copper or, more likely, copper bound to particles suspended in the water. Even though copper binds strongly to suspended particles and sediments, it is possible to suggest that some water-soluble copper compounds do enter groundwater.

Soil sorption studies are commonly performed to evaluate the extent of solute retention by a soil or soil constituents. Different soils possess different capacity to adsorb metals. Sorption studies are often used in an attempt to generate the equilibrium distribution coefficient (K_d), the ratio of metal sorbed to soil in solution at equilibrium which may be utilized in transport models. Sorption studies are also used for the comparison of the relative retention of several metals by a soil or the relative retention of a metal by several soils and are used in correlation studies to determine the relative importance of a soil's chemical and physical properties for metal retention (McLean and Bledsoe, 1992). Sorption studies also can be used to evaluate the effect that changing a soil solution parameter, e.g., adjusting of pH has on metal retention by a soil. All soil minerals are capable of adsorbing Cu ions from solution and these properties depend on the surface charge carried by the adsorbents. The surface charge is strongly controlled by pH; therefore, the adsorption of Cu ion can be presented as a function of pH (Kabata-Pendias, 2000). Spathariotis and Kallianou (2001) reported that the percentage of copper, zinc and cadmium adsorbed as

a function of pH increased in sigmoidal form. The interactions of metals with humic acids extracted from marine sediments (Rashid, 1971) and soils (Kerndorff and Schnitzer, 1980) have been reported. Metal adsorption capacity changes with pH, concentration and type of metal. In order to express the adsorption behaviour of metals to soil particles, sorption isotherms which describe equilibrium sorption are commonly used. The most widely employed are those proposed by Langmuir and Freundlich. A sorption isotherm is the relationship between the amount of metal sorbed and the equilibrium concentration of the metal.

Kocide 101 is an inorganic copper-based fungicide whose active ingredient is cupric hydroxide (77%) and inert ingredient (23%). The chemical name of this fungicide is copper hydroxide (cupric hydroxide) with chemical formula of CuH_2O_2 *(Cu (OH)$_2$)* .The metallic copper equivalent of the fungicide is 50% and it is commonly used by farmers in Nigeria to control fungi infection on beans, carrot, coffee, tomatoes, pepper and potatoes etc. It is a blue powder, which is hardly soluble in water. It is compatible with most other pesticides.

The main objectives of the study were therefore to quantify the adsorption of copper by two soil series of contrasting features from Southwestern Nigeria and to examine the influence of solution pH on the adsorption of the metal to soil particles. Adsorption isotherms were measured and modeled to see the correlation between copper adsorption and the pH. Sorption coefficients were also determined for copper in the two soils as influenced by the solution pH.

2. MATERIALS AND METHODS

The two soil types used in this work were common agricultural soils in Ile – Ife, southwestern Nigeria. The soils were collected from surface 0 – 15cm on a 5 – 10 year natural bush fallow plots from two sites in the area. The total annual rainfall of the study area is about 1350 mm. The average daily minimum temperature ranged between 20^{O}C and 22^{O}C, and the average maximum temperature between 27^{O}C and 35^{O}C. The two soils are classified at series level as *Apomu* and *Egbeda* series (*Ojanuga*, 1975). The physico – chemical properties of the two soils are summarized in Table 1.

The adsorption experiment was carried out by means of a batch sorption test (Ozanne and Shaw, 1967; Gray *et al*., 1998) at room temperature (28 ± 1^OC). Copper (II) solutions were prepared in 0.01M $CaCl_2$ using cupric hydroxide (*Kocide 101*). Air-dried soil sample of about 1g was equilibrated with 10 ml solution containing the desired concentrations of the copper fungicide in a centrifuge. The effect of the initial concentration of the metal in the background solution of 0.01M $CaCl_2$ (varied between 3.25 g/l and 4.5 g/l) and the influence of the pH (3, 4, 5 and 6) were studied in order to determine their effects on the removal of copper ions from the solution. The pH values were measured with a pH meter. The pH was varied using 0.1mol.md^{-3} HCl or 0.1mol.dm^{-3} NaOH. During the experiments the amount of soil (1g) and the stirring speed of the centrifuge (400rpm) were kept constant. The tubes containing the soil and fungicide solution were shaken for 3 hours. After equilibration and centrifugation, the supernatant was removed and taken to the laboratory for analysis for copper using Atomic Absorption Spectrophotometer. Adsorption was estimated from the decrease in concentration of the metal in the fungicide in the liquid phase after equilibration according to the formulas:

$$C_S = \frac{C_O - C_W}{(W/V)} \quad (1)$$

Where C_s is the amount adsorbed ($\mu g/g$), C_O is the initial concentration $(\mu g/ml)$, C_w is the final concentration in the solution $(\mu g/ml)$, W is the weight of the soil (g) and V is the solution volume (ml)

3. ANALYSIS OF DATA

3.1. Sorption Isotherms of copper

The experimental data on equilibrium sorption of copper by the two soils in six different initial solution concentrations and four levels of pH were subjected to analysis by means of the three commonly used sorption isotherm models, namely the Linear (McLaren and Cameron, 1990), Langmuir and Freundlich models (Wu, 1989; Atanassova, 1995; Atanassova and Okazaki, 1997)

The Linear isotherm model is:

$$C_S = a + K_d C_W \quad (2)$$

The Langmuir isotherm model is:

$$\frac{C_W}{C_S} = \frac{1}{kb} + \frac{C_W}{b} \quad (3)$$

The Freundlich isotherm model is:

$$Log.C_S = LogK_d + \left(\frac{1}{n}\right) LogC_W \quad (4)$$

where *a* is a constant which corresponds to the intercept on the C_s versus C_w plot, b is the maximum sorption capacity of the soil and k is the coefficient related to bonding energy. K_d is the adsorption coefficient in cm^3/g. $\left(\frac{1}{n}\right)$ is a constant that depends on the pollutant (in this case the trace metal) and b the maximum adsorption.

3.2. Sorption Isotherm

4.1.1 Equilibrium concentration and Amount of Copper Adsorbed

The sorption affinity of copper varied substantially with the solution pH, initial copper concentration in the solution and the soil types. In a two component system (sorbent and solution) a graph of copper concentration in the solid phase Cu_{ads} (mg/g) plotted as a function of copper concentration in the liquid phase Cu_{eq} (mg/*l*) at equilibrium is shown in Figure 1. The correlation coefficients derived from the plots for the two soil samples are higher than 0.95 for Langmuir model and 0.85 for Freundlich model. The Langmuir model provides the parameters of the maximum adsorption (b) and a constant related to bonding-energy of the adsorbate to the adsorbent (K) while Freundlich equations provide rough measurement of the adsorption intensity (1/n) and adsorption capacity (K_f) of the adsorbent. Table 3 lists all the adsorption parameters of b, K (for Langmuir equation), a and K_d (for Linear equation); K_f, and 1/n (for Freundlich equation) and their correlation coefficients, r^2.

Table 1: Some selected Physico – Chemical Properties of the soils

Soil series	Organic matter content (%)	CEC (cmol/kg)	Particle size distribution			Textural classification	Taxonomy
			Sand (%)	Silt (%)	Clay (%)		
Apomu	1.16	6.75	82.5	7.0	10.5	Loamy sand	Alfisols
Egbeda	1.85	10.12	68.0	10.0	22.0	Sandy clay loam	Inceptisols

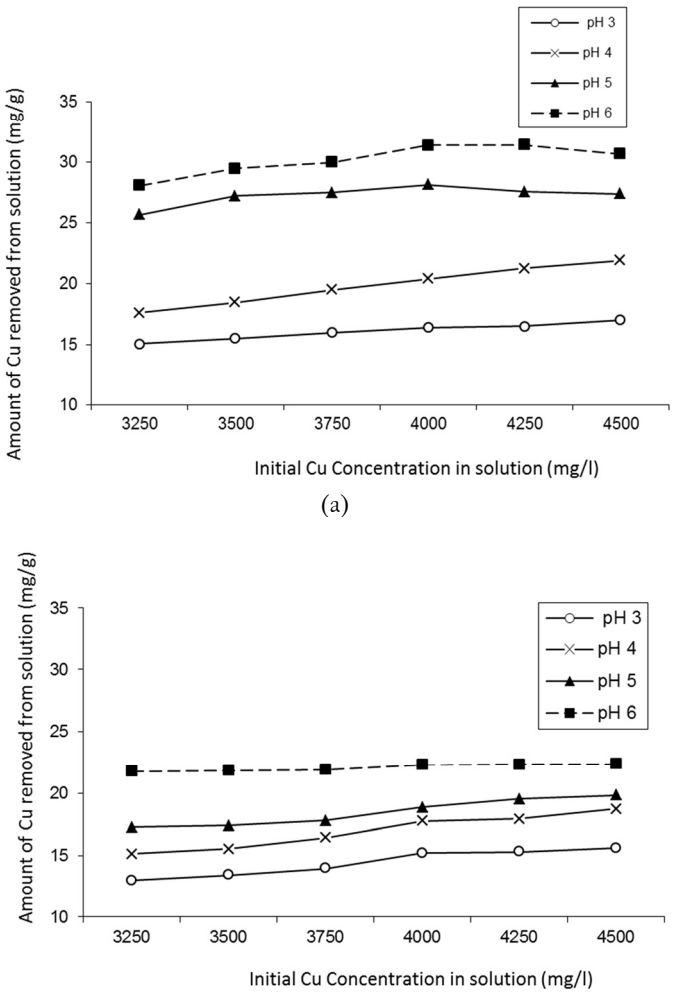

Figure 1: Effects of initial concentration on Cu removed from Kocide 101 solution per gram of soil (a) Egbeda soil and (b) Apomu soil as a function of solution pH

4. RESULTS AND DISCUSSION

The amount of copper adsorbed increased with the equilibrium copper concentration to a maximum value. This is typical of Langmuir type of Isotherms (Goldberg and Criscenti, 2008) and the results were in agreement with previous reports (Padmanabham, 1983; Wu, 1989; Atanassova, 1995; Wang et al., 1995; Atanassova and Okazaki, 1997; Yu et al., 2002). This is also evident from r^2 values (0.91 – 0.99) for the two soils at the four different solution pH considered (Table 3) for Langmuir Isotherm as against the r^2 ranges for the other two equations. Therefore, Langmuir equation is better for the adsorption properties of copper (II) ions to the two soil types considered in this study and thus should be used. The maximum adsorption of copper to the soil particles occurred at the pH of 6 for the two soil types. At this high pH, the ion is likely to be specifically adsorbed in the soil surface and may be bonded by covalent linkages.

4.1.2. Equilibrium concentration and initial copper concentration

The effect of initial copper concentration in the fungicide solution on the equilibrium concentration is shown in Table 2. For all the four pH considered in this work, the equilibrium copper concentration in the solution increases with the increase in the initial copper concentration in the solution for the two soils. The concentration of copper in the solution at equilibrium increases by 60.4 %, 55.4%, 156.9% and 224.9% for pH of 3, 4, 5 and 6, respectively, as the initial copper concentration increases from 3.25 g/l to 4.50 g/l for Egbeda soil. However the increases in the equilibrium copper concentrations reduced to 50.8%, 51.3%, 65.2%, and 110.7% for pH of 3, 4, 5 and 6, respectively, for Apomu series. This is because soils with high clay content and high organic matter content have a higher capacity to adsorbed chemicals (Riise and Salbu, 1992). Apomu series which contains a higher portion of sand shows lower sorption capacity for all the four pH considered.

Egbeda adsorbed more copper than Apomu series. At maximum initial concentration (4.5 g/l) of copper in the solution, 37.8 %, 48.6%, 60.9% and 68.2% of copper in the solution of Kocide 101 at the pH of 3, 4, 5 and 6, respectively, were adsorbed by Egbeda while 34.6%, 41.6%, 44.1% and 49.8% of copper were adsorbed by Apomu soil at the four different pH, respectively. However, the amount of copper adsorbed by Egbeda at solution pH 5 and 6 was not significant ($P < 0.05$). At these two solution pH, increasing the initial copper concentration in the solution did not affect the amount of copper adsorbed by the soil. Also for Apomu, the amount of copper adsorbed at solution pH of 6 was not significant ($P < 0.05$). However, the remaining three solution pH significantly affected the amount of copper adsorbed by this soil at the six initial concentration of copper in the solution. At solution pH of 6 (like for Egbeda soil), increasing the initial copper concentration in the solution did not affect the amount of copper adsorbed by the soil. This may be due to the fact that at this pH the adsorption capacity of the soil was low and additional input of the metal into the soil solution will not affect the amount of the metal adsorbed

The relationships between the amount of copper adsorbed and the initial copper concentration in the solution at the four solution pH are presented in Table 4. The regression between amount of copper adsorbed and initial copper concentration in the solution when done across all the four solution pH gave poor relationships for both Egbeda and Apomu soils (r^2 =0.03 and 0.09, respectively). However, the relationship within each solution pH was strong (except for the pH of 5) with r^2 values of 0.98, 0.99, 0.44, 0.71 for Egbeda soil and r^2 values of 0.94, 0.97, 0.95, and 0.89 for Apomu soil.

It is interesting to note that at lowest initial concentration (3.25 g/l) considered, it was observed that the amount of copper adsorbed by the two soils as a function of the initial copper concentration is higher than at the high initial copper concentration in the solution. At

Table 2: Equilibrium concentration of Cu as affected by solution pH and initial copper concentration

Soil series	pH	Initial Cu concentration in the fungicide solution (g/l)					
		3.25	3.5	3.75	4.0	4.25	4.5
Apomu	3	1.95 (0.01)[a]	2.16 (0.01)	2.35 (0.00)	2.40 (0.01)	2.72 (0.02)	2.94 (0.01)
	4	1.74 (0.01)	1.95 (0.01)	2.11(0.01)	2.22 (0.02)	2.46 (0.01)	2.63 (0.01)
	5	1.52 (0.01)	1.76 (0.01)	1.97 (0.01)	2.11 (0.01)	2.30 (0.01)	2.52 (0.01)
	6	1.07 (0.01)	1.32 (0.01)	1.56 (0.01)	1.77 (0.01)	2.02 (0.01)	2.26 (0.01)
Egbeda	3	1.75 (0.01)	1.95 (0.01)	2.15 (0.01)	2.36 (0.01)	2.60 (0.02)	2.80 (0.02)
	4	1.49 (0.02)	1.66 (0.01)	1.80 (0.01)	1.97 (0.02)	2.13 (0.02)	2.31 (0.01)
	5	0.69 (0.11)	0.78 (0.01)	1.00 (0.01)	1.19 (0.01)	1.49 (0.01)	1.76 (0.01)
	6	0.44 (0.01)	0.55 (0.01)	0.75 (0.01)	0.86 (0.02)	1.11 (0.01)	1.43 (0.01)

[a] *Standard deviation values are in bracket*

Table 3: Linear, Langmuir and Freundlich sorption isotherms constants based on batch equilibrium data of Copper in solution at the four solution pH

	Egbeda Solution pH				Apomu Solution pH			
	3	4	5	6	3	4	5	6
No of observations (Initial Conc.)	6	6	6	6	6	6	6	6
Linear isotherm constant								
a	12.05	9.69	25.99	28.00	7.49	7.65	12.44	21.11
K_d	0.0018	0.0054	0.0011	0.0025	0.0028	0.0042	0.003	0.0006
R^2	0.97	0.99	0.30	0.53	0.90	0.93	0.92	0.88
Langmuir isotherm constants								
K	0.0014	0.001	0.026	0.020	0.001	0.0004	0.0011	0.014
b (ml/mg)	21.37	40.16	28.33	32.26	27.62	37.17	27.25	23.09
R^2	0.99	0.99	0.99	0.99	0.93	0.91	0.97	0.99
Freundlich isotherm constants								
K_f	»100	2.09	17.33	17.12	2.76	3.44	1.72	16.59
1/n	5.67	0.49	0.06	0.08	0.47	0.52	0.31	0.04
R^2	0.68	0.99	0.55	0.71	0.89	0.93	0.87	0.74

Table 4: Relationships between adsorbed copper (mg/g) and initial copper concentration in the solution

Soil Type	Solution pH	Regression equation
Egbeda	3	$Cu_{ADS} = 0.0015Cu_{IC} + 10.213$ ($r^2 = 0.98^*$) n = 6
	4	$Cu_{ADS} = 0.0035Cu_{IC} + 6.308$ ($r^2 = 0.99^*$) n = 6
	5	$Cu_{ADS} = 0.0123Cu_{IC} + 22.609$ ($r^2 = 0.44^{NS}$) n = 6
	6	$Cu_{ADS} = 0.0023Cu_{IC} + 21.289$ ($r^2 = 0.71^{NS}$) n = 6
	Overall	$Cu_{ADS} = 0.002Cu_{IC} + 15.11$ ($r^2 = 0.03^{NS}$) ($n = 24$)
Apomu	3	$Cu_{ADS} = 0.0023Cu_{IC} + 5.662$ ($r^2 = 0.94^*$) n = 6
	4	$Cu_{ADS} = 0.003Cu_{IC} + 5.193$ ($r^2 = 0.97^*$) n = 6
	5	$Cu_{ADS} = 0.0023u_{IC} + 9.466$ ($r^2 = 0.95^*$) n = 6
	6	$Cu_{ADS} = 0.001Cu_{IC} + 19.909$ ($r^2 = 0.89^{NS}$) n = 6
	Overall	$Cu_{ADS} = 0.002Cu_{IC} + 10.06$ ($r^2 = 0.09^{NS}$) ($n = 24$)

Cu_{ADS}, *adsorbed Copper (mg/g);*
Cu_{IC}, *initial Copper concentration in the solution (mg/l);*
**significant at 5% probability level;*
NS not significant

the low initial copper concentration in the solution, 46.3 %, 54.2 %, 78.9 % and 86.4 % of the metal in the solution at the pH of 3, 4, 5, and 6, respectively, were adsorbed by Egbeda soil while 40 %, 46.6 %, 53.1 % and 70 % of the metal were adsorbed by Apomu soil at the four different pH at the low initial metal concentration in the solution. This is due to the fact that at low concentration, the metal added to the soil through the fungicide was below the adsorption capacity of the soils which is more dependent on the soil cation exchange capacity, Organic matter content and other physical and chemical properties of the soils. According to Mohamed et al. (1994), at low concentration, clay particles tend to disperse due to the full development of the diffuse double layer, therefore clay particle surfaces were in contact with solution at the maximum.

4.1. Effects of factors on copper adsorption

4.2.1 Effect of pH on the adsorption of copper

The interactive effect of soil types and pH on copper adsorption is shown in Figure 2. Each data is a mean of the six initial copper concentration considered. The pH of the solution was significant ($P < 0.05$) in its effects on the adsorption of copper to the two soils under consideration. The amount of copper adsorbed per unit mass of the soil on the average when the two soils were considered together increased from 15.24 mg/g when the solution pH was 3 to 26.13 mg/g when the pH was 6. The effect of pH was more pronounced in Egbeda soil than in Apomu soil. It is noteworthy here that relative higher copper was adsorbed by Egbeda soil as the solution pH changes from 3 to 4. This result was similar to what was reported by Schmuhl et al. (2001) that the most effective pH for Cu (II) removal was at pH range from 3 to 5. The increase in the amount of copper adsorbed by Apomu soil as the solution pH increases was relatively steady with the exception of solution pH of 6. However, relative higher copper was adsorbed by Apomu soil as the solution pH changes from 5 to 6.

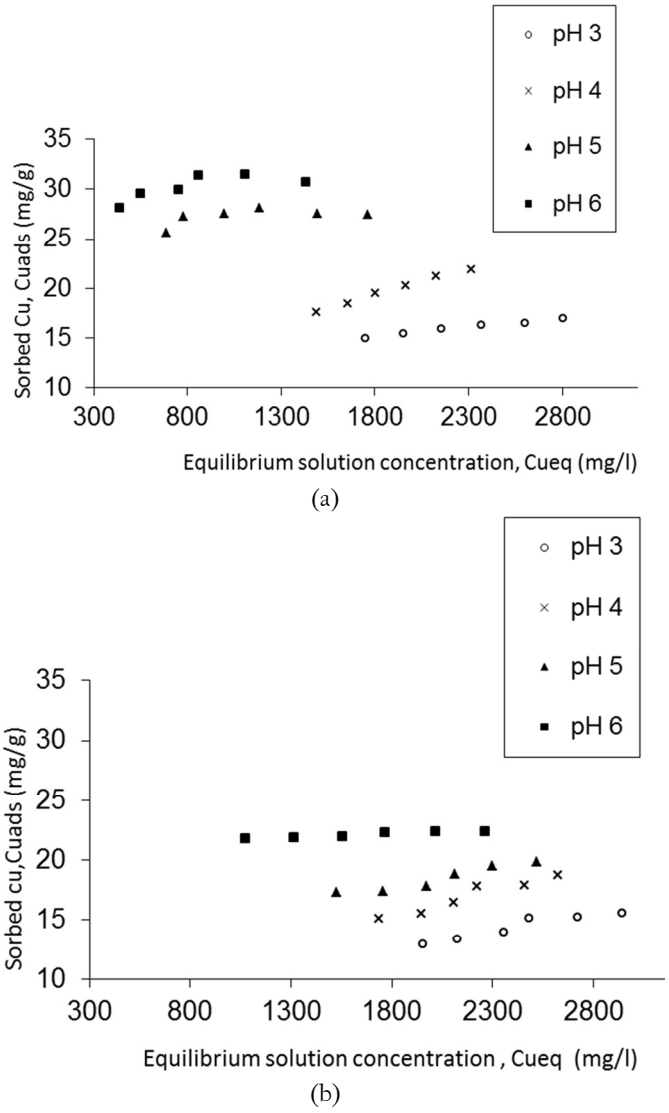

Figure 2: Isotherm for the adsorption of Copper ions from Kocide 101 solution onto soil at different pH(a) Egbeda soil and (b) Apomu soil

The relationships between the amount of copper adsorbed and the solution pH at the six different initial copper concentrations are presented in Table 5. The regression between amount of copper adsorbed and solution pH is stronger in Egbeda (r^2 =0.94) than in Apomu. (r^2 =0.87). Also, the relationship within each initial copper concentration in the solution was very strong with r^2 values not less than 0.94 for Egbeda soil and 0.95 for Apomu soil. The strong relationship observed when regression is done across all the six initial copper concentration considered in this work implies that the soil solution pH is one of the factors controlling the adsorption of copper to soil particles.

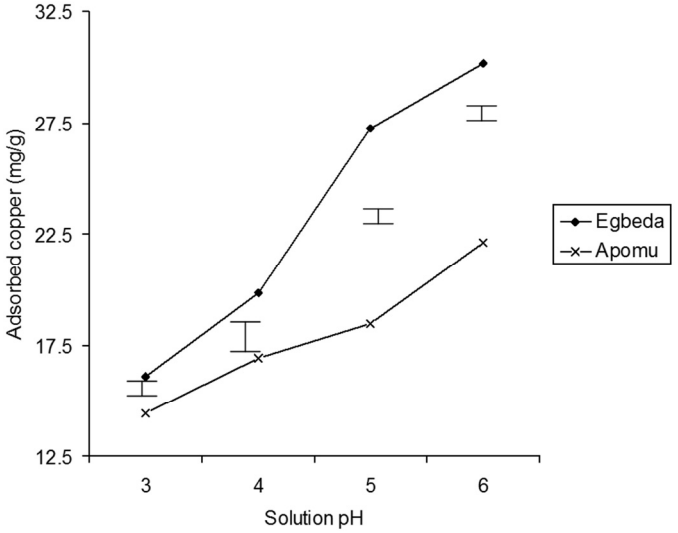

Figure 3 : Effect of solution pH and soil types on the amount of copper adsorbed (mg/g). The vertical bars represent Least Significant Difference (LSD) at 0.05.

Table 5: Relationships between adsorbed copper (mg/g) and solution pH

Soil Type	Initial conc. (mg/l)	Regression equation
Egbeda	3250	Cu_{ADS} = 4.715 pH + 0.385 (r^2 =0.95*) (n = 4)
	3500	Cu_{ADS} = 5.078 pH – 0.191 (r^2 =0.94*) (n = 4)
	3750	Cu_{ADS} = 4.995pH + 0.76 (r^2 =0.96*) (n = 4)
	4000	Cu_{ADS} = 5.287pH + 0.261 (r^2 =0.97*) (n = 4)
	4250	Cu_{ADS} = 5.101 pH + 1.233 (r^2 =0.95*) (n = 4)
	4500	Cu_{ADS} = 4.651 pH+3.308 (r^2 =0.99*) (n = 4)
	Overall	Cu_{ADS} = 4.9712pH + 0.959 (r^2 =0.94 **) (n =24)
Apomu	3250	Cu_{ADS} = 2.843 pH + 3.999 (r^2 =0.96 *) (n = 4)
	3500	Cu_{ADS} = 2.717 pH + 4.826 (r^2 =0.95*) (n = 4)
	3750	Cu_{ADS} = 2.525pH + 6.16 (r^2 =0.96*) (n = 4)
	4000	Cu_{ADS} = 2.244pH + 8.442 (r^2 =0.96*) (n = 4)
	4250	Cu_{ADS} = 2.273 pH + 8.539 (r^2 =0.99*) (n = 4)
	4500	Cu_{ADS} = 2.153 pH+ 9.444 (r^2 =0.97*) (n = 4)
	Overall	Cu_{ADS} = 2.4592pH + 6.902 (r^2 =0.87 **) (n =24)

Cu_{ADS}, *adsorbed Copper (mg/g); pH, solution pH;*
**significant at 5% probability level;*
***significant at 1% probability level.*

4.2.2. Effect of initial copper concentration on adsorption of copper

The initial copper concentration in the solution was also significant (P < 0.05) in its effects on the adsorption of copper to the two soils under consideration. Figure 4 shows the interactive effect of soil types and copper concentration on the adsorbed copper. The amount of Copper adsorbed was highest when the initial Copper concentration in the solution was 4.00 g/l (a mean of 21.69 mg/g) and lowest when the initial Copper concentration in the solution was 3.25 g/l (a mean of 19.20 mg/g). As the level of copper ion in the solution increases from 3.25 g/l to 4.50 g/l, the amount adsorbed also increases. At copper concentration of 4.00 g/l, monolayer capacity corresponding to complete surface coverage is likely to be reached and adsorption beyond this point is likely to be a surface precipitation or condensation of multi-layers. According to Duncan's multiple range tests, initial Copper concentrations of 3.25, 3.50 and 3.75 g/l were significantly different in their effect on the amount of Copper adsorbed at 5 % probability level. Initial Copper concentrations of 4.00 and 4.25 g/l were not significantly different as well as initial concentrations of 4.25 and 4.50 g/l (P< 0.05).

4.2.3. Effect of soil type on adsorption of copper

The influence of soil type on the amount of copper adsorbed to soil particles is shown in Figure 5. The two soil types were significantly different in their effect on the adsorption of Cu (p < 0.05). On the average, 17.97 mg/g of copper was adsorbed by Apomu series while 23.33 mg/g of the same metal was absorbed by Egbeda. This is expected because of the higher clay content and cation exchange capacity of Egbeda soil (Table 1).

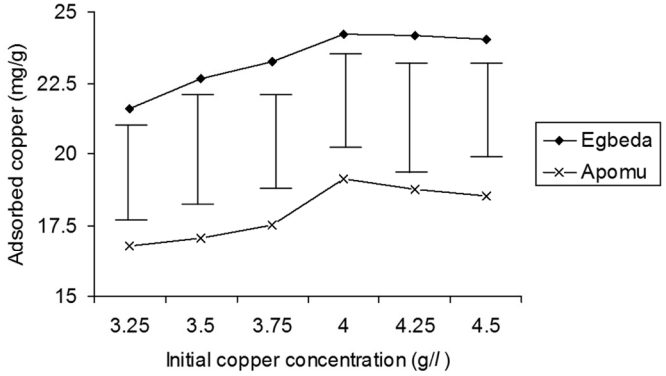

Figure 4 : Effect of soil types and initial copper concentration on the amount of copper adsorbed (mg/g) by the two soils. The vertical bars represent Least Significant Difference (LSD) at 0.05

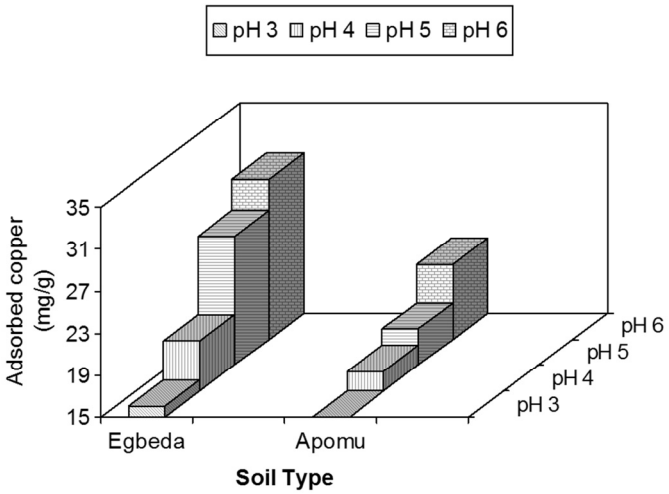

Figure 5 Effect of soil type on adsorbed copper

The regression equations between the equilibrium concentration and adsorbed copper for the different solution pH considered in this work based on Langmuir model (the model that best described the relationship) are presented in Table 6. The regression between amount of copper adsorbed and the concentration of Copper in equilibrium when done across all the solution pH gave a strong relationship (R^2= 0.91) with Egbeda soil and relatively strong relationship (R^2= 0.73) with Apomu. However, the relationship within

each solution pH was very strong and positive with R^2 value of 0.99 each for the four levels of solution pH for Egbeda soil and values 0.93, 0.91, 0.97 and 0.99 for solution pH 3, 4, 5 and 6, respectively, for Apomu. The strong relationship observed within the solution pH and when regression was done across all the four solution pH considered in this work implies that the equilibrium concentration of Copper in the solution is the major determining factor controlling the amount of Copper to be adsorbed to soil particles.

Table 6: Relationships between adsorbed Copper (mg/g) and equilibrium Copper concentration in the solution.

Soil Type	Solution pH	Regression equation
Egbeda	3	$Cu_{ADS} = Cu_{EQ}/(0.0468Cu_{EQ} + 34.304)$ $(r^2 = 0.99^{**})$ n = 6
	4	$Cu_{ADS} = Cu_{EQ}/(0.0249Cu_{EQ} + 47.894)$ $(r^2 = 0.99^{**})$ n = 6
	5	$Cu_{ADS} = Cu_{EQ}/(0.0353Cu_{EQ} + 1.379)$ $(r^2 = 0.99^{**})$ n = 6
	6	$Cu_{ADS} = Cu_{EQ}/(0.031Cu_{EQ} + 1.523)$ $(r^2 = 0.99^{**})$ n = 6
	Overall	$Cu_{ADS} = Cu_{EQ}/(0.067Cu_{EQ} - 26.72)$ $(r^2 = 0.91^{**})$ $(n = 24)$
Apomu	3	$Cu_{ADS} = Cu_{EQ}/(0.0362Cu_{EQ} + 80.121)$ $(r^2 = 0.93^{**})$ n = 6
	4	$Cu_{ADS} = Cu_{EQ}/(0.0269Cu_{EQ} + 69.707)$ $(r^2 = 0.91^{**})$ n = 6
	5	$Cu_{ADS} = Cu_{EQ}/(0.0367Cu_{EQ} + 34.987)$ $(r^2 = 0.97^{**})$ n = 6
	6	$Cu_{ADS} = Cu_{EQ}/(0.043Cu_{EQ} + 3.138)$ $(r^2 = 0.99^{**})$ n = 6
	Overall	$Cu_{ADS} = Cu_{EQ}/(0.070Cu_{EQ} - 24.69)$ $(r^2 = 0.73^{*})$ $(n = 24)$

Cu_{ADS}, adsorbed Copper (mg/g); Cu_{EQ}, concentration of Copper in equilibrium (mg/l);
** significant at 5% probability level;*
*** significant at 1% probability level.*

5. CONCLUSIONS

The equilibrium concentration of copper in soil solution increased with increase in the initial copper concentration and decreased with the solution pH. Sorption of copper to the two soil types considered in this work may be explained by all the three sorption isotherms tested with Langmuir equation fitting the data better than the other two isotherms. There appeared to be a strong correlation between sorption and equilibrium copper concentration in the solution ($r^2 > 0.90$). The adsorption process of copper to the two soils seems to be solution pH driven than the initial copper concentration in the solution. The effect of pH was more pronounced in Egbeda than in Apomu series. The most effective pH range for the removal of copper by the Apomu was between 4 and 5 while the range was between 3 and 4 for Egbeda soil. As the level of copper ion in the solution increases from 3.25 g/*l* to 4.50 g/*l*, the amount adsorbed also increases with maximum adsorption occurring at copper concentration of 4.00 g/*l*. A monolayer capacity corresponding to complete surface coverage is reached at copper ion concentration of 4.00g/*l*.

REFERENCES

Adriano, D.C. Trace Elements in Terrestrial Environments. New Yort: Springer-Verlug, 533p, 1986

Atanassova, I.D. Adsorption and desorption of Cu at high equilibrium concentrations by soil and clay samples from Bulgaria. Environ. Pollut. 87:17 – 21, 1995.

Atanassova, I.D. and Okazaki, M. Adsorption – desorption characteristics of high levels of copper in soil clay fractions. Water Air Soil Pollut. 98:213 – 228, 1997.

Baker, D.E. Copper. In: ALLOWAY, B.J.ed. Heavy metal in soils. Glasgow: Blackie Academic & Professional, pp 151 -176, 1993.

Gray, C.W.; McLaren, R.G.; Roberts, A.H.C. and Condron, I.M. Sorption and desorption of cadmium from some New Zealand soils: effect of pH and contact time. Australian Journal of Soil Research, *36, 199 – 216*, 1998.

Goldberg, S and Criscenti, L.J. Modeling Adsorption of Metals and Metalloids by soil components. In: Biophysico-Chemical Processes of Heavy Metals and Metalloids in Soil Environment. Edited by Antomio, V., Pan Ming, H and Geoffrey, M.G. John Wiley & Sons Inc., 215 – 263, 2008.

Goldberg, S.; Lessch, S.M. and Suarez, D.L. Predicting Trace Element Adsorption by soil using Soil Chemical Parameters. In: Proceedings of the International Salinity Forum, Managing Saline Soils and Water: Science, Technology, and Soil Issues. April 25-27, 2005. Riverside, CA pp. 197 – 200, 2005.

Kabata-Pendias, A. Trace Elements in Soils and Plants. CRC Press London, 106 -291, 2000.

Kerndorff, H. and Schnitzer, M. Sorption of metals on humic acid. Geoch. Et Cosm. Acta, vol. 44, 1701 – 1708, 1980.

Krumholz, L.R.; Elias, D.A. and Safita, J.M. Immobilization of cobalt by sulfite-reducing bacteria in subsurface sediments. Geomicrobiol J., 20:61 – 72, 2003.

McLaren, R.G. and Cameron, K.C. Soil Science, an introduction to the properties and management of New Zealand soils, 1990.

McLean, J.E and Bledsoe, B.E. Behaviour of Metals in Soils. Ground Water Issue. US EPA. EPA/540/S – 92/018, 1992.

Mohamed, A.M.O.; Young, R.N.; Tan, B.K.; Farkas, A. and Curtis, L.W. Geoenvironmental assessment of a micaceous soil for its potential use as an engineered clay barrier. Geotechnical Testing Journal, ASTM, 17 (3): 291 – 304, 1994.

Ojanuga, A.G. Morphology, Physical and Chemical Characteristics of Ife and Ondo areas. Nigerian Journal of Soil Sci., 9, 225 – 269, 1975.

Padmanabham, M. Adsorption – Desorption behaviour of copper (II) at the goethite – solution interface. Aust. Journal Soil Res. 21:309 – 320, 1983.

Raghupathi, H.B. and Vasuki, N. Copper adsorption of some soils of North Karnataka. Jour. Ind. Soc. Soil Sci., v.41, pp 70 – 74, 1993.

Rashid, M.A. Role of humic acids of marine origin and their different weight fractions in complexing di- and tr-valent metals. Soil Sci., vol. 111, 298 – 306, 1971.

Riise, G. and Salbu, B. Mobility of dichlorprop in the soil water system as a function of different environmental factors I. A batch experiment. The science of the Total Environment. 123/124, 399 – 409, 1992.

Sarkar, B. Heavy metals in the Environment. New York: Marcel Dekker., 344p, 2002.

Schmuhl, R.,; Krieg, H.M. and Keizer, K. Adsorption of Cu (II) and Cr (VI) ions by chitosan: Kinetics and equilibrium studies. Water SA, 27 (1), 1 – 8, 2001.

Singh, S.P.; Ma, L.Q. and Harris, W.G. Heavy metal interactions with phosphatic clay: sorption and desorption behaviour. Journal of Environ. Qual 30:1961 – 1968, 2001.

Spathariotis, E. and Kallianou, C. Adsorption of copper, zinc, and cadmium on clay fraction of two acid soils: Surface complexation modeling. Commun. Soil Sci., plant Analysis 32 (19 & 20), 3185 – 3205, 2001.

Sposito, G. The chemistry of soils. New York: Oxford University Press. 69pp, 1989.

Ozanne,P.G. and Shaw , T.C. Phosphate sorption by soil as a measure of phosphate requirement for pasture. Australian Journal of Agricultural Research, 18, 601 – 612, 1967.

Wang, W.; Shao, Z. and He, Q. Study on adsorption affinities of Co, Cu, Pb and Zn for different red soil clays. Acta Pedologica Sinica, 32: 167 – 178, 1995.

Wu, M. Study on the specific adsorption of copper ion by soils and its characteristics. Acta Pedologica Sinica, 26: 31 – 41, 1989.

Yu, S.; He, Z.L.; Huang, C.Y.; Chen, G.C. and Calvert, D.V. Adsorption – Desorption Behavior of Copper at contaminated levels in red soils from China. Journ. Of Environmental Quality 31:1129 – 1136, 2002.

Full Paper

APPLICATION OF ROOFTOP FUNCTIONS IN THE ANALYSIS OF ANTENNA SYSTEMS

E. Obayiuwana
Department of Electrical and Electronic Engineering, Obafemi Awolowo University, Ile-Ife, Nigeria
obayiuwanaenoruwa@oauife.edu.ng

S.A. Adeniran
Department of Electrical and Electronic Engineering, Obafemi Awolowo University, Ile-Ife, Nigeria

ABSTRACT

In this paper, we report the analyses of a single element antenna and array antenna using rooftop function as a basis and testing functions to model the current distribution on the antennas. The Method of Moments (MoM) was used to obtain matrix equation from the Electric Field Integral Equation (EFIE) from which the solution to the current distribution was obtained and validate using the Numerical Electromagnetic Code (NEC) software. The input impedance for dipole antenna was obtained and compared against measured results and other electromagnetic computational technique for a dipole antenna. A minimum convergence error percent of 0.03% was observed at the use of 30 rooftop functions. The single element wire antenna input impedance obtained produced better result and converged faster than the use of pulse testing technique. The antenna array characteristics simulated using the results obtained from a single dipole element, achieved the end-fire, broad-side and electronic beam steering (scanning) characteristics of linear array antenna.

Keywords: *Method of Moment, Rooftop Function, Antenna Systems Analysis, Computational Electromagnetics.*

1. INTRODUCTION

The earliest known rigorous approach to the analysis of wire antenna was by Pocklington in 1897. The integral equation he formulated was named after him. This Integral equation is an integro-differential type of the Electric Field Integral Equation (EFIE), with unknown current distribution along the cylindrical wire. It could not be solved numerically, such that for a long time its value was purely academic.

A different integral equation for modelling thin wire structures was put forward in 1938 (Hallen, 1938).This was derived from EFIE for thin cylindrical wires. Nomura and Hatta (1952) and Storm (1953) proposed the method of moment for the analysis of cylindrical antenna by means of the Hallen's Equation, the solution was very restricted, because the classical computational means available then were not suitable for numerical solution of integral equations. The Pocklington analysis is difficult to implement but gives a more accurate result compared to Hallen analysis for wire antenna.

The first numerical solution of wire–structure antenna was due to (Richmond, 1965). He applied the sub-domain rectangular basis function and entire–domain basis function to solve the Pocklington equation for cylindrical wire structures using the point matching procedure. Harrington, in his classical work in 1967, introduced the method of moment (MoM) for solving electromagnetic–field problems in general and the thin wire–antenna problem in particular. In tackling the wire antenna problems, he used both the point matching and Galerkin procedures for the first time to obtain its solutions (Harrington, 1967). Many of the works which followed thereafter were based on the MoM.

Most antenna problems are usually modelled using EFIE, which are derived from the Maxwell Equations (Wandzura et al., 1992). Various numerical /computer algorithms have been developed to solve the EFIE for various practical antennas. The most accurate algorithm for solving the EFIE is the MoM but this is usually complex and difficult to implement. The computational accuracy of results obtained, using Method of Moment are largely affected by the choice of basis functions in the modelling of the current distribution on the antenna system (Kolundzija *et al*., 1998), (Canning, 1993).

Therefore, it is important to look for an optimum basis function that will produce a fast converging result, easy to implement and that will give accurate results. The Numerical Electromagnetic Code (NEC) is the most powerful commercial code and was introduced by (Burke and Paggio, 1981). In this work, rooftop function is used as the basis function and testing function to model the unknown current distribution on the antenna. The result obtained is compared with the results obtained using NEC. The modelled current distribution on the antenna is then used to determine the input impedance, radiation pattern of single element wire antenna and to predict the beam scanning characteristics of the phase array. The input impedance results for single element are compared against experimental measurements and results obtained using other electromagnetic computational techniques

2. THE ELECTRIC FIELD INTEGRAL EQUATION

An antenna carrying current density $\vec{J}(\vec{r})$ has a radiated electric field given as

$$\nabla^2 \vec{E}(\vec{r}) + k^2 \vec{E}(\vec{r}) = j\omega\mu \vec{J}(\vec{r}') - \frac{1}{j\omega\varepsilon}\nabla\left(\nabla \bullet \vec{J}(\vec{r}')\right) \quad (1)$$

where $\vec{E}(\vec{r})$ is the radiated E-field, k is the wave number and $\vec{J}(\vec{r}')$ is the source current density. Maxwell's equations are linear, hence we consider $\vec{J}(\vec{r}')$ as a superposition of point sources distributed over some volume. Therefore, if we know the response of a point source or the Green's function of a point source we can solve the original problem by integrating this response over the volume. This idea is made use of to convert (1) into an Electric field integral equation

$$\vec{E}(\vec{r}) = -j\omega\mu \iiint_{V'} G(\vec{r},\vec{r}') \left(\vec{J}(\vec{r}') + \frac{1}{k^2} \nabla' \nabla' \bullet \vec{J}(\vec{r}') \right) dV' \quad (2)$$

where $G(\vec{r},\vec{r}')$ is the Green's function, $\vec{r}$ is the field observation point , $\vec{r}'$ is current source point and

$$G(\vec{r},\vec{r}') = \frac{e^{-jk\left|\vec{r}-\vec{r}'\right|}}{4\pi\left|\vec{r}-\vec{r}'\right|} \quad (3)$$

However, in many cases of practical interest, it may be difficult or impossible to directly solve this equation for the fields. A remedy, an auxiliary vector potential that can be used to solve for the radiated fields needs to be derived. The vector potential is obtained via integral equation of the currents, and the radiated fields are obtained directly from the vector potential. Vector potential formulation is used extensively in the analysis of antenna radiation and scattering problems, and used frequently in this work. The radiated E-field in terms of auxiliary vector potential $\vec{A}(\vec{r})$ is given by

$$\vec{E}(\vec{r}) = -j\omega\vec{A}(\vec{r}) - \frac{j}{\omega\mu\varepsilon}\nabla(\nabla \bullet \vec{A}(\vec{r})) \quad (4)$$

where

$$\vec{A}(\vec{r}) = \mu \iiint_{V'} \vec{J}(\vec{r}') \frac{e^{-jk\left|\vec{r}-\vec{r}'\right|}}{4\pi\left|\vec{r}-\vec{r}'\right|} dV' \quad . \quad (5)$$

2.1. Far Fields

When the observation point is located very far away from the source, $kr >> 1$, approximations can be made that greatly simplify the computation of the radiated field. In this case $\left|\vec{r}\right|$ and $\left|\vec{r}-\vec{r}'\right|$ are virtually parallel. Under this assumption, r can reasonably be approximated as,

$$r = \begin{cases} r, & \text{for amplitude variations} \\ r - \vec{r}' \bullet \hat{r}, & \text{for phase variations} \end{cases} \quad (6)$$

It has been shown that the far-field component becomes a proportional to $\frac{1}{r}$ (Morita *et al*, 1990). The far electric field will therefore be computed as

$$\vec{E}(\vec{r}) = -j\omega\vec{A}(\vec{r}) \quad (7)$$

$$= -\frac{j\omega\mu}{4\pi r} \iiint_{V'} \vec{J}(\vec{r}') e^{-jk(r-\vec{r}' \bullet \hat{r})} dV' \quad (8a)$$

$$= -\frac{j\omega\mu e^{-jkr}}{4\pi r} \iiint_{V'} \vec{J}(\vec{r}') e^{jk\vec{r}' \bullet \hat{r}} dV' \quad (8b)$$

3. MODELLING TECHNIQUE

For most problems of practical interest, the derived Integral Equation cannot be solved analytically, hence the application of computational methods to obtain the solution. The MoM is a technique used to convert the integral equation into a linear system that can be solved numerically using a digital computer.

The Rooftop function is used as the basis function to model the expected behaviour of the unknown current throughout the problem domain. A rooftop function is defined as

$$f_n(x) = \begin{cases} \dfrac{x - x_{n-1}}{x_n - x_{n-1}}, & x_{n-1} \le x \le x_n \\ \dfrac{x_{n+1} - x}{x_{n+1} - x_n}. & x_n \le x \le x_{n+1} \end{cases} \quad (9)$$

An inner product or moment between a basis function $f_n(\vec{r}')$ and a testing function $f_m(\vec{r})$ is defined as

$$\langle f_m, f_n \rangle = \int_{f_m} f_m(\vec{r}) \bullet \int_{f_n} f_n(\vec{r}') d\vec{r}' \, d\vec{r} \quad (10)$$

Requiring the inner product of each testing function with the residual function to be zero yields,

$$\sum_{n=1}^{N} a_n < f_m, L(f_n) > = < f_m, g > \quad (11)$$

which produces a $N \times N$ matrix equation given by

$$[Z_{mn}][a_n] = [b_m], \quad (12)$$

with matrix elements

$$z_{mn} = \langle f_m, L(f_n) \rangle \quad (13)$$

and right-hand side vector elements

$$b_m = \langle f_m, g \rangle . \quad (14)$$

where $L(\bullet)$, g operator and forcing are function, respectively.

In the MoM, each Rooftop function interacts with all others by means of the Green's function

3.1. Thin Wire Approximation

Consider the dipole antenna shown in Figure 1 to be a perfectly conducting thin wire with the length , $L = 1$ m and radius, $a = 5$ mm operating at a wavelength of 1m and (i:e $a << \lambda$ and $L >> a$), oriented in $\hat{z}$ -direction. An incident electric field $\vec{E}^i(\vec{r})$ excites on this wire a surface current $\vec{J}(\vec{r}')$ .Since the wire is very thin, and assuming that $\vec{J}(\vec{r}')$ can be written in terms of a $\hat{z}$ -oriented filamentary current $I_z(\vec{r}')$ as

$$\vec{J}(\vec{r}') = \frac{I_z(z')}{2\pi a}\hat{z} \quad . \tag{15}$$

In cylindrical coordinates, the corresponding magnetic vector potential A_z in terms of the surface integral is written as

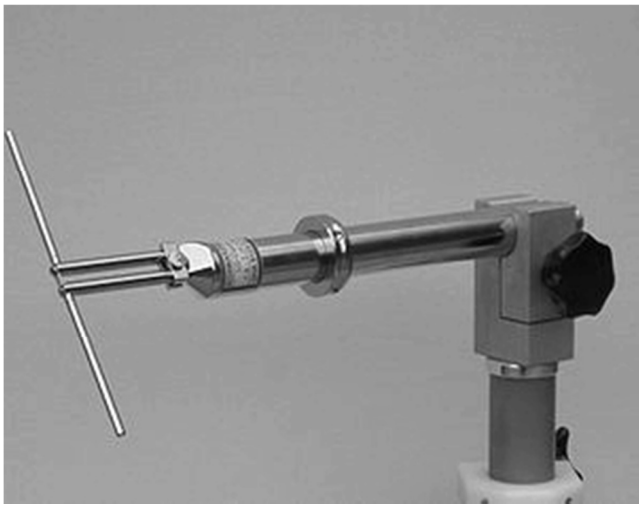

Figure 1: Single Dipole Antenna

$$A_z(\rho,\phi,z) = \mu \int_{\frac{-L}{2}}^{\frac{L}{2}} \int_{0}^{2\pi} \frac{I_z(z')}{2\pi} \frac{e^{-jkr}}{4\pi r} d\phi' dz' \tag{17}$$

noting that $\rho' = a,$ and that the source point is at the surface of the thin wire conductor, where a is the radius of the conductor. Therefore,

$$r = \sqrt{(z-z')^2 + \rho^2 + a^2 - 2a\rho\cos(\phi'-\phi)} \; . \tag{17a}$$

If a is assumed to be very small, r can be approximated as

$$r = \sqrt{(z-z')^2 + \rho^2} \tag{17b}$$

hence,

$$A_z(\rho,z) = \mu \int_{\frac{-L}{2}}^{\frac{L}{2}} I_z(z') \frac{e^{-jkr}}{4\pi r} dz' \quad . \tag{18}$$

The radiated field obtained from(4) is

$$E_z^s = -j\omega A_z - \frac{j}{\omega\mu\varepsilon}\frac{\partial^2}{\partial z^2} A_z \, , \tag{19}$$

by enforcing the boundary condition of zero tangential electric field on the surface of the wire,

$$E_z^s = -E_z^i \quad . \tag{20}$$

The thin wire EFIE in terms of the incident field E_z^i is

$$E_z^i(z) = \frac{j}{\omega\varepsilon} \int_{-L/2}^{L/2} I_z(z') \left[\frac{\partial^2}{\partial z^2} + k^2 \right] \frac{e^{-jkr}}{4\pi r} dz' \tag{21}$$

Equation (21) is called Pocklington's integral equation (Sadiku, 2001).

3.2. Source Excitation Modelling

The excitation source for the dipole antenna is modelled by a delta-gap source. The delta-gap source treats the feed as if the electric field impressed by the feed line exists only in the gap between the antenna terminals and is zero outside, that is, no fringing in the region of the feed, the current is of course displacement current, rather than conduction current; it is effectively the former which the MoM is approximating in the feed region, but it still needs a segment (even though it is fictitious) and its associated expansion function in order to do this (Davidson, 2005). The delta-gap source model assumes that the impressed electric field in the thin gap between the antenna terminals can be expressed as

$$\vec{E}_z^{\,i} = \frac{V_o}{\Delta_z}\hat{z}, \tag{22}$$

where Δ_z is the width of the gap, and V_o is usually set to unity. In the numerical simulation, this field exists inside one wire segment and is zero outside (Gibson, 2008). The resulting excitation vector will have nonzero elements only for basis functions defined within that segment.

3.2. Linear Array antenna

A single element antenna is usually not enough to achieve some required technical specifications. That happens because its performances are limited. Usually the radiation pattern of a single element is relatively wide, and each provides low values of directivity (gain). When an antenna array has elements arranged in a straight line, it is referred to as a linear array. A uniform array consists of equi-spaced elements, which are fed with current of equal magnitude and can have progressive phase-shift along the array. Figure 2 shows a uniform linear array of N elements equally spaced at distance d apart with identical amplitude excitation and has a progressive phase difference of β between the successive elements.

The radiated electric field of the linear array equals the product of the radiated electric field of single element antenna at the reference point and the array factor. The array factor (*AF*) is given by

$$AF = \sum_{n=1}^{N} e^{j(n-1)(kd\cos\theta+\beta)}, \tag{23}$$

where k the wave number, *d* is the element spacing, β is the phase shift and θ is the angle of radiation.

The linear array antenna is analysed using the radiated field from a single dipole antenna that serves as the reference element with the linear array factor (AF).

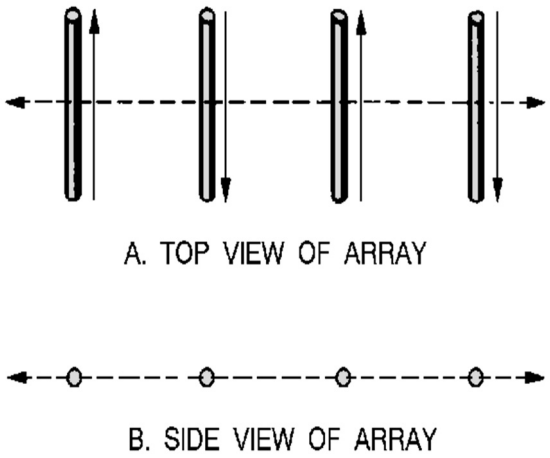

Figure 2: Linear Array (witn N-elements)

4. Results and Discussions

From equation (21), numerical computations for the input impedance matrix, which are generally complex Toeplitz Matrix, from which the current distribution, input impedance, and far field

radiation pattern are gotten for a radiating dipole antenna of signal frequency 300MHz, radiating in a free-space, are computed using 36, 48 and 60 unknown basis rooftop functions. The current distribution results obtained for wire dipole analysis are shown in figure 3. The current distribution plots showed that the magnitude of current values at both ends of the dipole antenna decays to zero. This result supports the electromagnetics boundary conditions that exist between the antenna and dielectric air medium. The current distribution obtained showed that the position of current anti-node is located at the mid-section of the dipole antenna, which is practically the feed or excitation point. This distribution showed that current nodes exit at the tips or ends of the dipole antenna of length $\lambda/2$ with the current Anti-node at its mid-section. Figure 4 shows that the current distribution result obtained compares well with that obtained using the NEC.

The Figure 5 and 6 compared the input impedance obtained in this work to that of experimental measurement of $72.0 + j0$ Ohms at resonance. The input impedance converges to the experimental value. The input impedance value for the dipole antenna improves as the number of roof top basis functions increases and the input impedance value converged approximately to $72.2 + j1.3$ Ohms. The computed convergence percentage error is 0.4% .

It is observed in this work that the real part of the input impedance converges better than the reactive part to the experimental value.

Figure 7 and 8 compared the input resistance and input reactance obtained in this work to that of reported by Eric D. Caswell against the number of basis function used. Figures 7 and 8 showed that the input impedance obtained from this work converges faster than that obtained using sinusoidal basis functions and testing functions. The input impedance convergence result of $77+j5$ ohms was reported by Eric D. Caswell (Caswell, 1998), using sinusoidal basis functions and testing functions. A perfect resonant single dipole antenna has an input Impedance of experimental measurement value of $72.0 + j0$ Ohms. This work shows improved results using rooftop basis functions and testing functions as compared to the use of sinusoidal basis functions and pulse testing functions. Figure 9 showed the input resistance percent error convergence result. The result showed a minimum convergence error of approximately 0.03% , at the use of 30 rooftop functions. The percent error convergence P_e is computed using the formula

$$P_e = \frac{O_V - T_V}{T_V} \times 100\ \% \qquad (24)$$

where O_v is the obtained value and T_v is the true value.

The far–field result obtained for a single element dipole antenna of length 0.5λ is presented in figure 10. The radiation pattern results for eight-element (N=8)\linear arrays are presented in figures 11 and 12. Figures 11 and 12 show the results obtained for End-fire and Broadside configurations using eight single element dipole antennas, with inter-element spacing (d) and phase shift (β) of 0.25λ , -90° , 0.5λ and 0° , respectively. The results for phase/ (scanning) array through arbitrary desired angle of radiation (θ_0) of 80° , 60° and 50° are presented in Figure 13, 14 and 15 respectively.

5. Conclusions

The EFIE equation for the analysis of wire antenna was implemented using MATLAB codes. The current distributions along the dipole antenna using rooftop functions compared well with NEC.

The input impedance for dipole wire antenna obtained using rooftop functions as basis and test functions are more accurate and converged faster than the results obtained using sinusoidal basis functions and testing functions. The input impedance value for the dipole antenna improves as the number of roof top basis functions increases and the input impedance value converged approximately to $72.2 + j1.3$ Ohms. The computed convergence percentage error is 0.4% .

Far–Electric field (E-field) agrees with the E-field radiation pattern of a practical dipole antenna. The result obtained from single element dipole antenna, when applied to linear array dipole antenna, produced good results.

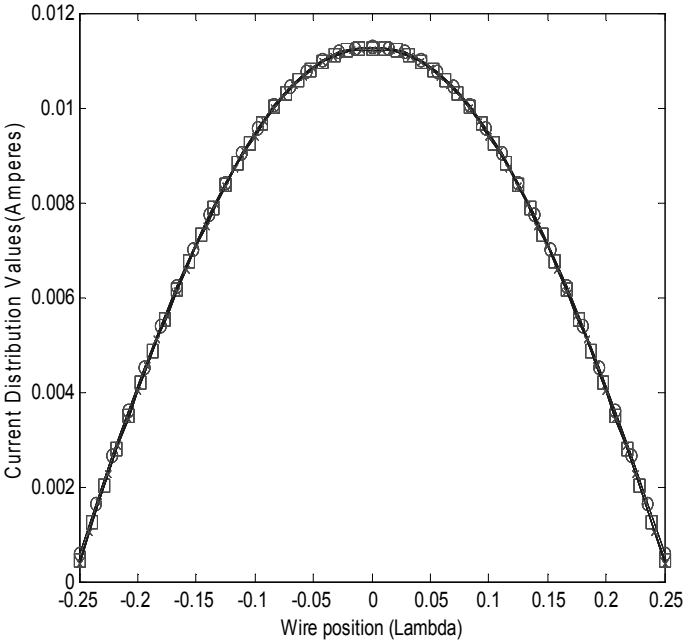

Figure 3: Current distributions over wire length of 0.5 λ , using 36(0), 48([]) and 60(X) rooftop basis Functions

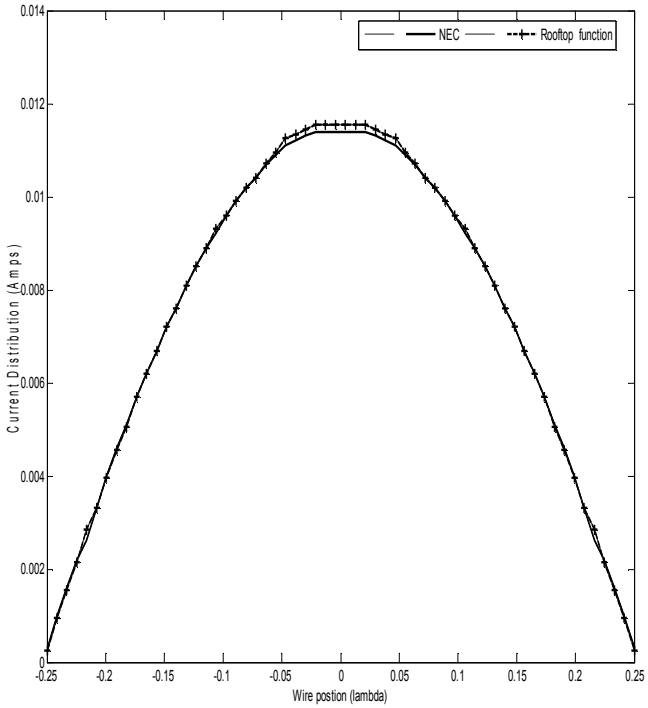

Figure 4: Comparison of results from rooftop function and NEC for Current distribution for dipole wire antenna operating at 300MHz

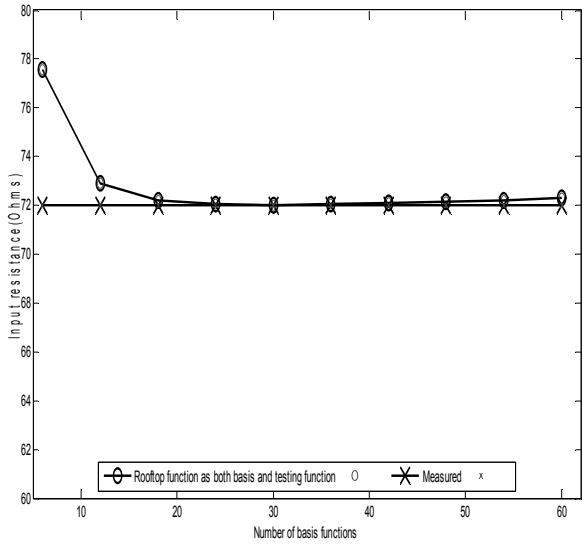

Figure 5: Comparison of results from rooftop function and experimental results for an input resistance of a dipole antenna at resonance

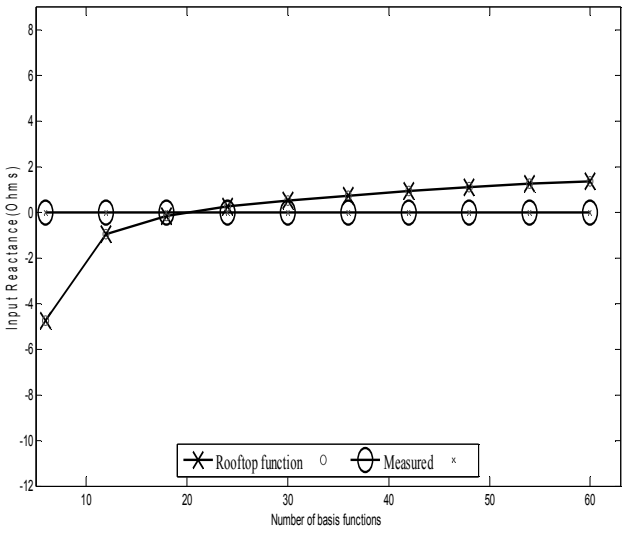

Figure 6: Comparison of results from rooftop function and experimental results for an input reactance of a dipole antenna at resonance

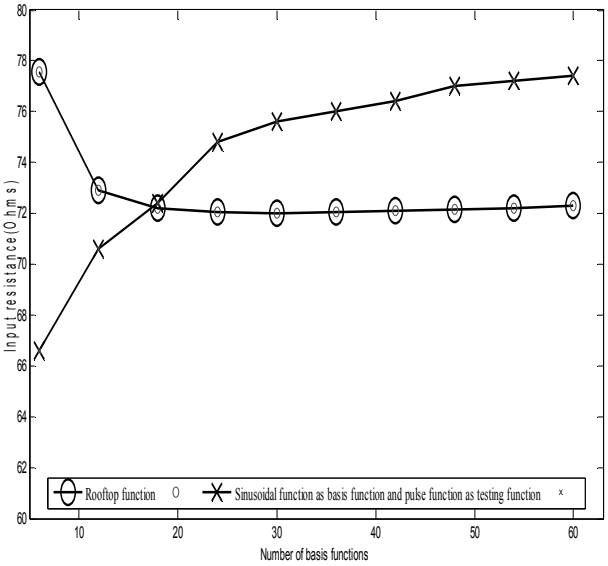

Figure 7: Comparison of results from rooftop function and sinusoidal function analysis for input resistance of a dipole antenna at 300Hz.

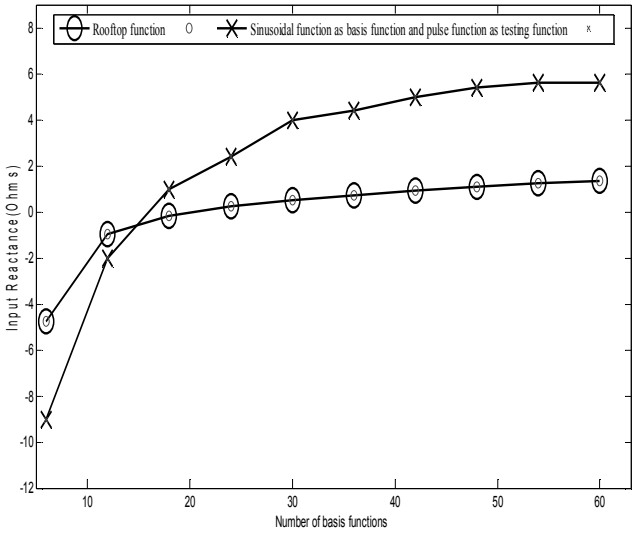

Figure8: Comparison of results from rooftop function and sinusoidal function analysis for input reactance of a dipole antenna at 300Hz.

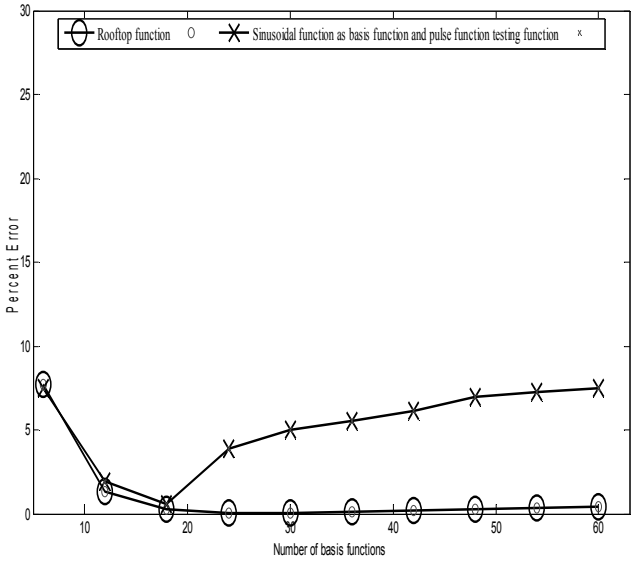

Figure 9: Comparison of input resistance percent error results for rooftop function and sinusoidal function for a dipole antenna at 300MHz

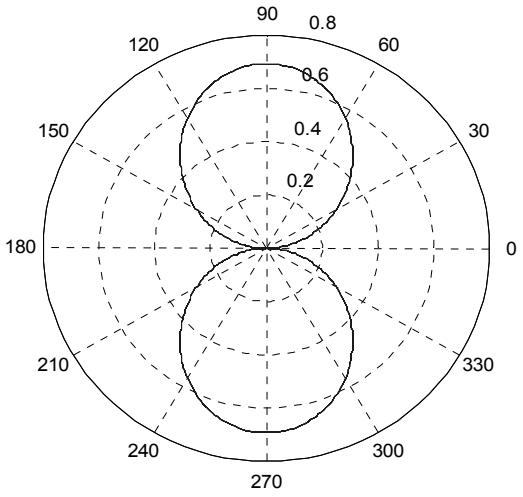

Figure 10: Far-Field radiation Pattern for single dipole wire antenna of length 0.5 λ, using 60 rooftop basis functions

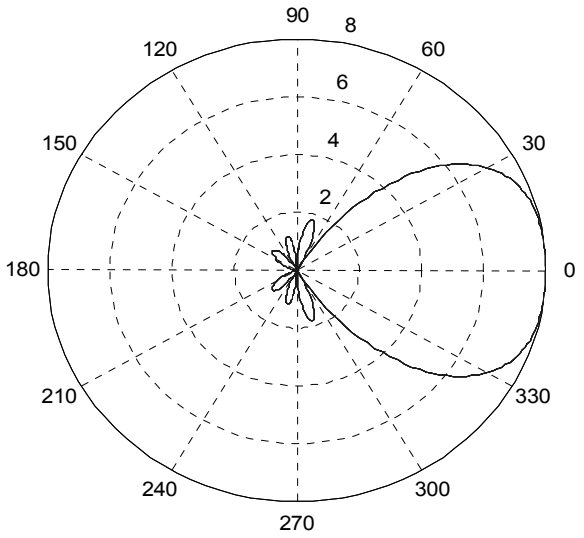

Figure 11: Radiation pattern for End-fire linear array with $N = 8, d = 0.25\lambda, b = -90^0$

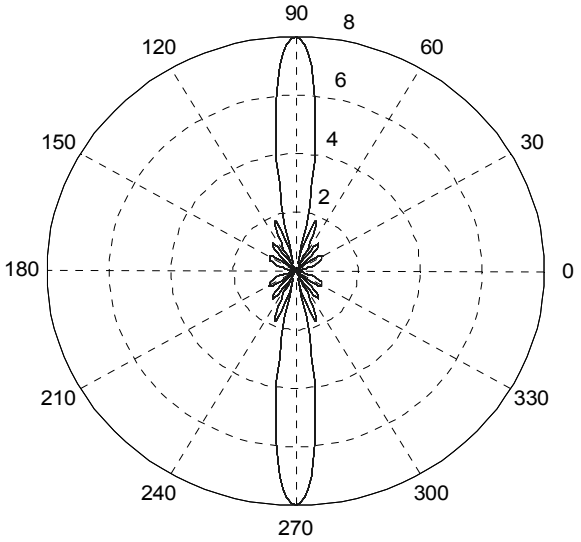

Figure 12: Radiation Pattern for Broadside linear array with $N = 8, d = 0.5\lambda, b = 0^0$

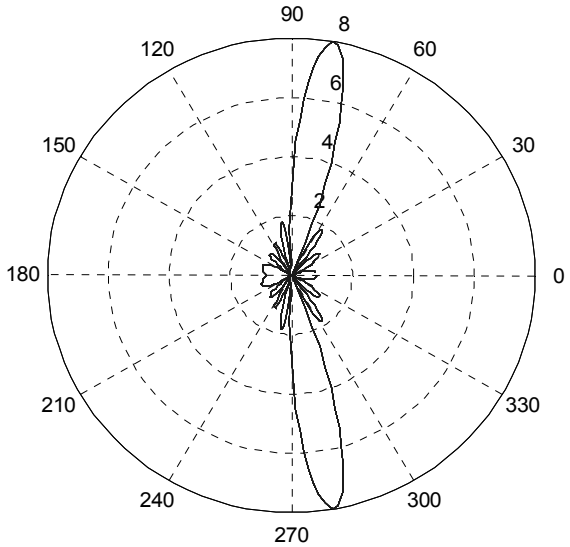

Figure 13: Polar plot result for Phase array with N=8, $d = 0.5\lambda$ *and* $\theta_o = 80^o$

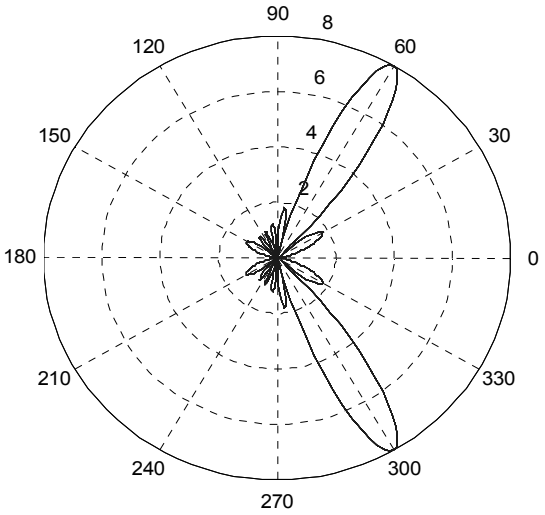

Figure 14: Polar plot result for Phase array with N=8, d=0.5 λ *and* $\theta_o = 60^o$

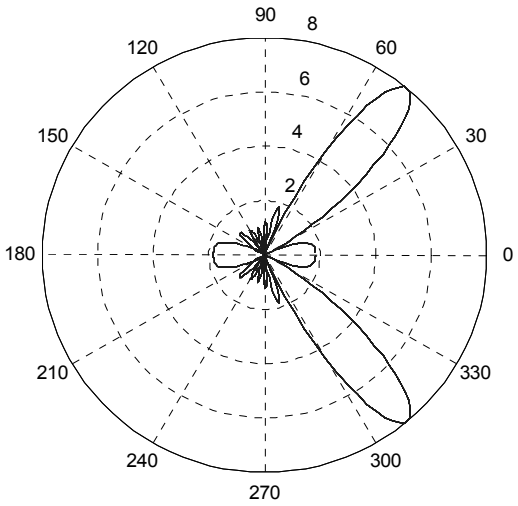

Figure 15: Polar plot result for Phase array with N=8, $d = 0.5\lambda$ *and* $\theta_o = 50^0$

REFERENCES

Canning, F. X., Improved impedance matrix localization method [EM problems], IEEE Trans. Antenna Propagation, 1993, 41, pp 659–667.

Caswell, E.D., Analysis of a Helix Antenna Using a Moment Method Approach with Curve Basis and Testing Functions, Virginia Polytechnic Institute and State University, U.S.A.

David, B. D., *Computational Electromagnetic and Microwave Engineering* (Department of Electrical and Electronic, University of Stellencosch, South Africa, 2005)

G. Burke and A. Poggio, Numerical Electromagnetics Code (NEC)-Method of Moments, Part 2: Program Description—Code, 1981

Gibson C. Walton, *Method of Moments in Electromagnetics* (Chapman & Hall/CRC Taylor & Francis Group New York, 2008)

Hallen, E. (1938) "Theoretical investigations into the transmitting and receiving qualities of antennae," Nova Acta (Uppsala), vol. 11, 1–44, 1938.

Harrington, R. F., *Field Computation by Moment Methods* (Macmillan, New York, 1968)

Kolundzija, B.M. and Sarkar, T.K.,On the choice of optimal basis functions for MoM/SIE, MoM/VIE, FEM and hybrid methods, *IEEE Trans. Antenna Propagation*,1998, 278 - 281 vol.1

Morita, N., Kumagai, N. and Mautz, J.R, *Integral Equation Methods for Electromagnetics* (Artech House, Boston, 1990)

Nomura, Y. and Hatta, T., the theory of a linear Antenna 1, *Technical report*, Tohoku University, Vol.17, Part 1, 1952

Pocklington, H. C., Electrical oscillations in wire, *Camb. Phil. Soc. Proc. 9*, 1990, 24- 332.

Richmond, J. H., Digital solutions of the rigorous equations for scattering problems *Proc. IEEE 53*, 1965, pp. 796-804.

Sadiku, M. N., *Numerical Techniques in Electromagnetics* (second Edition, CRC Press, Boca Raton London, 2001)

Storm, B., Investigation into Modern Aerial Theory and a new solution of Hallen's Integral Equation for Cylindrical Aerial, Imperial College, London, U.K. 1953.

WandzuraS.M. Thorington,C.B. Turley,C.B.Turley, R.S. and Hamilton, L.R. Fast Fourier transform techniques for solving the electric field integral Equation for a periodic body *Proc. IEEE, Microwave and Antenna propagation*. 1992, pp 401-406, Vol.139.

Full Paper

SPEECH INTELLIGIBILITY OF LECTURE THEATRES IN OBAFEMI AWOLOWO UNIVERSITY, ILE-IFE, NIGERIA

O. Osasona
Department of Electronic and Electrical Engineering, Obafemi Awolowo University, Ile-Ife, Nigeria.
ladiposasona@yahoo.co.uk

A. A. Fisusi
Department of Electronic and Electrical Engineering, Obafemi Awolowo University, Ile-Ife, Nigeria.

C.O. Osasona
Department of Architecture, Obafemi Awolowo University, Ile-Ife, Nigeria.

B. O. Onabanjo
Department of Architecture, Obafemi Awolowo University, Ile-Ife, Nigeria.

T.K. Yesufu
Department of Electronic and Electrical Engineering, Obafemi Awolowo University, Ile-Ife, Nigeria.

ABSTRACT

This work measured the speech intelligibility of lecture theatres in Obafemi Awolowo University (OAU), Ile-Ife, Nigeria using the Rapid Speech Transmission Index (RASTI) and Speech Transmission Index for Public Address (STIPA) methods. These methods are objective speech intelligibility measurement methods and they have been used in this work to determine definite and quantitative speech intelligibility values of lecture theatres in OAU unavailable before. RASTI is known to overestimate values when public address systems are involved and this was also observed to be true in this work. STIPA values are therefore recommended for making decisions related to speech intelligibility of the lecture theatres while RASTI values were evaluated for record purposes. Lecture theatres with architectural designs that minimize reverberation in addition to good interior acoustic enhancements were observed to have higher RASTI and STIPA values than lecture theatres with poor architectural design and poor acoustic enhancements.

1. INTRODUCTION

Other factors apart from the loudness level of speech can affect the comprehension of words by listeners. The major factors that affect comprehension of speech are noise and reverberation time. While noise is due to the presence of other sound sources (and/or external bodies), reverberation is due to the reflection of the original speech waveform by the walls and other structures in a room. Greenland, Shield and Dockrell (2009) stated that "design criteria for speech intelligibility in enclosed spaces are widely expressed as combinations of maximum background noise levels, and maximum mid-frequency reverberation times, assuming that students are quiet and listening to the teacher during lessons". Noise and reverberation times should be closely observed in the evaluation of speech intelligibility in a room designed for receiving lectures.

The measure of how well speech is understood or comprehended is termed *Speech Intelligibility*. Speech intelligibility is also defined as the score attained by live listeners to a live talker over a sound system (Davis and Patronis, 2006). When noise level is high and reverberation time is long in a room, the speech signal will be coloured by these interfering signals, making it difficult for listeners to comprehend what is being said. If the ambient noise level in a space is only 15dB below speech level, most listeners will have no trouble understanding the message, but many of them will complain about the noise level (Eargle and Foreman, 2002). Even though the noise level might be at an acceptable level for good word recognition in a room, the reverberation due to the make-up of the room might be excessive, leading to poor speech intelligibility in that room. Therefore, there is a need to measure the speech intelligibility in a room designed for teaching regardless of the noise level, in order to determine the suitability of the room for teaching. The speech intelligibility measurements obtained can be used as a basis for deciding on the need for improvement in acoustic enhancements in the room or otherwise.

This work measured the speech intelligibility of lecture theatres in Obafemi Awolowo University, Ile-Ife, Osun State, Nigeria using two objective methods: Rapid Speech Transmission Index (RASTI) and Speech Transmission Index for Public Address (STIPA).

2. SPEECH INTELLIGIBILITY MEASUREMENT TECHNIQUES

Formerly, speech intelligibility was measured only by using lengthy word-lists and a group of live listeners. However, today there are accurate and rapid methods of measuring intelligibility using acoustic instruments (Davis and Patronis, 2006). Intelligibility measurement and assessment techniques can be divided into two categories: subject based measures and objective acoustic measures of a parameter or parameters that correlate with some aspect of perception (Ballou, 2002). In subjective methods, trained speakers and listeners are used in the estimation of speech intelligibility. The speakers may be required to pronounce phonemes, syllables, words and/or sentences while the listeners respond. The response may be open or closed, for the open response case, the listener is required to respond to what he believes he heard. While, the listener must choose from a fixed number of options in the closed case, even when he presumably heard something not included in the options. At least four speakers and listeners are required for a useful estimation of speech intelligibility. This implies that a total of 16 speaker/ listener pairs are required.

A typical form of subjective testing is the syllabic testing. Syllabic testing is an accurate but tedious procedure (Eargle and Foreman, 2002). Intelligibility also depends on the acuity of individual listeners' ears; this makes it difficult to reproduce similar results for the same room when different sets of individuals are used for the test.

Objective methods are machine-based measurements of speech intelligibility. Speech intelligibility is estimated by using an

equipment that observe changes in certain features of the speech signal on reaching the listener position, and specifies the speech intelligibility value based on the observed changes. Usually, a sound source is placed at the speaker position while the intelligibility equipment is placed at the listener position.

One of the earliest objective methods of measuring speech intelligibility is the Articulation Index (AI) method. AI is based on the principle that the response of a speech communication system can be divided into twenty different bands. Each band has a distinct contribution to the overall speech intelligibility of the system. The contribution of each band is computed from a weighted value of the signal-to-noise ratio in that band. The overall speech intelligibility is the average of intelligibility taken over the twenty bands. Speech intelligibility is measured from 0 (completely unintelligible) to 1 (perfect intelligibility). AI does not account sufficiently for reverberation and other time-domain distortions. It has therefore been replaced by newer methods like the Speech Transmission Index (STI) method.

Speech Transmission Index (STI) is a machine measure of speech intelligibility that utilizes a speech-like test signal derived from a combination of 98 different waveforms. The 98 STI waveforms are generated by modulating (100% amplitude modulation) seven waveforms (one from each of seven octave bands ranging from 125 Hz to 8 KHz) by 14 different sinusoidal waveforms with frequencies ranging from 0.63 Hz to 12.5 Hz. The loss of modulation, known as the Modulation Transfer Function (MTF) is evaluated in each of the waveforms by comparing the received signal with the test signal and converting the MTF values into signal-to-noise values which are then averaged and normalized. The speech intelligibility is also measured from 0 (completely unintelligible) to 1 (perfect intelligibility).

STI has gained international acceptance as a useful measure of the ability of a transmission path to faithfully transmit speech intelligibility (Leembruggen, Hippler and Mapp, 2009). However, the standard STI takes about 15 minutes to be evaluated. Fortunately, simplified versions of the STI are now available that can be evaluated in about 15 seconds. These versions use fewer waveforms than the standard STI and the most common are Rapid Speech Transmission Index (RASTI) and Speech Transmission Index for Public Address (STIPA).

RASTI is a subset of STI. The RASTI method only considers the two octave bands 500 Hz and 2 kHz and each band is modulated with four and five frequencies respectively, making a total of 9 combinations (Bjor, 2009). The RASTI test signal is therefore a composite signal comprising 9 waveforms. Speech intelligibility is also obtained by computing MTF for the waveforms and mathematically combining these values to obtain a single value between 0 and 1. STIPA is a more comprehensive subset of STI than RASTI. The STIPA test signal is also a composite signal like the RASTI test signal, but the 9 waveforms in this case span all the octave bands from 125 Hz to 8 KHz specified for the full STI measurement.

When noise that is present is not correlated to the octave bands at which RASTI is calculated the modulation is not influenced and this leads to overestimation of the speech intelligibility (Zeilstra, 2009). RASTI does not account for distortion in time domain which can be present with the use of public address systems. It is best suited for person-to-person communications. For these reasons, STIPA which is more comprehensive and accurate than RASTI is recommended for making decisions pertaining to speech intelligibility of the lecture rooms. However, RASTI values were also evaluated for record purposes. STIPA handles reverberation in the room and distortions commonly found in public address systems. It delivers results closer to the values obtained by the full STI method (Bjor, 2009).

3. EXPERIMENTAL PROCEDURE

The speech intelligibility tests – RASTI and STIPA – were carried out using proprietary equipment called *Sencore SP495 Sound Pro Audio Consultant* in 14 different lecture theatres. The Sencore SP495 Sound Pro Audio Consultant (shown in Fig.1) is a high quality audio and acoustic analyser for design and consultation. It provides over 25 multiple audio analysing features including speech intelligibility, noise curves, signal generation, sound pressure level and impulse recorder. All functions, filters, and processing of the SP495 Audio Consultant are implemented in DSP firmware algorithms. The SP495 Audio Consultant can operate over the frequency range of 20 Hz to 22 KHz with a level resolution of 0.1 dB.

The speech intelligibility tests were carried out with a loudspeaker connected to a laptop (playing the RASTI or STI-PA test signal) acting as the sound source. For every reading taken, a measurement microphone connected to the Audio Consultant (placed at the listener position) received the sound signal. The Audio Consultant computes the Modulation Transfer Function (MTF) for each constituent waveform from the received signal and displays the RASTI or STIPA value. Two readings were taken for both RASTI and STIPA measurements in each lecture theatre. The readings were taken at the middle and back of the rooms with the sound source situated at the front of the rooms as suggested in the Audio Consultant Manual and also done by Zeilstra (2009).

Fig. 1. Sencore SP495 Sound Pro Audio Consultant

3.1. RASTI Measurements

RASTI values were estimated at the middle and back of each lecture theatre according to the following procedures:

1. The RASTI test signal CD was inserted into the CD drive of a laptop connected to a loudspeaker. The location of the loudspeaker was termed the "speaker location".
2. The Audio Consultant was placed at the listener location and a microphone was connected to it. The microphone received the sound signal from the loudspeaker and converted it to the corresponding electrical signal which is the input signal to the Audio Consultant.
3. The sound level of the test signal received at the listening location was set to fall between 75 – 85dB (this is the nominal listening level) by using the Sound Pressure Level (SPL) meter function on the Audio Consultant. Slow averaging was used for the SPL measurements as it averages the transients and provides the best indication of the sound level that the human ear hears (Sencore Operational Manual).
4. The RASTI function was then selected on the Audio Consultant menu to compute the RASTI value.
5. The ON/OFF field was selected to change "OFF" to "RUN" to evaluate the speech intelligibility value.
6. After some seconds, the RASTI value was displayed on the screen.

3.2. STIPA Measurements

STIPA values were also estimated at the middle and back of each lecture theatre using similar procedures to that used for the RASTI evaluation, except that the test signal was the STIPA test signal.

4. ARCHITECTURAL DESCRIPTION AND ACOUSTIC TREATMENT OF LECTURE THEATRES

4.1. The Ajose Lecture Theatre (AJSLT)

The essentially pentagonal shape of this auditorium (shown in Figs. 2 and 3) has been modified by converting the flanks into accordion-fold sections of alternating window and wall segments. This design articulation ensures there are no runs of parallel walls (which would have negatively impacted on the acoustic environment).

Acoustic treatment concentrates on ceilings and walls of the podium area, as well as the rest of the hall. In the podium area, wall treatment consists of 45mm-wide hardwood timber slats with 40 mm in-between spacing, on a plywood base; while the rear flanks and end wall, feature similar slats on mineral-wool ("fuzz") cladding. Ceiling treatment over the podium consists of triangularly-shaped acoustic panels, angularly suspended over the area. In the rest of the auditorium, polished timber panels are arranged in groups, with each group angularly-sloped and alternating with other groups sloping in the opposite direction. At the rear, the panels are beveled and also perforated. With these provisions, it was envisaged that there would be adequate absorption and appropriate reflection of sound for effective speech intelligibility.

4.2. Science Lecture Theatres

The Science Lecture Theatre complex features two auditoria, similar in design, but of varying capacities; the study analysed PY 102, the smaller of the two. It is a rectangular structure with severely raked seating, a stage area with exaggerated headroom, and a sitting area with parallel wall runs; the podium is flanked by short runs of angular walls (as shown in Figs. 4 and 5).

The stage area is panelled with 300 mm wide plain plywood planks, encompassing the flanking walls, and up to above the two front doorways into the auditorium. The rear and main flanks are treated with 50mm x 12mm studs (bevelled from bottom up), on a fibre-board base, with 35mm in-between spaces. Acoustic treatment of the ceiling is uniform over the whole hall, and consists of 300 x 300 mm corrugated chipboard tiles on 50 x 100 mm hardwood noggins, at 300 mm centres. The acoustic treatment of the walls and ceilings of this room minimize multiple reflections that can adversely affect speech intelligibility by absorbing sound energy impinging on them.

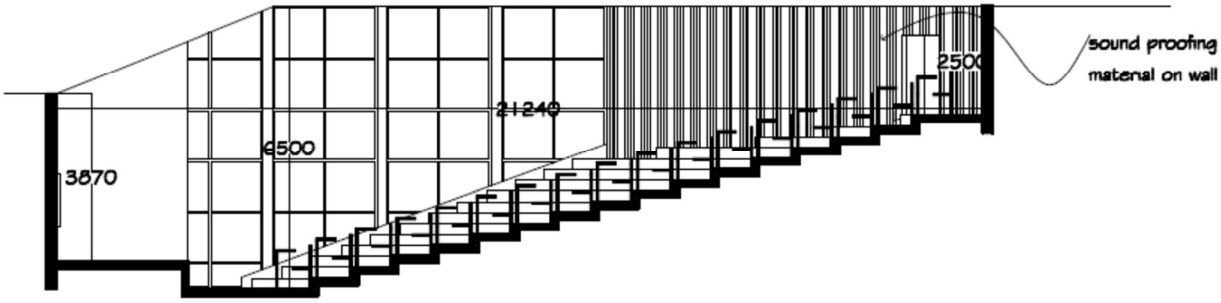

Fig. 2 Ajose Lecture Theatre Section

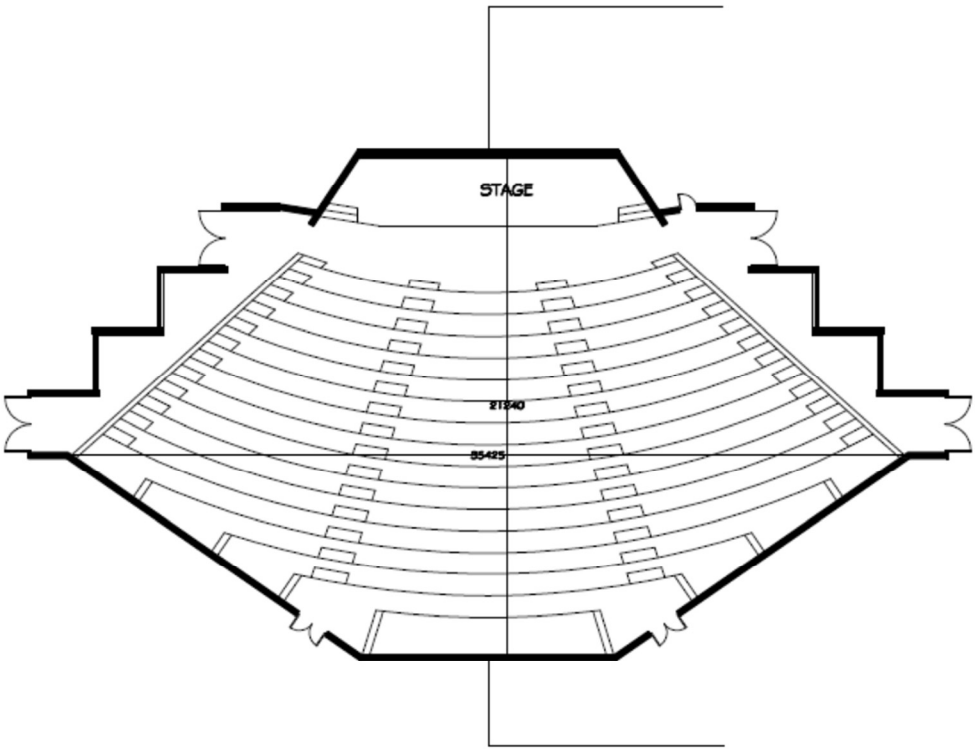

Fig. 3: Ajose Lecture Theatre Plan

4.3. Biological Sciences Lecture Theatres

The complex features three octagonal lecture theatres, of varying seating capacities; the largest, BOOC (shown in Figs. 6 and 7), was the subject of the study. In each case, the octagon is irregular, with the flanks, front and rear walls slightly longer than the remaining four wall-segments. This arrangement produces limited lengths of parallel-running walls – limiting the possibility of reflected sound that could worsen intelligibility.

Acoustic treatment of the stage area is the same as that of the rear wall of the auditorium, and comprises hardwood-timber plank panelling, grooved into 75mm slats.

The ceiling over this area consists of hardwood, overlapping slats, sloping upward from the blackboard, to meet a suspended ceiling over the central area of the auditorium.

The 1,200 x 1,200mm asbestos-cement sheets on timber noggins, constitute the finish to this suspended ceiling in which installations for artificial sound amplification are embedded. There are floor-to-ceiling louvre windows in the two flanking walls. Unfortunately, the remaining four walls defining the framework of the auditorium have been denuded of acoustic treatment. Nevertheless, it is apparent that, initially, the walls were once finished with timber slats on some fabric (presumably felt) base.

4.4. Humanities Lecture Theatres (Auditorium I & II)

Each of the two Humanities auditoria (AUD I and AUD II) has a rectangular floor plan, with the usual lecturer's podium in front, and a projection-room at the rear (Figs. 8 and 9). Wall treatment is varied in form (though not significantly in material). In the stage area, the section above the chalk-board is paneled in plain plywood;

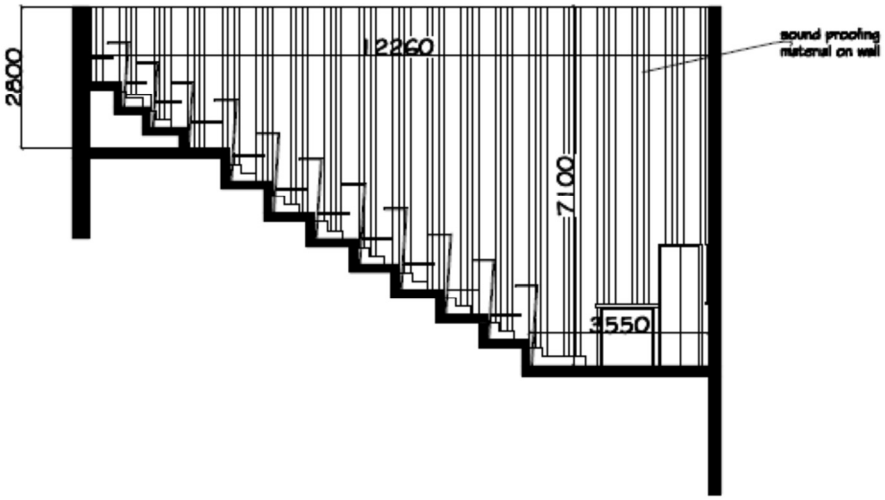

Fig. 4: Physics (PHY 102) Lecture Theatre Section

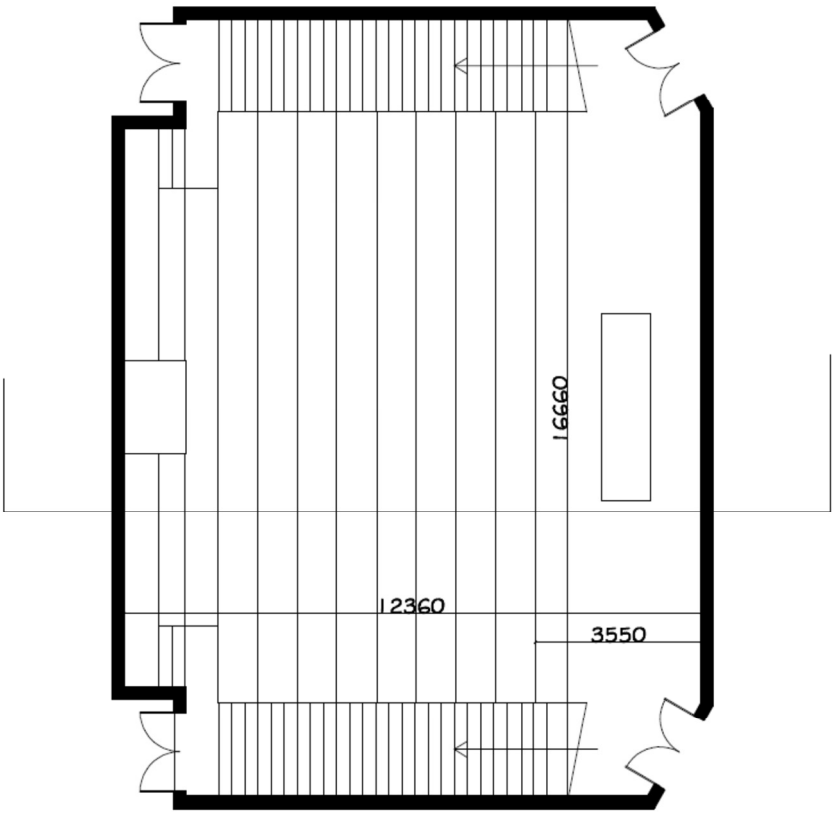

Fig. 5: Physics (PHY 102) Lecture Theatre Plan

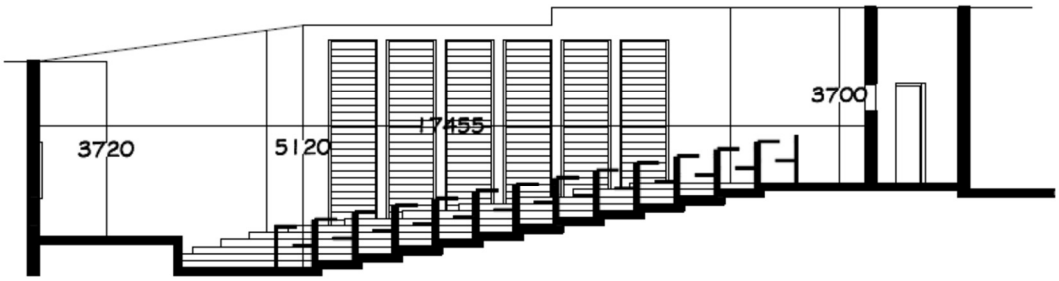

Fig. 6: BOOC Lecture Theatre Section

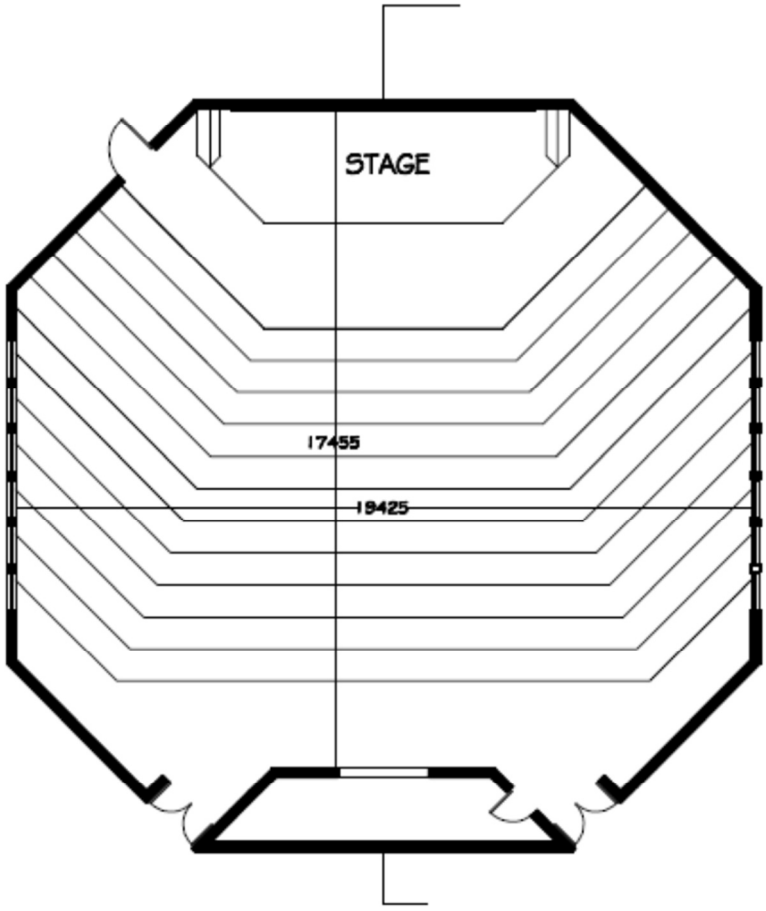

Fig. 7 BOOC Lecture Theatre Plan

Fig.8: AUD I and AUD II Lecture Theatre section

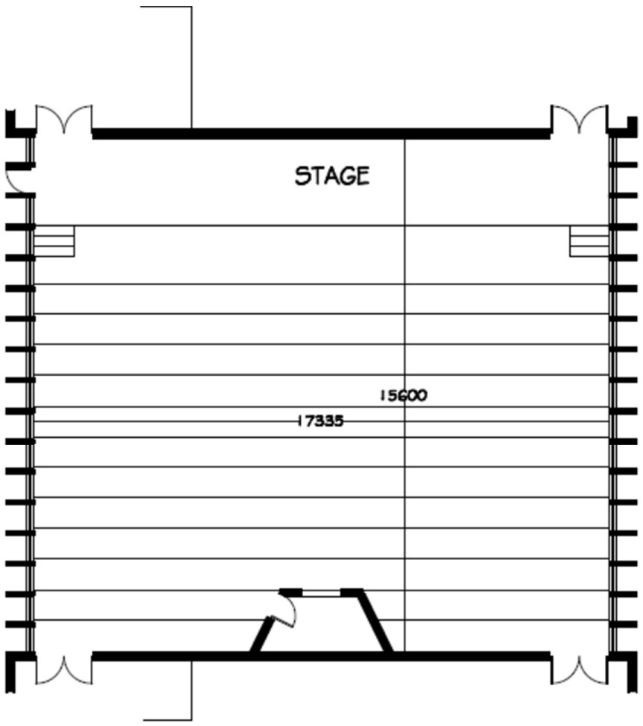

Fig. 9 AUD I and AUD II Lecture Theatre Plan

below, the finish is veneer-covered plywood. At the back of the hall – and excluding the projection-room area – 600mm-wide plywood panels provide cladding for the wall; paneling for the projection-room area comprises 150mm timber panels.

With 17 sets of floor-to-ceiling louvre windows on the flanks (separated by 100x 900mm reinforced concrete fins), the architectural configuration approximates a covered, but un-enclosed (tent) setting. The peculiar acoustics of this class of form is complemented by the use of glossy and reflective poly-vinyl chloride (PVC) slats as ceiling finish.

4.5. Oduduwa Lecture Theatres

The two Oduduwa Lecture Theatres are converted facilities in the Obafemi Awolowo University teaching spaces pool. Unlike the other lecture theatres (which were purpose-built teaching facilities), the ODLT auditoria were created by adapting free space under the raked seats of the Oduduwa Hall amphitheatre complex. As such, in general articulation, each of the two theatres is a-typical of the typology and characterized by unique vestigial features such as a tiered concrete ceiling and intervening concrete supports. Basically, these features constituting the structural supports of the amphitheatre above, define the spatial configuration of the lecture space (as shown Figs. 10 and 11). With the above seating area sloping down to the stage area, the headroom here is unusually low, and somewhat inadequate; the supporting beams of the raked seating above, converge on this area with a writing surface which is necessarily curvilinear (to reflect the orchestra area in the amphitheatre above); the tyrolene wall finish undoubtedly has implications for acoustic perception. Fan-shaped flanking wall segments consist of sandcrete block partitions, with matt-textured paint finish; louvre windows complement these wall sections. The rear of the fan-shaped hall comprises 12 window sections, framed by textured sandcrete party-walls.

4.6. Social Sciences Lecture Theatre (SSLT)

The Social Sciences Lecture Theatre (SSLT) (shown in Figs. 12 and 13) is a relatively small lecture hall, integrated into the ground floor of the Social Sciences general offices/ classrooms complex. It is

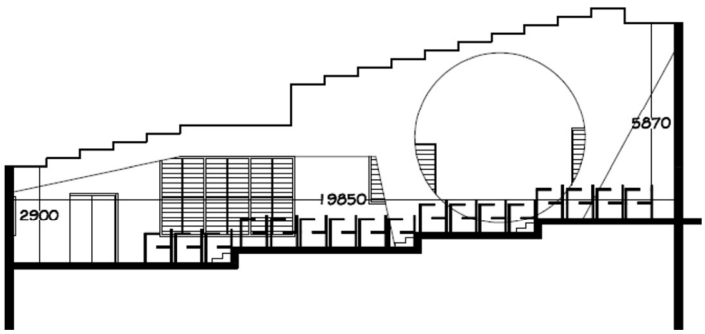

Fig. 10 ODLT Lecture Theatre Section

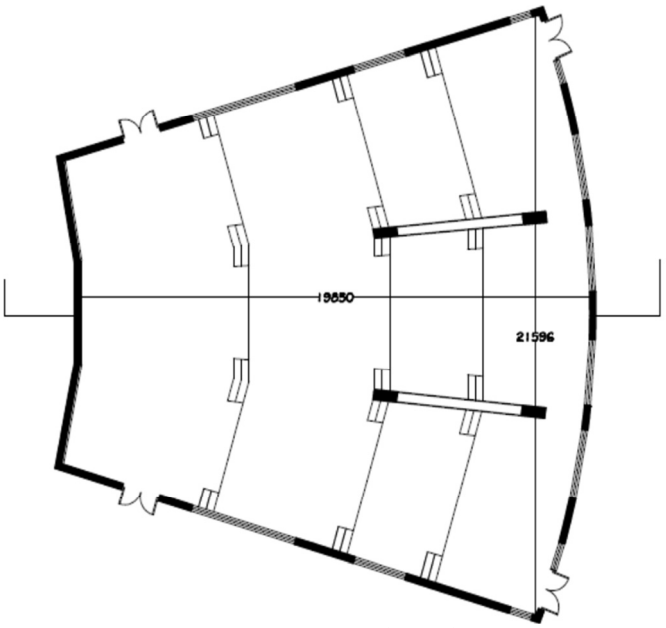

Fig. 11 ODLT Lecture Theatre Plan

rectilinear, with a volume that constitutes a rectangular pyramid frustrum i.e. the flanking walls slope inwards from bottom, halfway upwards, with louvre windows making up the rest of the wall segments; these walls are bare of any acoustic treatment.

In the stage area, 600mm-wide plain plywood panels constitute soffit treatment. At the rear of the theatre, 450mm timber slats alternate with 400mm gaps featuring some fabric-covered mineral-wool base. Ceiling treatment throughout the hall comprises 35mm timber slats on a plain plywood base.

4.7. Health Sciences Lecture Theatres (HSLT)

Similar in spatial configuration to the octagonal Biological Sciences lecture theatres, HSLTC (shown in Figs. 14 and 15) is the largest of three teaching spaces in the Health Sciences complex. The stage wall constitutes one end of the space, and the opposite end the entrance. The two parallel flanks – of an equal run as the other wall segments – provide floor-to-ceiling fenestration, with the glazing interrupted by 100 x 900mm reinforced concrete fins.

The walls are totally devoid of any acoustic treatment. The only consideration given to non-electronic acoustic performance appears to be with respect to the elaborate suspended, "egg-crate ceiling", uniformly provided over the whole auditorium; this is expected to produce differential reflection of sound. The egg-crate comprises perpendicular timber frames (of about 1,500 x 1,500mm), criss-crossed by diagonals; the timber panels are 750mm-deep, with the diagonals recessed to accommodate fluorescent tubes, providing artificial lighting with minimum glare.

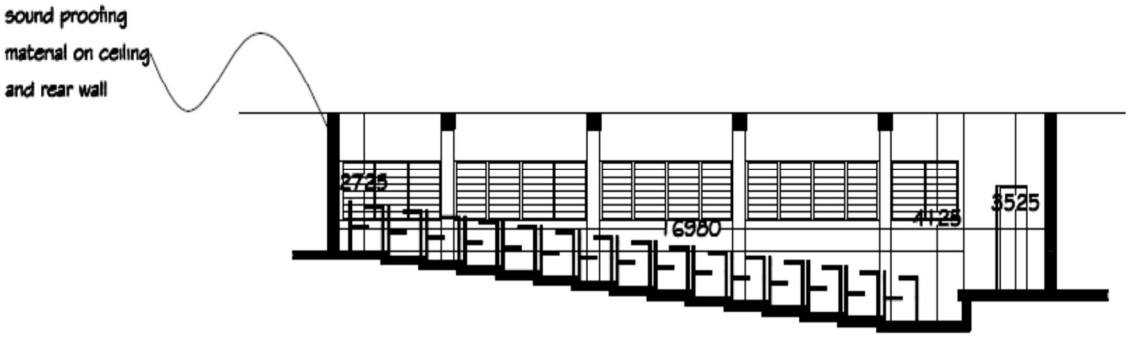

Fig.12 SSLT Lecture Theatre section

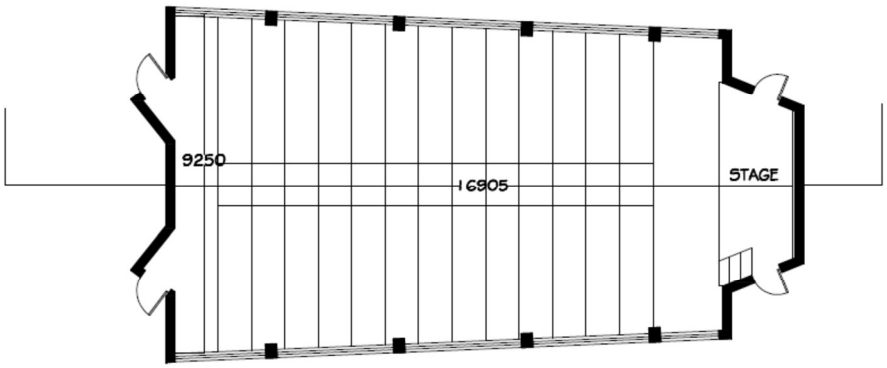

Fig. 13 SSLT Lecture Theatre plan

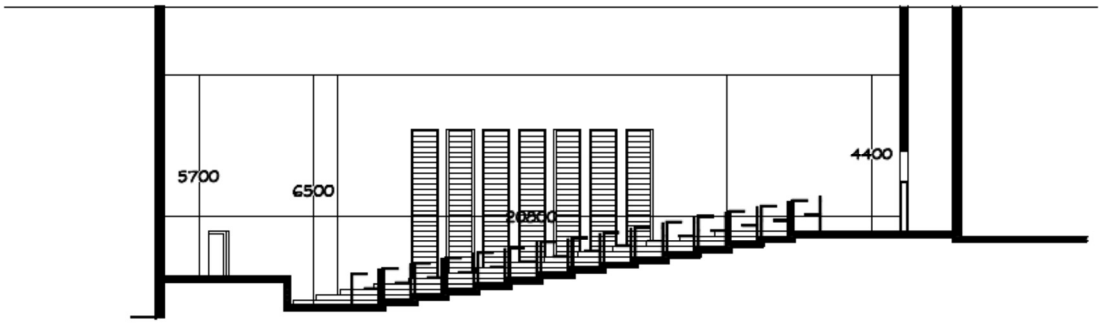

Fig. 14 HSLTC Lecture Theatre section

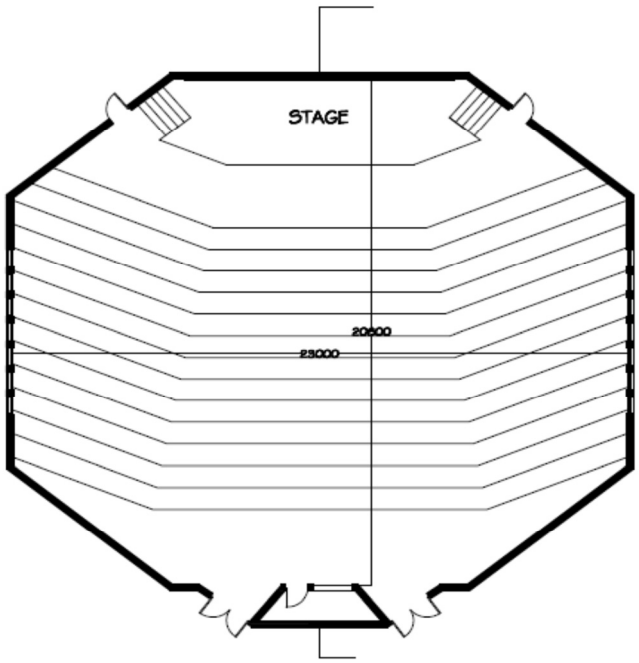

Fig. 15 HSLTC Lecture Theatre Plan

5. RESULTS AND DISCUSSIONS

RASTI and STIPA test values are usually decimal numbers between 0 and 1. Table 1 shows the guideline for interpreting the RASTI speech intelligibility test values. STIPA values are also interpreted in a similar way as shown in Table 2. RASTI and STIPA speech intelligibility measurements were taken in 14 lecture theatres as mentioned earlier. The values obtained for each lecture theatre are given in Table 3.

STIPA values were found to be higher at the middle of the lecture theatres than at the back as shown in Fig. 16. This is also true for RASTI values. This is expected since speech intelligibility of public address systems decreases with the distance from the loudspeaker which was placed in front of the room. This can be further explained by the reduction in the strength of the direct wave from the sound source (due to attenuation) as distance from source increases.

It was also observed that the RASTI values are higher than corresponding STIPA values at the middle of the lecture theatres as shown in Fig. 17. RASTI values are also higher than STIPA values at the back of the lecture theatres (see Table 3). This is due to the overestimation tendencies of RASTI mentioned earlier. Hence STIPA values should be used to specify the speech intelligibility capability of the rooms while the RASTI values can be kept for record purposes.

The dimensions of the lecture theatres were found not to be the main factor that determines the ratings of intelligibility in the rooms. Some large rooms were observed to have better speech intelligibility values than smaller rooms. For example, AJSLT has better speech intelligibility ratings than the ODLT lecture rooms which are smaller rooms. It is how well reverberation is handled in the rooms that determine whether reflections in the rooms would affect intelligibility or not, not just the sizes of the rooms.

Rooms with good intelligibility values are those that were well-designed to minimize reverberation from walls and ceilings. The architectural design and wall cladding of AJSLT and BOOC help to prevent excessive reverberation, while PY102 and CH102 lecture theatres have walls with acoustic cladding that absorbs sound, preventing reflection and reverberation from the walls. Such rooms have higher speech intelligibility ratings than rooms with poor architectural design and poor or no wall cladding (like HSLTC, HSTLB, HSLTA, ODLT I and ODLT II lecture theatres).

For the lecture rooms with poor speech intelligibility, one approach to improve the STI ratings is to implement good acoustic treatments for the walls and ceilings. It will be an arduous and costly task to change the architectural configurations of the rooms, so this option may have to be left out. For rooms with parallel louvre windows forming part of the walls, the windows should be kept open to reduce reflection of sound waves in the room thereby reducing the possibility of reverberation, leading to improvement in the speech intelligibility in such rooms.

Table 1: Guideline for Interpreting RASTI Speech Intelligibility Test Values

Rasti Values	Rating
0.2	Bad
0.25	Bad
0.30	Poor
0.35	Poor
0.40	Poor
0.45	Fair
0.50	Fair
0.60	Fair
0.65	Good
0.70	Good
0.75	Good
0.80	Excellent
0.85	Excellent
0.90	Excellent
0.95	Excellent
1.00	Excellent

Source: Sound Pro Audio Consultant Operational Manual

Table 2: Correspondence between STI or STIPA scores and perceived speech intelligibility

Subject Descriptor	Unintelligible	Poor	Fair	Good	Excellent
STI score	0 - 0.3	0.3 – 0.45	0.45 – 0.60	0.60 – 0.75	0.75 – 1.0

Source: Nestoras et al (2007)

Table 3: Speech Intelligibility Values of Lecture Theatres of Obafemi Awolowo University, Nigeria.

Lecture Theatre		Method	Location 1 (Middle)	Location 2 (Back)
Ajose Lecture Theatre	AJSLT	STIPA	0.65	0.44
		RASTI	0.64	0.57
Physical Sciences	PY 102	STIPA	0.56	0.51
		RASTI	0.65	0.58
	CH 102	STIPA	0.50	0.48
		RASTI	0.69	0.58
Biological Sciences	BOOC	STIPA	0.68	0.57
		RASTI	0.70	0.65
	BOOB	STIPA	0.68	0.65
		RASTI	0.70	0.68
	BOOA	STIPA	0.68	0.62
		RASTI	0.72	0.65
Health Sciences	HSLTC	STIPA	0.31	0.29
		RASTI	0.43	0.44
	HSLTB	STIPA	0.34	0.33
		RASTI	0.52	0.47
	HSLTA	STIPA	0.29	0.29
		RASTI	0.46	0.45
Humanities	AUD I	STIPA	0.73	0.55
		RASTI	0.90	0.73
	AUD II	STIPA	0.64	0.43
		RASTI	0.83	0.74
Oduduwa Lecture Theatre (Conversions)	ODLT I	STIPA	0.22	0.15
		RASTI	0.38	0.30
	ODLT II	STIPA	0.12	0.07
		RASTI	0.37	0.35
Social Sciences	SSLT I	STIPA	0.56	0.51
		RASTI	0.78	0.62

6. CONCLUSION

The speech intelligibility of 14 lecture theatres was evaluated using RASTI and STIPA methods. Speech intelligibility values ranging from poor to good were obtained for the rooms, depending on how well they were designed and whether provisions were made for proper handling of reverberation in the room. Based on the stated findings, there is a need to enhance the acoustic features of lecture rooms with poor or fair ratings, in order to improve speech intelligibility. It appears that all the studied lecture spaces can still be improved upon, based on the RASTI and STIPA values, as no room could be rated to have excellent speech intelligibility at the back.

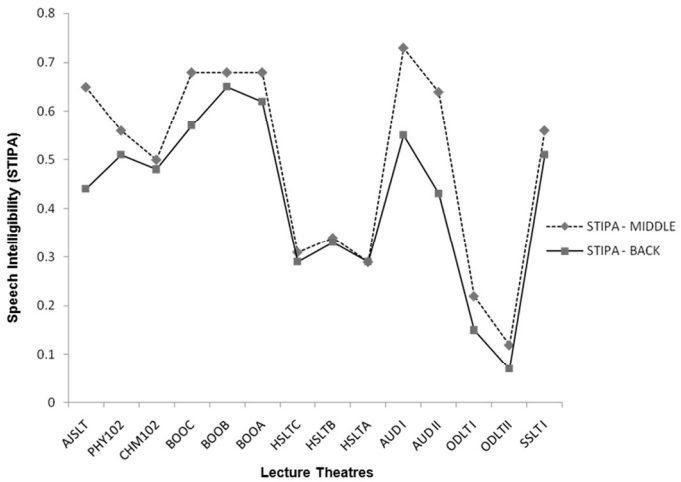

Fig. 16 Comparison of STIPA values at the middle and back of the lecture theatres

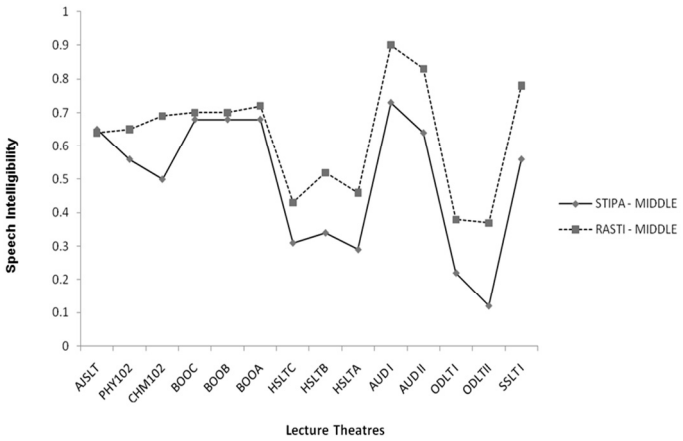

Fig. 17 Comparison of RASTI and STIPA values at the middle of the Lecture theatres

Garay-Vargas and Rodriguez-Manzo (2008) stated that "it is hard for architects to imagine how an architectural space will sound when there is not enough knowledge of the acoustic parameters, the behaviour of materials, the type of space, the dimensions, geometry, all of them are fundamental to define the sound characteristics of the space". Hence, subsequent lecture theatre building projects should take cognizance of the need to incorporate speech intelligibility capability into the project and this can be done at the design stage of the buildings. Therefore, acoustic parameters and other important parameters that will affect the speech intelligibility of the lecture room should be considered.

ACKNOWLEDGEMENTS

The authors wish to thank Pastor E. A. Adeboye and RCCG Electronics Services Department for the provision of Sencore SP495 SoundPro Audio Consultant used for this study. Shalom Productions, Ile-Ife is also appreciated for the audio system used.

REFERENCES

Eargle, J. and Foreman, C. "Audio Engineering for Sound Reinforcement", Hal Leonard Corporation, Milwaukee, US, 2002.

Garay-Vargas, E. and Rodriguez-Manzo, F.E. "Analysis of the impact of sound diffusion in the reverberation time of an architectural space – A proposal for the characterization of diffusive surfaces using scale model", Proceedings of Second ASA-EAA Joint Conference (Acoustic '08 Paris): 4521 – 4526, 2008.

Davis, D. and Patronis, E. "Sound System Engineering", Elsevier Inc., USA, 2006.

Ballou, G.M. "Handbook for Sound Engineers", Focal Press, United States, 2002.

Sound Pro Audio Consultant Operational Manual, Firmware Version 1.54, Sencore.

Greenland, E. Shield, B. and Dockrell, J., "Acoustics in open plan classrooms –towards revised speech intelligibility criteria", Proceedings of the Institute of Acoustics, 31(4): 50-61, 2009.

Leembruggen, G. Hippler, M. and Mapp, P., "Exploring ways to improve STI's recognition of the effects of poor spectral balance on subjective intelligibility", Proceedings of the Institute of Acoustics, 31(4): 133-169, 2009.

Bjor, O., "STIPA, The Golden mean between full STI and RASTI", Proceedings of the Institute of Acoustics, 25(7), 2003.

Nestoras, C. Gomez, L., Dance, S. and Murano, S., "Speech Intelligibility measurements a in diffuse space using open and closed loop systems",19th International Congress on Acoustics, Madrid, September, 2007.

Zeilstra, G.J., "Speech Intelligibility in Classrooms: A new measurement method", A Master Thesis Project, Applied Physics, Faculty of Applied Sciences, Delft University of Technology, Holland, 2009.

Full Paper

CARBON LOSS IN CHICKEN LITTER COMPOST AS AFFECTED BY CARBON TO NITROGEN RATIO AND TURNING FREQUENCY

G.A. Ogunwande
Department of Agricultural Engineering, Obafemi Awolowo University, Ile-Ife, Nigeria
gbolawande@oauife.edu.ng

ABSTRACT

Raw chicken manure was co-composted with sawdust in turned-windrow piles to study the effects of carbon to nitrogen (C:N) ratio and turning frequency (TF) on the loss of total carbon (C) during composting. Three levels of C:N ratio (20:1, 25:1 and 30:1) and TF (2, 4 and 6 days) were experimented in a two-factor completely randomized block design. During the composting process, temperature, pH, moisture content (MC), total C, phosphorus (P), potassium (K) and nitrogen (N), dry matter (DM) and C:N ratio were monitored. Also, MC of the piles was periodically replenished to 55%. The results showed that both C:N ratio and TF had significant ($p \leq 0.05$) effect on temperature, pH, total N, C, P and K losses and C:N ratio of the piles while only C:N ratio affected ($p \leq 0.05$) DM losses. It was observed that moisture loss increased as C:N ratio and TF increased. The decline of pile temperatures to near ambient temperature occurred at about 87 days in all treatments. The final total C losses ranged between 63.1 and 83.8%, with 65.2-97.1% occurring within the first six weeks when the pile temperatures and pH values were above 33 °C and 7.7, respectively. The total C losses were largely attributed to organic matter degradation and increased as C:N ratio and TF increased. The combined effects of C:N ratio and TF showed that treatment with 6 days TF and C:N ratio of 20:1 had the minimum total C loss (63.1%).

Keywords: *Composting, C:N ratio, Turning frequency, Total C loss.*

NOMENCLATURE

T_2R_{20}	composting pile with 2 days TF and C:N ratio 20:1
T_2R_{25}	composting pile with 2 days TF and C:N ratio 25:1
T_2R_{30}	composting pile with 2 days TF and C:N ratio 30:1
T_4R_{20}	composting pile with 4 days TF and C:N ratio 20:1
T_4R_{25}	composting pile with 4 days TF and C:N ratio 25:1
T_4R_{30}	composting pile with 4 days TF and C:N ratio 30:1
T_6R_{20}	composting pile with 6 days TF and C:N ratio 20:1
T_6R_{25}	composting pile with 6 days TF and C:N ratio 25:1
T_6R_{30}	composting pile with 6 days TF and C:N ratio 30:1

1. INTRODUCTION

Application of raw manure to agricultural soils could lead to serious environmental problems such as increased nutrient loss through leaching, erosion, and runoff from agricultural fields. These problems could be mitigated by chemically and biologically stabilizing the soluble nutrients in raw manure to more stable organic forms by composting before application to agricultural soils. Composting is viewed as a viable means of producing environmentally friendly humus-like material, and an important way of protecting ground and surface waters from excessive loading of litter nutrients. Composting stabilizes organic wastes and destroys most parasites, pathogens, and viruses contained in the wastes (Tiquia *et al.*, 2000). It also considerably reduces odour emissions by reducing levels of biodegradable hydrocarbons and dries up the waste making it unattractive to insects (Barrington *et al.*, 2002). However, one of the most negative effects of composting animal manures is the loss of valuable nutrients which reduces the fertilizer value of the manure and constitutes an important economic loss. During composting, nitrogen (N) is largely lost through ammonia (NH_3) volatilization. Ammonia emissions can result from aerobic or anaerobic bacteria activities in manure (Zhang *et al.*, 1991). Apart from N, carbon (C) is another key element of animal manure that is lost during the composting. Carbon may be lost due to either bio-oxidation, in which carbonaceous materials are lost as carbon dioxide (CO_2) (Eghball *et al.*, 1997) or mineralization of C, in which inorganic C are converted to organic C (Bernal *et al.*, 1998). Total C loss during composting varies depending on the composting method used. Nutrients that plants need in large amounts, called macronutrients, include oxygen, hydrogen, carbon and an array of minerals (Hynes, 2008). Carbon is what most of the plant is made of. It forms the backbone of many plant biomolecules, including starches and cellulose. Therefore, minimization of C loss during composting process should also be a research focus.

The control of parameters such as C:N ratio, temperature, moisture content (MC), bulk density, aeration, particle size and pH have demonstrated to be key for composting optimization since they determine the optimal conditions for microbial development and organic matter (OM) degradation (Haug, 1993). The initial C:N ratio of composting materials should be within 20:1-40:1 for rapid composting (Rynk *et al.*, 1992). Lower values could cause high emissions of NH_3 (Tiquia and Tam, 2000) while higher values could cause a slower beginning of the process and longer than usual composting time (Tuomela *et al.*, 2000). Turning is often cited as the primary mechanism of aeration and temperature control during windrow composting (Michel *et al.*, 1996; Tiquia, 1996), while turning frequency (TF) is commonly believed to be a factor which affects the rate of composting as well as compost quality (Tiquia, 1996).

Most composting studies have focused on N losses from manure during composting while C losses have been less investigated. For instance, the effects of C:N ratio (Hansen *et al.*, 1989; Eghball *et al.*, 1997; Huang *et al.*, 2004) and TF (Tiquia *et al.*, 1997; Wong *et al.*, 2001) on N losses during composting have been studied while information regarding the effects on C losses are rather scarce. As a result, the present study aims to: (1) investigate the effects of C:N ratio and TF on the changes in total C during composting of chicken litter in turned-windrow piles and (2) assess the combined effects of C:N ratio and TF with a view to determining the optimum combination that will minimize total C loss during composting.

2. MATERIALS AND METHODS

2.1. Composting Set Up

The experiment was conducted during the dry season on an open site at the Department of Agricultural Engineering, Obafemi Awolowo University, Ile-Ife, Nigeria. The ambient temperatures during the period ranged from about 22-35 °C. The raw chicken manure and sawdust used in the study were collected from a poultry farm and sawmill plant in Ile-Ife, respectively. The initial properties of the chicken manure and sawdust are summarized in Table 1. The total N, total phosphorus (P) and total potassium (K) contents of the sawdust were assumed to be traces (Eghball, 1997), hence they were not determined. The experimental set up was a 3 × 3 completely randomized block design with C:N ratios at 20:1, 25:1 and 30:1, and with TFs at every 2, 4 and 6 days. The C:N ratio of the chicken manure was raised to 20:1, 25:1 and 30:1 through the addition of sawdust (Brake, 1992), and in accordance with the recommendations of (Rynk *et al*., 1992) on rapid composting. Sawdust was used because of its low MC, high porosity and C:N ratio. The initial concentrations of ash, total C, total N, C:N ratio, total P, total K, and MC of the composting mixture were theoretically calculated based on the results of the analyses.

Nine piles of chicken litter were built in pits of size 1.2 m × 1.2 m square base and a height of 0.3 m, which each pile having a pyramidal shape with a square base of 1.2 m × 1.2 m and a height of about 0.76 m. Each pile was replicated three times and turned manually using a hand shovel. The MC of the litter was adjusted to 55% (wet basis) at the beginning of composting, as described by Brake (1992), measured periodically (precisely a day to turning operation) and replenished to 55% (wet basis) during turning operation such that every part received moisture.

2.2. Sampling and Analytical Procedures

Pile temperatures were measured daily, using a digital thermometer, at two levels (0.25 m and 0.50 m from the base of the pile) within the pile between the hours of 06:00 am and 08:00 am when the ambient temperature was fairly stable. Sampling was done fortnightly from the start to the end of the experiment. Three samples each were collected at three locations in each pile (0.25 m from the top, at the middle and 0.25 m from the base) and composited. Samples were analyzed at 105 °C dry weight basis for the following parameters: moisture content (105 °C for 24 h); ash content (expressed as a percentage of residues after ignition at 600 °C for 5 h); total N using regular-kjeldahl method (Bremner, 1996); total K (after acid digestion) using atomic absorption spectrophotometer (Alpha 4 model); total P (after acid digestion) using ultra-violet visible spectrophotometer (UNICAM UV1 model) of wavelength 660 nm; pH (1:10 w/v sample: water extract) using a pH meter with a glass electrode. The total C was estimated from the ash content according to the formula (Mercer and Rose, 1968):

$$Total\,C\,(\%) = [100 - Ash\,(\%)] / 1.8 \quad (1)$$

Initial and final concentrations of total N, P and K were determined while total C and pH determined fortnightly. Losses of dry matter (DM), total C, total N, total P and total K from the pile during composting were calculated according to the equation (Sanchez-Monedero *et al*., 1996):

$$Y\,loss\,(\%) = 100 - 100\left[\frac{X_1 Y_2}{X_2 Y_1}\right] \quad (2)$$

where X_1 and X_2 represent the initial and the final ash concentrations, Y represents DM, total C, N, P and K, and Y_1 and Y_2 represent the initial and final concentrations of Y.

2.3. Statistical Analysis

The data obtained were subjected to statistical analyses, using Statistical Analysis System (SAS, 2002) procedure. *T*-test was used to compare the upper and lower temperature readings within the piles. Regression analysis was used to determine the relationship among compost properties. Two-way analysis of variance (ANOVA) was performed to compare variations in compost properties, and where significance was indicated, Least Significant Difference (LSD) test was used to establish which treatment was significantly different.

Table 1: Initial properties of the composting materials

Property	Concentration (dry weight basis)	
	Chicken manure	Sawdust
MC (%)	54.0 ± 2.48*	30.0 ± 1.10*
pH	8.34 ± 0.04	7.60 ± 0.10
Ash (%)	52.3 ± 1.20	3.00 ± 0.17
Total C (%)	26.5 ± 1.13	53.9 ± 1.71
Total N (%)	2.10 ± 0.11	nd
Total K (ppm)	203.9 ± 4.10	nd
Total P (ppm)	2.70 ± 0.10	nd
C:N ratio	13:1	nd

Mean and standard error are shown (n = 3).

nd - not determined; ppm - parts per million.

**Value on wet weight basis.*

3. RESULTS AND DISCUSSION

3.1. Physico-Chemical Changes during Composting

The pile temperatures stabilized about the 87th day of composting. This duration was within the range of 15 and 180 days reported for converting manure into stabilized compost (Rynk *et al*., 1992; Michel *et al*., 1996). It was observed that moisture addition during composting increased from 161.67% to 270.57% (of total pile weight) as TF increased from 6 to 2 days, and increased from 176.90% to 248.37% (of total pile weight) as C:N ratio increased from 20:1 to 30:1. The final losses in compost elements are presented in Table 2. The increases observed in the ash concentrations of all the treatments revealed that effective OM degradation occurred during the composting process. Seepage losses were considered insignificant as the piles were not wet enough to drain water. Total P and K concentrations were significantly ($p \leq 0.05$) affected by both C:N ratio and TF. Table 3 shows the LSD test on compost properties. The final C:N ratios showed that, except for T_4R_{25}, all other treatments had increase in C:N ratio. This development could be attributed to vigorous NH_3 volatilization during composting, as reported by Eghball *et al.* (1997) and Tiquia and Tam (2000).

Table 2: Final loss in compost elements

Treatment	Dry matter loss (%)	Total N loss (%)	Total P loss (%)	Total K loss (%)
T_2R_{20}	16.1 ± 1.01	88.2 ± 0.28	62.8 ± 1.51	85.8 ± 0.17
T_4R_{20}	18.4 ± 1.71	82.7 ± 0.45	4.60* ± 9.16	79.6 ± 0.28
T_6R_{20}	15.2 ± 0.24	86.8 ± 0.32	53.9 ± 0.48	82.1 ± 0.12
T_2R_{25}	16.4 ± 1.50	82.9 ± 0.42	57.2 ± 1.48	70.9 ± 0.54
T_4R_{25}	7.72 ± 2.14	70.7 ± 0.80	1.77* ± 2.29	57.2 ± 0.62
T_6R_{25}	10.0 ± 0.80	87.4 ± 0.67	50.9 ± 1.21	50.6 ± 0.46
T_2R_{30}	17.9 ± 0.86	87.1 ± 1.06	53.7 ± 0.11	85.6 ± 0.15
T_4R_{30}	18.0 ± 2.15	83.9 ± 2.44	55.7 ± 3.55	82.8 ± 0.16
T_6R_{30}	22.9 ± 1.21	81.3 ± 1.10	67.2 ± 0.49	76.1 ± 0.27

Mean and standard error are shown (n = 3).

**Percent gain.*

3.1.1. Temperature

The pile temperatures during composting ranged between 28 °C and 71 °C. Both the C:N ratio and TF had significant ($p \leq 0.05$) effect on pile temperature (Table 3). The results of the *t*-test showed no significant ($p > 0.05$) difference between the two temperature readings within the piles. This was as a result of the mixing effect and it

Table 3: Least significant difference (LSD) test on the compost properties

Property	C:N ratio				TF (days)			
	20:1	25:1	30:1	LSD	2	4	6	LSD
Temperature (°C)	42.39^{b}	52.49^{a}	53.57^{a}	2.57	49.34^{a}	53.14^{b}	45.96^{c}	2.57
pH	8.03^{b}	8.26^{a}	8.09^{b}	2.45	8.17^{c}	8.09^{b}	8.12^{a}	2.45
DM (%)	16.55^{a}	11.36^{b}	19.61^{a}	2.44	ns	ns	ns	-
Total N (%)	85.90^{a}	80.33^{b}	84.13^{a}	1.80	86.05^{a}	79.13^{b}	85.19^{a}	1.80
Total C (%)	71.77^{a}	74.04^{b}	82.21^{c}	1.76	81.40^{a}	75.51^{b}	71.11^{c}	1.76
C:N ratio	40.89^{a}	37.85^{a,b}	34.74^{b}	3.28	33.90^{a}	30.14^{b}	49.45^{c}	3.28

Superscripts with the same letter are not statistically different at $p \leq 0.05$; ns - mean value not significant at $p \leq 0.05$.

implied that the composting rates and compost quality within the piles would be the same. The regression analysis performed on the pooled means showed that pile temperature had a significant ($p \leq 0.05$) correlation with pH and total C, according to the relationship:

$$Temperature = -29.49 + (1.02 \times total\,C) + (5.60 \times pH); \quad R^2 = 0.76 \tag{3}$$

This confirms the findings by Tiquia *et al.* (1998) on the correlation of temperature with compost properties. Thermophilic temperatures (56.3-70.7 °C) were attained within 24 h of composting (Figure 1a-c), an indication that the initial C:N ratios and MC were ideal for composting. The short thermophilic phase (17-22 days) observed is associated with turned windrow method (Diaz *et al.*, 2002), likely related to small size of piles involved (Ogunwande *et al.*, 2008) and also, as a result of the TFs ($p \leq 0.05$). The duration of temperatures › 55 °C (9-11 days, 10-11 days and 7-8 days in piles with C:N ratios 20:1, 25:1 and 30:1, respectively) indicated that the pathogens and weed seeds would have been abated during composting (Misra *et al.*, 2003). The slight increases noticed in the pile temperatures after each turning operation in the early days of composting were as a result of the re-activation of microbial activities. This could be explained by the incorporation of external material into the pile, providing degradable substrate for the microbial biomass (Gracia-Gomez *et al.*, 2003).

3.1.2. Dry Matter and Total Nitrogen

Dry matter loss ranged between 7.72% and 22.9% (Table 2) and was affected ($p \leq 0.05$) by C:N ratio (Table 3). These losses were lower than the range (35-50%) reported by Kithome *et al.* (1999) during composting of poultry manure. Both the C:N ratio and TF had significant ($p \leq 0.05$) effect on the final total N losses which ranged between 70.7% and 88.2% (Table 2).

3.1.3. pH

The initial pH values (8.35-8.63) (Table 4) were within the reasonable range (5.5-9.0) recommended for rapid composting (Rynk *et al.*, 1992). The pH values remained on the alkaline side throughout the composting process (Table 4). Both the C:N ratio and TF had significant ($p \leq 0.05$) effect on the alkalinity of the piles (Table 3). High pH values (8.73 to 9.34) observed during the second week in all the treatments (Table 4) was attributed to intense OM degradation in the piles and the consequent release of volatile NH_3 (Paredes *et al.*, 2000). The decrease in pH values after the second week was attributed to the production of organic acids during decomposition of OM contained in the chicken litter (Charest and Beauchamp, 2002). The final values (7.53-7.83) were close to 7.2 recommended for the improvement of agricultural soils (Rynk *et al.*, 1992) and for optimum plant growth (Campbell *et al.*, 1997).

3.1.4. Total Carbon

Total C concentration decreased gradually with composting time in all the piles due to OM degradation. The decrease synchronized with an increase in ash content of the chicken litter piles. It was observed that C:N ratio and TF had significant ($p \leq 0.05$) effect on total C loss, which increased as C:N ratio and TF increased (Table 3). Increase in C:N ratio is associated with increase in porosity of the piles, hence increase in air supply to the piles. Similarly, increase in TF increases air supply to the piles. Therefore, it can be concluded that total C loss was related to the air supplied to the piles. In view of these facts, with increased air supply, total C may have served as a source of energy for the micro-organisms and been

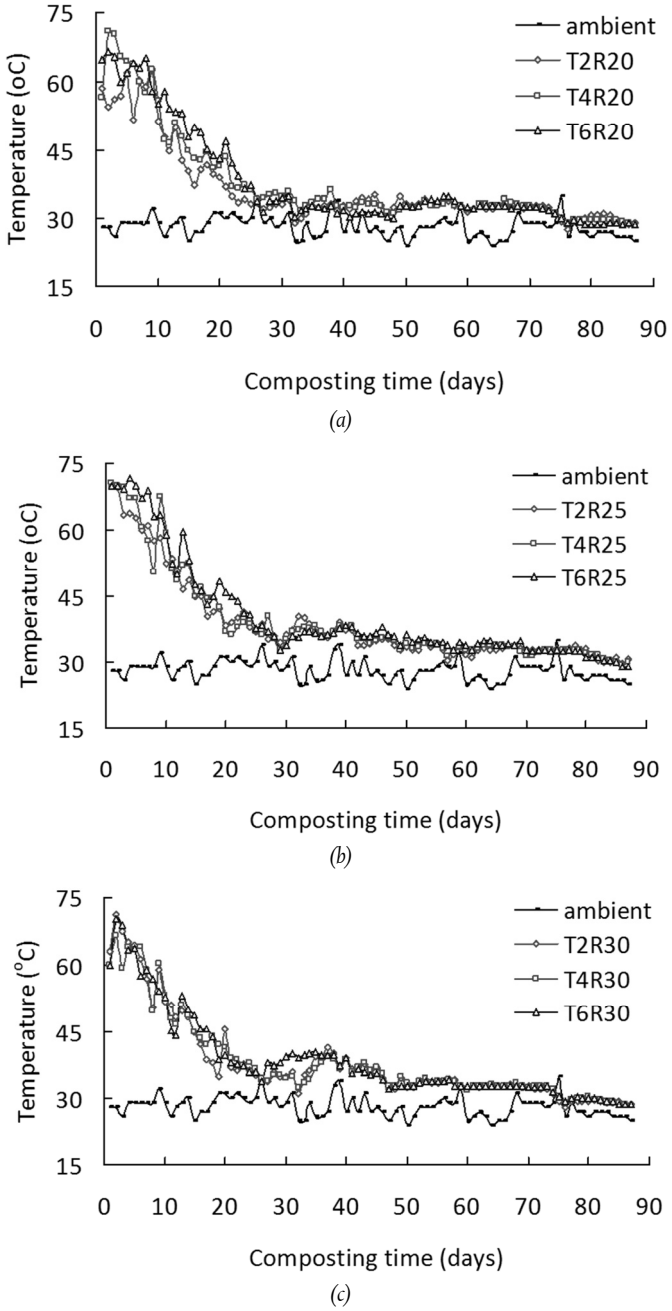

Figure 1: Changes in air and pile temperatures of composting piles with (a) C:N 20:1, (b) C:N 25:1, and (c) C:N 30:1

burnt up and respired as CO_2, or may have been mineralized, in which inorganic C would have been converted to organic C (Bernal *et al.*, 1998). The regression analysis showed that as TF decreased from 2 to 6 days, the rate of total C loss (% total C/day) was highest in treatment with C:N 20:1 (4.21, R^2=0.99), followed by treatment with C:N 25:1 (2.80, R^2=0.94) and then, treatment with C:N 30:1 (0.70, R^2=0.98). Also, it was shown that total C had a significant ($p \leq 0.05$) correlation with total N and C:N ratio, according to the relationship:

$$Total\ C = -11.54 + (0.21 \times temperature) + (17.59 \times total\ N) + (0.39 \times C:N\ ratio);\ R^2 = 0.9 \quad (4)$$

Table 4: Changes in pH of composting piles during composting

Treatment	Composting time (weeks)						
	0	2	4	6	8	10	12
T_2R_{20}	8.54	8.93	8.30	7.68	7.90	7.81	7.69
T_4R_{20}	8.49	8.87	7.87	7.65	7.72	7.76	7.74
T_6R_{20}	8.35	8.82	7.76	7.75	7.62	7.64	7.73
T_2R_{25}	8.63	9.29	8.24	8.17	8.19	7.99	7.82
T_4R_{25}	8.60	9.07	8.15	7.96	7.91	7.90	7.63
T_6R_{25}	8.46	9.34	8.08	8.19	8.06	7.94	7.83
T_2R_{30}	8.59	8.91	7.75	7.78	7.84	7.76	7.75
T_4R_{30}	8.43	8.73	8.02	7.96	7.95	7.76	7.80
T_6R_{30}	8.48	9.01	8.12	7.97	7.94	7.80	7.63

Figure 2a-c showed the changes in total C losses with composting time. It was shown that total C loss increased gradually in all the piles. The final total C loss ranged between 63.1% and 83.8% in all the treatments. This was an indication that the chicken litter contained high degradable OM (Fang *et al.*, 1999). Treatment T_6R_{20}, which had the least loss in total C, had pH and total N significantly ($p \leq 0.05$) correlated with total C. This implied that pH and total N contributed to the total C loss in the treatment. The final losses were higher than the range (44.5-61.5%) reported by Eghball *et al.* (1997), probably due to the higher initial C:N ratios or composting method used in this study. It was observed that 65.2-97.1% of the final losses occurred within the first 42 days of composting when the pile temperatures and pH values were above 33 °C and 7.7, respectively. This indicated that maximum OM degradation occurred within this period.

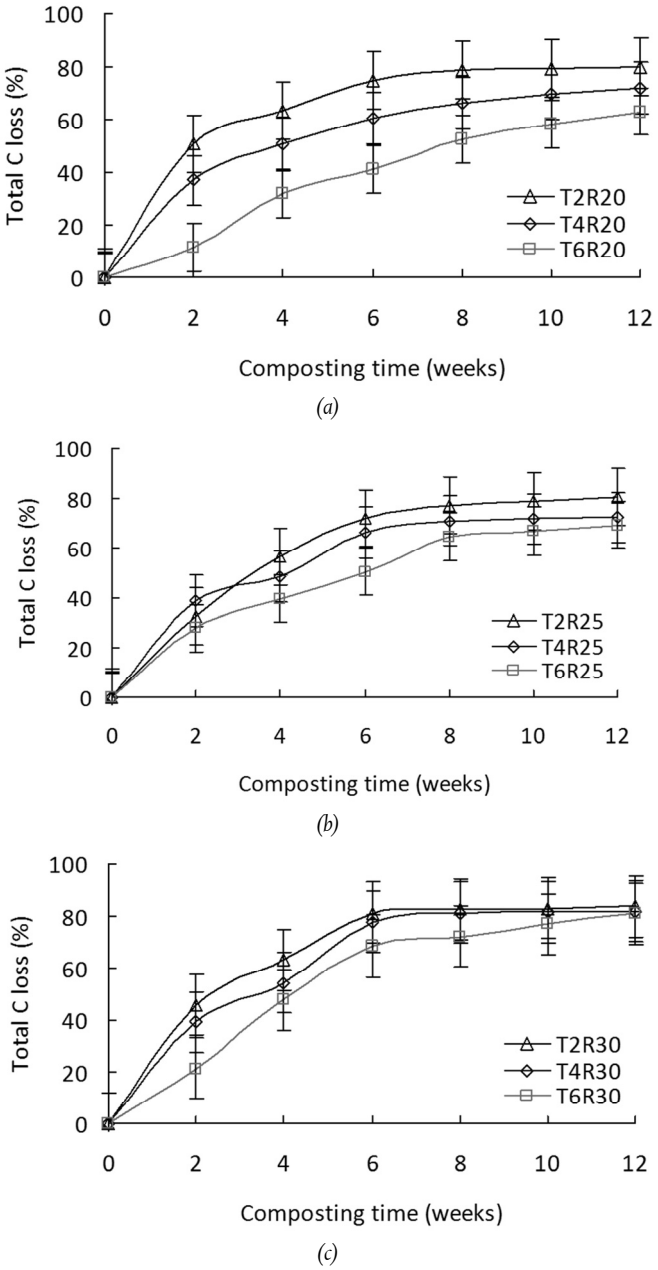

Figure 2: Changes in total C losses of composting piles with (a) C:N 20:1, (b) C:N 25:1, and (c) C:N 30:1. Error bars show standard errors of means (n = 3).

4. CONCLUSIONS

The main conclusions of the study are summarized as follows:

i. The stability of chicken litter compost was accompanied by a decline of compost temperatures to temperature near ambient level within a period of 87 days.
ii. Both C:N ratio and TF were significant ($p \leq 0.05$) on pile temperature, pH, total C, N, P and K losses and C:N ratio while DM was only affected ($p \leq 0.05$) by C:N ratio.
iii. The highest losses of total C occurred during the period of maximum OM degradation when the pile temperatures and pH values were above 33 °C and 7.7, respectively, and increased as C:N ratio and TF increased.
iv. Moisture loss increased as C:N ratio and TF increased.
v. A combination of 6 days TF and initial C:N ratio 20:1 (T_6R_{20}) produced the least total C loss.

REFERENCES

Barrington, S., Choiniere, D., Trigui, M. and Knight, W. "Effect of carbon source on compost nitrogen and carbon losses". Bioresource Technology 83: 189-194, 2002.

Bernal, M.P., Sanchez–Monedero, M.A., Paredes, C. and Roig, A. "Carbon mineralization from organic wastes at different composting stages during their incubation with soil". Agriculture, Ecosystems and Environment 69(3): 175-189, 1998.

Brake, J.D. "A practical guide for composting poultry litter". MAFES Bulletin 981, 1992.

Bremner, J.M. "Nitrogen-total". In: Sparks DL, editors. Methods of Soil Analysis. Part 3-Chemical methods. SSSA Inc., ASA Inc., Madison, WI, USA: 1085-1122, 1996.

Campbell, A.G., Folk, R.L. and Tripepi, R. "Wood ash as an amendment in municipal sludge and yard waste composting processes". Compost Science and Utilization 5, 62-73, 1997.

Charest, M.H. and Beauchamp, C.J. "Composting of de-inking paper sludge with poultry manure at three nitrogen levels using mechanical turning: behaviour of physico-chemical parameters". Bioresource Technology 81: 7-17, 2002.

Diaz, M.J., Madejon, E., Ariza, J., Lopez, R. and Cabrera, F. "Co-composting of beet vinasse and grape marc in windrows and static pile system". Compost Science and Utilization 10(3): 258-269, 2002.

Eghball, B. "Composting manure and other organic residues". Cooperative Extension, Institute of Agriculture and Natural Resources, University of Nebraska-Lincoln, 1997.

Eghball, B., Power, J.F., Gilley, J.E. and Doran, J.W. "Nutrient, carbon and mass loss during composting of beef cattle feedlot manure". Journal of Environmental Quality 26: 189-193, 1997.

Fang, M., Wong, J.W.C., Ma, K.K. and Wong, M.H. "Co-composting of sewage sludge and coal ash: nutrient transformation". Bioresource Technology 67: 19-24, 1999.

Gracia-Gomez, A., Roig, A. and Bernal, M.P. "Composting of the solid fraction of olive mill wastewater with olive leaves: organic matter degradation and biological activity". Bioresource Technology 86(1): 59-64, 2003.

Hansen, R.C., Keener, H.M. and Hoitink, H.A.J. "Poultry manure composting–An exploratory study". Transactions of the ASAE 36: 2151–2157, 1989.

Haug, R.T. "*The Practical Handbook of Compost Engineering*". Boca Raton, FL: Lewis Publishers, 1993.

Huang, G.F., Wong, J.W.C., Wu, Q.T. and Nagar, B.B. "Effect of C/N on composting of pig manure with sawdust". Waste Management 24: 805-813, 2004.

Hynes, E. "Gardening". Microsoft® Student 2008 [DVD]. Redmond, WA: Microsoft Corporation, 2008.

Kithome, M., Paul, J.W. and Bomke, A.A. "Reducing nitrogen losses during simulated composting of poultry manure using adsorbents or chemical amendments". Journal of Environmental Quality 28: 194–201, 1999.

Mercer, W.A. and Rose, W.W. "Investigation of windrow composting as a means for disposal of fruit waste solid". National Canners Association Research Foundation, Washington, DC: 20036, 1968

Michel, F.C., Forney, L.J., Huang, A.J.F., Drew, S., Czu Prenski, M., Lindeberg, J.D., Reddy, C.A. "Effects of turning frequency, leaves to grass mix ratio and windrow vs pile configuration on the composting of yard trimmings". Compost Science and Utilization 4: 26-43, 1996.

Misra, R.V., Roy, R.N. and Hiraoka, H. "On-farm composting methods". FAO Corporate Document Repository, 2003.

Ogunwande, G.A., Osunade, J.A., Adekalu, K.O. and Ogunjimi, L.A.O. "Nitrogen loss in chicken compost as affected by carbon to nitrogen ratio and turning frequency". Bioresource Technology 99(16): 7495-7503, 2008.

Paredes, C., Roig, A., Bernal, M.P., Sanchez-Mondero, M.A. and Cegarra, J. "Evolution of organic matter and nitrogen during co-composting of olive mill wastewater with solid organic wastes". Biology Fert. Soils 32(3): 222-227, 2000.

Rynk, R., van de Kamp, M., Wilson, G.B., Singley, M.E., Richard, T.L., Kolega, J.J., Gouin, F.R., Laliberty, L., Kay, JrD., Murphy, D.W., Hoitink, H.A.J. and Brinton, W.F. "On-farm composting". Northeast Regional Agricultural Engineering Services, Ithaca, New York, 1992.

Sanchez-Monedero, M.A., Bernal, M.P., Roig, A., Cegarra, J. and Garcia, D. "The effectiveness of the Rutgers system and the addition of bulking agent in reducing N-losses during composting". In: Van Cleemput O, Hofman G, Vermoesen A, editors. Progress in nitrogen cycling studies. Dordretch: Kluwer Academic: 133-139, 1996.

SAS. "Statistical Analysis Software Guide for Personal Computers". Release 9.1 SAS Institute Inc., Cary, NC 27513, USA, 2002.

Tiquia, S.M. "Further composting of pig manure disposed from the pig-on-litter (POL) system in Hong Kong". Ph.D. Thesis. The University of Hong Kong Pokfulam Road, Hong Kong, 1996.

Tiquia, S.M. and Tam, N.F.Y. "Fate of nitrogen during composting of chicken litter". Environmental Pollution 110: 535-541, 2000.

Tiquia, S.M., Richard, T.L. and Honeyman, M.S. "Effects of windrow turning and seasonal temperatures on composting of hog manure from hoop structures". Environmental Technology 21(9): 1037-1046, 2000.

Tiquia, S.M., Tam, N.F.Y. and Hodgkiss, I.J. "Changes in chemical properties during composting of spent litter at different moisture contents". Agriculture, Ecosystems and Environment 67(1): 79-89, 1998.

Tiquia, S.M., Tam, N.F.Y. and Hodgkiss, I.J. "Effects of turning frequency on composting of spent pig-manure sawdust litter". Bioresource Technology 62: 37-42, 1997.

Tuomela, M., Vikman, M., Hatakka, A. and Itavaara, M. "Biodegradation of lignin in a compost environment: A review. Bioresource Technology 72(2): 169-183, 2000.

Wong, J.W.C., Mak, K.F., Chan, N.W., Lam, A., Fang, M., Zhou, L.X., Wu, Q.T. and Liao, X.D. "Co-composting of soybean residues and leaves in Hong Kong". Bioresource Technology 76(2): 99-106, 2001.

Zhang, R., Ishibashi, K. and Day, D.L. "Experimental study of microbial decomposition in liquid swine manure, and generation rates of ammonia". In: Proc. Livestock Waste Management Conference. ASAE St. Joseph, Michigan, 1991.

Full Paper

EVALUATION OF SAWDUST AND SUGARCANE AS MOLECULAR SIEVE IN ADSORPTIVE CONCENTRATION OF AQUEOUS ETHANOL

E. A. Taiwo
Department of Chemical Engineering, Obafemi Awolowo University, Ile-Ife
etaiwo@oauife.edu.ng

O. Adeodu
Department of Chemical Engineering, Obafemi Awolowo University, Ile-Ife

ABSTRACT

Availability of ethanol in its absolute form is required for its use as automobile fuel additive. Purification of aqueous ethanol by conventional distillation is energy intensive with attendant difficulty of azeotrope formation. Effectiveness of dehydration of the aqueous ethanol mixtures past the azeotropic point by adsorption using hardwood sawdust and sugarcane fibre as adsorbents was therefore investigated in this study. Batch liquid-phase experiments were performed with both adsorbents at 10°C. Equilibrium data obtained from the experiments was fitted to Freundlich relation, Langmuir and BET correlation. Both the Langmuir and infinite form of the BET equilibrium theories were used to estimate the surface areas of the adsorbents. Sawdust preferentially adsorbed water from aqueous ethanol mixture while Sugarcane fibre relatively adsorbed ethanol from the mixtures. For the sawdust adsorbent, an improved ethanol concentration was obtained with increased concentration of ethanol in the feed as well as increased adsorbent to aqueous ethanol ratio. The experimental data fitted well into the Freundlich expression with an adsorption isotherm constant 'n' value of 1.3. However, BET and Langmuir gave a better fit with correlation coefficients of 0.9932 and 0.9978 respectively. Active surface area of adsorbent estimated using Langmuir and BET theories were 3.6339×10^6 and 3.3126×10^6 m^2kg^{-1}, respectively.

1. INTRODUCTION

World energy demand increased sharply over the last decade due to the recent heavy industrialization of populous countries like China and India. Nigeria energy sector depends heavily on petroleum fuel, especially, for transportation and electricity generation. To supplement the energy source, sustainable augmentation is required. This drives attention to renewable ones which will equally alleviate the attendant pollution problems. Ethanol, which is a popular alternative, presents several advantages over other fuels. As a renewable fuel, ethanol used in fuel-cell vehicles (Mattos and Noronha, 2005) or for stationary power plants generates far fewer greenhouse gases than conventional fuels such as gasoline or natural gas, since the CO_2 produced in the process is consumed in crop growths (Bentley and Derby, 2002, Duke 2003). The plan of NNPC to develop bioethanol in 10% blend with Premium Motor Spirit (PMS) as a first goal, would extend the life span of Nigeria's proven oil reserves of 36 billion barrels (CIA, 2006) appreciably.

Primarily, ethanol is produced on a commercial scale by the fermentation of sugar obtained from some local biomass: cassava in Nigeria, sugarcane in Brazil and corn in the United States. The fermentation product is quite dilute, containing about 10wt% ethanol. The high purity of ethanol requirement (greater than 99.5%) for automobile use is a dilemma (Adnadevic *et. al*., 2008). Distillation can only remove water from aqueous ethanol to a maximum ethanol concentration of 95%wt which is the azeotropic point of ethanol/water mixture. This is then followed by azeotropic distillation. Even, when distillation is used to obtain dehydrated ethanol, 50% of the total energy is consumed during this process (Carmo and Gubulin 1997). Thus, energy consumption problem in the process of dehydration of aqueous ethanol solutions obtained from fermentation broths is left to be solved. Also, the use of benzene as mass separation agent in azeotropic distillation makes the process not environmentally friendly. Selective adsorption onto zeolitic materials as an alternative to dehydration via distillation, is presently the most promising procedure for anhydrous ethanol production (Einicke *et. al*, 1995; Einicke, *et. al*., 2004; Bugaje and Muhammed, 2007). Adsorption of alcohols such as methanol (Badlani and Wachs, 2001) and ethanol (Benson, 2003) on the metal oxides surface occurs through an alkoxide species formed from the scission of the O–H bond.

The use of molecular sieves has grown quite rapidly mainly because sieves can be tailor-made to retain a specific adsorbate from a mixture. Regeneration characteristics were also impressive albeit at high temperatures. However, the relatively high manufacturing and regeneration costs of molecular sieves drove the need for investigation into cheaper adsorbents. The high density of hydroxyl groups present in both cellulosic and starchy biomass could enhance their water retaining capacity hence, the efficacy of local cellulosic biomass as adsorbent to dehydrate ethanol is investigated in this study towards enhancing the overall economy of bioethanol production.

2. THEORY

Adsorption occurs primarily on the walls of the pores or specific sites in the particle. The differences in the size, shape and polarity of species in the fluid mixture results into preferential adherent of some molecules (adsorbing species) on these sites. Adsorption isotherm, which is the relationship between the concentration in the fluid phase and the concentration in the adsorbent particles at equilibrium, can be used to assess the feasibility of adsorption operation for specific separation at a known temperature. In other words, the rate of adsorption is proportional to the adsorbate fluid concentration and the fraction of unoccupied space on the solid. The equation for liquid adsorption (Richardson *et. al*., 2002) is given as

$$\frac{C}{V} = \frac{C}{V_m} + \frac{1}{BV_m} \quad (1)$$

where,
C = solute concentration in liquid,
V = volume of solute adsorbed,
V_m = volume of solute in a monolayer spread over the adsorbent surface,
B = constant.

Equation (1) is Langmuir correlation. A system is described adequately by the Langmuir theory if a plot of (C/V) versus C gives a straight line. While Langmuir assumes a single layer of molecules, the theory developed by Brunauer *et. al.*, (1938) extended the Langmuir theory to a multilayer adsorption, built on different parts of the solid surface, with no interaction between each adsorption layer. The amount of surface associated with a particular thickness (monolayer, bilayer, etc.) is however constant. Richardson *et. al.*, (2002) detailed the mathematical derivation of the relation which can be adapted to liquid adsorption as

$$\frac{V}{V^1} = B_2 C \frac{1-(n+1)C^n + nC^{n+1}}{(1-C)[1-(B_2-1)C - B_2 C^{n+1}]} \quad (2)$$

where,
V = volume of solute adsorbed per unit adsorbent mass
V^1 = volume adsorbed contained in a monolayer spread over the surface
n = maximum number of adsorbate layers formed
B_2 = constant
C = initial concentration of the liquid phase

When n = 1, Equation (2) reduces to the Langmuir correlation, that is, Equation (1), but when n = ∞, Equation (2) is expressed linearly as

$$\frac{C}{V(1-C)} = \frac{1}{V^1 B_2} + \frac{B_2 - 1}{V^1 B_2} C \quad (3)$$

Equation (3) is an infinite form of the BET equation for dilute solute concentrations. A plot of the left hand term against C gives a straight line from which V^1 and hence active surface area can be calculated.

The empirical equilibrium relationship for liquid adsorption proposed by Freundlich (1926) is expressed as

$$C_s = \alpha (C^*)^n \quad (4)$$

where,
C_s=mass of solute adsorbed per unit adsorbent mass
C* =equilibrium concentration of solute in solution
α and n are constants.

The expression has been shown to be quite accurate for dilute solutions. A logarithmic plot of C_s versus C* gives a straight line from which α and n can be determined.

3. Methodology

The hardwood sawdust, and sugarcane fibre adsorbents studied were obtained locally in Ile-Ife. Sawdust was collected from the local sawmill industry while sugarcane fibre were obtained from the willd.

3.1. Adsorbent Pretreatment

Both the hardwood sawdust and sugarcane fibre were sundried, ground, sifted and clarified in a pretreatment process. These adsorbents were sifted first in a 40-mesh (0.0130 mm opening) screen to remove fine particles of material that might swell during operation. A 10-mesh (1.651 mm opening) screen was then used to filter out large particles. The adsorbents were then clarified in a pretreatment process to remove any impurities that may reside on the surfaces of the adsorbent particles. In pretreating the samples, 25 g of material were placed into a 500 ml Erlenmeyer flask, and enough distilled water added, to fill the flask to 500 ml. The mixture was stirred, the impurities were allowed to leach into the water medium and then drained. The washing was repeated several times until clear water was obtained. Then the adsorbent was oven dried at 90°C, chosen to keep the xylan and glucomannan polymers from changing to furfural polymers.

3.2. Determination of True Density

The adsorbent (20.0 g) was weighed and completely immersed in water using an overflow can. The true density was determined using the displaced volume of water by the equation:

$$\rho_{true} = \frac{m_{ads}}{v_{disp}} \quad (5)$$

where ρ_{true} is the true density, m_{ads} mass of the adsorbent and v_{disp} is the volume of water displaced.

3.3. Equilibrium Data Determination

The equilibrium data were obtained by the static method, which consists of placing inside 125ml flask a specific amount of the adsorbent in contact with specific mass of aqueous ethanol solution of known initial concentration. Several known initial concentrations were used in order to obtain wide range of isotherms at different temperatures. The flasks were maintained at constant temperature in a thermostatically controlled bath (NE2-D model supplied by Jenkon, UK) with an accuracy of ±0.1°C. Fluid phase concentrations were measured and the amount of water adsorbed by the adsorbent were determined by taking a mass balance between the phases, where ethanol was considered as the non-adsorbable component. This is given by the equation (Carmo and Gubulin, 1997)

$$q_x = \left[\frac{w_i - w_e}{w_i}\right]\left(\frac{M_{sol}}{M_{ads}}\right) \quad (6)$$

where,
q_x is the concentration of adsorbed phase after a specific time,
w_i is initial mass fraction of ethanol in solution
w_e is mass fraction of ethanol in solution at equilibrium
M_{sol} is mass of solution and M_{ads} is mass of adsorbent.

This equation assumes that the adsorbed material is primarily water, not ethanol. This hypothesis is in conjunction with the work of Rebar *et. al.* (1984), in which, the chemical affinity of starch to water was shown to be much greater than that of starch to ethanol. The same is also true for cellulosic materials with their high content of xylans (Benson, 2003).

3.4. Determination of the adsorption capacity

About 5 g of adsorbent sample was added to 50 g aqueous ethanol solution of known concentration in an adsorption vessel placed in the thermostatically controlled water bath (NE2-D model supplied by Jenkon, UK) at a pre-determined temperature. During the adsorption process, the adsorption system was homogenized by stirring at 400 rpm using electric motor-driven stirrer. Samples were taken from this adsorption system at regular time intervals. After centrifugation, the concentration of ethanol remaining in the supernatant was determined by measuring its refractive index using a Reichart-Jung Auto Abbe refractometer. The specific adsorption capacity of adsorbent (x) at a given temperature after certain adsorption period was calculated from the equation:

$$x = \frac{C_O - C}{m}(m_s) \quad (7)$$

where,
C_o is the initial concentration of the ethanol solution before adsorption (wt%),
C is the concentration of the ethanol solution after a certain adsorption time (wt%),
m_s is the mass of the solution (g),
m is the mass of adsorbent (g).

The adsorption degree of ethanol (α) was calculated from equation:

$$\alpha = \frac{x}{x_{max}} \quad (8)$$

where,
x_{max} is the maximum specific adsorption capacity of adsorbent for ethanol at a given temperature.

3.5. Determination of active surface area

The active surface area was determined from the plot of Langmuir and BET correlation, using Equations (1) and (3).

4. Results And Discussion

Fig. 1 shows the particle size distribution of the adsorbents studied. High percentage of both the sugarcane fibre and the sawdust has particle size in the range of 10 and 40 mesh sizes representing 0.013 and 1.651mm diameter. This particle range was used for the adsorption because particles of lower sizes can easily sift away. Thus, if used in column for adsorptive separation, it may result into clogging. This may lead to excessive column flooding which is undesirable for adequate column performance (Black, 1980). Higher particle size adsorbent on the other hand, may inhibit adsorption by reducing the surface area available for mass transfer, and hence, the amount of available adsorption sites.

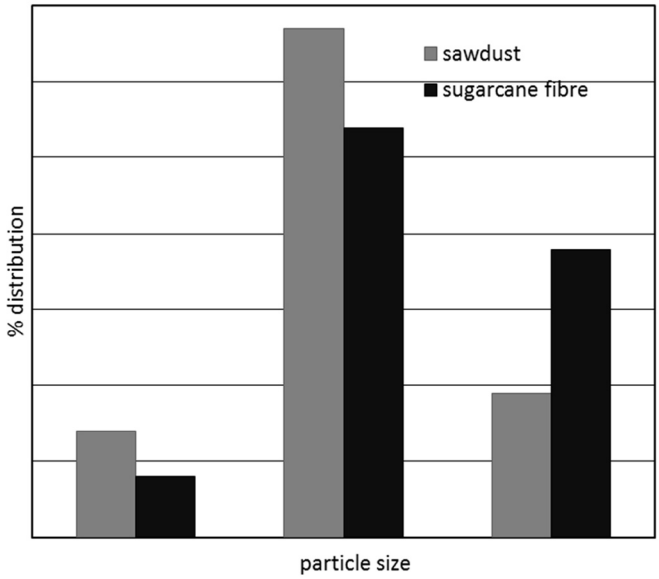

Figure 1: Particle size distribution for the adsorbents

The measured true density of sawdust and sugarcane adsorbents was 0.218 and 0.132 gcm^{-3} respectively. Thus, sawdust adsorbent having higher true density is expected to be more suitable adsorbent. It would provide a greater intimate contact since a more compact arrangement of the particles would be achieved inside the adsorption column. Greater surface area per unit volume would therefore be provided for adsorption to take place. The physical properties of the solvents (ethanol and water) used are reported in Table 1.

Table 1. Physical Properties of Ethanol and Water

Property	Ethanol	Water
Molecular Formula	CH_3CH_2OH	H_20
Molecular Weight	46.07	18.016
Specific Gravity	0.789	1.00
Melting Point(°C)	-112 0	0
Boiling Point(°C)	78.4	100
Solubility	∞ (in water)	

The preliminary adsorption experiments showed that sawdust adsorbed water from the aqueous ethanol solution, while sugarcane showed no significant adsorption for aqueous ethanol system. Adsorption capacity of 0.00022 g H_2O/g adsorbent was observed as the highest capacity for sugar cane fibre. Thus, sugarcane fiber was not experimented further. The equilibrium adsorption isotherms for the ethanol-water/ sawdust system at the temperatures of 30, 40, 50 and 60 °C are reported in Fig. 2. It is noticeable from this figure that its adsorption capacity decreased with increasing temperature. This might be due to increased kinetic and vibrational energy of the molecules with temperature, rendering only small net fraction of the molecules available for adsorption at equilibrium. At increased temperature, equilibrium shifts towards region unfavorable for adsorption due to exothermic character of adsorption process. The horizontal plateau zone in Fig. 2 represents the adsorbing capacity of the adsorbent at the varying temperatures.

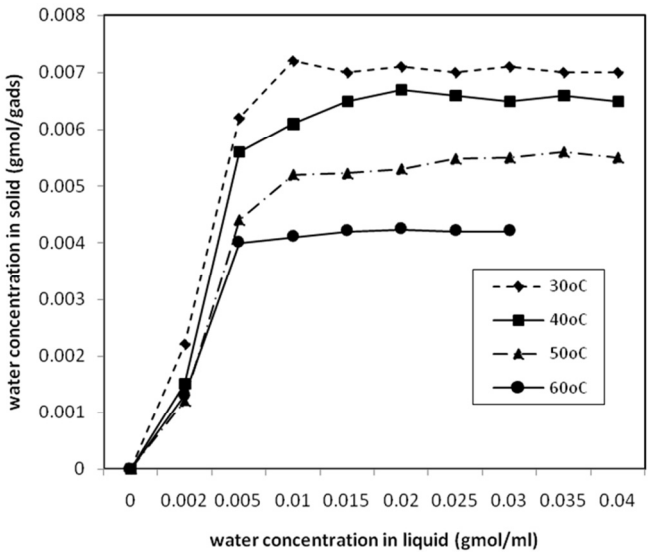

Figure 2: Equilibrium adsorption isotherms for the ethanol-water system on sawdust adsorbent

The adsorption capacity increases with increased initial water concentration in the mixture. This increased adsorption capacity with moisture content supports the theory of increasing capacity with increased water content until saturation point whereby no further site is available for adsorption. In this context, the uptake of water by sawdust adsorbent as the water concentration in the ethanol/ water mixture increases from 1 to 10 wt% reflected progressive water molecules uptake by hydroxyl group adsorption sites as the number of water molecules per unit volume increases. This increase in the concentration gradient leads to a significantly higher driving force. The cellulosic adsorbent has lignin, xylans and glucans. These polysaccharides, and the lignin, contain abundance of hydroxyl groups for the attachment of the water molecules. Thus the ligno-cellulosic substance offers the structural basis for adhesion to the cellulosic mass.

Investigation of the variation of concentration by adsorption using sawdust shows a progressive increase in concentration over time (Fig. 3). At about 120 – 200 mins, the concentration gradient (slope of curves) dropped indicating saturation zone. Above this point, no further adsorption takes place hence the maximum capacity of the adsorbent. This zone increases with decreasing concentration of

water content in the feed mixture. Fig. 3 also shows a dependence of final concentration on the initial feed concentration. At a feed concentration of 94 % ethanol by mass, an almost absolute ethanol was obtained. This significantly reflects purification pass the azeotropic point. Thus, by successive adsorption runs, absolute ethanol could be obtained using sawdust as adsorbent. As water moves from ethanol-water solution and adheres to the adsorbent particles, the thermodynamics of ethanol-water system is altered which in turn, modify the azeotropic situation resulting to breakage of the azeotropic tie between water and ethanol molecules.

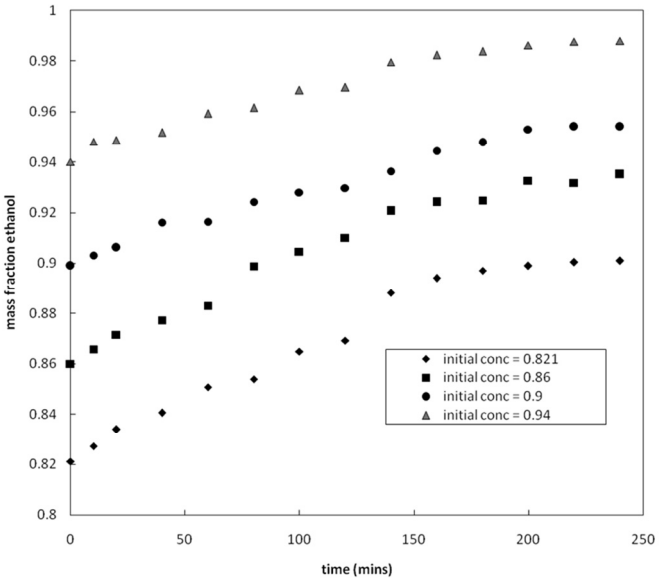

Figure 3: Adsorption characteristics of sawdust at varying ethanol concentration

The adsorption equilibrium data for sawdust adsorbent was fitted to the empirical Freundlich relation (Equation 4) in the MATLAB environment. The graph of logarithmic plot of Cs versus C* is shown in Fig. 4. The values of n and α were calculated from the slope and intercept and were found to be 1.3 and 26.3755, respectively. Since n is a measure of performance of adsorbent, the value obtained, coupled with the correlation coefficient value, R2 of 0.8930 suggests that dehydration of ethanol using sawdust as adsorbent is favorable, but there is need to improve upon the adsorbent to produce higher capacity for industrial application.

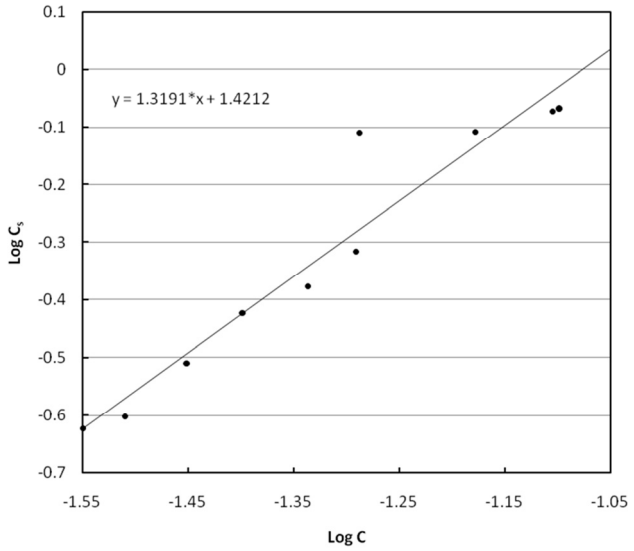

Figure 4: Freundlich correlation for sawdust adsorbent

By fitting the equilibrium data to a linear form of Langmuir and BET correlations represented by Equations (1) and (3), respectively, good correlation having correlation coefficients 'R^{2}' values of 0.9978 and 0.9932 for Langmuir and BET correlations respectively were obtained (Fig. 5). These values reflect a nearly homogeneous sorbent surface with a monolayer spread of adsorbed solute. An estimated volume of adsorbed solute contained in a monolayer spread over the homogeneous adsorbent surface was in the range 1.6505 and 1.8083 cm^3/g. Similarly, the active surface area in the range of 3.6339×10^6 and 3.3126×10^6 m^2kg^{-1} were obtained from the slope and intercept of plot.

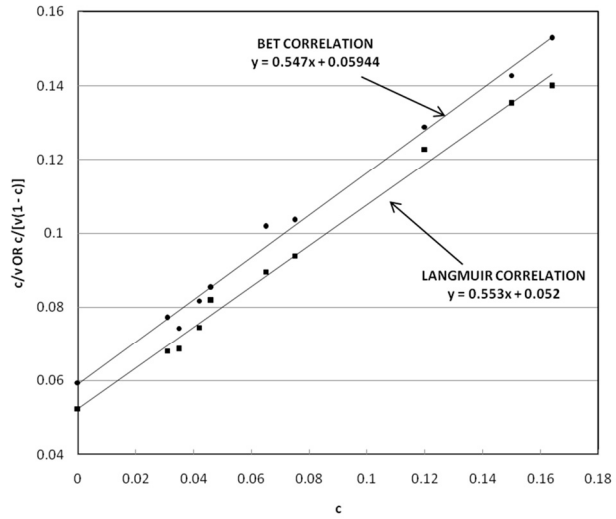

Figure 5: Langmuir and BET correlations for sawdust adsorbent

5. CONCLUSION

Sawdust preferentially adsorbs water from aqueous ethanol mixture and would be a good adsorbent for the purification of aqueous ethanol pass the azeotropic point with little or no energy consumption. This is of significance to ethanol/ biofuel production and national economy.

Adsorption capacity of the sawdust adsorbent is as high as 0.007gmol H_2O/g of adsorbent and decreases with increasing temperature. The active surface area fell between 3.6339×10^6 and 3.3126×10^6 m^2kg^{-1} with monolayer spread volume of 1.6505 and 1.8083 cm^3/g for the adsorbed solute.

REFERENCES

Adnadevic B.; Mojovic Z. and Abu-Rabi A. " The kinetics of ethanol adsorption from the aqueous phase onto zeolite NaZSM-5" Adsorption. 14:123-131. 2008

Badlani, M. and I. Wachs I. "Adsorption of methanol and methoxy on α-CrO(0001) surface Catal. Lett. 75, 137-139. 2001.

Benson T. J. "Dehydration of an ethanol-water mixture using lignocellulosic based Adsorbents", Unpublished M.Sc thesis, Dave Swalm School of Engineering, Mississippi State University. 2003.

Bentley, J. and Derby, R. "Ethanol and Fuel Cells: Converging Paths of Opportunity" Report for the Renewable Fuels Association, 2002.

Black C. "Distillation Modeling of Ethanol Recovery and Dehydration Processes for Ethanol and gasohol". Chemical Engineering Progress. 1980

Brunauer, S., Emmett, P.H. and Teller, E. "Adsorption of gases in multimolecular layers", Journal of American Chemistry. 60, 309 -314 , 1938

Bugaje I. M. and Muhammed I. A. "Biofuels as Petroluem extenders: Prospects and challenges in Nigeria". Petroleum Training Journal,4(1), 11-21, 2007

Carmo M. J. and Gubulin J. C. "Ethanol-Water Adsorption on commercial 3A zeolites: Kinetic and Thermodynamic data". Brazilian Journal of Chemical Engineering. 14(3), 1-12. 1997

CIA (2006) World Fact Book, available at http://www.cia.gov/cia/publications/factbook/nigeria. (Accessed in 3rd March 2008).

Duke J. S. "Burning Buried sunshine: Human consumption of ancient solar energy". Climatic Change, 61. 31-44. 2003.

Einicke W. D.; Gläser B.; Lippert R. and Heuchel M. "Liquid-phase adsorption of ethanol–water mixtures on NaZSM-5 zeolite with inorganic and organic binders". J. Chem. Soc. Faraday Trans. **91**(5), 971–974. 1995

Einicke W. D., Gläser B. and Schöllner R. "In-situ recovery of ethanol from fermentation broth by hydrophobic adsorbents". Acta Biotechnol. **12**(4), 353–358. 2004

Freundlich H. "Colloid and Capillary Chemistry". Methuen, London. 1926

Mattos, L.V. and Noronha F.B. "Hydrogen production for fuel cell applications by ethanol partial oxidation on Pt/CeO2 catalysts: the effect of the reaction conditions and reaction mechanism". Journal of Catalysis. 233, 453–463. 2005

Rebar V., Fischbach E. R., Apostolopoulos D., and Kikini J. L. "Thermodynamics of Water and Ethanol Adsorption on Four Starches as Model Biomass Separation Systems," Biotechnology and Bioengineering, Vol. XXVI, 513 – 517. 1984.

Richardson J. F., Harker J. H. and Backhurst J. R. "Particle Technology and Separation Processes' 5th ed. Elsevier, New Delhi, pp.979-986. 2002.

Full Paper

PRODUCTION OF MAYONNAISE FROM CORN OIL AND SOYAOIL USING SKIM MILK AS EMULSIFIER

O. C. Otitoola
Department of Science Laboratory Technology
Federal Polytechnic
Ede, Nigeria
lolaotitoola@yahoo.com

C. T. Akanbi
Department of Food Science And Technology
Obafemi Awolowo University
Ife, Nigeria

ABSTRACT

The objective of this study was to investigate the use of skim milk as an emulsifier in salad dressings and to compare its chemical, rheological and sensory properties with egg yolk based mayonnaise. Mayonnaises were produced (with or without gum) from corn oil and soya oil using egg yolk or skim milk as emulsifiers. The emulsification capacity (EC) of the emulsifiers, proximate composition, rheological and sensory properties of the mayonnaises were determined. The emulsification capacity was 50 and 57% for skim milk and egg yolk respectively. Addition of 0.2% sodium carboxyl methylcellulose increased the EC to 86 and 90% respectively. Moisture, protein, fat, sugar and starch of the samples were found to be in the range of 17.2-47.7%, 0.4-2.0%, 11.0-70.0%, 1.0-13.0 and 0.4- 6.1%. Egg yolk based dressings were more viscous (216-315Nsm^{-2}) than skim milk based dressings (90-216Nms^{-2}), although all products were found to be pseudo plastic. The results of sensory evaluation showed that egg yolk based dressings were preferred for such quality attributes as smoothness, texture, hand feel and mouth feel. However there was no significant difference ($P<0.05$) between skim milk based dressings and egg yolk based dressings in terms of taste, colour and flavour.

Keywords: *salad dressing, rheology, emulsifying property, proximate composition, sensory evaluation.*

1. INTRODUCTION

Mayonnaise is a stable emulsion consisting of oil, egg yolk with vinegar or lemon juice, condiments and spices. The emulsion is formed when the egg yolk coats the tiny droplets of oil in suspension thereby preventing it from separating out. Mayonnaise is generally regarded as a high-fat and energy-dense food because the oil content of a traditional mayonnaise is more than 65% (Depree and Savage, 2001). Research has found a positive association between high dietary fat consumption and development of chronic heart diseases and cancer. Several studies have been conducted to reduce the fat content of mayonnaises using fat replacers (Worrasinchai et al. 2006; Liu *et al.*, 2007). Oat dextrin (Shen *et al.*, 2011), polysaccharide gums (Su *et al.*, 2010) and enzyme (4-alpha-glucanotransferase) treated rice starch (Mun, et al, 2009) have been used as fat replacers in low fat mayonnaise and the fat content was reduced to half that of the conventional mayonnaise. It is important to know that while reducing the fat content of mayonnaise, the quality attributes (such as flavor and taste) contributed by fat in the mayonnaise is also reduced (Su *et al.*, 2010).

Although egg is the emulsifier used in mayonnaise it has been found to contribute significantly to high blood cholesterol as it contains a substantial amount of cholesterol which is naturally produced in the body. In traditional mayonnaise gums are generally used as emulsion stabilizers. Apart from stabilizing emulsion, gums are used for suspension of particulates and control of crystallization, inhibition of syneresis, encapsulation, formation of films and thickening in various industries (Benhura and Marume; 1993). Studies have shown that groundnut protein isolate; soybean isolate and casein also have good emulsifying properties and could be used as emulsifiers in mayonnaise production (Ramanathan *et al.*, 1978). Low calorie dressings have been developed using milk and locust bean as stabilizers (Chiralt *et al.*, 1992) however, not much information is documented on the physico-chemical, rheological and sensory properties of mayonnaise produced with skim milk as alternative emulsifiers. This study sought to bridge the gap.

2. MATERIALS AND METHODS

2.1. Materials

The ingredients used in the study included vinegar (8% acetic acid) and mustard cream, which were purchased from Leventis stores in Ibadan, Nigeria. Soybean oil and corn oil were obtained from Foodco supermarket, Ibadan. Sugar and salt were purchased from a local market in Ife. Skim milk powder was obtained from UTC stores, Ibadan. Eggs were obtained from Agricultural farms of the Obafemi Awolowo University and Sodium carboxyl methylcellulose from Neimeth Plc Lagos. All ingredients purchased were of standard quality and grade.

2.2. Preparation of the mayonnaises

The oil in water emulsions were prepared as presented in Table 1. These emulsions were prepared as described by Tressler and Sultan (1975) and Li -Hsieh and Regenstein (1991). The liquid phase containing the egg yolk (or skim milk powder), water, mustard cream, sugar and salt was blended into a smooth paste at speed 2 using Kenwood mixer for 2 minutes (during which sodium carboxyl methyl cellulose was added for emulsions with gum). The oil was then added while blending for 5 minutes after which vinegar was added and blended for 1minute. The emulsions were filled manually in bottles with caps, sterilized at 121°C for 15 minutes, cooled with chilled water then stored at between 8-10°C inside a refrigerator. Fig 1 shows the processing steps involved in the production of the mayonnaises.

2.3. Emulsification capacity of the emulsifiers

Emulsification Capacity (EC) of egg yolk and skim milk powder was determined by the method described by Yasumatsu *et al.* (1972). About 3.5g of each emulsifier was dispersed in 50ml of water followed

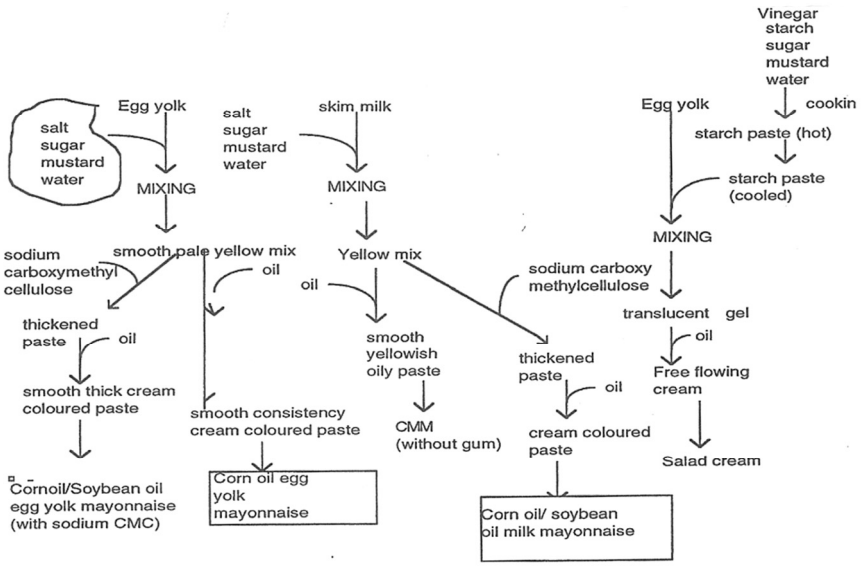

Fig 1: Processing steps in dressing production

Table 1 Percentage Composition of Mayonnaise

	CEM	CMM	CEM*	CMM*	SEM	SMM*
Corn oil	78.5	65.09	72.70	59.25	-	-
Soya oil	-	-	-	-	72.79	59.25
Egg yolk	5.90	-	16.28	-	18.28	-
Skim milk	-	5.40	-	3.33	-	3.33
Mustard	0.30	0.30	0.29	0.30	0.29	0.30
Vinegar	4.80	7.88	5.81	5.93	5.81	5.93
Sugar	1.80	1.80	1.45	1.48	1.45	1.48
Salt	1.20	1.20	0.45	0.44	0.45	0.44
Water	7.50	18.33	3.00	28.14	3.00	28.14
Sodium CMC	-	-	0.02	0.02	0.02	0.02

CEM = Corn oil egg mayonnaise
CMM = Corn oil milk Mayonnaise
CEM= Corn oil egg mayonnaise (with Gum)*
CMM= Corn oil milk Mayonnaise (with Gum)*
SEM = Soya oil egg mayonnaise
SMM = Soya oil milk Mayonnaise

by the addition of 50ml of oil and the mixture was homogenized at 10,000rpm for 1.0 minute. Equal volume of the emulsion formed was filled into centrifuge bottle and centrifuged at 2,050 rpm for 10 minutes. The emulsification capacity was then expressed as:

$$EC = \frac{\text{Height of the emulsified layer}}{\text{Height of the total contents in the tube}} \times 100 \quad (1)$$

2.4. pH of Mayonnaise

The pH values were measured at a temperature of 25°C using a pH meter

2.5. Composition Analysis

The official methods of analysis (AOAC, 1995) was used for the determination of protein, fat and moisture while sugar and starch were determined calorimetrically by the phenol-sulfuric acid method of Dubois *et al.* (1956) and Joslyn (1970). Caloric values were calculated using Atwater.

2.6. Rheological measurements

Rheological measurements of samples were made in a rheometer BS viscometer (Tokyo Keiki Co Ltd) equipped with rotors of varying sizes and numbers (1-7). Rotor 4 was used for the measurement. All the samples were kept at 25°C before measurement. The rheological properties of the samples were measured at various speeds: 1000, 2000, 5000 and 10,000 rpm. The conversion table as contained in the operation manual for the model and rotor was used to obtain the viscosity in Nm/s^2. The method of Chiralt *et al.* (1992) was used for thixograms. Thixograms were produced for each sample at 25 °C, using rotor 4 during a 4 minute- shearing at 5 seconds interval to reach constant shear stress.

2.7. Sensory evaluation

Sensory evaluation was carried out in the Department of Food science and Technology using a panel of eighteen assessors. Samples were assessed under normal illumination. Portions of 30g each of salad dressings were served in a randomized order within replicates and with respect to each assessor. The profiles – sourness, sweetness, saltiness, colour, mouth feel, hand feel, spread ability, texture, smoothness, consistency, flavour and overall acceptability- were assessed using five hedonic scale (1=dislike very much, 5=like very much). Values above 3 shows the samples were Data from hedonic assessment were averaged over all the panelists. The sample presentation order was randomized (Lin and Yeh, 2003).

2.8. Statistical Analysis

All analyses were replicated thrice. Data were subjected to One-way Analysis of Variance (ANOVA). Comparison of means used Duncan's multiple range tests. Differences of $P<0.05$ were considered to be significant. The statistical analyses were conducted using science analysis system (SAS)

3. RESULTS AND DISCUSSION

3.1. Emulsification capacity

Table 2 shows the emulsification capacity (EC) of the two emulsifiers. The EC of egg yolk was higher than that of the skim milk. This shows that egg yolk will form a stable emulsion more easily than skim milk. However addition of 0.2% CMC almost doubled the emulsification capacity. This observation showed that the ability of skim milk to form a stable emulsion can be greatly improved by gum. Carboxymethyl cellulose has been shown to increase viscosity of syrups (Collins and Dincer, 1973). Another factor influencing emulsification capacity include rate of mixing (Hegarty *et a.l*, 1963; Carpenter and Saffle, 1964; Swift et al, 1961) which was believed to be to due the fact that increased speeds produced greater shear rate which decreased the particle size of the oil droplet (Carpenter and Saffle, 1964). The addition of sodium chloride has been shown to increase EC over a pH range of 7-10 but at lower pH 3-6 (the pH of

mayonnaise) the increase in EC was observed only at 0.1M NaCl concentration (Ramanathan *et al*., 1978). This shows that the salt added to the mayonnaises has no effect on the emulsification capacity of the emulsifiers.

Table 2: Emulsification Capacity of the Emulsifiers

Emulsifier	% Emulsification capacity
Skim milk	50.00±0.41[b]
Egg yolk	57.14±1.51[b]
Skim milk with Na CMC*	86.21±0.69[a]
Egg yolk with Na CMC*	89.89±0.48[a]

** Sodium carboxylmethyl cellulose*

Means with the same letter in the same row are not significantly different at p < 0.05

3.2. pH of mayonnaise

The pH values of the mayonnaise are shown in Table 3. The pH of commercial mayonnaise was significantly lower than the prepared mayonnaises. Earlier studies had shown low fat mayonnaise to have higher pH than full fat mayonnaise due to the effect of the fat replacer used (Hathcox *et al*., 1995). Su et al (2010) observed the contrary, there was no significant difference between low fat mayonnaise and full fat mayonnaise.

Table 3: pH of Mayonnaise

Mayonnaise	pH
CEM*	4.17±0.01[c]
CMM*	4.09± 0.02[c]
SEM*	4.83±0.02[b]
SMM*	4.97±0.01[a]
CEM	4.76±0.05[b]
CMM	5.11±0.03[a]
Commercial Mayonnaise	3.77±0.02[d]

CEM = Corn oil egg mayonnaise
SEM = Soya oil egg mayonnaise
CMM= Corn oil milk Mayonnaise (with Gum)*
SMM = Soya oil milk Mayonnaise
CEM= Corn oil egg mayonnaise (with Gum)*
Means with the same letter in the same row are not significantly different at P < 0.05

3.3. Chemical composition and caloric values

The chemical compositions and caloric values of control (commercial mayonnaise) and prepared mayonnaises containing either egg yolk or skim milk are listed in Table 4. The moisture content of prepared salad dressings ranged between 17.24 and 46.30%. The moisture content of the prepared mayonnaise without gum (SEM and CEM) was very close to that of commercial mayonnaise (13.79%). These values agreed with 16.6% obtained earlier for full fat mayonnaise (Su et al, 2010). The mayonnaises prepared with gum had moisture values of 26.1%-46.3%. These values were within the range reported in literature (Tressler and Sultan, 1975; Su *et al*., 2010). Due to the high moisture content of the fat replacers (sodium carboxymethyl cellulose and skim milk) the moisture content of the samples increased (Su *et al*., 2010; Akoh and Min, 2002). The high moisture content could encourage lipid oxidation of the mayonnaise during storage. The reported protein value for commercial mayonnaise was found to be 0.9%, while the prepared dressing ranged from 0.42-1.97%. Addition of some egg white could greatly upgrade the protein level of egg yolk based dressings, although a weak mayonnaise (which may break due to the diluted emulsifier) will be produced (Meyer, 1960). The fat content of the prepared dressings (40% -70%) compared well with Literature value, 41-80% (Shen *et al*., 2011; Su et al. 2010).

The sugar content of milk based dressing (2.0 -2.8%) was higher than that of egg yolk based dressing (1.0 -1.8%). This is due to the effect of lactose in skim milk. The starch content of dressing with gum (0.7 – 0.9%) was about twice those without gum (0.4%). The milk based mayonnaise had lower caloric values (379-494 kcal/100g) compared to the egg based mayonnaise (537-639kcal/100g). Similar result was obtained for low fat mayonnaise, 385-398kcal/100g (Su *et al*., 2010) and 598kcal/100g (Shen *et al*., 2011). This shows that using skim milk as emulsifier could greatly reduce the caloric content of mayonnaise.

Table 4: Chemical Composition of Mayonnaise

Salad Dressings	Protein %	Fat %	Moisture %	Starch %	Sugar %	Energy kcal
CEM*	0.42	62.0	26.09	0.7	1.6	569
CMM*	1.15	47.0	36.75	0.8	2.8	442
SEM*	1.97	58.0	32.49	0.8	1.0	537
SMM*	1.60	40.0	46.30	0.9	2.0	379
CEM	0.49	70.0	17.24	0.4	1.8	640
CMM	1.20	53.0	17.50	0.4	2.8	495
Commercial Mayonnaise	0.90	57.0	13.79	0.4	1.8	628

CEM = Corn oil egg mayonnaise
SEM = Soya oil egg mayonnaise
CMM= Corn oil milk Mayonnaise (with Gum)*
CMM = Corn oil milk Mayonnaise
SMM = Soya oil milk Mayonnaise
CEM= Corn oil egg mayonnaise (with Gum)*
Means with the same letter in the same row are not significantly different at p < 0.05

3.4. Rheological properties of mayonnaise

All samples exhibited similar flow behavior with relation to speed. Most protein dispersions exhibit pseudo plastic flow behaviour in which the fluid exhibit shear thinning over a wide range of shear stress. The results obtained compared well with literature (Ramanathan *et al*., 1978). This shear rate thinning effect is due to the fact that in polymer dispersions, molecules are oriented and entangled when fluid is at rest. This random structure gives the system the tendency to maximize entropy. The material behaviour when sheared may be imagined to change over different shearing conditions. As the shear rate is increased, the asymmetric dispersed molecules tend to align themselves with the shear planes so that frictional resistance is reduced resulting in a decreased apparent viscosity (Collins and Dincer, 1973).

The thixogram curve is shown in Fig. 2. The dressings were found to be thixotropic. The shear stress decayed very quickly in the first minute of shearing and slowed afterwards (Chiralt *et al*., 1992). After about 1.5 minutes the rate of decay became constant for dressings without gum. The thixogram obtained for dressings without gum similar to that of mayonnaise, though it took a longer time to reach equilibrium.

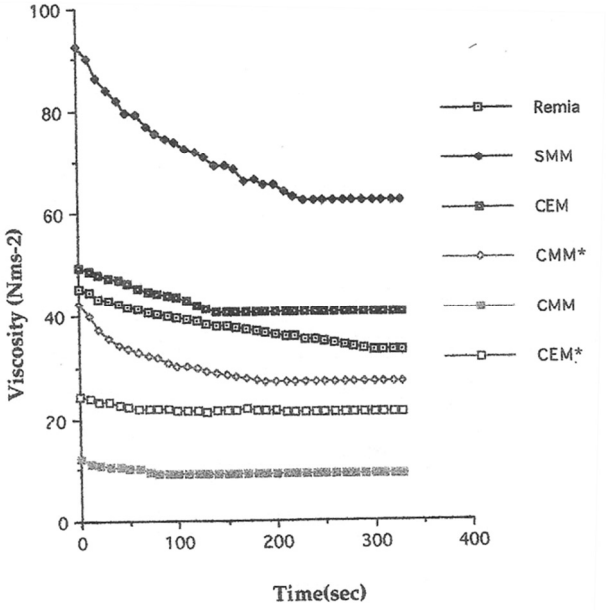

Fig 2. Thixogram curve of the salad dressings

3.5. Sensory properties of mayonnaise

The data for mean sensory scores of the quality attributes of the mayonnaise are listed in Table 5. The colour, taste and flavour of prepared mayonnaises were not significantly different (P<0.05) from the commercial mayonnaise. However, all samples were significantly different (P>0.05) in Textural attributes such as mouthfeel, smoothness, handfeel and consistency. In all quality attributes egg yolk mayonnaise was rated next to the commercial mayonnaise. Products of the same emulsifier were not significantly different (P<0.05) from each other in all quality attributes. Generally, all mayonnaises were acceptable to the panelists.

Table 5: The Means of Sensory Scores of Mayonnaise

Attributes	SEM	SMM	CEM	CMM	Commercial mayonnaise	F-value
Sweetness	2.42ab	1.81b	2.44ab	1.94b	2.78a	3.03
Saltiness	2.17a	2.19a	2.00a	1.81a	2.28a	0.64
Colour	3.31a	2.72a	3.25a	2.86a	2.56a	1.61
Mouth feel	3.33b	2.25c	3.28b	2.19c	4.16a	13.79
Hand feel	4.28b	2.78c	4.22b	2.70c	4.94a	31.83
Spread-ability	4.56a	3.67b	4.39a	3.66b	4.97a	5.32
Texture	4.03b	2.53c	3.47b	2.56c	4.76a	24.14
Smoothness	4.17b	2.83c	3.81b	2.94c	4.94a	22.55
Consistency	3.69b	2.67dc	3.22bc	2.25c	4.61a	20.68
Flavour	3.58b	3.00c	3.56b	3.67b	4.22a	6.38
Overall Acceptability	3.61b	2.92c	3.69b	3.33bc	4.44a	9.37

Means with the same letter in the same row are not significantly different at p < 0.05
CEM = Corn oil egg mayonnaise
SEM = Soya oil egg mayonnaise
SMM = Soya oil milk Mayonnaise
CMM= Corn oil milk Mayonnaise*

4. CONCLUSION

The rheological properties and chemical composition of salad dressings produced compared well with commercial mayonnaise. The egg yolk based dressings were found to be closer to the commercial mayonnaise in composition, rheological and sensory properties than the milk based dressings. The study has shown that skim milk could be used as an alternative emulsifier in mayonnaise. However the textural properties (to improve the mouthfeel) and the shelf life need further investigations.

REFERENCES

Akoh, C. C. and Min, D. B., *Food Lipids*. Marcel Dekker, New York, 2002.

AOAC *Official Methods of Analysis of the Association of Analytical Chemists* (15th edn). AOAC,Washington, DC, 1995.

Benhura, M.A.N. and Marume, M., Emulsifying properties of the mucilage extracted from Ruredzo (*Dicerocarum zanguebarium*). BSSC Biotechnology-Biochemistry Journal 57(12):1995-1998, 1993.

Carpenter, J.A. and Saffle, R.L., Simple method of estimating the emulsifying capacity of various sausage meats. Journal of Food Science. 29:774-781, 1964.

Chiralt A., Ferragut, V. and Salazar J.A., Rheological characterization of low-calorie milk based salad dressings. Journal of Food Science 57(1):200-202, 1992.

Collins, J.L.D. and Dincer, B., Rheological properties of syrups containing gums. Journal of Food Science 38:489-492, 1973.

Depree , J.A. and Savage G.P., Physical and flavor stability of mayonnaise. Trends Food Sci Technol 12:157–163, 2001.

Dubois, M.K.A., Gilles, J.K., Hamilton, P.A.R. and Smith, F., Colorimetric method for determination of sugars and related substances. Anal. Chem. 28:350-356, 1956.

Hathcox, A. K., Beuchat, L.R. and Doyle, M.P., Death of enterohemorrhagic *Escherichia coli* O157:H7 in real mayonnaise and reduced-calorie mayonnaise dressing as influenced by initial population and storage temperature. Appl Environ Microbiol 61:4172–4177, 1995.

Hegarty, G.R., Batilzer, L.J. and Pearson, A.M., Studies on the emulsifying properties of intercellular beef muscle protein. Journal of Food Science. 28:663-668, 1963.

Joslyn, A. M. Methods in Food Analysis. 2nd ed. A series of monographs. Academic Press NewYork, 1970.

Li Hsieh, Y.T. and Regenstein, J.M., Factors affecting quality of oil mayonnaise. Journal of Food Science 56(5):1298-1301, 1991.

Lin, C.S. and Yeh, R.Y., *Application and Practice of Sensory Evaluation*. Rui Yu, Taipei, Taiwan, 2003.

Liu, H., Xu, X.M. and Guo, S.D., Rheological, texture and sensory properties of low-fat mayonnaise with different fat mimetics. *LWT Food Sci Technol* 40:946–954, 2007.

Meyer, L. H., Oils and fat in Food Chemistry. 3rd edition Reinhold, New York, 1960.

Mun, S., Kim, Y.L., Kang, C.G., Shim, J.Y. and Kim, Y.R., Development of reduced fat mayonnaise using 4 alphaGTase-modified rice starch and Xanthan gum. Int J Biol Macromol 44(5):400-407, 2009.

Ramanathan, G., Ran, L.H. and Urs, L.N., Emulsification of groundnut protein. Journal of Food Science. 43:1270-1273., 1978.

Shen, R., Luo, S. and Dong, J., Application of oat dextrin for fat substitute in mayonnaise. Food Chemistry 126 (1):65-71, 2011.

Su, H.P., Lien, C.P., Lee, T.A. and Ho, J.H., Development of low-fat mayonnaise containing polysaccharide gums as functional ingredients J Sci Food Agric 90(5):806-812, 2010.

Swift, C.E., Lockett, C. and Fryer, A.J., Comminuted meat emulsions- The capacity of meats for emulsifying fat. Food Technology Journal. 15:468-473, 1961.

Tressler, D.K. and Sultan, W.J. Mayonnaise and Salad dressing in Cereals baked goods dairy and egg products vol. 2 AVI Food Product Formulary Series, 1975.

Worrasinchai, S., Suphantharika, M., Pinjai, S. and Jamnong, P., β-Glucan prepared from spent brewer's yeast as a fat replacer in mayonnaise. Food Hydrocoll 20:68–78, 2006.

Xu, S.Y., Stanley, D.W., Golf, H.D., Davidson, V.J. and Magner, M.L., Hydrocolloid/ milk gel formation and properties.Journal of Food Science 57:96-102, 1992.

Yasumatsu, K., Sawad, K., Moritaka, S., Toda, J. and Ishi, K., Whipping and emulsifying properties of soybean products Agricultural Biological Chemistry 36:719-727, 1972.

Full Paper

ARCHITECTURAL FRAMEWORK FOR MOBILE ONLINE HOTEL RESERVATION IN NIGERIA USING GSM TECHNOLOGY

A.I. Oluwaranti
Department of Computer Science and Engineering
Obafemi Awolowo University, Ile-Ife, Nigeria
aranti@oauife.edu.ng

O.O. Abiona
Department of Computer Information Systems
Indiana University Northwest
Garry, USA

O.S. Samson
Department of Computer Science and Engineering
Obafemi Awolowo University, Ile-Ife, Nigeria

ABSTRACT

Going by the continuous spread in the number and geographical coverage of mobile operators and facilities of the Global System for Mobile Communication (GSM) technology in Nigeria, there exists a compelling need for creating more value added services to the network. One example of a value added service is the mobile online Hotel Reservation Systems. This paper focuses on Hotel rooms' reservation being a vital part of the growing tourism industry in Nigeria, where quality of service could be critical; hence, it sets out to improve upon the existing Hotel reservation system. This it achieved by designing and evaluating an architectural framework for mobile hotel reservation system using the Global System for Mobile communication, which will create a platform for hotel reservation from any location. In order to achieve this, the existing hotel reservation systems in Nigeria were reviewed. We examined the development of hotel reservation system from manual method to computerized system to online reservation system. The problems and challenges inherent in these systems were highlighted. Arising from the challenges in the existing system, an improved GSM-based model was designed using the traditional *Model-View-Controller (MVC)* architectural pattern. This pattern consist of three parts: the Model which represent the data and business logic of the application; the View which is the actual screen that displays data and related commands to the users; and finally the Controller which receives user actions and dispatches them to the Model. The following performance parameters were used in the evaluation of the proposed architecture: response time, bandwidth consumption and cost per request.The results revealed that using the HTTP-based design approach, instead of the WAP based approach; a performance evaluation of the architecture used was carried out. The result revealed an improved response time; reduced bandwidth consumption leading to reduced bandwidth cost per request. Evaluation shows that the architectural framework is highly implemental and that it is of greater advantages over the existing hotel reservation systems in Nigeria because of its flexibility, availability, ease of use and reliable.

Keywords: *GSM, Hotel Reservation, Mobile, HTTP, WAP, WML*

1. INTRODUCTION

The hotel industry is a sub-system in the travel and tourism industry, which is concerned with the provision of lodging and other such services to different categories of people. However, for the hotel industry to flourish and meet the different demands placed on it by its teaming customers, it needs a fast and reliable reservation system that will help in handling its reservation processes. Hotel reservation system is, therefore, any process that helps in efficient and optimized allocation of hotel facilities to willing customers. Such systems, apart from being able to keep necessary information about the specific user hotel, it should be able to make informed decisions based on the information provided by customers on their hotel facilities preferences. Nigeria is taking a leading role in the mobile market. Since, the sector opened up in 1999 (IT-Edge, 2004), the mobile market has ushered in a once unknown competition amongst the Information Technology Providers in the Telecommunication industry. Companies have been licensed as global system for mobile communication (GSM) operators in Nigeria and, the operators have within five years connected over 20 million subscribers and evidently still growing. Because of this, there exist needs for value-added services to be added to the wireless network provided by the viable GSM technology in Nigeria. The paper focuses on developing a mobile reservation system for hotels through which customers can carry out booking for hotel facilities. This will invariably lead to increase in the number of users of GSM technology and coupled with the fact that people want dynamic change in location while they still have seamless access to remote information, the best solution to hotel reservation can never be best conceived than a mobile/wireless one.

Therefore, design and analysis of an architectural framework for the operation of a mobile hotel reservation system (christened mHotReservator) in Nigeria, is being proposed which would allow allocation of hotel facilities via micro devices such as mobile phones and other handheld devices.

The hotel business is an important industry in many countries, especially in those attracting a large tourist trade and as such has gone through a series of developmental stages over these past decades (Jacques, 2003; Bureau of Labor Statistics, 2005).

A hotel management system's function is to coordinate the different subcomponents involved in the planning, direction, and control of the operations of a hotel business. The subcomponents in hotel management system include: facility reservation/booking, building cleaning departments, hotel bars and restaurants, room services, security system, gaming surveillance, counter and rental clerks. Hotel reservation system is organized process/methods that assist in efficient and optimized allocation of hotel facilities to customers. Such systems, apart from being able to keep necessary information about the specific user hotel, it should be able to make informed decisions based on the information provided by customers on their hotel facilities preferences. Reservation as regards to hotel means advance booking, for instance of hotel room, train, coach, cars

Increased competition among establishments in the hotel industry has spurred many independently owned and operated hotels and other lodging places to evolve reliable reservation systems, which allow travelers to make hotel facility reservations.

The reservation system can be used to reserve a wide variety of entities, including: Hotel, motel, and resort rooms, Conference rooms; However, this work focuses on hotel rooms' reservation.

2. Related Works

Basically in Nigeria, the most rampant implementations of hotel reservation solutions are the following:

i. Manual hotel reservation system

Manual hotel reservation system, employs booking/reservation processes carried out by an assigned front-desk clerk who is responsible to the hotel as a public eye and, who, through his/her attitude and behavior, greatly influence the public's impressions of the hotel. Suffice to say that this method is fraught with many problems. (Samson, 2005)

ii. Computerized hotel reservation system.

It is however noteworthy to say that nowadays, front-desk clerks' work have been enhanced by the use of computer for the automation of the booking process (computerized hotel reservation). This of course, does take place at the hotel. This reservation system is just an enhanced manual method of hotel reservation where the record of individual customer is kept on the computer instead of the usual paper and ink form so that data could be more organized and safe. Aside the computer enhancement, the method has all the disadvantages of the manual system. (Samson, 2005)

iii. Call-in hotel reservation system

Many hotels in Nigeria encourage their customers to call-in to make lodging reservations via telephone. This method also has the disadvantage that the customer must know the hotel phone number and it could be expensive since call cost varies with duration of calls and because voice transmission is involved. Furthermore, a single hotel could be reached at a time; hence it could be time-wasting if the hotel cannot meet the requirement needed. (Samson, 2005)

iv. Online hotel reservation system

In the on-line hotel reservation system willing customers visit the web site of the hotel of interest where they would provide information concerning their preferred hotel facilities such as type of hotel room, number of room etc. The information is then used by the hotel to decide which facilities to make available for such customers. Payment facilities are also provided.

Galor System and Software Development Ltd developed Gilboa Software which was originally developed for PCs operating in a Local Area Network (LAN) under the DOS operating system but it has been designed to parallel the manual work of the travel agents. Wilkinson (1999) of Oceanic Consultancy Company Ltd developed Globekey, hotel reservation software designed for hotels, resort, guest houses, motel, villas, bed and breakfast etc.

Bug Softwares (1998) also developed web-based hotel reservation software called Bug Hotel Reservation system software. Bug was designed to simplify the task of online booking. When customers book online, they receive notification in 3 days by email and/or fax.

All of the above reservation systems have common features such as:

i. Provision of internet users with ability to make reservation when they browse their web sites.
ii. They allow travel agents to manually make reservations for their clients.
iii. They allow instant or between 2 to 3 days notification of reservation either through email, fax etc.

One of the problems with these methods is that the user/client needs a physical point of connection to the Internet. This restricts the users/customers from physical mobility. Similarly there is the need for the customer to know the existence of a hotel (especially its URL) before he/she can browse for its reservation information. Another demerit of these methods is that it links the user with a single hotel at a time. This can be time-wasting, especially if the hotel does not meet one's requirements.

3. Proposed Architecture

In view of the problems facing the afore-mentioned hotel reservation systems, this work seeks to proffer an alternative method of reservation that will eliminate the problems above. This solution christened mHotReservator uses M-commerce technology combining the telephone/fax using the Hypertext Transfer Protocol (HTTP). Nigeria is presently occupying the front seat in the global system for mobile phone market in Africa. Moreso, cost of mobile phone SIMs are getting cheaper. This invariably leads to increase in the number of users of hand-held devices. Conveniences in term of unhindered physical mobility are a welcome development by most users. Therefore, a reliable and a widely-acceptable solution which is also an improvement to the existing hotel room reservation systems is needed, and this can be found in *mHotReservator*. This work would allow hotel users to reserve hotel rooms via the use of hand-held devices such as mobile phones.

The feasibility of this work hinges on the following:

i. Acceptability and Relevance of the system
ii. Cost of Resources
iii. Availability of the needed technology (Wireless Network)

A mobile hotel reservation system in Nigeria is of utmost importance and relevance now, as it bring ease of operation to the Tourism and Hospitality business. Though, Cost is always a paramount factor in every decision-making procedure. The survey of the resources needed shows that the price of most computing equipment is falling by 50% every year. It is also a fact that GSM operators are expanding and extending the reach of their infrastructure making it readily available in most cities and local communities in the Nigeria. Suffice to say that this expansion more than anything else account for the projected success of Mobile Hotel Reservation System. A mobile hotel reservation system architecture would have the following components among others:

i. The client component
ii. The hotel registration component
iii. The host hotel component.

The relationship among the three parts are depicted in figure 1.

The client component

This component resides with the user of the mobile hotel reservation system. The component runs on mobile phones, pager or PDA. This component determines which host hotel component a request for room reservation belongs to, and dispatches it to that host hotel component. This component consists of

i. Facility for supplying customers' information.
ii. Facility for payment on successful room reservation.

Facility for supplying customers' information: It is a well-designed mobile hotel reservation system interface through which the customers put their information through to the system itself. Some of the costumer's information include name, customer's state of interest, particular location in the state, hotel category (this can be 5-star, 3-star or others),check-in date, check-out date, number of rooms etc.

Facility for payment on successful room reservation: This component also provides a means of payment for the reserved hotel room. This can be via a credit card.

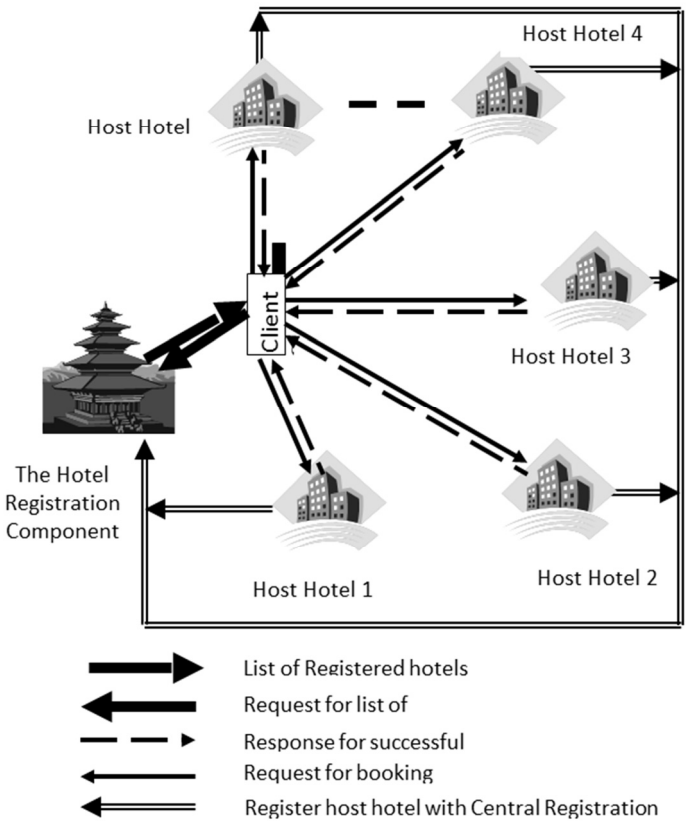

Figure 1 The three components of mHotReservator architecture and how they relate with one another

The central hotel registration component

It is also responsible for the registration of the host hotel components. This component has a house-keeping facility that allows the host hotel components to get registered and/or unregistered. Therefore, it keeps all records of registered host hotels. This component is responsible for deciphering and responding to requests for hotel list from the client component.

Facility for house-keeping: House-keeping facilities are used for record management activities. These can be any data base management system or any proprietary web-based record management application such as oracle and MySQL servers.

The host hotel component

This is the component that determines room availability, price if room is available. It also keeps all records of reservation made in the host hotel. It has a facility for acknowledgement of successful room reservation. It also has a local facility for house-keeping work.

Mobile device limitations impose many constraints on the design of wireless mHotReservator. The system must offer useful and usable interfaces even though the devices on which it runs have limited screen size, input capabilities, processing power, memory, persistent storage, and battery life. Wireless enterprise applications such as mHotReservator, are especially constrained because of their dependence on the network. The constraints imposed by a mobile network are significantly larger than those of a typical Web browser connected to the Internet (e.g. on-line hotel reservation system). It may be necessary for clients to operate offline or disconnected from the network for two reasons: the network quality may be poor (compared to wireline networks) and the typical use to which mobile wireless devices is put may justify it.

Wireless devices generally do not maintain a dedicated connection to the network, but connect only intermittently due to imperfect network coverage and poor network reliability (such as when the user enters an area where the network cannot be reached). These will be resolved by: Connecting to the network only when needed, consuming only as much data from the network as needed and remaining useful when disconnected.

The constraints faced would be taken into consideration under the following:

- The client design (presentation)
- The central hotel registration and the host hotel components
- Communication protocol
- Design tools used.

The client design

The client design of the reservation system used the traditional *Model-View-Controller (MVC)* architectural pattern. MVC is categorized as an architectural style, while others think of it as a design pattern (Mikko, 2004). The MVC pattern solves the problem of updating an application's views (UI screens) as its data changes. The MVC pattern consists of three parts: model, view, and controller.

Figure 2 shows the MVC pattern. The view contains the graphical user interface, which is the part of the application the user can see. When the user alters the data on the screen and then initiates an action, that action goes to the controller. The controller determines what kind of action has been requested and calls the appropriate interfaces of the model. The model consists of several components, classes, or packages, depending on the technology that implement the application's business logic.

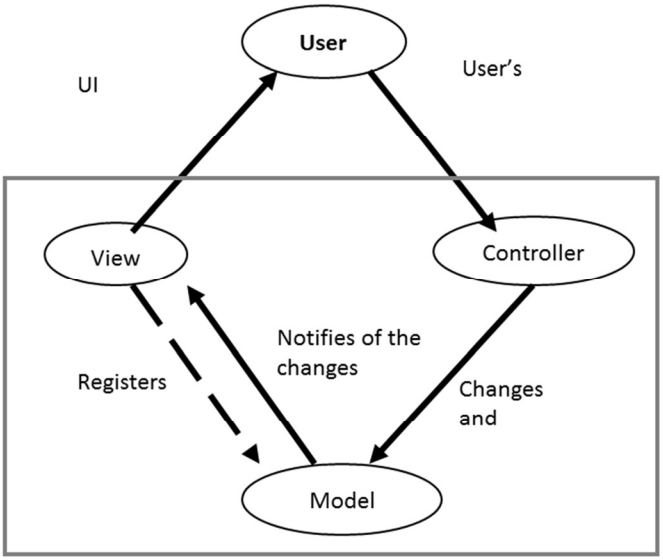

Figure 2 Elements of Model-View-Controller design pattern

Using MVC architecture offers benefits that may outweigh the costs.

Application flow is kept isolated from data and presentation: By separating the controller from the view and the model, the flow of the application is isolated in one place. Consequently, developers can look at just the controller to understand the client's perspective. They can also change the flow of the application by modifying the controller, with little, if any, disruption to the rest of the code.

Data is insulated from presentation: Separating the model from the view insulates the model from changes to the view. In other words, developers can alter the look of the client without having to change the model.

Presentation is not contingent on how the data is stored: Separating the view from the model insulates the view from the details of how the model works.

The view is not affected by how the model manages data: the model may get its data from local storage, from a server using HTTP net-working, or from an in-memory cache, or a combination of these sources.

The last benefit is probably the most important reason to use MVC for mobile clients. To use the network sparingly and remain

useful when disconnected, a client must decide when to fetch data from the server or from local storage. Local data strategies may be based on caching or synchronization to improve responsiveness and maintain data coherence. Partitioning these details into a model makes implementation, testing, and maintenance easier than if those details were spread out across the application. The client is the system component that resides with the client mobile device and is responsible for presenting responses from the central hotel registration and the host hotel components. The client design can be achieved using: Wireless Markup Language (WML)-based design approach and Hypertext Transfer Protocol (HTTP)-based design approach. In this work, the HTTP-based design approach was used based on its many merits over the WAP-based approach.

The central hotel registration and the host hotel components

The central hotel registration component and the host hotel component comprises of the web server and the database server. The database server is mainly is a database server employed in the paper is the hardware on which the data resides (Deitel and Deitel, 1999; Yank, 2003). The important feature of consideration in the design of this aspect is in order to ensure safe data sharing and durability. Durability implies that committed updates are permanent. Failures that occur after a commit cause no loss of data. Durability also implies that data for all committed transactions can be recovered after a system or media failure. These features ensures that persistent data always conform to their structure, that a series of operations can assume a stable set of inputs and working data, and that persistent data changes are recoverable after system failure (Samson, 2005).

The communication and messaging techniques

Under the communication and messaging techniques, we considered different communication and messaging method/format employed between: i. client and web server; ii. Web server and database server; and, iii.Client and database server.

Client-webserver messaging format: The simplest and most flexible messaging format involves sending HTTP GET or POST requests to a web server in a proprietary format (Taylor, 2002; Day, 2004). The web server then responds with a HTTP response in a proprietary format. In a HTTP GET request, the proprietary request data is encoded into the URL.

Webserver-database server messaging format: The web server and the database communicate via the use of some native communication techniques such as through Structured Query Language (SQL) embedded in Open Database Connection (ODBC) which allows for connection to different databases (Sun Microsystems, 2003).

Client-database messaging format: Here, there is no direct communication between the client and the database. Generally, clients should not connect directly to the database. Clients require a powerful interface, such as the ODBC API, via the web server to manipulate data on a remote resource. In some circumstances, it may be acceptable for clients to access the database directly; such clients could be database administrator for management tasks. As mentioned earlier, mHotReservator's design is a three-tier application and the architecture for it is as shown in figure 3.

4. System Preformation Evaluation

Evaluation was meant to justify mHotReservator by comparing its design approach to the existing mobile application design approaches. Essentially, the wireless application protocol (WAP)-based design approach and the hypertext transfer protocol (HTTP)-based design were compared. The parameters used for the evaluation are Response Time, Bandwidth Consumption, Bandwidth cost and Request Optimization.

The **response time** of the framework is the amount of time required for information requested from the Mobile Hotel Reservation

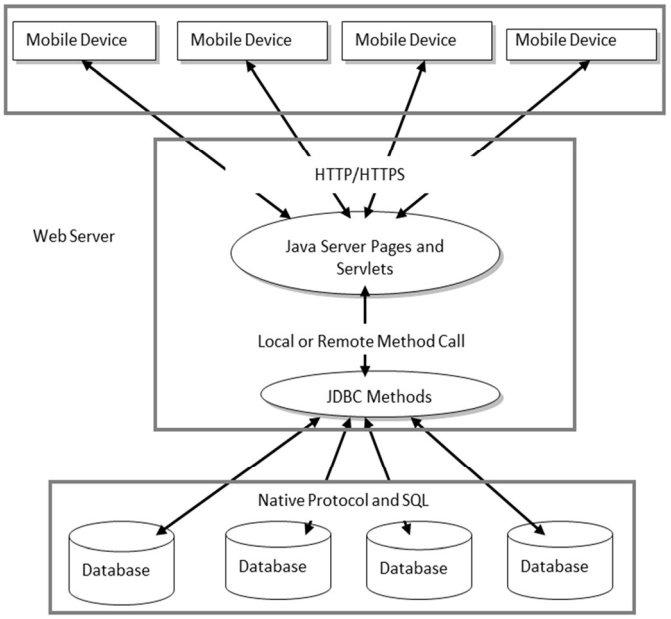

Figure 3 The three-tier system communication architecture of the three components

system to get to the requestor (the user). This is simply the time that elapses between when a request was made and the time a response to the request arrives. If we assume a fixed and a hypothetical bandwidth, *Bw*, then the relation for Response time for WAP and HTTP are given below:

$$Rt_{HTTP} = \frac{(rq + rp)}{Bw} \quad (1)$$

$$Rt_{WAP} = \frac{(rq + rp + fi)}{Bw} \quad (2)$$

Where *rq* is request size (in kilobyte), *rp* is response size (in kilobyte) and *fi* is formatting information size (in kilobyte). If we let Total request-response size (in kilobyte)

$$Trr = rq + rp$$

Then we can rewrite (1) and (2) generally as

$$Rt_{HTTP} = \frac{Trr}{Bw} \quad (3)$$

$$Rt_{WAP} = \frac{(Trr + fi)}{Bw} \quad (4)$$

$$Rt_{WAP} = \frac{Trr}{Bw} + \frac{fi}{Bw} \quad (5)$$

which gives

$$Rt_{WAP} = Rt_{HTTP} + \frac{fi}{Bw} \quad (6)$$

Since $\frac{Trr}{Bw}$ is the same for both WAP and HTTP, it shows that for any request, $Rt_{WAP} > Rt_{HTTP}$ because as *fi* increases, Rt_{WAP} increases. This relationship is depicted in Figure 4 using *Bw* of 64kbps while varying *fi*.

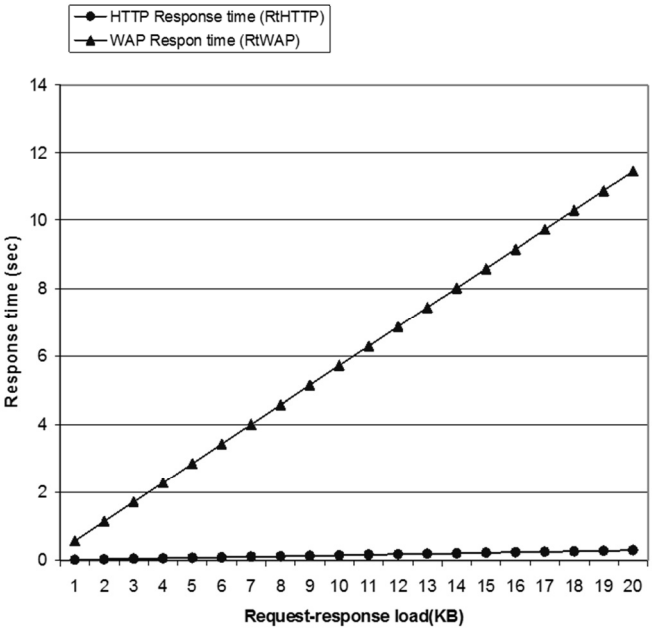

Figure 4 Response time for HTTP and WAP at Bw = 64kbps while varying fi

Bandwidth consumption of the architecture is the amount of data being sent through a data-transmitting medium, that is, a computer network in a given amount of time while considering WAP and HTTP. If the transmission time for request, *rq* is t_{rq} and transmission time for response, *rp* is t_{rp} then;

$$\text{Bandwidth requirement} = \frac{\text{Total request- response load}}{\text{Transmission time for total request-response load}}$$

therefore,

$$Bandwidth_{HTTP} = \frac{(rq+rp)}{(t_{rq}+t_{rp})} \quad (7)$$

$$Bandwidth_{WAP} = \frac{(rq+rp)}{(t_{rq}+t_{rp})} + B_{fi} \quad (8)$$

That is,

$$Bandwidth_{HTTP} = \frac{Trr}{T_{Trr}} \quad (9)$$

$$Bandwidth_{WAP} = \frac{Trr}{T_{Trr}} + B_{fi} \quad (10)$$

that is,

$$Bandwidth_{WAP} = Bandwidth_{HTTP} + B_{fi} \quad (11)$$

Where *Trr* is the total request-response size (in kilobyte), T_{Trr} is the total time for transmitting *Trr* in seconds and B_{fi} is the additional bandwidth required by the formatting information, *fi*. As B_{fi} increases, $Bandwidth_{WAP}$ increases. There is no doubt that for any request, $Bandwidth_{HTTP} \leq Bandwidth_{WAP}$. This is depicted in Figure 5 by varying $\frac{Trr}{T_{Trr}}$ between 5.5 – 550 kbps and randomly assigning values to B_{fi}.

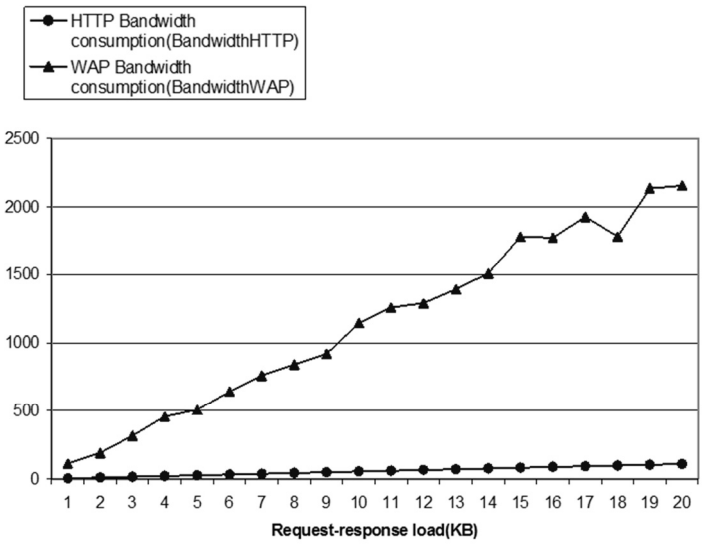

Figure 5 Bandwidth consumption for HTTP and WAP

Bandwidth Cost is the amount paid on bandwidth consumption while using the system. From equations (3) and (4), total response time were given as

$$Rt_{HTTP} = \frac{Trr}{Bw} \quad \text{from (3)}$$

$$Rt_{WAP} = Rt_{HTTP} + \frac{fi}{Bw} \quad \text{from (6)}$$

But $Bandwidth\cos t = Rt * Cost\ of\ 1kb/s$ therefore,

$$Bandwidth\cos t_{HTTP} = Rt_{HTTP} * Cost\ of\ 1kb/s \quad (12)$$

$$Bandwidth\cos t_{WAP} = Rt_{WAP} * Cost\ of\ 1kb/s \quad (13)$$

From (12) and (13) and following from (3) and (6), $Bandwidthcost_{WAP} > Bandwidthcost_{HTTP}$. This is depicted in Figure 6 at 1kbps costing ₦ 200.00.

Request optimization of the framework is a means of reducing the number of times requests are sent to server, thereby reducing access cost. Suppose that *n* is the number of supposed requests to the server and that *m* is the number of requests out of *n* made to local store of information on the mobile device. Hence,

$$Optimization\ index, e = n - m \quad (14)$$

As m increases, cost is greatly reduced and vice versa. Therefore,

$$Optimization\ index, e_{HTTP} = n - m \quad (15)$$

$$Optimization\ index, e_{WAP} = n \quad (16)$$

But optimization, $O \propto 1/e$. Therefore, as *e* decreases *O* increases and vice versa. This shows that $m = 0$ for e_{WAP} hence, for any group of requests $e_{WAP} \geq e_{HTTP}$ showing that $O_{WAP} < O_{HTTP}$. This can be depicted as shown in Figure 7.

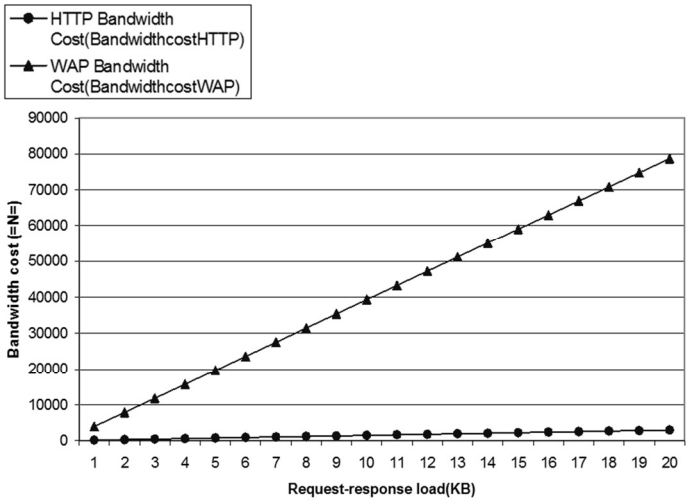

Figure 6 Cost per request for HTTP and WAP at 1kbps costing ₦200.00

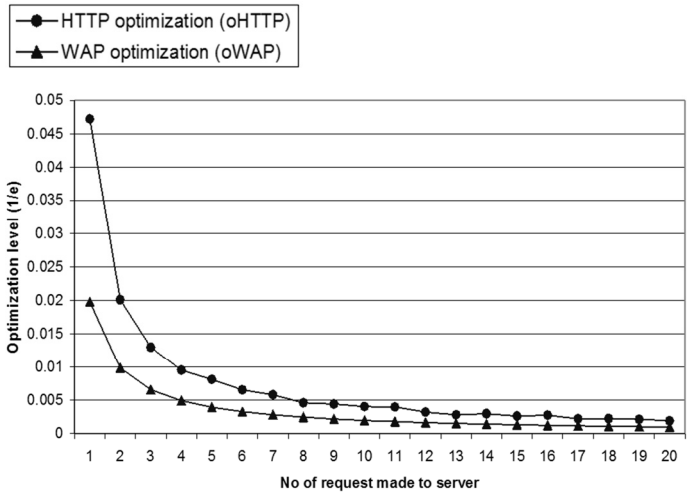

Figure 7 Request optimization for HTTP and WAP

5. CONCLUSION

The growth of Tourism and Hospitality business is predicated on an efficient technology driven industry that meet the basic needs of Clients with ease and convenience. The review threw light on the problems associated with the existing hotel reservation systems in Nigeria. Such problems include among others time-wasting processes, insecurity of information, need to physically to book, need for knowledge of hotel existence, error-prone processes.

The existing method requires Client to be physically available the hotel site or use a computer Terminal for online reservation. The designed architecture for mHotReservator proposed uses adaptable interfaces such as PDA, Mobile Phone, other handheld devices and it support flexible User interfaces. The framework empowered the Users of the system in making Hotel Reservation possible at any time, anywhere using GSM technology. Further research work is being considered to extend the technology to the West and Central African region and possibly, to incorporate the concept of Geographic Information System (GIS) into the evaluation of Hotels location relative to GSM base station locations.

REFERENCES

Anand Systems Inc. (2003) "*ResMe.Com: Online Hotel Reservation Software*". Internet document online at: http://www.resavenue.com/index_resav.jsp.

Armstrong, E.; Ball, J.; Bodoff, S.; Carson, D. B.; Evans, I,; Green, D.; Haase, K.; Jendrock, E. (2004), *The J2EE™ 1.4 Tutorial*, Sun Microsystems, Inc., California, 1.4 edition, pp.2-10

Bug Software LLC (1998) "*Bug Hotel Reservation: Online Reservation Software*". Internet document online at: http://www.bug_hotel.org/index.html.

Bureau of Labor Statistics, U.S. Department of Labor, (2005), *Hotels and Other Accommodations*, In: Career Guide to Industries, 5th Edition. Internet document online at: http://www.bls.gov/oco/cg/cgs036.htm.

Day, B. (2004), *Developing Wireless Applications using the Java 2 Platform, Microedition.* Day is a Technology Evangelist in Sun Microsystems, Inc. Internet document online at: www.billday.com.

Deitel, P. and Deitel, J (1999) *Java How to Program*, Prentice Hall, New Jersey, 3rd edition, p.888.

Galor Systems and Software Development Ltd. (1994) "*Gilboa: Online Hotel Reservation Software*". Internet document online at: http://www.galor.com/index.html.

Internet Merchandising Systems (2003) "*Voyager: Online Hotel Reservation System*". Internet document online at: http://wwwimscart.com/index.html.

IT-Edge (2004) No *More Fishing in Dangerous Water*, July/August 2004. ed, p10.

Jacques L. (2003), *Hotels: A Brief History.* Internet Article. Jacques is the Manager of the Hotel Marketing Department of Siemens Landis & Staefa in Zug, Switzerland. Internet document online at: http://www.ehlite.com/

Mikko K. (2004), *Simplify your GUI development process with MVC.* Internet Article, Mikko is the Technology manager, Enfo Solutions, USA. Online document at: http://www.ibm.com/

Sun Microsystems, Inc.(2003) *Designing Wireless Clients for Enterprise Applications with Java Technology. In:* A Java BluePrints for Wireless White Paper, p.3

Samson O. S. (2005) *Design and Simulation of a mobile hotel reservation system using global system for mobile communication (GSM) technology in Nigeria.* Unpublished thesis submitted to the Department of Computer Science & Engineering. Obafemi Awolowo University, Ile-Ife.

Taylor, M. (2002), *Strategies For J2ME MIDP/J2EE Integration Over HTTP*, Development Consulting Limited, North Yorkshire, U.K, Version 1.1. Online document at: http://www.developnet.co.uk.

Wilkinson, R. (1999) "*Globekey: Online Hotel Reservation Software*". Rod Wilkinson is a technical director of Oceanic Consultancy Company Ltd. UK..

Yank, K. (2003), *Build Your Own Database Driven Website Using PHP and MySQL*, SitePoint Books, U.S.A, 1st edition, pp.29-92.

Full Paper

INFLUENCE OF NUT CRACKING METHODS ON KERNEL QUALITY AND SEPARABILITY OF PRODUCT

O. A. Koya
Department of Mechanical Engineering,
Obafemi Awolowo University, Ile-Ife, Nigeria.
femikoya@oauife.edu.ng ; afemikoya@yahoo.com

M. O. Faborode
Department of Agricultural Engineering,
Obafemi Awolowo University, Ile-Ife, Nigeria.

ABSTRACT

In order to provide rational basis for design considerations to reduce kernel breakage in palm nut cracking using the conventional centrifugal nutcracker and enhance subsequent kernel and shell separation, comparison was made between the qualities of products from manually and mechanically cracked nuts. Furthermore, a 23 factorial experiment was conducted to determine the effects of the machine operational parameters and size of nut on nut cracking efficiency, quality of recovered kernels, and fragmentation of the nutshell. The nutcracker with a throughput capacity of 250 kg/h and a rotational of 1100 rpm gave a cracking efficiency of 97.2%, but kernel breakage was up to 9.7%; however, kernel breakage was 5.5% when the nutcracker was driven at a lower speed of 800 rpm and unbroken nuts were recycled. In contrast, cracking the nuts manually yielded 100% cracking efficiency and 2.0% kernel breakage, but the process was cumbersome and time consuming. In relation to the separation of the product, shell particles passing through a sieve with 10 mm aperture were 71.3% of the total shell produced using the nutcracker; compared with 58.3% from nuts broken manually.

Keywords: *Palm kernel, Nutshell, Nutcracker, Separation, Sieving, Palm nut.*

1. INTRODUCTION

The challenges of cracking the palm nut more effectively, while protecting the embedded kernel from being crushed has attracted some research attention (Manuwa, 1997; Obiakor and Babatunde, 1999; Koya and Faborode, 2005). The nutshell possesses high resistance to fracture, while the embedded kernel is friable. Therefore, the nuts are sufficiently dried to enable the kernel shrink away from the shell, to reduce the possibility of crushing the kernel during nut cracking process. At failure, the nut fractures in a catastrophic brittle manner with the shell breaking into pieces. Because the physical properties of the kernels and shells are close (Akubuo and Eje, 2002; Koya et al., 2004) the resulting mixture presents a difficult problem of separation, In addition, kernel breakage during nut cracking makes the separation more difficult and, the market value of the kernels is reduced. It is worthwhile therefore, to control the nut cracking process to enhance the separation of the mixture.

Existing methods employed in nut cracking are manual and the use of powered mechanical nutcrackers. In the manual method, the processor breaks the nuts, one at a time between two stones, and by experience, judging the magnitude of force applied once or repeatedly. The impact is controlled to prevent kernel breakage. Although, a hand-held nutcracker is described in the literature (Meriam and Kraige, 1998) it is rarely employed in palm nut cracking. Using the hand-held nutcracker is equivalent to loading a nut to failure between two parallel plates, which in a previous work (Koya and Faborode, 2005) was shown to be approximately equivalent to breaking the nut without multiple impacts in a centrifugal nutcracker. However, manual methods are cumbersome and time consuming, but have the advantage that the separation of kernel from shell is done simultaneously.

On the other hand, mechanical nutcrackers are usually of the centrifugal type: the nuts are fed into a slot turning at a very high speed and are hurled against a cracking ring; or with other types, fed against impact beaters turning at high speed. Therefore, large quantities of nuts are processed at a time, but efficient separation techniques are required to retrieve the kernels. The nut experiences multiple impacts, bouncing on the cracking wall, and secondary collisions with the walls of the rotating channels, or with the beaters. In spite of the repetitive impacts, however, some of the nuts are discharged uncracked; while, some kernels from cracked nuts are crushed. It may be assumed that broken kernels result because the kernels were further impacted excessively after the nutshell had been broken. Furthermore, because the palm nut is non-homogeneous and non-isotropic, variations exist in the nuts of same grade; the force required to crack a nut also depends on its diameter and its orientation against the cracking wall (Manuwa, 1998; Koya and Faborode, 2005). It is therefore reasonable to anticipate some optimum operating conditions, with lower impacts (as obtainable in the manual method) where, recycling uncracked nuts in the machine, all the nuts may be broken with no kernel breakage. The most challenging process in kernel recovery, once the nuts are broken, is the separation of the kernel and shell mixture. Whilst, most separators are liquid based, requiring enormous energy in re-drying the product; attempts to separate the kernels from the shell without admission of liquid have not yielded satisfactory results (Olie and Tjeng, 1974; Hartley, 1977; Akubuo and Eje, 2002; Koya and Faborode, 2006). Sophisticated equipment consisting of hydro-cyclone, conveyors and bin dryers are also too expensive for most farmers who operate as clusters of small scale processors, but providing about 77% of total yearly production (Owolarafe et al., 2002). Evidently, most difficulties in the dry systems were experienced with kernels and shell particles of comparable size grade; but better efficiencies were anticipated with shell particles of uniform but distinct sizes from the kernels.

Consequently, the focus of this work was to investigate the benefits of low impact nut cracking (represented by the manual method) in terms of kernel quality and separation of product, in comparison with the use of the conventional powered nutcrackers. It was expected that such investigation would lead to the identification of necessary modifications in the design of the conventional powered nutcrackers.

2. Materials And Methods

2.1. Sampling Technique

A local palm oil processing settlement in Ayekoka, South of Ile-Ife, Nigeria, was chosen for the purpose of the study. Only Dura variety of the oil palm was available on the farm. The farmers operate as clusters of processors, cracking the nuts in turns in the community based mechanical nutcracker; alternatively, the farmers break the nuts manually between two stones. The nuts were sufficiently dried but not graded before being cracked, using any of the two methods.

In course of the experiment, a measure of 150 kg of the dried palm nuts was procured. The exact moisture content of the nuts was later determined in the laboratory, using the oven method, drying at 130°C for 6 hours, as specified for oil-bearing seeds (ASAE, 1982). Furthermore, a representative sample of the nuts was passed through a set of sieves BS 410 (Endecotts Limited, London) with 25, 20, 14 and 10 mm apertures to grade the nuts, to provide a description of the size distribution.

2.2. Determination of Nut Cracking Efficiency, Product Quality and Distribution of Nutshell Particles

2.2.1. Process Equipment and Preliminary Experiment

The centrifugal nutcracker available at the cracking station was powered by a 5 hp Lister engine, with the provision for adjusting its mean speed. As a prelude to the main experiment, the exact operating speed of the nutcracker was measured using a hand-held electronic tachometer. The internal diameter of the cracking ring was measured with a venier caliper. The nuts were gradually fed into the machine in 10 kg batches; and the feed rate was estimated, dividing by the average time taken. The product (kernel and shell mixture) for each experimental run of three replicates was analysed separately. The least speed at which nut cracking was feasible and the highest speed yielding reasonably low kernel breakage were noted. These speeds were designated as low and high speeds, respectively, in the subsequent main experiment.

2.2.2. Influence of Cracking Methods

(a) Manual Method

In the manual nut cracking, five of the skilled processors on the farm were randomly selected and each was commissioned to crack 5 kg of nuts. Although, the processor separated the whole kernels from the shells simultaneously, as in practice, the lot from each processor was kept separately for further analysis.

(b) Mechanical Method

Based on the results of the preliminary experiment, a 2^3 factorial experiment was designed to determine the effects of machine speed, nut size and the loading times on nut cracking efficiency and percentage kernel breakage.

The nutcracker was driven at 800 or 1100 rpm, which were respectively, the low and the high speeds. The nut sizes were those retained on the 14 and 20 mm apertures; while the two loading times referred to running the nuts through the machine at once, or twice (sorting and recycling the uncracked nuts only).

2.2.3. Performance Indices

The kernels were sorted from the shells. The weights of the whole and the broken kernels were determined, measuring on an electronic top balance (Mettler, PL 1200) to estimate the cracking efficiency and the percentage kernel breakage. The cracking efficiency ϵ_c was computed using Eqn. 1.

$$\epsilon_c = \frac{N_b}{N_T} \times 100\% \quad (1)$$

where, N_B is the mass in kg of broken nuts; and N_T is the mass in kg of nuts fed into the machine.

The percentage kernel breakage η_K was defined as

$$\eta_K = \frac{K_b}{K_T} \times 100\% \quad (2)$$

where, K_b is the mass in kg of damaged kernels, and K_T is the mass in kg of all the kernels recovered from the nuts.

The percentage kernel recovery K_R was therefore defined as follows:

$$K_R = (100 - \eta_K) \quad (3)$$

The shell particles from each cracking method were graded using the set of sieves. This was to determine the difference in the shell particles size distribution compared with that of the kernels, in view of separating the mixture.

3. Results and Discussion

The moisture content (percentage wet basis) of the nut at the time of the experiment was 13.4%. The size distribution of the nut is shown in Fig. 1, which shows the cumulative proportion of nuts retained on the sieves with 20, 14 and 10 apertures as 23, 97 and 100%, respectively. The result implies that the nuts may be divided into two grades, defined by those retained on the sieves with 20 and 14 or 10 mm apertures; but about 3% of the nuts (consisting of small-sized nuts) will be lost if the sieve with 14 mm aperture is used. The average feed rate was calculated to be 250 kg/h.

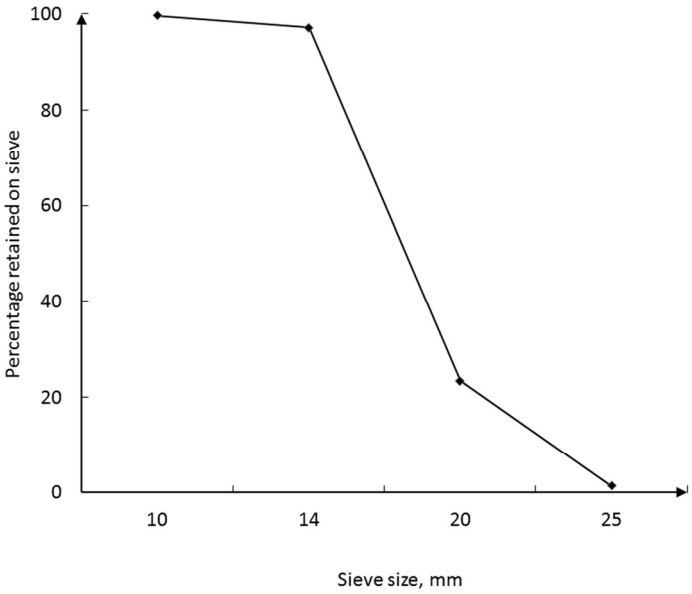

Fig. 1: Size Distribution of Nut Samples used in the Experiments

3.1. Effect of Nut Cracking Methods on Cracking Efficiency

The cracking efficiency and the percentage kernel breakage from the two cracking methods are shown in Table 1. The 100% cracking efficiency obtained in manual cracking is reasonable, since the processor ensures that all the nuts are broken; albeit, some kernels (2.0%) are also broken in the process. The mechanical nutcracker gave a cracking efficiency of 97.2%, but 9.7% of the kernels were broken, when driven at 1100 rpm. Although, this efficiency is lower than the 100% cracking efficiency obtained when the nutcracker was operated at the conventional speed of 1450 rpm, kernel breakage was reduced by about 52%. The percentage kernel recovery (90.3%) is also an improvement over the data reported by Obiakor and Babatunde (1999)

in respect of a similar nutcracker, with 95% cracking efficiency and 85% kernel recovery when driven at 1500 rpm.

Table 1: Efficiencies of Two Palm Nut Cracking Methods

Method of Nut Cracking	Cracking Efficiency, %	Kernel Breakage, %
Manual (between two stones)	100.0 (0.0)*	2.0 (0.0)
Centrifugal Nutcracker		
driven at:		
1450 rpm	100 (0.0)	20.0 (0.2)
1100 rpm	97.2 (0.2)	9.7(0.5)
800 rpm	89.4(1.5)	5.5(0.4)

**Numbers in parentheses are the standard deviations.*

However, operating the nutcracker at too low a speed (800 rpm and below) may not be beneficial, except the unbroken nuts are sorted out and re-introduced into the machine. It was observed that the unbroken nuts consisted of the small-sized nuts.

3.2. Effect of Nut Cracking Methods on Shell Fractions

The sieve analysis of shell particles obtained from the two nut cracking methods are shown in Fig. 2. From the result, mechanically cracked nuts yielded smaller shell fractions than the manually cracked nuts, and the difference, using paired t-test (Barnes, 1994) is significant at the 95% confidence level. Shell particles passing through the sieve with 10 mm aperture are 71.3% of the total shell produced using the nutcracker and 58.5% of shell from manually broken nuts. This result may be attributed to the fact that the nutcracker breaks the nut by impact, and with repeated impacts, the brittle nutshell is shattered into smaller fractions; albeit, with attendant kernel breakage, because the kernel is similarly affected. On the other hand, manually cracked nut is impacted skillfully by the processor until the nut breaks and without further impact on the nutshell once the kernel is extracted; thus, terminating the shell comminuition process.

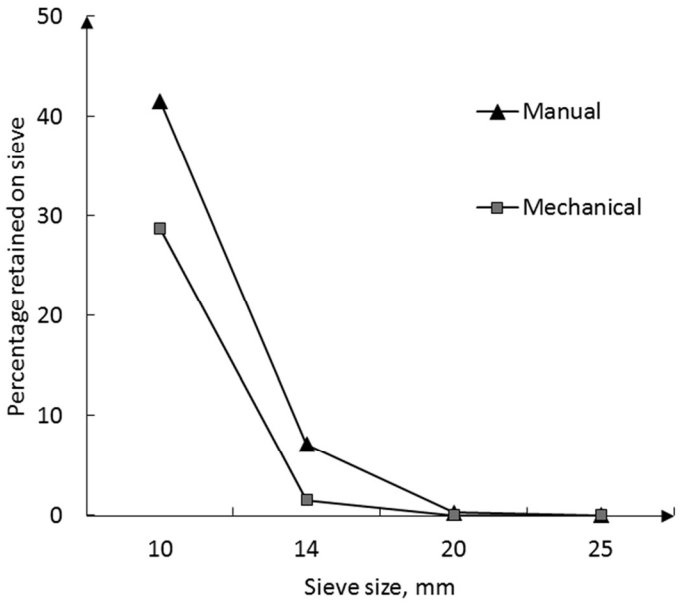

Fig. 2: Size Distribution of Shell Particles from Palm Nuts Cracked Manually and Mechanically

It is worthy of note that the least mean diameter of Dura kernels is more than 10 mm (Koya, 2004). Hence, the large percentage of shell particles smaller than the kernels suggests benefits in the use of sieves to pre-clean palm kernel and shell mixture when mechanical nutcracker is used. The remaining mixture may then be further separated by other methods.

3.3. Effects of Machine Operational Parameters on Product Quality

The result of the 2^3 factorial experiments on the effects of machine's rotational speed, nut size and the loading times on the quality of product from mechanically cracked nuts is shown in Table 2. The mean value of each experimental run was compared with the associated standard error to determine the bound of the statistic (Box et al., 1998). The effects of kernel size and machine, as well as kernel size and loading times have large interactions, so that the contributions of each pair are confounded statistically.

Table 2: Estimated Effects from 2^3 Factorial Design On Quality of Product From A Mechanical Nutcracker

Effect	Estimate ± Standard Error	
	Cracking Efficiency, %	Kernel Breakage, %
Average	95.5 ± 1.0	7.7 ± 0.1
Main effect:		
Kernel size, K	8.0 ± 1.9	5.6 ± 0.2
Speed, S	6.0 ± 1.9	4.3 ± 0.2
Number of runs, N	4.6± 1.9	0.4 ± 0.2
Two factors interactions:		
K x S	-6.8± 1.9	0.0 ± 0.2
K x N	-3.8± 1.9	-0.6 ± 0.2
S x N	-1.8± 1.9	0.0 ± 0.2
Three factors interaction:		
K x S x N	2.5± 1.9	-0.3 ± 0.2

Cracking efficiency increased up to 100% ($p < 0.01$) at 1100 rpm for both nut sizes; similarly, 100% cracking efficiency was obtained running the unbroken nuts through the machine while operating at 800 rpm. Kernel breakage increased by 5.6% ($p < 0.05$) when bigger nuts were fed into the machine compared with when the smaller nut were fed at the same speed, confirming the need to grade the nuts for cracking at different speeds. Operating the nutcracker at the 1100 rpm increased kernel breakage by 4.3% ($p < 0.05$) compared with cracking the same grade of nuts at 800 rpm. The foregoing observations are justified because the bigger nuts are subjected to higher impacts when the two grades are hurled at the same speed. When the nut is recycled at the lower speed, the nutshell fractures at lower impact; thus, reducing the incidence of kernel breakage; but the shell particles, being brittle, are further broken into smaller factions. This development is beneficial because the finer shell particles will enhance the use of sieves in pre-cleaning the mixture.

Based on these results, therefore, the conventional mechanical nutcracker will give better performance in terms of cracking efficiency and kernel recovery, if it is operated at lower speed and unbroken nuts are recycled. Alternatively, a multistage nutcracker, equipped with twin cracking chamber in series, and driven at speeds lower than the operating speed of an equivalent conventional nutcracker should give similar result. The lower limit of the driving speed will be determined by the fracture resistance of the nutshell and the hardness of the cracking chamber.

4. Conclusion

The performances of manual and mechanical nut cracking methods were compared in the study. Operating the conventional centrifugal nutcracker at 1100 rpm gave minimum cracking efficiency of 97.2% at a higher throughput capacity; albeit, with higher kernel breakage, compared with breaking the nuts manually. Shell particles from the nutcracker were finer, enhancing pre-cleaning of the kernel and shell mixture.

Furthermore, the study showed that the undesirable kernel breakage, associated with the use of the conventional centrifugal nutcracker, can be reduced by driving the machine at lower speeds;

and recycling the unbroken nuts. Consequently, the study provides the basis for future modification of the conventional nutcracker as a multistage nutcracker, to reduce kernel breakage while enhancing subsequent separation of the resulting palm kernel and shell mixture.

REFERENCES

Akubuo, C. O. and Eje, B. E., "Palm kernel and shell separator" Biosystems Engineering, 81(2): 193-199, 2002.

ASAE "Standard S352. Moisture measurement – grains and seeds". Agricultural Engineers Year Book, ASAE, St. Joseph MI, p. 345; 1982.

Barnes, J. W., "Statistical analysis for engineers and scientists; a computer-based approach".McGraw-Hill, Inc., New York, 1994.

Box, G. E. P., Hunter, J. S. and Hunter, W. G., "Statistics for experimenters: design innovation and discovery, 2nd Edition". John Wiley, New York, 1998.

Hartley, C. W. S., "The oil palm". Longman Publishers, London, 1977.

Koya, O. A., "Studies of the mechanics of nut cracking and centrifugal separation of palm kernel and shell mixture". Unpublished PhD thesis, Obafemi Awolowo University, Ile-Ife, Nigeria, 2004.

Koya, O. A. and Faborode, M. O., "Mathemetical modeling of palm nut cracking based on Hertz theory". Biosystems Engineering. 91(4): 471 – 478, 2005.

Koya, O. A. and Faborode, M. O., "Separation theory for palm kernel and shell mixture on a spinning disc". Biosystems Engineering. 95(3): 405 – 412, 2006.

Koya, O. A., Idowu, A. and Faborode, M. O., "Physical properties of palm kernel and shell relevant in nut cracking and product separation". Journal of Agricultural Engineering and Technology, 12: 33 – 45, 2004.

Manuwa, S. I., "Design, fabrication and testing of a low cost palm nut cracker". Paper presented at the 19th Annual Conference of the Nigerian Society of Agricultural Engineers, at the Federal University of Technology, Owerri, Nigeria, 1997.

Manuwa, S. I., "Fracture resistance of palm nuts to compressive loading". Paper presented at the 20th Annual Conference of the Nigerian Society of Agricultural Engineers at Lagos Airport Hotel, Lagos, Nigeria, 1998.

Meriam, J. L. and Kraige, L. G., "Engineering mechanics, volume 2: dynamics, 4th edition". John Wiley and Sons, Inc., New York, 1998.

Obiakor, S. I. and Babatunde, O. O., "Development and testing of the NCAM centrifugal palm nut cracker". AGRIMECH Research and Information Bulletin of the National Centre for Agricultural Mechanization (NCAM), 1999.

Olie, J. J. and Tjeng, T. D., "Kernel recovery in the extraction of palm oil", The Netherland Stork Amsterdam, Amstelveen, p. 63 – 72, 1974.

Owolarafe, O. K., Sanni, L. A., Edinowe, O. S., Ogunyomi, O. T., Faborode, M. O. and Ajibola, O. O., "Development of an oil palm fruit stripper". Journal of Agricultural Engineering and Technology. 10: 59 – 64, 2002.

Full Paper

EROSION CORROSION IN THE OIL AND GAS INDUSTRY: A REVIEW

O.O. Ige
Department of Materials Science and Engineering
Obafemi Awolowo University
Ile –Ife, Nigeria

L.E. Umoru
Department of Materials Science and Engineering
Obafemi Awolowo University
Ile –Ife, Nigeria

O.E. Olorunniwo
Department of Materials Science and Engineering
Obafemi Awolowo University
Ile –Ife, Nigeria

M.O. Adeoye
Department of Materials Science and Engineering
Obafemi Awolowo University
Ile –Ife, Nigeria

ABSTRACT

This paper reviews the various factors that affect erosion corrosion in the oil and gas industry. The mechanisms are highlighted and explained, with a view to understanding the underlying principle of the degradation phenomena. There are many monitoring techniques that are used in evaluating erosion corrosion but three are commonly employed in the laboratories. The benefits and limitations associated with these methods - rotated disc, rotated cylinder and jet impingement are reviewed. Erosion corrosion is regarded as a surface process that can be controlled via surface engineering for example, using coatings and inhibitors coupled with materials selection. Some of the critical parameters, such as inhibitor concentration as a function of flow parameters are discussed.

Keywords: *Erosion corrosion, corrosion monitoring, inhibitor, corrosion resistant alloys*

1. INTRODUCTION

The oil and gas industry exposes a variety of materials to corrosive fluids, often containing solids such as sand. The combination of a corrosive environment, high fluid velocity, and entrained solids typically lead to the loss of material from the surfaces in contact with the flowing hydrocarbon fluid. Sweet corrosion in carbon steel pipelines carrying oil-water mixtures has long been a problem in the oil industry. Corrosion - related problems in oil-gas production and processing operations result in loss of millions of dollars each year in downtime, lost production and damaged pipelines (Evans et al., 2004). With the use of enhanced oil recovery techniques, CO_2 corrosion in oil-water pipelines has become common causing much concern in transportation of these multiphase fluids over long distances from remote wells to separation sites (Evans et al., 2004; Vuppu and Jepson, 1994).

In the oil and gas industry, it has been discovered that there is continuous growing demand in energy consumption and also that convectional energy sources are depleting at a fast rate. Then new sources such as oil sands are expected to be increasingly relied upon to make the difference in future global oil and gas production. The most energy – and cost–efficient manner to transport oil sands from excavation to the excavation plant is by using a hydrotransport system. In the hydrotransport process, oil, sand and water are mixed together to make a slurry and this is transported via pipeline (Tian and Cheng, 2008). This multiphase system will definitely lead to some degradation mechanism.

The effect of flowing liquid streams on the degradation of engineering components is of great importance in many industrial processes. Flow induced corrosion is often used to describe the accentuation of corrosion resistance when mass transfer of reactants and products is enhanced. They are described according to their appearances and causes, which are brought about by the flow mechanisms of the system, when the mechanical forces of the flowing fluid prevail at the metal/environment interface then erosion corrosion and cavitation corrosion occur (Hu and Neville, 2002). Flow induced corrosion is defined as a process whereby the corrosion rate of a material is increased in a moving fluid. The effects of flow velocity on flow induced corrosion have been categorized into three, namely; low, medium, and high velocities regimes of erosion corrosion (Neville and Hu, 2001).

Typically, corrosion research is conducted in static solutions. Hydrodynamic factors are often ignored in the analysis of corrosion kinetics, or at best a hydrodynamic regime is used that does not effectively simulate the industrial environment of interest (Wharton and Wood, 2004). One significant contributing factor in the degradation of pipeline in oil and gas production is erosion-corrosion. It is seen that the contributions of corrosion and erosion to erosion-corrosion rate rank approximately 30% and 70%, respectively (Wang et al., 2005; Tian and Cheng, 2008). Erosion-corrosion is a degradation phenomenon that falls into a broad category of tribo-corrosion processes, which includes, for example, abrasion, corrosion and cavitation corrosion. These are not specific forms of corrosion but are degradation processes that involve the action of a mechanical process (for example, the impact of a solid particle) in conjunction with an electrochemical corrosion process. The material loss mechanism is caused by flowing fluid (containing or free from solid particles) disrupting or thinning the protective film of the corrosion product (Reyes and Neville, 2001; Neville et al., 2003; Dave et al., 2008; Fan et al., 2011).

Industries like chemical, material processing, pump manufacture, offshore and marine technologies, mining, metallurgical, oil and gas among others experience considerable deterioration processes as a result of erosion-corrosion (Wood and Hutton, 1990; Heitz, 1996; Stack and Paungwiwat, 2002; Chen et al., 2003; Wood and Speyer, 2004; Xu and Zhuo, 2010). Some of the equipment affected are pumps, impellers, valves, heat exchanger tubes, tees and elbows in pipework, manifolds, inspection omegas, agitators and so on (Wood and Hutton, 1990; Heitz, 1996; Neville and Dougal, 2002;

Chen et al., 2003; Hernandez-Rodriguez et al., 2007; Mohammed, 2010). Generally, the economic and effective operation of machinery and plant involved in fluids handling is increasingly dependent on the utilization of materials that combine high corrosion resistance and good wear resistance. The synergistic effect between erosion and corrosion is significant and is dependent on the material (Heitz, 1996). In multiphase systems the effect of each constituent needs to be defined and clearly understood. This review highlights these and the various factors that have profound effects on the erosion corrosion mechanism in the oil and gas industry.

1.1. Sand Management

Sand production is a common problem in oil and gas production and this may cause considerable erosion damage in critical parts of the transport and processing equipment leading to expensive failures and loss of production time (McLaury et al., 1999; Shirazi et al., 1999; Mohammed, 2010). The mechanical influence, frequency and extent of impacts by sand or other impacting species can cause the material to make a transition into a regime where active and passive sites are constantly forming on one surface (Aracic et al., 2010). It has been established that erosion rate is proportional to sand production rate as well as other factors like fluid properties, flow regime, pipe material properties and sand characteristics (Shirazi et al., 2000).

1.2. Oil and Sand

Concerted efforts are being deployed by industry to enhance the rate of oil and gas recovery to meet the global demand for energy. The mining of oil sand and the shift towards subsea developments, particularly associated with deep well production, horizontal drilling and the use of hydrotransport systems where oil, sand and water are mixed together (slurry), increases the risk of material degradation by erosion corrosion. Slurry erosion corrosion is regarded as a major problem in the oil and gas industry (Stack and Paungwiwat, 2002; Nesic et al., 2008; Neville and Wang, 2009). The presence of some active substances such as fine particles of sand, dissolved salts, CO_2, H_2S, bacterial activity and in some cases even the presence of oxygen aggravates corrosion in formation water. Crude oil also contains an important quantity of highly mineralized water, rich gases with a large percentage of CO_2, and sand grains from the petroliferous bed (Ripeanu et al., 2007). From the corrosion standpoint, CO_2 corrosion is one of the most important problems in the oil and gas industry (Cabrini et al., 1998; Wood, 2006).

1.3. Carbon Dioxide Corrosion

It is believed that one significant factor of pipelines in oil and gas production is CO2 corrosion. In carbon steel piping systems handling fluids containing water and dissolved CO2 under a range of conditions, and FeCO3 (iron carbonate) scale can form on the pipe wall and provide a measure of protection against CO2 corrosion. If the fluid also contains sand, particles of sand impinging the pipe wall can remove the protective scale or prevent it from adhering to the wall. Without the scale to protect the pipe, CO2 corrosion can progress at an accelerated rate (Shadley et al., 1996). Due to greater solubility of the precipitable corrosion products, the presence of CO2 therefore lowers the flow rate thresholds corresponding to the appearance of erosion-corrosion phenomena. Indeed, the pronounced erosion corrosion often observed in CO2 fields has led to confusion between CO2 corrosion and erosion-corrosion. With or without CO2, erosion-corrosion attack has unmistakable characteristic features (Houghton and Westermark, 1983; Crolet and Boris, 1991). The presence of solids is known to induce erosion and its interaction with corrosion is poorly understood in CO2 environments. The mechanism of CO2 is still considered to be a grey area despite the volume of work that has been carried out. The effect of fluid dynamics on this type of corrosion needs to be determined and some of the parameters are flow velocity, flow regimes and the effect of liquid shear stress at the pipe wall (Hu and Neville, 2008).

1.4. Flow Induced Corrosion

The effect of flow on CO_2 corrosion has been the subject of a large number of investigations. The studies can be grouped into four main topics (Figure 1): i) effect of mass transfer; ii) effect of flow on removal of corrosion products; iii) effect on corrosion inhibition; and iv) effect on erosion and erosion-corrosion. It was shown that erosion corrosion causing flow-induced localized materials attack is mainly found under conditions when the material is covered with protective layers. Local destruction of such layers by fluid dynamic forces is the primary reason (Gulbrandsen, 2005; Schmitt and Bakalli, 2008).

1.5. Erosion corrosion

Erosion is defined as the removal of material from a solid surface by the repeated application of mechanical forces. These forces are induced by solid particles, liquid droplets, or cavitation. Erosion may be attributed to removal of the metal, the inhibited film, and/or protective corrosion scales. In a recent survey, erosion-corrosion was rated in the top five most prevalent forms of corrosion damage in the oil and gas industry (Cabrini et al., 1998; Salama, 2000; Wood, 2006).

Erosion corrosion of carbon steel in CO_2 environments involves the synergistic action of metal loss due to impingement and corrosion of an active surface. In the presence of suspended solids, the erosion

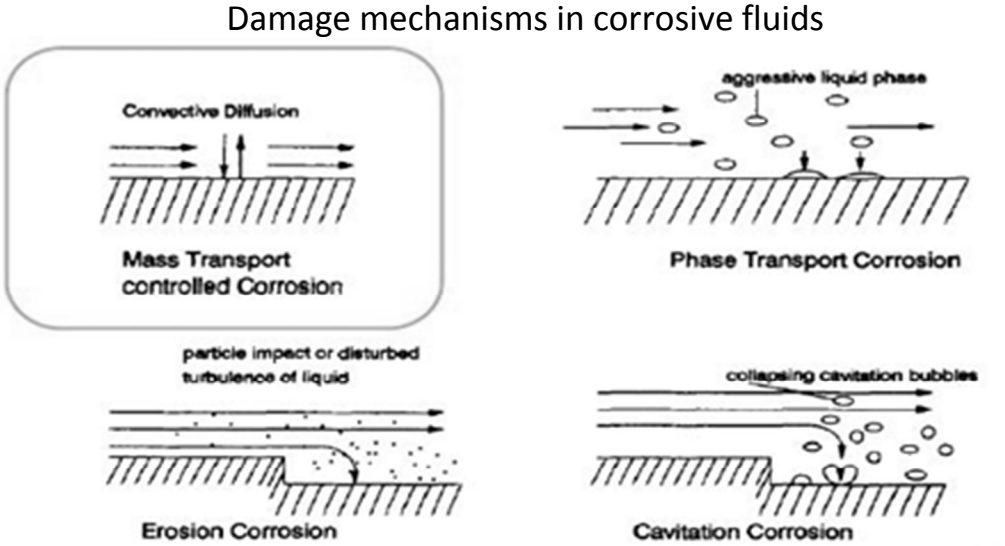

Fig. 1: The effect of flow on CO_2 corrosion (Heitz, 1996)

corrosion rate can increase by 25 – 100 times greater than the uniform corrosion rate (Ramachandra et al., 2005; Neville and Wang, 2009). Under suitable conditions $FeCO_3$ scale is the corrosion product formed in CO_2 – saturated conditions and the corrosion regimes have been determined as a function of the flow condition (French et al., 1989; Neville et al., 2003):

- $FeCO_3$ scale formation and low metal loss rates at low velocity
- Sand abrasion and removal of the scale and high metal loss rates at high velocities, and
- Partial removal of scale and localized pitting at intermediate velocities

These regimes depend on the environment and the material of construction (de Moraes et al., 2000; Neville et al., 2003).

Erosion in oil and gas production systems is mainly due to the presence of sand along with liquid and gas. Since erosion is due to mechanical forces occurring on the metal surface, erosion can be difficult to control. Erosion corrosion occurs when corrosion is accompanied by solid particle impingement (Dave et al., 2008). Erosion corrosion is defined as accelerated corrosion following the removal of surface films. It is associated with production velocities and is most severe when production velocities are high. The erosion corrosion effect is induced by rapid relative movement between a flowing electrolyte, for example, slurry and metal parts, pipes or containers. All metals can be affected to a greater or lesser degree. The presence of CO_2 in oil and gas has made the environment very corrosive and special attention must be paid to their degradation mechanism especially erosion-corrosion (Keating and Nesic, 1999; Ajeel and Ahmed, 2008; Tian and Cheng, 2008;Tandon et al., 2009).

1.6. Cost of erosion corrosion

For some decades, it has been acknowledged that erosion corrosion is the largest threat to the integrity of multiphase oil and gas pipelines. Erosion and corrosion problems in oil and gas production cost the industry hundreds of millions of dollars each year (Wood and Hutton, 1990). While GE Technologies believed that the negative effects of corrosion and erosion cost the oil and gas, and power industries billions of dollars annually, they argued that 20% to 25% of these costs could be avoided (Hedges and Bodington, 2004). It has been stated that massive costs are directed annually to alleviate corrosion and erosion corrosion costs. The cost impact of corrosion to the USA economy totalled nearly $300 billion annually and it has been suggested that erosion corrosion is about 30% of the total corrosion form (Novak and Macenauer, 1993). Erosion corrosion problems provide significant health, safety and environmental risks to the oil and gas industry due to unexpected material failure, unscheduled plant or pipeline shutdowns, inefficient or lost production, and high maintenance costs or imposed fines (Wood and Hutton, 1990; Novak and Macenaeur, 1993; Hedges and Bodington, 2004; Wang et al., 2005).

1.7. Factors that affect erosion corrosion

There are several factors affecting erosion corrosion and they can be classified as flow dynamics, concentrations, geometry, environment, solid particles among others.

Erosion corrosion is often associated with areas where fluid flows are altered and there is increased turbulence, the presence or absence of solid particles, the fluid corrosiveness and so on. The relationship between erosion corrosion rates and some variables such as (geometry, fluid velocities, fluid properties, flow regime, pipe material properties, particle diameters, and densities) have been established. Also the effects of the presence of solid particle- like sand and their characteristics, such as sharpness, geometry, and hardness has been evaluated (Heitz, 1991; Shiraz et al., 2000; Neville et al., 2003; Fan et al., 2011). The presence of contaminants and corrosive species such as oxygen, water combined with salts containing chloride, bicarbonate and sulphate accelerates erosion corrosion (Tian and Cheng, 2008; Mohammed, 2010). Table 1 listed some of the important variables related to slurry erosion (Wood et al., 2004).

Unlike erosion in sand free systems where erosion rate is related to two parameters, it was observed that the degree of damage associated with erosion corrosion in the presence of sand is a function of the following (Stack and Paungwiwat, 2002; Salama, 2000):

- Fluid characteristics: flow rate, composition, density, viscosity
- Sand characteristics: concentration, impact velocity, impact angle, number of particles hitting the surface, shape, sharpness, hardness, size distribution and density
- Component geometry: bend, tee, choke, joint
- Material properties: hardness, microstructure
- Environment: pH, electrochemical potential, chemical composition, temperature and pressure.

Table 1: Some of the main variables which influence erosion (Wood et al., 2004)

Slurry Variables	Component Variables
Liquid; viscosity, density, surface activity, lubricity, corrosivity, temperature	Bulk properties; ductility or brittleness, hardness and toughness, melting point, microstructure, shape and roughness
Particle; brittleness, size, density, relative velocity, shape, relative hardness concentration, particle/particle interaction	Surface properties; work hardening, corrosion layers, surface treatments, coating type, coating bond, microstructure
Flow field; angle of impingement, particle impact, efficiency, boundary layer, particle rebound, degradation, particle drop – out, turbulence intensity	Service variables; contacting materials, pressure, velocity, temperature, surface finish, lubrication, corrosion, hydraulic design, intermittent slurry flows

2. MECHANISM OF EROSION CORROSION

There are a number of mechanisms to describe the conjoint action of flow and corrosion that result in four types of flow-induced corrosion, viz: - mass transport controlled corrosion, phase transport controlled corrosion, erosion corrosion and cavitation corrosion (Heitz, 1991). Erosion corrosion is characterized by the combined action of flow-induced mechanical forces and electrochemical processes. The mechanical action is comprised of the following types:-

- Shear stress and pressure variations by high flow velocities mainly in disturbed flow
- Particle impact in multiphase flows (liquids containing solid particles and gas bubbles)

The interaction between erosion and corrosion is complex. In the absence of sand, corrosion is a major concern for the integrity of pipelines while the presence of sand may result in erosion, erosion-influenced corrosion (EIC), corrosion-influenced erosion (CIE), sand settling, corrosion under sand beds (underdeposit corrosion), and loss of inhibitor effectiveness. Both corrosion and erosion are essentially surface-dependent degradation related to microstructure and composition of only the near-surface region (Wood and Speyer, 2004; Wood et al., 2004).

It was pointed out that increasing flow velocities generally augments corrosion rates but they also have beneficial effects. It may enhance passivation and inhibition in such a way as to improve the transport of the passivator and inhibitor to the phase boundary (Heitz, 1991; Chen et al., 2003). In this work, the mechanisms considered are as follows: erosion, corrosion, erosion-corrosion and the underlying principle of synergism associated with erosion-corrosion.

2.1. Mechanisms of Erosion

In erosion the significant factor that defines the mechanism is the flow velocity of the fluid. At low velocity there is scale formation and low corrosion rates, while for high erosivity there is uniform corrosion which occurs at high rates and for intermediate velocity,

pitting is most often observed and the penetration rates can be extremely high. The material wastage associated with erosion is called wear and it is caused by three major mechanisms: chemical dissolution of the pipe, mechanical erosion caused by fluid flow and impingement of particles on the pipe wall (Cardoso Filho and Orazem, 2001; Papavinasam and Revie, 2004).

2.2. Mechanisms of Corrosion

Corrosion mechanism is well understood and documented but in this work, we are considering CO_2 erosion corrosion in the oil and gas industry. It must be noted that the CO_2 corrosion principle is still under intensive investigation. CO_2 is found to cause an enhanced rate of general corrosion and localized corrosion and the kind of corrosion caused by dissolved CO_2 varies considerably according to the precise environmental conditions. In addition, CO_2 associates to give carbonic acid and can then dissociate further into bicarbonate and carbonate anions. These mechanisms are influenced by the resulting acidic pH. The buffering action of this carbon–containing species may also play an important role. The mechanism of the effects of dissolved CO_2 on the corrosion of steel has been successfully resolved and established (Ikeda et al., 1984; de Waard et al., 1991).

Although there is some debate about the mechanism of CO_2 corrosion in terms of which dissolved species are involved in the corrosion reaction. There is a consensus that iron carbonate is the main corrosion product and that formation (dissolution) depends on various environmental and fluid parameters. It is clear that irrespective of the exact mechanisms involved, the formation of iron carbonate films is a major controlling factor that influences the final corrosion rates observed. It is generally accepted that the CO_2 partial pressure and temperature influence the corrosion rate. Velocity effects are also very important in the CO_2 system such that turbulence is often a critical factor in pushing a sweet system into a corrosive regime. Notwithstanding this, the mechanisms of CO_2 corrosion are complicated and are influenced by many factors (Ikeda et al., 1984; de Waard et al., 1991; Gulbrandsen, 2005). The erosion corrosion of carbon steel in CO_2 environments involves the synergistic action of metal loss due to impingement and corrosion of an active surface (Cabrini et al., 1998).

2.3. Mechanisms of Erosion-Corrosion

Erosion-corrosion is a complex mechanism of material degradation resulting from interactions between electrochemical corrosion and mechanical erosion processes. The mechanism of this form of material damage is very complex due to the interaction between erosion and corrosion, and the overall damage is higher than the summation of pure erosion and corrosion. Erosion corrosion was regarded as a form of material degradation by simultaneous attack of erosion plus corrosion. It is clear that the mass loss rate by combined erosion corrosion is not simply the sum of erosion and corrosion mass loss rates. Instead, of this some synergistic effects can occur. Corrosion is often assumed to be controlled by mass transfer while erosion is controlled by the flow of a second particulate (Kang et al., 2003; Hu and Neville, 2005; Wang et al., 2005; Aracic et al., 2010; Mori et al., 2010).

Erosion-corrosion that produces the maximum impact originates from two sources. The first is the mechanical source and this is the result of high velocity of the corrosive medium (gas-oil-water emulsion) which produces cavitation and impingement. The other is electrochemical and is as a result of chemical reaction between the medium and the exposed parts. Erosion corrosion produces weight loss as a result of removal of large parts of clear-cut metal portions due to impingement and cavitation (Neville and Dougal, 2002).

The mass loss can therefore be caused by several mechanisms which can either be flow and/or impingement of suspended particles on the pipe wall and electrochemical corrosion enhanced erosion or vice versa (Birks et al., 1993; Neville et al., 2003). Substantial progress has been made towards understanding the mechanisms of erosion-corrosion of pure metals and specific alloys in particular the role of oxygen formation and its removal. Though the interaction between erosion and corrosion processes is complex, it can be rationalized into a series of regimes with a smooth transition from one regime to the next as the relative intensity of one process is varied with respect to the other (Stack et al., 2007). The modes of erosion-corrosion are diverse and may vary from being "erosion-dominated", where erosion of metal is the dominant process, to "corrosion-dominated", where erosion of oxide scale is the dominant process. The intermediate situation in which erosion of transient oxygen is the predominant process is termed "erosion-corrosion dominated" and describes the regime in which continual formation and removal of oxygen occurs down to the scale/metal interface (Malka et al., 2006).

2.4. Synergism of Erosion-Corrosion

Erosion and corrosion have a synergistic effect on each other, and as a result, the two are often grouped together as one phenomenon. Although the problem associated with this interaction is enormous, the mechanism of synergism is still not thoroughly understood because of its complexity (Papavinasam and Revie, 2004; Dave et al., 2008). It is extremely difficult to clearly separate the damage due to erosion and corrosion and this may be due to the fact that most of the work done on erosion corrosion is on a laboratory scale which is different from field work. Despite the extensive work in the past there has been no clear understanding of erosion corrosion synergistic effect on each interaction under realistic flow conditions (Wood and Hutton, 1990; Stack and Paungwiwat, 2002; Stack et al., 2006).

Synergism can be defined as the difference between erosion-corrosion and the sum of its two parts and can be expressed by the following relationships (de Waard et al., 1991):

$$T = E + C + S \quad (1)$$

$$S = T - (E + S) \quad (2)$$

where

T is the material loss due to erosion corrosion,
E is the material loss by pure mechanical erosion process,
C is the material loss by electrochemical corrosion processes, and
S is the combined interaction between corrosion and erosion processes.

In addition the synergistic term can further be divided into two additional components, ΔE and ΔC, where:

ΔC is the corrosion enhanced erosion, and

ΔE is the erosion-corrosion

such that

$$S = \Delta E + \Delta C \quad (3)$$

The synergistic effects during erosion-corrosion processes may be influenced by changes in hardness induced by the surface damage, during slurry jet impingement tests. Synergism can be evaluated by using an experimental programme which includes three types of test:

- Pure erosion tests to determine the erosive wear rate
- Pure corrosion tests to determine the corrosive wear rate, and
- Combined tests to determine the total wear rate when conditions in both tests 1 and test 2 are acting

Several mechanisms have been proposed and it was reported that the magnification of the wear rate by synergism is due to fresh surfaces being created during erosion which are not immediately passivated by corrosion products and are therefore allowed to corrode at an accelerated rate (Wood and Hutton, 1990). Also it was stated that the most significant damage process was determined to be the synergistic effect and this is as a result of property degradation due to corrosion processes translated to mean that the resistance to erosion on the surface is reduced (Hu and Neville, 2009).

3. MONITORING OF EROSION CORROSION

It is well known that corrosion tests are very difficult to replicate and also that there are many factors which affect these measurements. Some of these factors include surface/sample preparation and the environment like flow velocity, pH, temperature, concentration of corrosive species and others. It is also assumed that reproducibility of these tests in various laboratories differ between 55 – 75% (Groysman and Shvarts, 2006; Papavinasam et al., 2002). Erosion corrosion may occur in the presence or absence of sand but generally it is believed that sand is present. Also it is argued that due to economic and technical reasons, new sources of energy are being developed and as such oil sands will increasingly be relied upon to make the difference in future global oil production. The quantity of sand produced in a well is regarded as unknown and as such there is a need to evaluate the sand that is produced. This can be achieved by using sand monitors and/or erosion or corrosion monitors (Shirazi et al., 2000; Tian and Cheng, 2008).

Electrochemical methods are used in the field and laboratories to measure corrosion and erosion corrosion rates. Some of the techniques include weight loss, Linear Polarization Resistance (LPR), Electrochemical Impedance Spectroscopy (EIS), Electrochemical Noise (EN), and externally monitored hydrogen permeation foils. The use of LPR to investigate erosion-corrosion has been established and it has been able to identify the conditions quickly for which erosion-corrosion may be a serious threat (Papavinasam et al., 2002; Groysman and Shvarts, 2006; Hu and Neville, 2009). In conjunction with the electrochemical techniques, there are many devices that are used for erosion-corrosion studies out of which three kinds of test techniques are extensively used. These tests are used in the laboratory to simulate the hydrodynamic conditions exerted on the materials experiencing erosion-corrosion, viz; Rotating Disk Electrode (RDE), Rotating Cylinder Electrode (RCE), and Submerged Impingement Jet system (SIJ) (Tian and Cheng, 2008).

A study discussed all three major methods of measuring flow induced corrosion critically and outlined their benefits and shortcomings. They considered jet impingement as a powerful tool that is suitable for investigating susceptibilities of materials to flow induced localized corrosion under severe flow intensities and to study the efficiency of chemical mitigation of these problems. While the rotated cylinder has the advantage that the complete flow regime from laminar to turbulent can be tested in the same arrangement. They stated that the rotated disc is preferred when studying the flow effects under laminar flow conditions, because this flow regime exists at rotated discs up to high angular velocities. Also, rotated disc is considered for investigating the mass transport phenomena because there is a direct relationship between the mass transport rate and angular velocity. They now concluded that there is a distinct differentiation between corrosion experiments and electrochemical measurements, because the limited depth of information obtained from flow influenced electrochemical measurements is often underestimated and sometimes even ignored (Schmitt and Bakalli, 2006). However, another study demonstrated the correlation of steel corrosion in pipe flow with jet impingement and rotating cylinder tests. The flow field established for a circular jet impinging on a flat plate with the jet central axis normal to the plate is as shown in Figure 2. Based on the results obtained it can be concluded that submerged impinging jet and rotating cylinder electrode laboratory test methodologies give the optimum field conditions (Effird, 2000).

Laboratory – tests for inhibitor evaluation consist of two main components – laboratory methodology and measurement technique. The combinations of laboratory methodology and measurement technique for inhibitor evaluation for multiphase systems are presented in Table 2 (ASTM G170 – 01a (2001). The features of different flow systems and related experimental tools applied in flow – related corrosion research and protection are listed in Tables 3 - 5 with respect to the flow intensity typically achieved the availability of equations for quantitative and predictive evaluation of experimental data, and whether this tool is better applied in the laboratory or in the field (Effird, 2000).

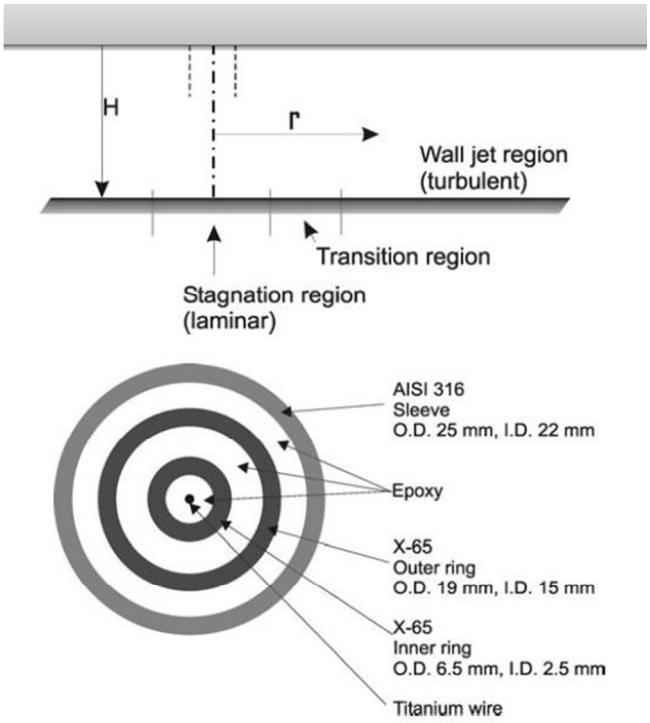

Figure 2: Hydrodynamic characteristics of jet impingement on a flat sample showing the three characteristic flow (Cabrini et al., 1997)

Table 2: Laboratory Methodologies and Measurement Techniques for Corrosion Inhibitor Evaluation (Nesic et al., 2004)

Laboratory Methodology	Measurement Techniques	Aqueous/Oil/Gas Phase	Remarks
RCE	Mass loss, electrochemical	Aqueous Phase	Specimen is cylinder
RCE	Mass loss	Aqueous/Oil Phase	Specimen is cylinder
JI	Mass loss, electrochemical	Aqueous Phase	Specimen is disc
JI	Mass loss, electrochemical	Aqueous/Oil Phase	Specimen is disc
JI	Mass loss, electrochemical	Aqueous Phase	Specimen is ring
RC	Mass loss	Aqueous or aqueous/Oil Phase	Electrochemical measurements cannot be carried out

Table 3: Remarks of Different Flow Regimes (Fan et al., 2011)

Flow System	Flow Velocity or Reynolds Number	Evaluation	Application
Simple stirred	Small	Qualitative	Laboratory
Rotated disc			
Free	Moderate	Quantitative (Levich Equation)	Laboratory
In front of wall	High	Quantitative (empirical)	Laboratory
Rotated disc			
Free	Moderate	Quantitative	Laboratory
Coaxial	High	(empirical)	
Rotated Cage	High	Quantitative (empirical)	Laboratory
Channel flow	High	Quantitative (empirical)	Laboratory, Plant
Tube flow	High	Quantitative (empirical)	Laboratory, Plant
Jet Impingement	High	Quantitative (empirical)	Laboratory

Generally, RDE and RCE are used to investigate the effects of hydrodynamic conditions of fluids on corrosion and erosion-corrosion of metals, while the impingement jet system is suitable for studying mechanical impingement of solid particles. They are also used to generate laminar and turbulent flows, respectively. When the rotating speed is sufficiently high, RDE could also generate transition and relatively turbulent flows. Devices such as slurry pots, rotating cage, slurry drum and coriolis tester can also be used for erosion-corrosion research (Schmitt and Bakalli, 2006).

4. MODELLING OF EROSION CORROSION

Generally, modelling is useful to help understand the mechanisms of degradation, predict the damage level, failure mode and the most likely location of corrosion in the oil and gas industry. These predictions can help support the development of practical guidelines to assist the pipeline industry in mitigating existing, or preventing future corrosion failures (Ryborg, 2002). The majority of erosion corrosion research has been undertaken using experimental methods. Nowadays the trend has moved towards utilization of modelling techniques which provide an additional tool for investigation. The models differ considerably in how they predict the effect of protective corrosion films and the effect of oil wetting on CO_2 corrosion, these two factors account for the most pronounced differences between the various models (Cabrini et al., 1997; Nesic et al., 2004).

4.1. Modelling of CO_2 Corrosion

There are many varieties of prediction models for CO_2 corrosion of carbon steel. Most of these models are semi-empirical, or even fully empirical with only a handful of the more recent models being based on mechanistic descriptions of the processes underlying CO_2 corrosion. The modern history of CO_2 corrosion prediction started in 1975 with the introduction of de Waard and Milliams model. The model combined the effect of CO_2 partial pressure and temperature on the corrosion rate. Over the years new approaches to CO_2 corrosion prediction and models were introduced (NORSOK, 1998; Nyborg et al., 2000).

Nyborg (2002) highlighted the advantages and limitations of models that are being used currently for CO_2 corrosion. He categorized these models into academic based organizations and industry driven, some of the former were Tulsa, Ohio, ULL, Dream among others and the former were HydroCor, NORSOK, Dream, Corpos and so on. He stated that the major factors in CO_2 corrosion are pH, protective films, oil wetting, presence or absence of H_2S, top-of-line corrosion and fluid dynamic parameters. In this work, the latter parameter is our area of interest and it must be noted that, theoretically, CO_2 corrosion is dependent on the flow velocity and these models have varying degrees of flow dependence. One of the shortcomings of these models is that they have simplified fluid flow calculation and only a few of them have a version that incorporates fluid flow. These models assumed that there is a tendency to over-emphasize the effects of flow parameters on CO_2 corrosion, however during the past decade several workers have established the importance of hydrodynamic factors in CO_2 corrosion in the oil and gas industry (Crolet and Boris, 1991; Cabrini et al., 1997; Cabrini et al., 1998; Nyborg et al., 2000).

Table 4: Mass Transport Relationship for Important Flow Regimes (Fan et al., 2011)

Flow System	Power $Sh = a.Sc^b.Re^c$	Interval of validity	Characteristic length and Reynolds Number
Free rotated disc			L = r,
Laminar flow	$0.60.Sc^{1/3}.Re^{1/2}$	$10^2 < Re < 10^5$	$Re = (\omega.r^2)/v$
Turbulent flow	$0.11.Sc^{1/3}.Re^{0.87}$	$Re > 10^6$	
Rotated disc in front of wall			L = r,
Laminar flow	$17.3.Sc^{1/3}.Re^{0.34}$	$9.10^4 < Re < 6.10^5$	$Re = (\omega.r^2)/v$
Turbulent flow	$0.50.Sc^{1/3}.Re^{0.78}$	$Re > 6.10^5$	
Free rotated cylinder			L = r,
Turbulent flow	$0.079.Sc^{0.35}.Re^{0.7}$	$10^2 < Re < 4 . 10^5$	$Re = (\omega.r^2)/v$
Coaxial cylinder	$0.0027.Sc^{1/3}.Re$	$Re < 2.7. 10^5$	
Flat plate in channel and tube flow			$L = d_e$,
Laminar flow	$2.54.Sc^{1/3}.Re.(d_e/l)^{1/3}$	Re < 2300	$Re = (d_e.u)/v$
Turbulent flow	$0.079.Sc^{0.35}.Re^{0.7}$	Re < 2300	d_e = (4.cross section area)/perimeter
Flat plate in free area (Laminar flow)	$0.34.Sc^{1/3}.Re^{1/2}$	$Re < 5.10^5$	L = l, Re = (l.u)/v
Rotated cage (Turbulent)	N/A	N/A	$Re_{RC} = [\omega.(r_{RC})^2]/v$
Impinging Jet			L = d,
Region A (Laminar)	$Sh = 1.51.Re^{0.5}.Sc^{0.33}.(H/d)^{-0.054}$	Re < 2000	Re = (d.u)/v
Region B (Transition)	$Sh = 1.12.Re^{0.5}.Sc^{0.33}.(H/d)^{-0.054}$	4000 <Re <16000	d: nozzle diameter
Region C (Wall-jet)	$Sh = 1.51.Re^{0.5}.Sc^{0.33}.(H/d)^{-0.054}$		u: flow velocity in nozzle

Table 5: Wall Shear Stress and Limiting Current Density Equations used in Different Experimental Setups for Investigations on Flow Influenced Corrosion (Papavinasam et al., 2002)

Experimental Tool	Methods used: Mass loss	Methods used: Electro-chemical	Wall Shear Stress	Limiting Current Density
Rotated Disk	+	+	$\tau_w = 6.302.\upsilon.\rho.\omega.(Re)^{1/2}$	$j_D = 0.6205.n.F.D^{0.66}.\upsilon^{-0.167}.\omega^{0.5}.C_{bulk}$
Rotated Cylinder	+	+	$\tau_w = 0.0791.\rho.(r_c)^2.\omega^{2.3}.(Re_c)^{-0.3}$	$j_D = 0.0791.n.F..C_{bulk}.(\omega/r)^{0.7}.(r/\upsilon)^{-0.3}.(\upsilon/D)^{-0.644}$
Rotated Cage	+	+	$\tau_w = 0.0791.\rho.(r_{RC})^2.\omega^{2.3}.(Re_{RC})^{-0.3}$	$j_D = k.\tau$, Leveque equation at microelectrodes under stationary condition
Flow Loop	+	+	$\tau_w = (\Delta P/\Delta L).(d/4)$	Tube: $j_D = 0.320.n.F.D^{2/3}.\upsilon^{-1/6}.l^{-1/3}r^{-1/3}.u^{0.33}.C_{bulk}$, l,r is the tube electrode length and diameter respectively Channel: $j_D = 0.81.n.F.D^{2/3}.\upsilon^{-1/6}.u^{1/2}.C_{bulk}$
Impinging Jet	+	+	$\tau_w = 0.0447.\rho U_o.(Re)^{-0.182}.(x/d)^{-2}$	$j_D = k.n.F.D^{2/3}.\upsilon^{1/6}.(0.637.u/r)^{1/2}.C_{bulk}$, r is the electrode radius $j_D = k.\tau$, Leveque equation, stationary condition

4.2. Modelling of Erosion Corrosion

It is assumed that the corrosion factors in erosion models have been generally overlooked and as such, there are no integrated erosion-corrosion models (Gulbradsen, 2005). It is observed that the estimation of corrosion rate in a multiphase system is complex due to the high number of parameters involved. The advent of the computer has expanded the horizon of the inputs that can be processed, such that what was considered unfeasible some years back can now be solved within a short time. The correlation between model output and the field experience is not satisfactory and it is still a problem (Dugstad, 1997; Stack, 2002).

One significant parameter in erosion corrosion is the velocity of the impacting particles and the general form of the equation that relates erosion to velocity and it is given as:

$$\varepsilon = k.\, V^{n} f(\theta) \quad (4)$$

where, ε is the erosion rate; k is a constant and is a function of particles and targets, V is the velocity; n is the velocity exponent and θ is the impact angle in degrees.

It was concluded that there is a wide variation of velocity exponents derived for different erosion-corrosion conditions, which reflects the differences in erosion resistance of the scale formed between impacts (Groysman and Shvarts, 2006). There is a need to explain the contribution of erosion maps to the development of erosion-corrosion modelling techniques in general and emphasize the role these maps play in understanding some of the obscure principles in erosion corrosion.

Erosion maps are one of the basic results obtained by using modelling and it is regarded as one of the few design guides for erosion corrosion. They are engineering maps that have been used to describe erosion corrosion interactions at elevated temperatures. A mathematical model has been developed to construct the boundaries of such maps and to predict wastage rates. The material loss is dependent on a wide range of variables such as the impacting particle properties, the target material and the environment. Erosion corrosion maps are often used to give a visual representation of these interactions and to isolate regimes in terms of flow parameters, which are "erosion-dominated" or "corrosion-dominated". The interactions between the basic processes of erosion and corrosion is complex, but can be rationalized into a series of regimes with a smooth transition from one regime to the next as the relative intensity of one process is varied with respect to the other (Birks et al., 1993; Stack et al., 1997; Neville and Hu, 2001; Stack and Paungwiwat, 2002; Bousser et al., 2008).

It must be stated that erosion-corrosion modelling has greatly enriched the understanding of the mechanism, measurement techniques and ultimately the prevention and control methods of erosion-corrosion.

5. Prevention and Control

Erosion corrosion is a surface phenomenon and there are a wide variety of surface modification techniques by which we can improve the corrosion or tribological properties. There are various ways of controlling erosion-corrosion (Heitz, 1991; Chen et al., 2003; Wood and Speyer, 2004), these include cathodic protection, materials selection, design, coating, inhibitors among others. Several workers have used highly erosion-resistant ceramic coatings such as TiN, CrN but they found that these ceramic materials are brittle and ultimately fail leading to catastrophe. They are very expensive and are used in critical applications, however, the used of novel metallic coatings is still under investigation (Wood and Hutton, 1990; Stack, 2002).

It is also suggested that at the design stage, flow barriers such as blind tees, sharp corners and others should be removed (Birks et al., 1993) and the use of cathodic protection has been proposed as a viable option to reduce materials wastage significantly (Reyes and Neville, 2001). Industrially, two mitigation strategies are usually deployed and they are proper materials selection and inhibitors.

5.1. Materials Selection

Selection of materials capable of withstanding sand erosion is one of the major problems encountered in the oil and gas industry and low carbon steel is the material of construction. This is attributed to many factors but technically, mild steel can be improved with the aid of heat treatment and alloying.

Materials selection for erosion-corrosion is based on the use of corrosion resistant alloys, coatings which include hard-metals, cermets and ceramics. Since it is a surface phenomenon, surface degradation control techniques other than surface selection may well include the use of inhibitors as well as controlling fluid temperature, pH and dissolved oxygen. Cost considerations are one of the major factors in selecting coating materials. Cheap organic coatings tend to perform relatively poorly under high energy solid particle impingement but have a use as corrosion barrier coatings within low energy flow components. The use of ceramic coatings is limited to critical applications because they are usually expensive. Importantly in order to achieve a long-term corrosion resistance, it is important to understand the consequence of selecting anodic and cathodic coatings relative to their substrate. It was concluded that materials selection for tribocorrosion systems is extremely challenging and is based on optimising performance against the combined degradation processes. A wide range of corrosion resistant materials relies on a relatively thin surface film to provide a barrier (of high impedance) to charge transfer (and thus corrosion) between the relatively active bulk material and the corrosive environment (Stack et al., 1997).

In severe operating conditions such as erosion-corrosion conditions, corrosion resistance alloys are commonly used but generally they do not resist erosion very well. Materials selection for oil and gas production can be summarized as (Wood and Hutton, 1990; Wang et al., 2005; Schmitt and Bakalli, 2006; Tian and Cheng, 2008; Neville and Wang, 2009; Aracic et al., 2010):

- Use of carbon steels with suitable chemical inhibitors
- Use of corrosion resistant alloys (CRAs) without adding corrosion inhibitors, and
- Mixed compilations where the upper part is carbon steel with inhibitor and the lower part is made of corrosion resistant alloys.

5.2. Inhibitors

Inhibitor action may involve both the reduction of metal loss during impingement and subsequent retardation of active corrosion. It is well known that carbon and low alloy steels suffer metal loss via a synergistic erosion-corrosion mechanism in corrosive solids-containing environments. Also, that corrosion inhibiting chemicals are frequently used to mitigate the corrosion component in hydrocarbon systems. Achieving effective corrosion inhibition in high velocity systems suffering from erosion-corrosion has historically been considered difficult (Stack et al., 1997).

It has been established that chemical inhibitors must be able to recognize the corrosion agents present in the system such as chloride, oxide, carbonate and others (Stack et al., 2006; Dave et al., 2008; Neville and Wang, 2009). Corrosion inhibitor prevents attack by formation of a film on the metal surface as illustrates in Figure 3. The inhibitor may interfere with either the anodic or cathodic reaction. Also the efficiency of corrosion inhibitors in flowing media depends on local flow intensities. Above critical flow intensities inhibitors lose their efficiency as shown in Figure 4a. While in Figure 4b the critical flow intensities initiation can also depend on the inhibitor concentration which depends on the chemical structure of the active inhibitor compounds and the formulation of inhibitor packages in erosion-corrosion. It has been demonstrated that inhibitor performance is a function of the type of inhibitor at a particular concentration and flow intensity (Schmitt et al., 1990; Wang, 2007).

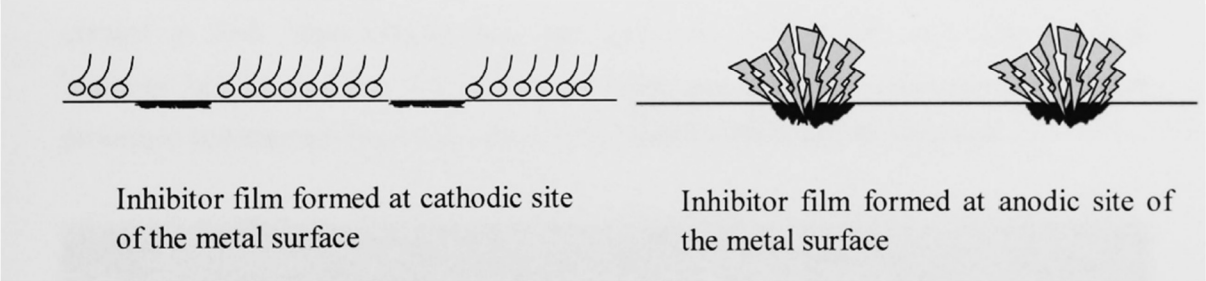

Figure 3: Corrosion inhibitor preventing attack by formation of a barrier on the metal surface (Wang, 2007).

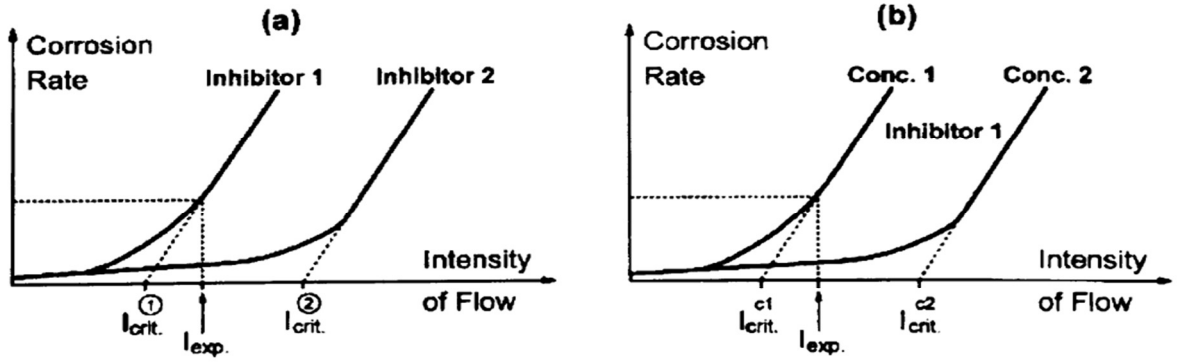

Figure 4: Effect of flow intensity on corrosion inhibitor performance (Schmitt, 2001)

Organic, adsorption-type corrosion inhibitors are used in the oil and gas industry generally and they act on the metal surface. This phenomenon is strongly dependent on the nature and surface charge of the metal, the type of aggressive electrolyte and the chemical structure of the inhibitor. The most important prerequisite for compounds to be efficient inhibitors under erosion/corrosion conditions is that they should chemisorb on the metal surface forming a barrier layer (de Damborenea et al., 1997; Durnie et al., 2001).

6. Conclusions

This paper has highlighted the several studies on erosion corrosion and the general mechanisms have been established. The mechanisms are regarded as being driven by synergistic effects of both erosion and corrosion. The degradation is a surface phenomena and this makes application of surface engineering to be an ideal procedure for its prevention and control. In the oil and gas industry, materials selection, coatings and inhibitors are the most common choices of prevention and control. It is believed that the former is more critical to the success of the prevention strategies. It is apparent that the general mechanism is well understood but some areas are still under consideration such as the fluid dynamics and the utilization of inhibitors. Hence concerted efforts need to be deployed in evaluation of the effect of the hydrodynamics and inhibitors characteristics.

Acknowledgements

We will like to thank the following organizations for their financial assistance: ETF, NIGERIA; NASENI, NIGERIA; Carnegie Corporation through OAU Linkages, NIGERIA and School of Mechanical Engineering, University of Leeds, UK.

References

Ajeel S.A. and Ahmed, M.A., "Study Synergy effect on erosion corrosion in oil pipes", Eng and Tech. 26(9):12-13, 2008.

Aracic, S., Krumes, D., and Vitez, I., "Tribocorrosion of low carbon steel C15E in 5% NaCl and 5% NaCl + SiO_2", Metalurgija. 49(2):111-114, 2010.

ASTM G170 – 01a, "Standard Guide for Evaluating and Quantifying Oilfield and Refinery Corrosion Inhibitors in the Laboratory", ASTM International, West Conshohocken, 2001.

Birks, N., Pettit, F.S., and Rishel, D.M. "Erosion corrosion and wear", Journal de physique IV, http:11dx.doi.org/10.1051/jp:1993970. Access on 21/11/2010, 1993.

Bousser, E., Benkahoul, M., Martinu, L., and Klemberg-Sapieha, J.E., "Effect of Microstructure on the erosion resistance of Cr-Si-N coatings", Surface and Coatings Technology. 203(2):776 – 780, 2008.

Cabrini, M., Hoxha, G., Kopliku, A., and Lazzari, A.L., "Prediction of CO_2 corrosion of carbon steel", Eurocorr '97, paper15. 1997.

Cabrini, M., Hoxha, G., Kopliku, A., and Lazzari, L. "Prediction of CO_2 corrosion in oil and gas wells analysis of some case histories" CORROSION/98. 24: 1998.

Cardoso Filho, C., and Orazem, M.E., "Application of a submerged impinging jet to investigate the influence of temperature, dissolved CO_2, and fluid velocity on corrosion of pipeline grade steel in brine", CORROSION 2001, paper 01058, 2001.

Chen, J., Shadley, J.R., Rincon, H., and Rybick, E.F. "Effects of temperature on erosion corrosion of 13CR", NACE 2003, paper 03320, 2003.

CO_2 corrosion rate calculation model, NORSOK Standard no M-506, Norwegian Technology Standards Institution, http://www.nts.no/norsok, 6, 1998.

Crolet, J., and Boris, M.R., "Prediction of the Risks of CO_2 corrosion in Oil and Gas Wells", SPE Production Engineering, November 1991, Offshore Technology Conference. 16 (449), 1991.

Dave, K., Roberts, K.P., Shadley, J.R., Ramachandran, S., Rybick, E.F., and Jovancecic, V., "Effects of a corrosion inhibitor for oil and gas wells when sand is produced", CORROSION/08, Aberdeen UK, paper 08750, 2008.

de Damborenea, J., Bastidas, J.M., and Vazquez, A.J., "Adsorption and inhibitive properties of four primary aliphatic amines on mild steel in 2M Hydrochloric acid", Electrochemica Acta. 42(3): 455 – 459, 1997.

de Moraes, F.D., Shadley, J.R., Chen, J., and Rybicki, E.F., "Characterization of CO_2 corrosion product scales related to environmental conditions", CORROSION 2000, paper 00030, 2000.

de Waard, C., Lotz, U. and Milliams, D.E. "Predictive model for carbon dioxide corrosion engineering in wet natural gas pipelines", Corrosion. 1991: 976 – 985, 1991.

Dugstad, A., "Formation of Protective Corrosion Films during CO_2 corrosion of carbon steel", Eurocorr '97, 1997.

Durnie, W.H., Kinsella, B.J., De Marco, R., and Jefferson, A., "A study of the adsorption properties of commercial CO_2 corrosion inhibitor formulations", Journal of Applied Electrochemistry, 13(11):1221 – 1226, 2001.

Effird, K.D., "Jet impinging testing for flow accelerated corrosion, CORROSION 2000, NACE International, Houston, Texas, paper 00052, 2000.

Evans, T.N., Sun, Y., Babaian-Kibala, E., Bennett Jnr, H.R., Martins, J.W., and Alvarez, J., "Studies of inhibition and monitoring of metal loss in gas systems containing solids", CORROSION/2004, Houston, Texas. paper362, 2004.

Fan, J., Masur, J., Melicharek, N., and Schmittdel, M., "Erosion, cavitation and fretting corrosion", www.mse.berkeley.edu/group/doyle/serdar/...../COURSE...../erosion.pdf accessed on 03/01/11.

French E.C., Martin R.L., and Dougherty J.A., "Review of corrosion inhibitors for gas wells", Materials Performance.28(8): 46-49,1989.

Groysman, A., and Shvarts, I. "Study of efficiency of industrial corrosion inhibitors for cooling water systems at oil refining industry", CORROSION NACExpo 2006, San Diego. paper 06097, 2006.

Gulbrandsen E., "How does fluid flow affect performance of CO_2 corrosion inhibitors?", SPE 95095, SPE International Symposium, Aberdeen, 2005.

Hedges, B, A, and Bodington, A.A., "Comparison of monitoring techniques for improved erosion control: A field study", NACE International, Houston, TX, 2004.

Heitz E., "Chemo-mechanical effects of flow on corrosion", Corrosion. 47:135-146, 1991.

Heitz E., "Mechanically based prevention strategies of flow – induced corrosion", Electrochemita Acta. 41(4):474-488, 1996.

Hernandez-Rodriguez, M.A.L., Martinez-Delgado, D., Gonzalez, R., Perez Unzueta, A., Mercado-Solis, R.D., and Rodriguez, J., "Corrosive wear failure analysis in a natural gas pipeline", Wear. 290:567-571, 2007.

Houghton, C.J., and Westermark, R.V., "North Sea Downhole Corrosion: Identifying the problem: Implementing the solution", Journal of Petroleum Technology. 1983(1):239-246, 1983.

Hu, X. and Neville, A. "The electrochemical response of stainless steels in liquid-solid impingement", Wear. 258:641-648, 2000.

Hu, X., and Neville, A. "CO_2 erosion-corrosion of pipeline steel (API X65) in oil and gas conditions – A systematic approach", Wear, doi: 10:1016/j.wear.2009.07.023 accessed on 02/12/2010, 2009.

Hu, X., and Neville, A., "Assessing the role of corrosion in erosion corrosion of high – grade alloys in aggressive marine environments", CORROSION 2002, paper 02189, 2002.

Hu, X., and Neville, A., "Prediction of erosion-corrosion in oil and gas – A systematic approach", CORROSION 2008, paper 08540, 2008.

Ikeda, A., Ueda, M., and Mukai, S. "Carbon dioxide behaviour of carbon and chromium steels", Advances in carbon dioxide corrosion, NACE, Houston, Texas.1(2):39 – 51, 1984.

Kang, C., More, P.P., Magalhas, A.A.O., and Guisso, R.M. "Effect of flow on erosion corrosion at extreme gas flow rate and the performance of corrosion inhibitor" www.dnvcolumbus.com/files/dsp_recent_publications_6_1_9.pdf. Accessed on 18/11/2010, 2003.

Keating A, and Nesic, S., "Prediction of 2 – phase erosion-corrosion in bends, 2nd International Conference on CFD in minerals and process industries", CSIRO, Melbourne, Australia, 6-8 December, 1999.

Malka, R., Nesic, S., and Gulino, D.A. "Erosion corrosion and synergistic effects in disturbed liquid-particle flow", CORROSION 2006. NACE International, Houston, TX, paper 06594, 2006.

McLaury, B.S., Shiraz, S.A., Shadley, J.R. and Rybicki, E.F., "How operating and environmental conditions affect erosion", CORROSION 99. 34, 1999.

Mohammed, T., "Factors increasing corrosion rates of oil field pipes and their inhibition", Petroleum and Coal. 52(3):215-219, 2010.

Mori, G., Vogl, T., Harberl, J., Havlick, W., and Schoberl, J. "Erosion Corrosion and Synergistic Effects under high velocity multiphase conditions", CORROSION/2010, NACE. paper 382, 2010.

Nesic, S., Neville, A., and Papavinasam, S., "Sand management for reliability of oil and gas pipelines", www.corrosioncenter.ohio.edu/documents/sand20%-----pdf accessed on 21/12/2010, 2008.

Nesic, S., Wang, S., Cai, J., and Xiao, Y. "Integrated CO_2 corrosion – multiphase", SPE International, SPE 87555, 1st International Symposium on Oilfield Corrosion, Aberdeen, 2004.

Neville, A. and Dougal, B.A.B.I., "Electrochemical assessment of erosion corrosion of commercially pure titanium and a titanium alloy in slurry impingement", Proceeding Institution Mechanical Engineers,; Journal of Materials: Design and Applications. 216(1):31-41, 2002.

Neville, A. and Wang, C., "Erosion corrosion of engineering steels – can it be managed by use of chemicals?", Wear. 267: 2018-2026, 2009.

Neville, A., and Hu, X., "Mechanical and electrochemical interactions during liquid-solid impingement on high-alloy stainless steels", Wear. 251:1284-1294, 2001.

Neville, A., and Wang, C., "Erosion-corrosion mitigation by corrosion inhibitors – An assessment of mechanisms", Wear. 267:195-203, 2009.

Neville, A., Wang, C., Ramachandran, S., and Jovancecic, V., "Erosion corrosion mitigation using chemicals", NACE 2003. 03319:1-12, 2003.

Novak, P., and Macenauer, A., "Erosion control of passive metals by solid particles", Corrosion Science. 35(1-4):635-640, 1993.

Nyborg R., Andersson, P., and Nordsreen, M., "Implementation of CO_2 corrosion models in a Three – Phase Fluid Flow Model", CORROSION/2000, Houston, TX: NACE International, 48, 2000.

Papavinasam, S., and Revie, R.W., "Review of Testing Methods and Standards for oilfield corrosion inhibitors", Proceedings of EUROCORR 2004, Nice, paper10, 2004.

Papavinasam, S., Revie, R.W., Demiz, A., and Michaelian, K. "Comparing and Ranking of Techniques for monitoring general and pitting corrosion rates inside pipelines", CORROSION 2002, NACE International, Houston, Texas, paper 02495, 2002.

Ramachandra, S., Ward, M.B., Bartrip, K.A., and Jovancicevic, V., "Inhibition of the effects of particle impingement", CORROSION 2002, NACE International, Houston TX, paper 02498, 2002.

Ramahandra, S., Ahn, Y.S., Bartrip, K.A., Jovancicecic, V., and Bassett, J., "Further Advances in the development of erosion corrosion inhibitors", CORROSION 2005, paper 05292, 2005.

Reyes, M., and Neville, A., "Mechanisms of erosion corrosion on a cobalt base alloy and stainless steel UNS S17400 in aggressive slurries", Journal of Materials Engineering and Performance (JMEPEG). 10(6):723-730, 2001.

Ripeanu, R.G., Ioanu Tudor, Dinu, F., and Grigore, V., "The effect of cathodic protection upon erosion corrosion wears", ROTRIB '07,. www.rotrib.pub.07/029.pdf;2007; Nov 8-10, World Trade Center, Bucharest, 7:1-3, 2007.

Ryborg, R.N., "Overview of CO_2 Corrosion models for wells and pipelines", CORROSION/02, paper 233, 2002.

Salama, M.M., "An alternative to API 14E erosional limits for sand laden fluids", Journal of Energy Resources Technology. 122:71-77, 2000.

Schmitt, G. and Bakalli, M.A. "Critical Review of Measuring Techniques for Corrosion Rates under Flow Conditions", NACE 2006, paper 593, 2006.

Schmitt, G., "Drag reduction by corrosion inhibitors – a neglected option for mitigation of flow induced localized corrosion", Materials and Corrosion. 52:329 – 343, 2001.

Schmitt, G., and Bakalli, M., "Advanced models for erosion corrosion and its mitigation", Materials and Corrosion. 2:181-182, 2008.

Schmitt, G., Simon, T., and Hausler, R.H. "CO_2 erosion corrosion and its inhibition under extreme shear stress: I Development of Methodology", CORROSION/90, NACE, Houston TX, paper 022, 1990.

Schmitt, G., Simon, T., and Hausler, R.H., "CO_2 erosion corrosion and its inhibition under extreme shear stress: II Performance of Inhibitors", CORROSION/93, NACE, Houston TX, paper 086, 1993.

Shadley, J.R., Shirazi, S.A., Dayalan, E., and Rybicki, E.F., "Velocity guidelines for preventing pitting of carbon steel piping when the flowing medium contains CO_2 and sand", CORROSION/96, paper 15, 1996.

Shalaby, H.M., Attari, S., Riad, W.T., and Gouda, V.K., "Erosion corrosion behaviour of some cast alloys in seawater", Corrosion. 48:206-217,1992.

Shirazi, A., McLaury, S., and Ali, M.M., "Sand monitor evaluation in multiphase flow", Corrosion 2000, paper no 00084, 2000.

Stack, M.M., "Mapping tribo-corrosion processes in dry and in aqueous conditions: som new directions for the new millennium, Tribology International. 35:679-687,2002.

Stack, M.M., and Paungwiwat, N., "Particulate erosion-corrosion of aluminium in aqueous conditions: some perspectives in pH effects on the erosion corrosion maps", Tribology International. 35:651-660, 2002.

Stack, M.M., Corlett, N., and Zhou, S., "A methodology for the construction of the erosion-corrosion maps in aqueous environments", Wear. 203-204:474-488, 1995.

Stack, M.M., Stott, F.H., and Wood, G.C. "The significance of velocity exponents in identifying erosion-corrosion mechanisms", Journal de physique IV, dx.doi.org/10.1051/jp4:1993972 access on 21/11/2010, 3, 2007.

Tandon, S., Gao, M., and McNealy, R., "Erosion corrosion failure of a carbon pipe elbow – A case study", NACE CORROSION 2009, March 22-26, Atlanta, Georgia. paper 09479, 2009.

The Erosion/Corrosion Research Center. The University of Tulsa, Tulsa, Oklahoma, USA, http://www.ecrc.utulsa.edu; accessed on 22/01/2011.

Tian, B.R., and Cheng, Y.F., "Electrochemical corrosion behaviour of X-65 steel in the simulated oil sand slurry I: Effects of hydrodynamic condition", Corrosion science. 50: 773-779, 2008.

Tian, B.R., and Cheng, Y.F., "Electrochemical corrosion behaviour of X-65 steel in the simulated oil sand slurry II: Synergism of erosion and corrosion", Corrosion science. 50:1469-1474, 2008.

Vuppu, A.K., and Jepson, W.P., "Study of Sweet Corrosion in Horizontal Multiphase, Carbon Steel Pipelines", OTC 7494, 1994, Houston, TX, 1994.

Wang, C., "Erosion-corrosion mitigation using chemicals, Ph.D. Thesis, School of Mechanical Engineering, University of Leeds, UK, 2007.

Wang, C., Neville, A., Ramachandran, S., and Jovancecic, V., "Alleviation of erosion – corrosion damage by liquid – sand impact through use for chemicals", Wear. 258:649-658, 2005.

Wharton, J.A., and Wood, R.J.K., "Influence of flow conditions on the corrosion of AISI 304L SS", Wear. 256:525-536, 2004.

Wood, R.J.., Jones, T.F., Ganeshalingam, J. and Miles, N.J., "Comparison of predicted and experimental erosion estimates in slurry ducts", Wear. 258:937 – 947, 2004,

Wood, R.J.K. and Hutton, S.P., "The synergistic effect of erosion and corrosion trends in published results", Wear. 140:387-394, 1990.

Wood, R.J.K.,"Erosion-Corrosion interactions and their effect on marine and offshore materials", Wear. 261:1012-1023, 2006.

Wood, R.J.K., and Speyer, A.J., "Erosion-corrosion of candidate HVOF aluminium-based marine coatings", Wear. 256:545-556, 2004.

Xu, E.J., and Zhuo, C., "Erosion corrosion characteristic of nano-particulates reinforced Ni-Cr-Mo-Cu surface alloying layer in acidic flow and acidic slurry flow", Materials and Corrosion. 61(1):7-15, 2010.

Full Paper

SOME NUTRITIONAL AND ENGINEERING PROPERTIES OF *KARIYA* (*HILDEGARDIA BARTERI*) SEEDS

B.S. Ogunsina,
Department of Agricultural & Environmental Engineering, Obafemi Awolowo University, Ile-Ife, Nigeria.
bsogunsina@yahoo.com

I.O. Olaoye,
Department of Agricultural Engineering. The Polytechnic Ibadan, Nigeria.

A.O. Adegbenjo
Department of Agricultural & Environmental Engineering, Obafemi Awolowo University, Ile-Ife, Nigeria.

B.D. Babawale
Department of Agricultural & Environmental Engineering, Obafemi Awolowo University, Ile-Ife, Nigeria.

ABSTRACT

Kariya is an ornamental tropical tree which produces an underutilized edible seed. Some nutritional and engineering properties of *kariya* seeds were investigated. The results show that *kariya* seeds contain 17.5, 13.8, 2.8, 37.5 and 6.5% of crude protein, moisture, ash, fat and crude fibre, respectively. The crude fat was largely made up of myristic, palmitic, stearic and linolenic acids. The length, width, thickness, equivalent diameter and mass were 14.1, 10.2, 9.6, 11.1 mm and 0.5 g for the nut and 10.2, 7.20, 7.2, 8.1 mm and 0.4 g for the kernel, respectively. The volume, surface area, sphericity and aspect ratio were respectively 719.81 mm^3, 387.13 mm^2, 79.26, 73.78% for the nut and 324.28 mm^3, 203.60 mm^2, 80.45, 71.33% for the kernel. The true and bulk density, and porosity were 787.2, 375.4 kg/m^3 and 47.7% for the nuts and 1058, 508 kg/m^3 and 52% for the kernels, respectively; while the angle of repose and coefficient of friction on wood, aluminum and galvanized steel surfaces were 38.22°, 0.32, 0.34 and 0.35 for the nut and 33.37°, 0.23, 0.30, 0.31 for the kernel. The rupture force of the nut in the longitudinal axis (91.65 N) was less than in the transverse direction (104.87 N) and the corresponding values of stiffness and maximum deformation at nutshell rupture were 29.71 and 13.53 N/mm; and 3.39 and 4.18 mm, respectively. Knowledge of these properties will be useful for designing various systems for processing of *kariya* seeds.

Keywords: *Hildegardia barteri, nuts, kernels, nutritional and engineering properties*

1. INTRODUCTION

Kariya (Hildegardia barteri) belongs to a genus of *Malvaceous* trees comprising eleven species that are found in the dry tropical forests of West Africa from Ivory Coast to southeastern Nigeria (Hinsley, 2009). Although it grows mostly in the wild, it is specifically grown for ornamental purpose tree due to the bright red flowers it produces during the dry season (Fig. 1). The flowers, usually born on leafless branches mature into one-seeded pods; each about 50 mm in length ((Inglett *et al.*, 1973), bearing a peanut-like seed in a nutshell (Fig. 2).

Fig. 1: A typical kariya (Hildegardia barteri) tree on Obafemi Awolowo University Campus, Ile Ife, Nigeria.

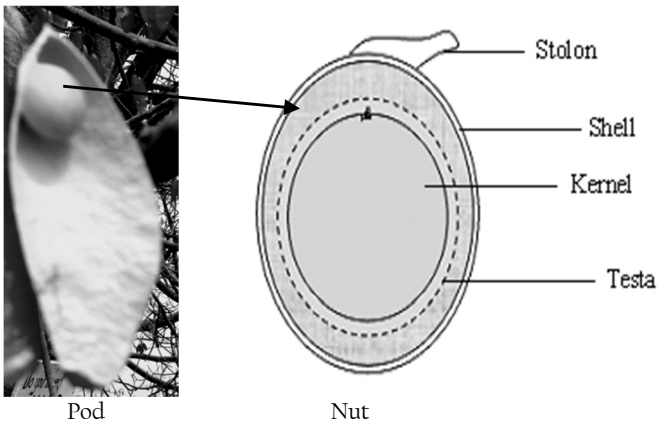

Pod Nut

Fig. 2: Longitudinal section through kariya pod and nut

Kariya wood, due to its light weight is reported to be useful in making fishing net floats and traditional household utensils. Fibre ropes and gum obtainable from the bark have also been found to be of high industrial value if properly harnessed. In some parts of West Africa, raw or roasted *kariya* kernels are eaten like peanuts (Inglett *et al.*, 1973)

or used as a traditional food condiment. However, in Nigeria and most other places where it is grown as ornament, when the mature pods dry up and get completely shed, they are disposed or incinerated as refuse.

The properties of agricultural materials have been widely studied. Physical and mechanical properties such as axial dimensions, mass, volume, equivalent diameter, sphericity, bulk density, true density, porosity, projected area, coefficient of friction and cracking force provide useful information for designing threshing, separating, handling, pneumatic conveying and storage systems. For most oil seeds and legumes, knowledge of nutritional properties provides useful information on their exploitation for industrial or food purposes. Some of the previously researched seeds include peanut (Aydin, 2007); filbert nut (Pliestic *et al.*, 2006); pistachio (Kashaninejad *et al.*, 2004); walnut (Koyuncu *et al.*, 2004); almond (Aydin, 2003); hazelnut (Aydin, 2002); macadamia nut (Braga *et al.*, 1999) and neem (Viswanathan *et al.*, 1995).

The sizes of these products were determined by measuring their axial dimensions as documented by Dutta *et al.* (1988) and Mohsenin (1986) using linear measurement tools such venier callipers and micrometer screw gauge. The axial dimensions of a material give information about its natural position at rest and this is useful when applying compressive force to induce fracture in a nutshell. The one thousand seed weight is a measure of seed size in grams of 1,000 seeds; it is important when calculating seeding rates, calibrating seed drills and estimating shattering and combine losses (Agri-Facts, 2007). Dutta *et al.* (1988) and Aviara *et al.* (2005) determined 1,000 seed weight by weighing one thousand randomly selected seeds using high-precision electronic balances. Ogunjimi *et al.* (2002) and Shepherd & Bhardwaj (1986) determined the true or particle density of locust beans and pigeon pea respectively using the liquid displacement method. Aviara *et al.* (2005) coated balanite nuts with a thin layer of epoxy resin to prevent the sample from absorbing water during determination of true density by water displacement. In a similar study, Omobuwajo *et al.*, (1999) packed African breadfruit seeds in a sinker made from mosquito wire net. The relationship between porosity, true density and bulk density documented by Mohsenin (1986) has been frequently used for determining the porosity of agricultural products. The mass and density characteristics of agricultural products are quite useful in estimating product yield and throughput of processing machines. Hull-seed or shell-kernel ratio as an index of maturity was first proposed by Troeger *et al.* (1976) and Pattee *et al.* (1977) especially for groundnuts. It is obtained as a percent ratio of the mass of the hull (kernel) to mass of the entire seed (nut) obtained on the basis of fresh or dry seed mass. It gives an idea of what percentage of the whole seed is the hull and this has been used subsequently by other researchers (Pattee *et al.*, 1980, 1981; Nautiyal, 2002). The extent of maturity of seeds in nutshell affects their behaviour during processing and resistance to static and dynamic forces. For instance, an immature seed will yield less oil than mature one. The static coefficient of friction of several agricultural products on several structural surfaces has been determined using the inclined plane method (Ramakrishna, 1986; Dutta *et al.*, 1988; Joshi *et al.*, 1993; Aviara *et al.*, 2000, Aviara *et al.*, 2005). Fraser *et al.* (1978), Dutta *et al.* (1988), Aviara *et al.* (1999 and 2005) used a specially constructed box with removable front panel to determine the angle of repose of grains and seeds.

Although, information on the production statistics of *kariya* seeds is quite sparse, it is reported to be an edible oil seed (Inglett *et al.*, 1973) which could be exploited for food or industrial purposes. Consequently, this study was carried out to investigate some nutritional and engineering properties of *kariya* seeds.

2. Materials and Methods

2.1. Source of materials

Dry *kariya* pods were gathered on Obafemi Awolowo University campus, Ile-Ife during the month of January, 2008. About 5 kg of nuts that were extracted from the pods were winnowed manually to remove stones and other extraneous particles. About 2 kg of the nuts were dehulled manually and cleaned with an air screen cleaner to remove all dust, chaff, broken, shrivelled, immature kernels and broken seeds.

2.2. Determination of proximate composition and fatty acid profile

Moisture content: The moisture contents of the nuts and the kernels were determined according to American Society of Agricultural and Biological Engineers standard S410.1 (ASABE, 1998). Approximately 10 g of nuts and kernels were weighed to the nearest 0.01 g inside aluminium dishes of known weights; each in three replicates. Samples were oven dried at 130°C for 6 h and removed afterwards from the oven, cooled in desiccators and weighed. The moisture content (w.b.) was calculated from the percent difference in weight before and after oven-drying.

Proximate composition: The proximate composition of the samples was determined according to AOAC (2002) method. Nitrogen estimation was done by micro-Kjeldhal method. The protein content was determined by multiplying the nitrogen value with 6.25. The greyish white residue formed after charring and incineration of sample in a muffle furnace at 600°C for 6–8 h comprised of the total ash. Fat content was estimated by soxhlet extraction and total carbohydrate was obtained by difference. All values were averages of three determinations.

Fatty acid analysis: Fatty acid methyl esters (FAMEs) of the extracted crude fat were prepared by transesterification using methanolic KOH according to method Ce 2-66 of AOCS (1997). The FAMEs were separated in a gas chromatograph (Model GC-15A, Shimadzu corporation, Japan) equipped with a hydrogen flame detector (FID) using a S.S. column coated with 15% DEGS on chromosob w/HP 80-100 mesh as the stationary phase. The column oven temperature was 180°C. Injector and detector temperatures were 220 and 230°C respectively and the carrier gas, nitrogen was maintained at a flow rate of 40 ml/min. The fatty acids in the oil were identified by comparing retention times of FAMEs with those of standard FAME mix C8 – C24 (Supelco, Belle, USA). There were three observations and the average was expressed as relative percent.

2.3. Determination of physical and mechanical properties

Axial dimension, Shape indices and Gravimetric properties: To determine the average size of the seed, 100 nuts and kernels were picked randomly and their three linear dimensions namely, length L, width W and thickness T were measured using a micrometer reading to 0.01 mm (Ö̈zarslan, 2002; Vilche *et al.*, 2003; Yalcin, 2007). From the axial dimensions, the equivalent diameter, D_e mm; sphericity, ϕ %; and aspect ratio, R_a % were calculated using the following equations (Mohsenin, 1986; Aydin, 2002, 2003; Joshi *et al.*, 1993; Isiaka *et al.*, 2006):

$$D_e = (LWT)^{1/3} \tag{2}$$

$$\varphi = \frac{D_e}{L} \times 100 \ ; \tag{3}$$

$$R_a = \frac{W}{L} \times 100 \tag{4}$$

The following equations were used to obtain the volume, *V* (Pliestic *et al.*, 2006; Du & Sun, 2006) and arithmetic mean diameter, D_a (Dursun & Dursun, 2005; Mohsenin, 1986; Rasavi *et al.*, 2007):

$$V = \frac{\pi LWT}{6} \quad (5)$$

$$D_a = \frac{L + W + T}{3} \quad (6)$$

Surface area, S_a was calculated according to Equation (7) below (McCabe *et al.*, 1986; Koocheki *et al.*, 2007)

$$S_a = \pi D_e^2 \quad (7)$$

The respective mass of the individual nuts and kernels and one thousand seeds mass were determined using a precision electronic balance Mettler Toledo PB153 weighing to 0.001g degree of accuracy. Density of the sample was determined by water displacement method. Ten nuts of known mass coated with a thin layer of epoxy resin were immersed inside a known volume of water inside a measuring cylinder using a sinker made of mosquito wire netting (Omobuwajo *et al.*, 1999). From preliminary investigation, the average increase in mass of the sample due to the epoxy resin coating was 2.23%. The ratio of the mass of the nuts to the net volume of water displaced due to the immersion was used to calculate the average density of one nut. For bulk density, a measuring cylinder of pre-determined weight and known volume was filled to the top with the sample, the excess was removed by a strike off stick without any compaction and the weight was determined afterwards (Dutta *et al.*, 1988). The ratio of the weight of the nuts to the volume of the cylindrical container was calculated to obtain the bulk density (ρ_b). In both cases, there were ten replicates. Based on Mohsenin (1986), density ratio (ρ_r) was calculated as the ratio of true density to the bulk density of the material while porosity (p) was calculated using equation (8):

$$\text{Porosity, } \varepsilon = \frac{\rho_t - \rho_b}{\rho_t} \times 100 \quad (8)$$

Hull-seed ratio (HSR) was obtained as a percent ratio of the mass of hull (shell) to the mass of the entire seed (nut). Five nuts of known total weight were dehulled, the total weight of the hull was determined and HSR was calculated. The indicated value was an average of ten replicates.

Frictional Properties: The coefficient of friction of the material was determined using the inclined plane method described by Dutta *et al.* (1988); Suthar and Das (1996) and Aviara *et al.*, (2005). Three structural surfaces were considered; namely, wood (with grains parallel to the direction of slide), aluminum and galvanized steel, each in three replicates. As soon as the material began to slide on the selected surface, the angle at which the plane was inclined to the horizontal (β) was measured with a protractor and the coefficient of friction (μ) was calculated as:

$$\mu = \tan\beta \quad (9)$$

This was carried out in ten replicates. The angle of repose (Φ) was determined using a 200 × 200 × 200 mm transparent fibre box which had a removable front panel. The box was filled with the samples to level and afterwards, the front panel was quickly removed, allowing the nuts or kernels to flow and assume a natural slope (Aviara *et al.*, 2005; Ozdemir & Akinci, 2004; Baryeh, 2001; Joshi, *et al.*, 1993). The angle made by the slope with the horizontal was calculated as the angle of repose and there were ten replicates.

Force Deformation Characteristics: The cracking force of *kariya* nuts was determined in the longitudinal and transverse axis using the Instron Universal Testing Machines (UTM 3369 series, 50 kN capacity). Individual nut was loaded between two parallel plates and compressed at a fixed cross-head speed of 10 mm/min until the shell ruptured. The bio-yield point was taken as the point at which rupture occurred after which there was a sudden drop in force on the force deformation curve. As soon as the bio-yield point was attained, loading was discontinued. The magnitude of the load applied on the sample and the deformation during compression was read through the monitor of the desktop computer fitted with the Instron UTM. The software has an X-Y plotter which generates the force-deformation curve of each sample. This was carried out in fifteen replicates.

3. Results and Discussion

Proximate composition: The results showed that *kariya* kernels contain 17.54, 37.45, 2.79, 6.48 and 21.91% of crude protein, crude fat, ash, crude fibre and carbohydrate respectively (Table 1). The crude protein content *kariya* compares favourably with 18.3% for gingelly seeds; 15.6% for walnut and 19.8% for both pistachio and sunflower seeds; whereas, it is less than 21.2 % for cashew nut; 20.8 % for almond; 26.25 for groundnut; 20.3 % for linseed and 20 % for mustard seeds (Gopalan *et al.*, 2007). The crude fat content can be compared with 39.3 % for sponge gourd seeds (Ogunsina *et al.*, 2009); 39.8 % for groundnut; 37.1 % for linseed; 39.7 % for mustard and 39 % for niger seeds (Gopalan *et al.*, 2007). Given its relatively high protein content, and subject to investigation of its anti-nutritional components, defatted *kariya* flour may be explored as a good source of vegetable protein.

Table 1: Proximate composition of kariya kernel

Constituent	% composition
Moisture	13.83±0.13
Crude Protein	17.54±0.25
Ash	2.79±0.15
Fat	37.45±1.18
Crude Fiber	6.48±0.57
Carbohydrate	21.91±0.46

Table 2: Fatty acid composition of kariya seed oil

Fatty acids	% Composition
Saturated fatty acids	
Lauric	0.60
Myristic	23.32
Palmitic	29.38
Stearic	23.74
Total	77.04
Unsaturated fatty acids	
Oleic	0.03
Linoleic	1.43
Linolenic	21.50
Total	22.96

Fatty acids: The fatty acid profile of *kariya* seed oil is presented in Table 2. A total of 77.04% of saturated fatty acids comprising 29.38% palmitic, being the most abundant; 23.32% myristic, 23.75% stearic and trace amount of lauric (0.6%) were observed in *kariya* seed oil. Unsaturated fatty acids totaled 22.96% with 21.5% of linolenic acid as the most abundant; and a small amount of linoleic acid (1.43 %) and trace amount of oleic (0.03%) were also observed. Oils with a high proportion of saturated fats are generally important for energy, hormone production, cellular membranes and organ padding. They are usually stable under oxidative conditions (Rossel *et al.*, 1985) and serve important dietary functions in human nutrition and immune system. Enig (2000) reported that myristic and palmitic acid are important to

body metabolism and proper functioning of vital body organ among other things. Subject to further investigation, the suitability of *kariya* seed oil may be exploited for edible industrial products.

Physical and mechanical properties: Data on axial dimensions, shape indices, gravimetric properties, density characteristics and frictional properties of *kariya* nuts and kernels are shown in Table 3. The average axial dimensions (*i.e.* length, width, thickness, geometric mean diameter) and mass of *kariya* were 14.06, 10.02, 9.57, 11.1 mm and 0.47 g, for the nuts and 10.16, 7.20, 7.16, 8.05 mm and 0.35 g for the kernels respectively. The volume and the surface area were 719.81 mm^3 and 387.13 mm^2 for the nuts and 324.28 mm^3 and 203.60 mm^2 for the kernels. These axial dimensions are close to 10.5, 9.48 and 8.50 mm for bambara groundnut (Baryeh, 2001), whereas with an average width and thickness of 16.68 and 15.71 mm respectively, *kariya* is smaller than peanut (Aydin, 2007). Similarly, when compared with other nuts such as cashew, almond, pistachio and filbert nuts for which length, width and thickness were 32.24, 23.23 and 17.02 mm (Oloso & Clarke, 1993); 25.49, 17.03 and 13.12 mm (Aydin, 2003); 16.86, 12.1 and 11.81 (Kashaninejad, *et al*., 2004) and 25.32, 20.54 and 17.93 mm (Pliestic *et al*., 2006), respectively, *kariya* is smaller in size. It is however bigger in size than sweet corn which has 10.47, 8.33 and 3.83 mm of length, width and thickness, respectively (Karababa & Coskuner, 2007). It was observed that *kariya* nut is lighter in weight compared to peanut, filbert, pistachio and almond which weigh 2.16, 3.88, 1.09, 1.15 and 2.64 g, respectively (Aydin, 2007; Pliestic *et al*., 2006; Kashaninejad *et al*., 2004; Aydin, 2003). The following general expressions were derived for the relationship between the principal dimensions and mass for the nut and the kernel.

$$L=1.38W = 1.47T = 31.15M, \quad (10)$$

$$l= 1.42w = 1.43\ t = 29.54\ m; \quad (11)$$

The relationships between the respective parameters for the nut and kernel are derived as follows:

$$L= 1.39l, \quad (12)$$

$$W = 1.47w, \quad (13)$$

$$T= 1.40t, \text{ and} \quad (14)$$

$$M = 1.24m. \quad (15)$$

where mass, length, width and thickness are *M*, *L*, *W*, *T* for nut and *m*, *l*, *w*, *t* for the kernel, respectively.

A lower mass ratio of 1.24*l* of nut indicates a relatively high yield of kernels per unit weight of *kariya* nuts which is greater than that of sunflower seeds (Gupta & Das, 1997) and sponge gourd seeds (Ogunsina *et al*., 2009). The frequency distribution curves of *kariya* nut and kernels for length, width and thickness are shown Figs. 3 and 4. Table 4 shows the dimension and mass of *kariya* nuts and kernels based on their size distribution. The trend shown by each curve is that of normal distribution. The geometric mean diameter of *kariya* is less than 13.38 mm for pistachio (Kashaninejad, *et al*., 2006); 20.96 mm for filbert (Pliestic *et al*., 2006) and 12.6 mm for pea nut (Aydin, 2007). These properties of *kariya* seeds are essential for the design of equipment and facilities for handling, conveying, separation, drying, aeration, storing and processing. Various types of cleaning grading and separation equipment are designed on the basis of their physical properties.

The sphericity of *kariya* nut (79.26) and kernel (80.45%) compares favourably with that of palm nut, 80% (Sanni & Adegbenjo, 2002); pistachio 79.54% (Kashaninejad, *et al*., 2006) and filbert nut, 82.86% (Pliestic *et al*., 2006), but are less that of bambara groundnut

Table 3: The Physical Properties of kariya Seeds

Property	Nuts	Kernels
Axial dimension and Shape indices		
Length (mm)	14.06±1.1	10.16±0.64
Width (mm)	10.2±0.59	7.2±0.41
Thickness (mm)	9.57±0.40	7.16±0.50
Geometric mean diameter (mm)	11.1±0.47	8.05±0.32
Volume (mm^3)	719.81±2.22	324.28±8.31
Surface area (mm^2)	387.13±2.34	203.60±1.86
Sphericity (%)	79.26±4.34	80.45±0.05
Aspect ratio (%)	73.38±0.07	71.33±0.07
Gravimetric properties		
Mass (g)	0.47±0.08	0.35±0.04
Thousand seeds mass (g)	485.61±10.2	396.23±8.54
True density (kg/m^3)	787.17±31.63	1058.02±78.3
Bulk density (kg/m^3)	375.39±10.81	508.02±22.01
Density ratio (%)	56.42±4.29	45.37±4.01
Porosity (%)	47.69±4.27	51.98±3.97
Hull-Seed Ratio (%)	24.73±0.06	-
Frictional properties		
Coefficient of static friction		
-on wood (with grain parallel to axis of slide)	0.32±0.05	0.23±0.04
-on aluminum	0.34±0.04	0.3±0.02
-on galvanized steel sheet	0.35±0.04	0.31±0.01
Dynamic angle of repose (°)	38.22±2.09	33.37±2.59

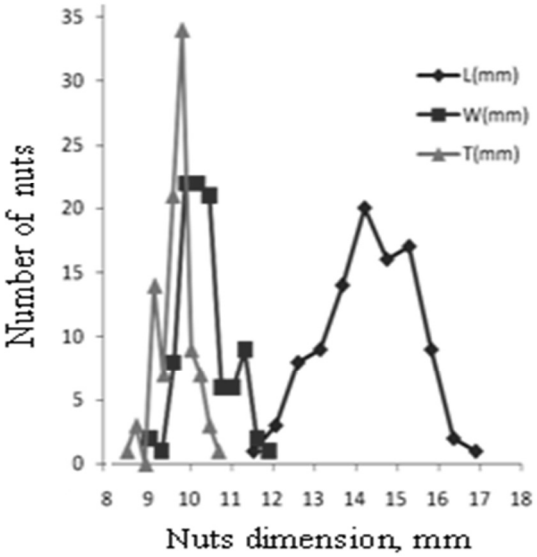

Fig. 3: Frequency distribution curves of kariya nuts dimensions

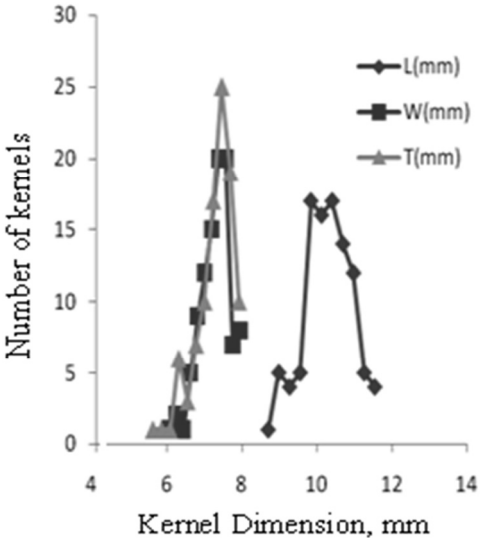

Fig. 4: Frequency distribution curves of kariya kernels dimensions

Table 4: Dimension and mass of kariya nuts on size distribution

Properties	Size distribution		
	Large	Medium	Small
Nut			
Length (L), mm	15.48±0.48	14.05±0.53	12.32±0.39
Width (W), mm	11.25±0.24	10.19±0.29	9.54±0.21
Thickness (T), mm	0.13±0.22	9.63±0.13	9.04±0.24
Mass (M), g	0.58±0.03	0.48±0.04	0.36±0.06
Kernel			
Length (l), mm	10.90± 0.33	10.03±0.29	9.03±0.25
Width (*w*), mm	7.69± 0.16	7.25±0.15	6.64±0.25
Thickness (*t*), mm	7.69± 0.15	7.14±0.27	6.12±0.25
Mass (*m*), g	0.40± 0.03	0.34±0.02	0.28±0.03

which varied from 87-90% (Baryeh, 2001). These values indicate that *kariya* has a near spherical shape and provides useful information for the design of nutcracker, kernel-shell separator, milling machine for *kariya* seeds and other similar agricultural products where the flow pattern of the material on flat surfaces is an important factor.

The true density, bulk density, density ratio and porosity are 787.17, 375.39 kg/m^3 56.42 and 47.69% for the nut and 1058.02, 508.02 kg/m^3, 45.37 and 51.98% for the kernel, respectively. The bulk density of *kariya* kernels is greater than 213.5 kg/m^3 for peanuts (Aydin, 2007) and 492 kg/m^3 for filbert nut (Pliestic *et al.*, 2006); but lesser than 520.79, 590, 585.8 and 795 kg/m^3 for pistachio (Kashaninejad *et al.*, 2006), almond (Aydin, 2003), chestnut (Yildiz *et al.*, 2009) and bambara groundnut (Baryeh, 2001), respectively. Similarly, the true density of *kariya* nuts is greater than 484.5 for peanut and lower than 868 for filbert; 1141.77 for pistachio; 1285 for bambara groundnut and 1135.68 kg/m^3 for chest nut. The porosity of kariya nuts compares with that of almond and balanite which ranges from 35.32 - 53.21 and 41.86 - 47.46%, respectively (Aydin, 2003; Mamman, *et al.*, 2005) but higher than 41.53 - 45.24%; for filbert nuts (Pliestic *et al.*, 2006), and sunflower seeds (Gupta & Das, 1997). Bulk density and porosity affect structural loads of most biomaterials. The HSR of *kariya* compares with 24.5% for *Moringa oleifera* seeds (Ogunsina, 2009) and far below 70-75% for cashew nut (Andrighetti *et al.*, 1994). Hull seed ratio measures the extent of maturity of a particular seed in a nutshell and provides information regarding its further processing and utilization.

The angle of repose of *kariya* nut and kernel are 38.22 and 33.37º respectively. The static coefficient of friction on wood, aluminum and galvanized sheet are 0.32, 0.34, and 0.35 for the nut and 0.23, 0.3 and 0.31 for the kernel, respectively. The angle of repose compares very closely with that of balanite which varies from 22.36 to 33.66 (Aviara *et al.*, 2005). It was observed that for the kernel, angle of repose is lower than that of the nut and this may be attributed to the rough nature of the hull which offers resistance to motion when sliding on the test surface. Both the nut and the kernels are near spherical in shape thus they both glide easily on one another. The hopper walls are mostly inclined at an angle greater than the angle of repose to allow material flow by gravity (Sanni & Adegbenjo, 2002). The static coefficient of friction of *kariya* kernel on all the surfaces considered is lesser than that of the nut due to the smoother surface of the kernel. Information about the frictional properties of biomaterials is important in the design of hopper and conveyor systems.

The force deformation curve of *kariya* nuts during quasi-static compression tests in both axial and longitudinal directions are shown in Fig. 5 and Table 5. The average compressive force required to cause nut rupture during longitudinal loading (91.65 N) was less than during transverse loading (104.87 N). The average maximum deformations of kariya nuts at nutshell rupture were 3.39 and 4.18 mm and the corresponding values for stiffness were 29.71 and 13.53 N/mm. It was observed that maximum rupture force occurred in the transverse axis while minimum force was in the longitudinal axis. Similar behaviour had been reported for almond (Aydin, 2003) and green gram (Nimkar & Chattopadhyaya, 2001). The converse was true for filbert (Pliestic *et al.*, 2006). This implies that the nutshell is more resistant to fracture in the transverse axis as compared to the longitudinal. These are contrary to the findings of Aydin (2002) for hazelnut, Braga *et al.* (1999) for macadamia nut and Koyuncu *et al.* (2004) for walnut. This contradiction could be due to differences in the shape of *H. barteri* and filbert nut in comparison to these other nuts.

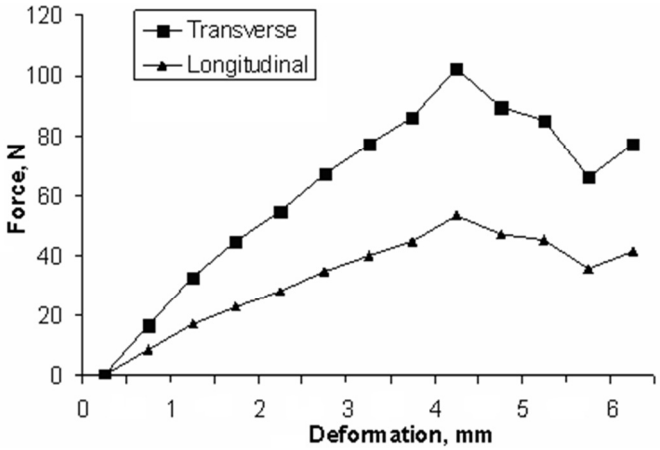

Fig. 5: Force-Deformation of kariya nuts under quasi-static compression

Table 5: Some strength characteristics of kariya nuts during quasi-static loading

Quantity	Orientation of load application	
	longitudinal axis	transverse axis
Stiffness, N/mm	29.71	13.53
Maximum elastic deformation, mm	3.39	4.18
Load at nutshell rupture, N	91.65	104.87

4. CONCLUSIONS

The following conclusions can be drawn from this study:

i. *Kariya* though an underutilized seed is rich in protein (17.54%) and crude fat (37.45%). The fatty acids profile indicates an almost equal amount of myristic, palmitic, stearic and linolenic acids.

ii. The average values of length, width, thickness, equivalent diameter and mass were 14.06, 10.2, 9.57, 11.10 mm and 0.47 g for the nut and 10.16, 7.20, 7.16, 8.05 mm and 0.35 g for the kernel respectively. The volume, surface area, sphericity and aspect ratio were 719.81 mm^3, 387.13 mm^2, 79.26 and 73.78% for the nut and 324.28 mm^3, 203.60 mm^2, 80.45 and 71.33% for the kernel respectively.

iii. The true and bulk density, density ratio and porosity were 787.17, 375.39 kg/m^3, 56.42 and 47.69%, for the nuts and 1058.02, 508.02 kg/m^3, 45.37 and 51.98% for the kernel respectively.

iv. The angle of repose and coefficient of friction on wood, aluminium and galvanized steel surfaces were 38.22º, 0.32, 0.34 and 0.35 for the nut and 33.37º, 0.23, 0.30, 0.31 for the kernel.

v. The average compressive force required to cause nut rupture during longitudinal loading (91.65 N) was less than during transverse loading (104.87 N). The average maximum deformations of kariya nuts at nutshell rupture were 3.39 and 4.18 mm and the corresponding values for stiffness were 29.71 and 13.53 N/mm.

REFERENCES

AOAC. Official Methods of Analysis. Association of Analytical Chemists. Gaithersburg, Maryland, USA. 2002.

AOCS. *Official Methods of the American Oil Chemists' Society*, Vol. I, 6th Ed., AOCS Press, Champaign, IL. 1997.

Andrighetti, L., Bassi, G. F., Capella, P., De Logu, A. M., Deolalikar, A. B., Haeusler, G., Franca F. M. C., Rivoira, G., Vannini, L. and Deserti, R. N. *The World Cashew Economy*. (2nd Edtion). Linchiostroblu, Italy. p 11 - 48, 79 – 80, 1994.

ASABE Standards S 410.1. Moisture Measurement-Peanuts American Society of Agricultural Engineers. 1998. http://www.google.com/search?hl=en&q=ASAE+standards+%2B+moisture+content+%2B+pea+nuts&aq=f&oq=&aqi=

Aviara, N.A., Gwandzang, M.I. and Haque, M.A. Physical properties of guna seeds. *Journal of Agricultural Engineering Research*, 73(2): 105-111, 1999.

Aviara, N.A., Haque, M.A. and Izge, I.A. Physical and frictional properties of sheanut. *Agro-Science*, 1: 19-34, 2000.

Aviara, N.A., Mamman, E. and Umar, B. Some physical properties of *Balanites aegyptiaca* nuts. *Biosystems Engineering*, 92(3): 325–334, 2005.

Aydin, C. Physical properties of hazel nut. *Biosystems Engineering*, 82(3): 297-303., 2002.

Aydin, C. Physical properties of almond nut and kernel. *Journal of Food Engineering*, 60: 315–320, 2003.

Aydin, C. Some engineering properties of ***peanut*** and kernel. **J***ournal of Food Engineering,* 79(3):810-816***, 2007.***

Baryeh, E.A. Physical properties of bambara groundnuts. *Journal of Food Engineering.* 47: 321–326, 2001.

Braga, G.C., Couto, S.M., Hara, T. and Almeida-Neto, J.T.P. Mechanical behaviour of macadamia nut under compression loading. *Journal of Agricultural Engineering Research*, 72: 239–245, 1999.

Du, C.J. and Sun, D.W. Estimating the surface area and volume of ellipsoidal ham using computer vision. *Journal of Food Engineering*, 73: 260–268, 2006.

Dursun, E. and Dursun, I. Some physical properties of caper seeds. *Biosystems Engineering*, 92(2): 237–245, 2005.

Dutta S.K., Nema, V.K. and Bhardwaj, RK. Physical properties of gram. *Journal of Agricultural Engineering Research*, 39: 259–268, 1988.

Enig, M.G. *Know Your Fats: The Complete Primer for Understanding the Nutrition of Fats, Oils, and Cholesterol*. Bethesda Press, US. Pp 45, 2000.

Fraser. B.M., Verma, S.S. and Muir, W.E. Some physical properties of faba beans. *Journal of Agricultural Engineering Research*, 23: 53–57, 1978.

Gopalan, C., Rama Sari, B.V. and Balasubramanian, S.C. *Nutritive value of Indian foods.* National Institute of Nutrition, Indian Council of Medical Research, 52, 2007.

Gupta, R.K. and Das, S.K. Physical properties of sunflower seeds. Journal of Agricultural Engineering Research. 56(2): 89-98, 1997.

Hinsley, S.R. The Hildergadia Page. Hildergadia Galery. Malvaceae Home Info. 2009. http://www.malvaceae.info/Genera/Hildegardia/Hildegardia.php

Inglett, G. E., Cavins, J.F. and Spencer, G. F. Seed composition of *Hildegardia barteri*. Economic Botany, 27(1): 128-130, 1973.

Isiaka, M., El-Okene, A.M.I. & Oyedele, T.A. Determination of physical properties of melon seeds. In *Proceedings of the 7th International Conference and 28th Annual General Meeting of the Nigerian Institution of Agricultural Engineers*, Zaria, Nigeria. November 6-10, 2006, 28: 322-326, 2006.

Joshi, D.C., Das, S.K. and Mukherjee, R.K. Some physical properties of pumpkin seeds. *Journal of Agricultural Engineering Research*, 54: 219–229, 1993.

Karababa, E. and Cokuner, Y. Moisture dependent physical properties of dry sweet corn kernels. *International Journal of Food Properties*, 10(3): 549-560, 2007.

Kashaninejad, M., Mortazavi, A., Safekordi, A. and Tabil, L.G. Some physical properties of pistachio nut (*Pistacia vera* L.) and its kernel. *Journal of Food Engineering,* 72: 30-38, 2004.

Koocheki, S.M.A., Razavi, E., Milani, T.M., Moghadam, M., Abedini, S.A. and Izadkhah, S. Physical properties of watermelon seeds as a function of moisture content and variety. *International Agrophysics*, 21: 349-359, 2007.

Koyuncu, M.A., Ekinci, K. and Savran, E. Cracking characteristics of walnut. *Biosystems Engineering*, 87: 305-311, 2004.

Mamman, E., Bobboi, U. and Aviara N.A. Effect of moisture content and loading direction on the mechanical properties of *Balanites aegyptica* nuts. Agricultural Engineering International. *The CIGR E-journal*. Manuscript FP 04 015, Volume. VII. December, 2005 *International Commission of Agricultural Engineering.* USA. 2005.

McCabe, W.L., Smith J.C. and Harriott P. *Unit Operations of Chemical Engineering*, McGraw-Hill Press, New York, 1986.

Mohsenin, N.N. *Physical properties of plant and Animal Materials.* Gordon and Breach Science Publishers. New York. Pg 1-31, 1986.

Nautiyal, P.C. Groundnut –Post harvest operations. A post harvest compendium for groundnut by National Research Centre for Groundnut (ICAR), India, (2002). www.fao.org/fileadmin/user_upload/inpho/docs/Post_Harvest_Compedium_Groundnut.pdf. Accessed on October 6, 2011.

Nimkar, P.M. and Chattopadhyaya, P.K. Some physical properties of green gram. *Journal of Agricultural Engineering Research*, 80: 183-189, 2001.

Ogunjimi, L.A.O., Aviara N.A. and Aregbesola, O.A. Some engineering properties of locust bean seed. *Journal of Food Engineering*, 55: 95–99, 2002.

Ogunsina, B.S. Value addition to Drumstick (*Moringa* oleifera) seeds using various adaptable technologies. A report of United Nations University Research fellowship undertaken at Central Food Technological Research Institute, Mysore, India. Pp 50, 2009.

Ogunsina, B.S., Adegbenjo A.O. and Opeyemi, O. Compositional, mass-volume-area related and mechanical properties of sponge gourd *(Luffa aegyptiaca*) seeds. *International Journal of Food Properties*, 13(4): 864-876, 2009.

Oloso A.O. and Clarke, B. Some aspects of strength properties of cashew nuts. *Journal of Agricultural Engineering Research*, 55: 27-43, 1993.

Omobuwajo, T., Akande, F.A. and Sanni, L.A. Selected physical, mechanical and aerodynamic properties of african breadfruit (*Treculia africana*) seeds. *Journal of Food Engineering*, 40: 241-244, 1999.

O¨zarslan, C. Physical properties of cotton seeds. *Biosystems Engineering*, 83(2): 169–174, 2002.

Ozdemir, F. and Akinci, I. Physical and nutritional properties of four major commercial Turkish hazelnut varieties. *Journal of Food Engineering,* 63: 341–347, 2004.

Pattee, H.E., Wynne, J.C., Young, J.H and Cox, F.R. The seed hull weight ratio as an index of peanut maturity. *Peanut Science*, 4: 47-50, 1977.

Pattee, H.E., Wynne, J.C., Sanders, T.H and Schubert, A.M. Relation of the seed/hull ratio to yield and dollar vaue in peanut production. *Peanut Science*, 7: 74-77, 1980.

Pattee, H.E., Giesbrecht, F.G., Dicken, J.W and Whitaker, T.B. Variation in the seed hull maturity index in commercial peanut fields. *Peanut Science*, 8: 97-96, 1981.

Pliestic, S., Dobricevic; N.D. and Filipovic, Z.G. Physical properties of filbert nut and kernel. *Biosystems Engineering,* 93(2): 173-178, 2006.

Ramakrishna, P. Melon seeds: evaluation of physical characteristics. *Journal of Food Science and Technology*, 23: 158–160, 1986.

Razavi, S.M.A., Emadzadeh, B., Rafe, A. and Mohammad, A.A. The physical properties of pistachio nut and its kernel as a function of moisture content and variety: Part I. Geometrical properties. *Journal of Food Engineering*, 81(3): 209–217, 2007.

Rossel, J.B., King, B. and Downes, M.J. Composition of oils. *Journal of American Oil Chemist Society*, 62(2): 221-229, 1985.

Sanni, L.A. and Adegbenjo, A.O. Properties of palm nuts and fiber that influence mechanical separation after palm oil extraction. In the *Proceedings of Regional Workshop on Promotion of Appropriate Agro-Processing Technologies in West Africa*, Ile-Ife, Nigeria. British Council and PHTRG .186-196, 2002.

Shepherd H. and Bhardwaj, R.K. Moisture dependent physical properties of pigeon pea. *Journal of Agricultural Engineering Research*, 35: 227–234, 1986.

Suthar, S.H. and Das, S.K. Some physical properties of karingda (*Citrullus lanatus* thumb Mansf) seeds. *Journal of Agricultural Engineering Research*, 65: 15-22, 1996.

Troeger, J.M., Williams, E.J and Butler, J.L. Factors affecting peanut peg attachment force. *Peanut Science*, 3: 37-40, 1976.

Vilche, C., Gely, M. and Santalla, E. Physical properties of quinoa seeds. *Biosystems Engineering*, 86(1): 59–65, 2003.

Viswanathan, R., Palanisamy, P.T., Gothandapani, L. and Sreenarayanan, V.V. Physical properties of neem nut. *Journal of Agricultural Engineering Research*, 63: 19-26, 1995.

Yalcın, I. Physical properties of cowpea (*Vigna sinensis* L.) seeds. *Journal of Food Engineering*, 79: 57–62, 2007.

Yildiz, M.U., Ozcan, M.M., Calisir, S., Demir, F. and Er, F. Physico-chemical properties of wild chest nut (*Castanea sativa*) fruit grown in Turkey. *World Applied Sciences Journal*, 6(3): 365-372, 2009.